

**Variations in cyclical carbonate-evaporite
depositional architectures**

By

Heero Ghareeb Abdullah

Submitted in accordance with the requirements for the degree of

Doctor of Philosophy

University of Leeds

School of Earth and Environment

June, 2016

Declaration

The candidate confirms that the work submitted is her own and that appropriate credit has been given where reference has been made to the work of others.

This copy has been supplied on the understanding that it is copyright material and that no quotation from the thesis may be published without proper acknowledgement.

The right of Heero Ghareeb Abdullah to be identified as Author of this work has been asserted by her in accordance with the Copyright, Designs and Patents Act 1988.

©2016 The University of Leeds and Heero Ghareeb Abdullah

Abstract

Cyclical carbonate-evaporite successions provide an important record of palaeoenvironmental fluctuations in the geologic record. They also have significance as economic resources, either as a part of petroleum systems or as an industrial-scale source of halite and/or gypsum. Few basins with such carbonate-evaporite stratigraphic architectures have been studied in detail, the best known being the Zechstein Basin of north-central Europe and the Paradox Basin of the western United States of America. In this study, sedimentological and sequence stratigraphical investigations of the late Early Miocene deposits of the Fatha Formation at the periphery of the Zagros foreland basin, Kurdistan region, NE Iraq, were carried out. To achieve this, nine complete exposures of the Fatha Formation were logged and correlated across the study area. This was in order to determine depositional environments, a depositional model, and basin configuration, in addition to analyse sequence stratigraphic relationships, high-frequency cyclicities, and to determine average cycle duration. Results are used to evaluate the mechanisms that originated the high-frequency cycles, and to compare their development with the well-developed high-frequency cycles of the Paradox Basin (Pennsylvanian-Permian) in the United States and the Zechstein Basin (late Permian) in north-central Europe.

This study reveals a cyclical arrangement of carbonate-evaporite ramp cycles on the north-eastern margin of the Zagros Basin, each recording basinward progradation and a shallowing-upward trend from lower energy calcareous mudstone and mudstone-wackestone carbonate microfacies at the base, to higher energy packstone-grainstone-rudstone and/or low energy algal mat/stromatolitic carbonate facies at the top. Each carbonate unit is capped by evaporite deposits of supratidal sabkha origin. Red clastic sediments that advanced south-westward into the basin from the adjacent Zagros hinterland overlie each evaporite unit. The investigations reveal inner ramp facies of different environments that included normal marine salinity open lagoons, hypersaline lagoons, restricted and shallow lagoons, sand shoals, beaches, intertidal and supratidal flats, tidal flats, supratidal ponds. These are overlain by the sabkha deposits and above these a distal coastal alluvial coastal plain developed that included palaeosols and infrequent channel deposits. This south-westwards progradation of the red siliciclastic deposits into the Miocene Zagros foreland first occurred during deposition of the Fatha

Formation. This progradation and shoreline migration toward the basin caused thickness variation and both lateral and vertical facies changes.

The late Early Miocene carbonate-evaporite cycles of the Fatha Formation display two superimposed orders of stratigraphic cyclicity and two different stacking patterns. Fourth-order parasequences (17-42 parasequences, each 5-13m thick in the lower part of the succession and 1-5m thick in the upper part of the succession, and have a mean periodicity of approximately 60,000 years. They are packaged into a third-order cycle of accommodation evolution, represented by the 50-300m total thickness and a duration of approximately 2.5 Myr. The fourth-order parasequences are composed of the shallowing-upward cycles, separated by flooding surfaces, that each grade up from more basinal carbonate mudstone facies into normal marine carbonates and then into intertidal and supratidal facies, sabkha evaporites and then into fluvial deposits. By using Fischer plot analyses, two different stacking patterns are recognized. The retrogradational set, comprising 10-20 thick cycles with thicknesses that are more than the average cycle thickness, onlaps a sequence boundary at the base of the succession and was deposited during a period of relatively high accommodation space generation and subsidence. In contrast, a progradational set, including 10-20 thinner cycles with thicknesses that are less than the average cycle thickness, prograded toward the SW of the basin and was deposited during decelerating accommodation creation and subsidence in the upper part of the succession. This systematic variation in thickness of fourth-order parasequences, characterised by this thickening upward followed by thinning upward trend, defines a third-order accommodation cycle. Both stacking patterns and the third-order accommodation cycle are regionally correlative over the whole study area, and individual cycles may be correlated throughout the area, demonstrating continuity of at least several tens of kilometres. This is a characteristic feature of high-frequency glacio-eustatic sea-level fluctuations that are controlled by Milankovitch cycles and such depositional geometries unlikely to be controlled by tectonic oscillations. Autocyclic controls on the depositional geometries may occur within each fourth cycle, in particular in the inner ramp facies associations.

A secondary, literature-bases analysis has been carried out of two well-developed carbonate-evaporite cyclical successions, namely of the Paradox (Pennsylvanian-Permian) and Zechstein (late Permian) Basins. These are characterised in terms of their sedimentological features, vertical facies trends within cycles, and more regional

depositional geometries. These examples are then compared to the cyclical succession of the Fatha Formation. Their tectonic settings, palaeo-climates, and stratigraphic trends are analysed, as well as their hierarchical divisions and sequence stratigraphic styles. The mechanisms that controlled the high-frequency cyclicities are inferred and compared those that controlled the Fatha Formation. Climate, glacio-eustatic sea-level fluctuation and the tectonic configuration of a basin are considered to be the major variables in the determination of the stratigraphic architectures of each carbonate-evaporite cyclical succession. The presence or absence of boundstone bioherm constructors additionally influences whether a basin margin architecture will remain as a gradually sloping ramp, in the absence of such bioherms, or develops a distally-steepened slope, in the case of coral or algal bioherms being present. The new sequence stratigraphic model for cyclical carbonate-evaporite deposition on ramp margins, as developed for the Fatha Formation, applies to the former. More classical type-1 sequence boundaries and associated systems tract geometries remain appropriate for describing the latter.

Acknowledgment

First of all, I would like to express my sincere gratitude to my supervisors, Dr. Richard Collier and Dr. Nigel Mountney for their continual supervision, constructive criticism, and encouragement during the period of this study. Without their guidance and persistent help, this thesis would not have been possible.

I would like to thank the Ministry of Higher Education and Scientific Research of the Kurdistan Regional Government (KRG) for funding this study. In addition, I wish to thank Professor Dr. Salahaddin Saeed Ali, president of the University of Sulaimani, and Assistant Professor Dr. Dyary Ali, head of the Department of Geology at the University of Sulaimani, for their guidance. I acknowledge with gratitude the aid and support I received from all the academic staffs at the Department of Geology, Sulaimani University.

I am grateful to the entire academic and technical staffs of Earth and Environment School, University of Leeds for their help and guidance throughout my study, in particular Fiona Gill, Crispin Little, Ivan Savov, Harri Wyn Williams, Linda Forbes, and Lesley Neve.

I am grateful to Professor Kamal Haji Karim for his scientific assistance and counseling during fieldworks in Kurdistan Region. As well as, I would like to thank Mr. Soran Othman for his assistance during fieldworks.

I would like to thank Dr. Wyn Hughes and Professor Maurice Tucker for their scientific assistance.

I wish to express my deeply appreciation to my friends, Dr. Fraidoon Rashid and Dr. Devan Hussein for their continual accompaniment and fillip. In addition, I would like to thank my friends Zida Karim and Araz Sabir, for their inspirations and supports, as well as Baban Yousef, Shelan Hussein, and Nawzad Aziz.

Finally, I would like to express the deepest appreciation to my family for their patience and support, especially my father, Ghareeb Abdullah, and my husband, Dyary Hiewa.

Conference Abstracts

Abdullah, H., Collier, R.E.L., and Mountney, N.P., 2013. Carbonate-evaporite cyclicity in the Middle Miocene Fatha Formation of the Mesopotamian Basin, Kurdistan, NE Iraq. The 52nd British Sedimentological Research Group Annual General Meeting, University of Hull.

Abdullah, H., Collier, R.E.L., and Mountney, N.P., 2015. Variations in carbonate-evaporite ramp facies trends: Middle Miocene Fatha Formation, Kurdistan. The 15th Bathurst Meeting of Carbonate Sedimentologists, University of Edinburgh.

List of Content

Declaration	ii
Abstract	iii
Acknowledgment	vi
Conference Abstracts	vii
List of Content	viii
List of Figures	xiv
List of Tables.....	xx
Chapter One	1
1 Introduction.....	1
1.1 Background	1
1.2 Aims and objectives of the study	4
1.3 Thesis structure.....	6
Chapter Two.....	9
2. Geological Settings	9
2.1 Introduction	9
2.2 Tectonics of the area.....	12
2.3 The Zagros foreland basin during the Cenozoic.....	14
2.4 Palaeogeography of Miocene	14
2.5 Regional Correlation	18
2.6 Palaeoclimate.....	19
2.7 Study areas	19
2.8 Data collection.....	21
2.9 The stratigraphy of the studied areas.....	24
2.9.1 Late Eocene Pila Spi Formation.....	27
2.9.2 Oligocene formations	28

2.9.3	Basal Fars Conglomerate	28
2.9.4	Euphrates Formation	28
2.9.5	Dhiban Formation	29
2.9.6	Jeribe Formation.....	31
2.9.7	Fatha Formation	31
2.9.8	Injana Formation	35
Chapter Three.....		36
3. Variations in carbonate-evaporite ramp facies trends: Late Burdigalian Fatha Formation, Kurdistan		36
3.1	Introduction	36
3.2	Methods	39
3.3	Divisions of the Fatha Formation	40
3.3.1	The lower evaporite-dominated part	40
3.3.2	The upper clastic-dominated unit.....	40
3.4	Sedimentary facies	43
3.4.1	Calcareous mudstone facies (CM)	43
3.4.2	Carbonate microfacies.....	46
3.4.3	Evaporite facies	72
3.4.4	Red clastic facies (RC).....	75
3.5	Fatha Formation cyclicity.....	76
3.6	Variations in carbonate-evaporite ramp models.....	80
3.7	Discussion	82
3.8	Conclusion.....	86
Chapter Four		120

4.	Sequence Stratigraphy of the Fatha Formation.....	120
4.1	Introduction	120
4.2	Methods	122
4.2.1	Strontium isotope $^{87}\text{Sr}/^{86}\text{Sr}$ method.....	123
4.2.2	Age of the Fatha Formation from strontium isotope dating.....	124
4.3	Review of sequence stratigraphy methods	126
4.3.1	Sequence	126
4.3.2	System Tract.....	127
4.3.3	Parasequences and their bounding surfaces	128
4.4	Sequence stratigraphic model of high-frequency carbonate-evaporite cycles and mechanisms of their origins.....	129
4.5	Review of vertical facies variations within the Fatha Formation.....	132
4.5.1	Vertical facies variations within the calcareous mudstone unit.....	133
4.5.2	Vertical facies variations within the carbonate unit.....	133
4.5.3	Vertical facies variations within evaporite unit	138
4.5.4	Vertical facies variations within red clastic unit.....	138
4.6	High-frequency cycles of the Fatha Formation	138
4.7	Correlation panels and lateral facies changes.....	142
4.8	Types of parasequences	147
4.8.1	Type A.....	147
4.8.2	Type B.....	147
4.8.3	Type C.....	148
4.8.4	Type D.....	148

4.8.5	Type E.....	148
4.8.6	Type F.....	148
4.8.7	Type G.....	149
4.8.8	Type H.....	149
4.9	Parasequences and Fischer plots - methods.....	155
4.9.1	Results of Fischer plot analysis.....	157
4.9.2	Parasequence sets.....	167
4.9.3	Distributions of the parasequences on the Fischer plots.....	169
4.10	Sequence boundaries.....	173
4.10.1	The lower boundary.....	173
4.10.2	The upper boundary.....	175
4.10.3	The upper boundary of Injana Formation.....	175
4.11	Mechanisms controlling the Miocene high-frequency parasequences.....	176
4.11.1	Glacio-eustasy and orbital forcing.....	177
4.11.2	Tectonics.....	182
4.11.3	Sedimentary process.....	184
4.12	Conclusion.....	186
	Chapter Five.....	189
5.	Comparison of carbonate-evaporite cyclical successions of the Zechstein, Paradox and Zagros Basins.....	189
5.1	Introduction.....	189
5.2	Zechstein Basin.....	190
5.2.1	Tectonic development of the Zechstein Basin.....	192

5.2.2	Permian climate in Central Europe	193
5.2.3	Zechstein stratigraphy	195
5.2.4	Zechstein cycles	196
5.2.5	Sequence stratigraphy of the Zechstein cycles.....	202
5.2.6	Origin of cyclicity	206
5.3	Paradox Basin.....	208
5.3.1	Development of the Paradox Basin.....	210
5.3.2	Palaeo-tectonic setting	210
5.3.3	Stratigraphy	212
5.3.4	Palaeoclimate	216
5.3.5	Paradox cyclicity	219
5.3.6	Sequence stratigraphy of the Paradox succession.....	223
5.3.7	Origin of cyclicity	225
5.4	Comparison between basin types and their evolution	226
5.4.1	Basin-fill stratigraphy.....	226
5.4.2	Basin configuration	231
5.4.3	Stratigraphy	232
5.4.4	Sedimentary facies	234
5.4.5	Carbonate-evaporite cycles	237
5.4.6	Palaeoclimate	238
5.4.7	Mechanisms controlling cyclicity	239
5.5	Conclusions	242

Chapter Six.....	244
6. General Discussion	244
Chapter Seven	255
7. Conclusions.....	255
References	260
Appendices.....	278
Appendix 1 - Stratigraphic logs of the study areas.....	279
Appendix 2 - Tables of number, thickness, cumulative thickness, and cumulative departure of the cycles.....	289

List of Figures

Figure 1-1 Map showing the distribution of major evaporite basins, including the Miocene, Paradox, and Zechstein evaporite basins (Kendall, 1992).	4
Figure 2-1 Tectonic developments and megasequences of the Arabian Plate (Sharland <i>et al.</i> , 2001).	11
Figure 2-2 Structural elements of Iraq (Aqrawi <i>et al.</i> , 2010).	13
Figure 2-3 Palaeofacies map of the Miocene spanning deposition of the Jeribe, Fatha and Injana formations from Iraq and their time equivalents, the Gachsaran, Mishan and Agha Jari Formations in Iran (Ziegler, 2001).	15
Figure 2-4 Palaeogeographic map and palaeofacies distributions of the Middle Miocene Fatha Formation (Goff <i>et al.</i> , 1995). Two main depocentres were developed in Iraq, including Sinjar sub-basin that extended to Syria and Zagros sub-basin that extended to Iran where Gachsaran Formation was deposited.	17
Figure 2-5 Location and geological map of the study area in Kurdistan, Sulaimani Government, NE Iraq. The Fatha Formation and the studied outcrop sections are illustrated.	23
Figure 2-6 Chronostratigraphic column for NE Iraq during the Tertiary (van Bellen <i>et al.</i> , 1959).	25
Figure 2-7 Chronostratigraphic column of north eastern Iraq from the Eocene to Recent (Karim, 2010).	26
Figure 2-8 Field photographs of the Early Miocene Euphrates and Jeribe formations.	30
Figure 3-1 Field photographs of the Fatha cycles of the lower evaporite (A) and upper clastic-dominated (B) units from Basara and Sangaw sections, respectively.	42
Figure 3-2 A column diagram showing percentages of the extracted fossils from the calcareous mudstone unit from the Mamlaha section. B: bryozoas, O: ostracods and R: rotaliids. The samples are stratigraphically ordered. The percentage of rotaliids is relatively high at the lower part of the succession. However, it becomes low toward the upper part where bryozoan, oyster and bivalve are high.	46
Figure 3-3 Variations of the carbonate-evaporite cycles of the Fatha Formation from the lower to upper parts of the succession. The cycles, as well as the marine deposits, become thinner toward upper part, and the evaporite deposits are ceasing.	77
Figure 3-4 Two dimensional pie diagrams showing the percentages of the sedimentary facies, which are making the cycles from all the studied sections. The percentages of evaporite deposits are increasing toward the basin centre. In contrast, the percentages of clastic deposits are decreasing. Ma: Mamlaha; Ba: Basara; Ta: Takiya; Aj: Azh-Dagh; Sa: Sangaw; Da: Darbandikhan Dam; Kr: Krbchna; Kf: Kfri and Ch: Chnarah sections.	78
Figure 3-5 Bar diagrams between cycle numbers and thickness of the cycles from all the studied sections; Ma: Mamlaha; Ba: Basara; Ta: Takiya; Aj: Azh-Dagh; Sa: Sangaw; Da: Darbandikhan Dam; Kr: Krbchna; Kf: Kfri and Ch: Chnarah sections.	79

Figure 3-6 The depositional model of the Fatha Formation showing different depositional environments on a gently ramp platform. The model is presenting the progradation and migration of the Miocene shoreline along three vertical sections A, B, and C. In addition, D and E block diagrams are maximized to show detailed depositional settings of two cycles and to represent the lateral variation possible within these.	85
Figure 3-7 Scanning electron photomicrographs of the rotaliids foraminifera from the calcareous mudstone units of the Fatha Formation.	87
Figure 3-8 Scanning electron photomicrographs of the ostracod specimens from calcareous mudstone units of the Fatha Formation.	88
Figure 3-9 Scanning electron photomicrographs of extracted microfossils from the calcareous mudstone units of the Fatha Formation.	89
Figure 3-10 Thin section photomicrographs of calcareous mudstone unit (CM)	91
Figure 3-11 Field photographs and thin section photomicrograph of a thin cycle at the upper part of the succession.	92
Figure 3-12 Thin section photomicrographs of carbonate mudstone microfacies (SK1).	94
Figure 3-13 Thin section photomicrographs of carbonate microfacies.	96
Figure 3-14 Field samples with their representatives thin section photomicrographs of carbonate microfacies.	98
Figure 3-15 Thin section photomicrographs of non-skeletal microfacies (NS1-NS2).	100
Figure 3-16 Thin section photomicrographs of non-skeletal microfacies (NS2-NS5).	102
Figure 3-17 Field photographs of non-skeletal microfacies (NS4-NS5)	104
Figure 3-18 Thin section photomicrographs of non-skeletal microfacies (NS5-NS7).	106
Figure 3-19 Thin section and field photographs of algal bindstone and dolo-mudstone microfacies (AG1 & D1).	107
Figure 3-20 Field and thin section photographs of stromatolite microfacies (AG2). ...	109
Figure 3-21 Thin section photomicrographs of sandy carbonate microfacies (S1).	111
Figure 3-22 Field and thin section photographs of evaporites (NE & LE).	113
Figure 3-23 Field photographs of laminated evaporites (LE).	115
Figure 3-24 Field photographs of red clastic unit (RC).	117
Figure 3-25 Field photographs of siliciclastic sandstone (RC).	119
Figure 4-1 Comparison of Miocene strontium-isotope ratios (Sr^{87}/Sr^{86}) from the Fatha Formation (blue rectangles) with the Lowess 5 Miocene strontium-isotope ratio Sr^{87}/Sr^{86} curve (red line). The value of Miocene sea water Sr^{87}/Sr^{86} has increased through time and the Sr^{87}/Sr^{86} values of the Miocene Fatha Formation have matched the curve.	125
Figure 4-2 A general sequence stratigraphy model, including type-1 sequence boundary, systems tracts, and parasequences. LST: Lowstand System Tract, TST:	

Transgressive System Tract, and HST: Highstand System Tract (Van Wagoner, 1995).	128
Figure 4-3 Tidal flat progradational model on a carbonate ramp. Each cycle terminates with a disconformity surface (heavy line) and is capped by tidal flat deposits. Subtidal deposits onlap the disconformity surface toward the margin, and then tidal flat deposits start to prograde toward the basin and continue to extend completely across the platform (Read <i>et al.</i> , 1991).	132
Figure 4-4 A representative schematic log of vertical facies variations of a high-frequency shallowing-upward cycle of the Fatha Formation. The facies variations form a high-frequency shallowing-upward package that is repeated throughout the succession.	140
Figure 4-5 Lithostratigraphic correlation of the shallowing-upward parasequences from basin margin to basin centre in the lower and upper part of the succession. The evaporite thickens toward the basin centre (Al-Juboury and McCann, 2008) and the fluvial unit progrades toward the basin.	141
Figure 4-6 Lateral and vertical correlations of the studied cycles along the Qishlagh-Sargrma-Darbandikhan Mountains. The cycles are traceable for tens of kilometres but the microfacies within the individual cycles vary laterally. A higher number of siliciclastic-dominated cycles are recorded along these sections.	145
Figure 4-7 Lateral and vertical correlations of the studied cycles along the Aj Dagh-Qara-Wais anticlines. The cycles are traceable for tens of kilometres but the microfacies within the individual cycles vary laterally. A higher number of evaporite-dominated cycles are recorded in the thicker successions.	146
Figure 4-8 Types of parasequences and their distribution from the lower carbonate-evaporite-dominated part to the upper siliciclastic-dominated part.	149
Figure 4-9 Field photographs of parasequence types in the lower part of the succession.	150
Figure 4-10 Representative logs of the shallowing-upward cycles or parasequences, type of cycles, their thickness ranges and distributions from the lower to upper parts of the succession and from the basin margin to basin centre. Overall, the cycles vary from evaporite-dominated in the lower part to siliciclastic-dominated in the upper part. Basin centre parasequence styles are after (Tucker, 1999).	151
Figure 4-11 Field photographs of cycle (parasequence) types in the upper part of the succession.	152
Figure 4-12 Standard curve of Fischer plot constructed between cumulative departure from mean cycle thickness and cycle number (Sadler <i>et al.</i> , 1993).	157
Figure 4-13 Fischer plot of the carbonate-evaporite cycles of the Fatha Formation from Kfri section. The plots represent the standard Fischer plot as constructed between cumulative departure of mean cycle thickness and cycle number (upper plot), as well as revised Fischer plot as presented between cumulative departure of mean cycle thickness and cycle thickness (lower plot).	158
Figure 4-14 Fischer plot of the carbonate-evaporite cycles of the Fatha Formation from Mamlaha section. The plots represent the standard Fischer plot as constructed between cumulative departure of mean cycle thickness and cycle	

number (upper plot), as well as revised Fischer plot as presented between cumulative departure of mean cycle thickness and cycle thickness (lower plot).	159
Figure 4-15 Fischer plot of the carbonate-evaporite cycles of the Fatha Formation from Aj Dagh section. The plots represent the standard Fischer plot as constructed between cumulative departure of mean cycle thickness and cycle number (upper plot), as well as revised Fischer plot as presented between cumulative departure of mean cycle thickness and cycle thickness (lower plot).....	160
Figure 4-16 Fischer plot of the carbonate-evaporite cycles of the Fatha Formation from Sangaw section. The plots represent the standard Fischer plot as constructed between cumulative departure of mean cycle thickness and cycle number (upper plot), as well as revised Fischer plot as presented between cumulative departure of mean cycle thickness and cycle thickness (lower plot).....	161
Figure 4-17 Fischer plot of the carbonate-evaporite cycles of the Fatha Formation from Basara section. The plots represent the standard Fischer plot as constructed between cumulative departure of mean cycle thickness and cycle number (upper plot), as well as revised Fischer plot as presented between cumulative departure of mean cycle thickness and cycle thickness (lower plot).....	162
Figure 4-18 Fischer plot of the carbonate-evaporite cycles of the Fatha Formation from Takiya section. The plots represent the standard Fischer plot as constructed between cumulative departure of mean cycle thickness and cycle number (upper plot), as well as revised Fischer plot as presented between cumulative departure of mean cycle thickness and cycle thickness (lower plot).....	163
Figure 4-19 Fischer plot of the carbonate-evaporite cycles of the Fatha Formation from Krbchna section. The plots represent the standard Fischer plot as constructed between cumulative departure of mean cycle thickness and cycle number (upper plot), as well as revised Fischer plot as presented between cumulative departure of mean cycle thickness and cycle thickness (lower plot).....	164
Figure 4-20 Fischer plot of the carbonate-evaporite cycles of the Fatha Formation from Darbandikhan section. The plots represent the standard Fischer plot as constructed between cumulative departure of mean cycle thickness and cycle number (upper plot), as well as revised Fischer plot as presented between cumulative departure of mean cycle thickness and cycle thickness (lower plot).	165
Figure 4-21 Fischer plot of the carbonate-evaporite cycles of the Fatha Formation from Chnarah section. The plots represent the standard Fischer plot as constructed between cumulative departure of mean cycle thickness and cycle number (upper plot), as well as revised Fischer plot as presented between cumulative departure of mean cycle thickness and cycle thickness (lower plot).....	166
Figure 4-22 Correlation of the Fischer plots from the studied sections and distributions of parasequences types along the plots. The shape of the plots are nearly similar in all the studied sections. Most of the parasequences at the lower succession are of type-D, whereas type-H is predominate at the upper succession. The dotted blue line is the position of the laminated evaporite.	171
Figure 4-23 Schematic illustration of the distribution of parasequence types on a Fischer plot. Thick carbonate-evaporite parasequences are located in the lower part of the succession with high accommodation space creation; however, the parasequences in the upper part of the succession become thinner due to decelerating accommodation space. Furthermore, siliciclastics become abundant and evaporites are missing.	173

Figure 4-24 Lower boundary of the Fatha Formation with the Early Miocene formations (Euphrates, Dhiban and Jeribe). There is an unconformity surface toward the margin that represents a sequence boundary at the Oligocene-Miocene boundary. Both the Early Miocene formations and the Fatha Formation onlap the sequence boundary.	175
Figure 4-25 3 rd order sea-level changes including system tracts during deposition of the Fatha Formation marginal deposits, and variations in cycle types throughout the regressive succession.....	176
Figure 4-26 Eustatic sea-level estimations and global oxygen isotope ratios between 50 Ma and the present. The eustatic sea-level estimations are after Haq <i>et al.</i> , (1987, the green curve), Miller <i>et al.</i> , (2005, the blue curve), Haq and Al-Qahtani (2005, the black curve) and Kominz <i>et al.</i> , (2008, the red curve). The Haq <i>et al.</i> curve estimates higher amplitudes of sea-level variations. In contrast, the other curves of Kominz <i>et al.</i> , and Miller <i>et al.</i> , estimate lower amplitudes. The global oxygen isotope curve is after Zachos <i>et al.</i> (2001), against which Fatha Formation deposition occurred during the mid-Miocene Climatic Optimum (from ca. 18.0 to 15.5 Ma, the purple line).	181
Figure 4-27 Components of orbital forcing of the earth, showing their periodicities and causes.....	182
Figure 4-28 Isopach map of the Fatha (Gachsaran) Formation on the Arabian Plate. The (possibly syn-sedimentary) basement Khanaqin fault (KHF) and Hail Ga'ara lineament (HRA) are shown in the context of the separate Sinjar and Kirkuk salt sub-basins in Iraq (Bahroudi and Koyi, 2004).	183
Figure 4-29 The effects of relative sea-level changes and subsidence on the Fatha cyclicity, based on the Mamlaha section. The subsidence is high at the lower succession, where the thicker cycles were deposited. Whereas, it shows a dramatic decrease in subsidence upward through the upper succession.....	185
Figure 5-1 Late Permian palaeogeography of the Zechstein Sea, including both Northern Zechstein Basin (NZB) and Southern Zechstein basin (SZB). The shallow and deep water areas of sedimentation are also included (Taylor, 1998).....	191
Figure 5-2 Lithostratigraphic diagram of the Zechstein cycles, including five carbonate-evaporite cycles (Z1-Z5). The Upper Claystone Formation overlies the Zechstein cycles unconformably (Van Adrichem Boogaert and Kouwe, 1994). Two thick halite deposits were accumulated during the Z2 and Z3 cycles, and carbonate deposition ceases toward the upper cycles.	195
Figure 5-3 Field photographs of the Zechstein carbonate units in England.	198
Figure 5-4 Field photographs of the Zechstein carbonate units in England.	201
Figure 5-5 Sequence stratigraphy and lithostratigraphy of the English Zechstein group (Tucker, 1991).	203
Figure 5-6 Lithostratigraphic cycles and chronostratigraphic division of the Zechstein cycles in German and sequence stratigraphic comparison of the Zechstein succession in German, England, and Poland.	204
Figure 5-7 Chronostratigraphic division of the Zechstein cycles in Poland showing the four 3 rd -order sequences (PZS1-PZS4) (Wagner and Peryt, 1997).....	206

Figure 5-8 Structural and location map of the Paradox Basin and basement lineaments showing north-western Olympic-Wichita Lineament and north-eastern Colorado Lineament with bounding uplifts (Baars and Stevenson, 1982).	209
Figure 5-9 Structure and stratigraphic cross-section of the Paradox Basin showing the north-eastern evaporitic basin, and the south-western shelf carbonates (Baars and Stevenson, 1982).	213
Figure 5-10 Stratigraphic relationships of the Paradox Basin during Pennsylvanian to Permian times (Wengerd and Matheny, 1958; Baars and Stevenson, 1981). The basin overfilled with the Pennsylvanian carbonate-evaporite cycles, and then the siliciclastics, derived from the Uncompahgre Uplift, prograded south-westward into the basin through time.....	215
Figure 5-11 Carboniferous to Permian eustatic sea-level curve, including long- and short-term sea-level fluctuations, showing eustatic rise in the latest Pennsylvanian, and eustatic falls at the Mississippian-Pennsylvanian boundary and in the latest Permian (Haq and Schutter, 2008). The eustatic fall at the Mississippian-Pennsylvanian boundary was related to the main Gondwana Glaciation. The magnitude of sea-level changes during the Palaeozoic is estimated to have varied from a few tens metres to nearly 125 metres.....	218
Figure 5-12 Stratigraphic logs of an idealized carbonate and evaporitic cycle bounded by disconformities. Each cycle represents a full cycle of sea-level change and salinity variations (Hite and Buckner, 1981; Trudgill and Arbuckle, 2009).....	221
Figure 5-13 Correlation of depositional cycles showing three types of cycles from tectonically-active siliciclastic-dominated through basinal evaporite-dominated cycles to shelf carbonate cycles (Weber <i>et al.</i> , 1995).	222
Figure 5-14 Sequence stratigraphic model for the carbonate-evaporite cycles of the Paradox Basin (Weber <i>et al.</i> , 1995).	224
Figure 5-15 Cross-section through Cataract Canyon showing cycle sets, high-frequency cycles, and tectonic settings of the Pennsylvanian-Permian of the Paradox Basin, as well as the approximate location of the measured logs (Williams, 2009). The red dash-lines represent the cycle-set boundaries, and black dash-lines are cycle boundaries. The basin underwent three tectonic stages of basin-fill, basin-reconfiguration, and basin progradation.	229
Figure 5-16 Stratigraphic logs of the Pennsylvanian-Permian cycles of the Paradox Basin in Utah (Williams, 2009), showing the carbonate-siliciclastic cycles. the dotted red line is the boundary between cycle-sets C and D.....	230
Figure 5-17 Stratigraphic relationships between the Miocene formations showing the final stage of progradation of the Zagros foreland basin and conceptual location of the measured logs from basin margin. Approximate horizontal scale (from basin margin to basin centre): 200km.	233

List of Tables

Table 2-1 Geographical and structural locations of the studied sections.....	21
Table 2-2 Geographical locations, thicknesses and sample numbers of the studied sections.....	22
Table 3-1 Microfacies associations and divisions of the carbonate members.	47
Table 3-2 Descriptions and interpretations of the carbonate microfacies.....	67
Table 4-1 Sr ⁸⁷ /Sr ⁸⁶ ratios and inferred numerical ages of the carbonate and evaporite samples from the Fatha Formation, sampled in Mamlaha section.	124
Table 4-2 Shallowing-upward facies changes within the carbonate microfacies of the Fatha Formation.	136
Table 4-3 Types, characteristics, occurrences of the cycles of the Fatha Formation....	153
Table 4-4 Descriptions and definitions of the high-frequency cycles, cycle-set, and 3 rd -order sequence of the Late Burdigalian Fatha Formation.	169
Table 6-1 Comparison of three carbonate-evaporite basins, including Zagros, Zechstein, and Paradox, in terms of their depositional developments, climates, and tectonics.....	247

Chapter One

Introduction

1.1 Background

Carbonate-evaporite cycles that developed on shallow-dipping ramp margins are important deposits in both the ancient and modern sedimentary records, providing a major record of palaeogeographic, palaeoclimatic and palaeo-environmental change (Tucker, 1991). Also, over 50% of the world's hydrocarbon reserves are found in carbonates, and over 60% of these reservoirs are sealed by evaporite deposits (Kendall *et al.*, 2009). Many hydrocarbon-bearing reservoirs in the world are associated with carbonate-evaporite successions, including in ramp settings, for example the Miocene carbonate-evaporite cycles of the Middle East (Beydoun, 1991; Beydoun *et al.*, 1992), the carbonate-evaporite cycles of the Paradox Basin in the USA (Peterson and Hite, 1969; Weber *et al.*, 1995), the second carbonate cycle of the Zechstein Basin (Late Permian) (Ingo and Lehmann, 2002), and the Cretaceous carbonate-evaporite cycles of the Albian Acatita Formation of NE Mexico (Ingo and Lehmann, 2002). The depositional processes that result in the accumulation of cyclical evaporite-prone sequences are typically more complex than those involved in the deposition and accumulation of carbonate deposits alone. Although numerous important studies have been undertaken to consider the origin of and controls upon the accumulation of mixed carbonate-evaporite successions in both ancient and modern environments, especially on the evaporite elements (Warren and Kendall, 1985; Schreiber *et al.*, 1986; Logan, 1987; Schreiber, 1987; Tucker, 1991; Sarg, 2001; Warren, 2006), each studied example is unique and the number of studied ancient outcrop examples is currently limited. Most evaporite successions represent chemical compositions that record precipitation from a seawater-derived brine (Kinsman, 1969; Warren, 2006). Consequently, most large-scale and long-lived marine evaporite deposits required a water body that was mixed or exchanged with ocean waters but with limited circulation, typically in an arid or semi-arid climatic regime, where evaporation is intensive (Warren and Kendall, 1985; Warren, 2006). Marine-derived evaporites are believed to accumulate subaqueously in shallow marine shelves and enclosed basins (lagoons and salinas), and subaerially in coastal plains (sabkhas) (Nissenbaum, 1980; Warren and Kendall, 1985; Flugel, 2004).

The late Early Miocene cyclical carbonate-evaporite-siliciclastic succession of the Fatha Formation is well-exposed in Kurdistan, northern Iraq. Until recently it has received little attention for political and security reasons. It now offers a chance to re-evaluate the architecture and controls upon this type of sedimentary succession. It should be considered a significant ancient outcrop example, allowing comparison with those systems mentioned above.

Studies have previously been undertaken of carbonate-evaporite cycles to unveil their distribution and architectures in the geologic record, including, as mentioned, the Late Permian Zechstein Basin from Europe (Tucker, 1991; Strohmenger *et al.*, 1996a; Wagner and Peryt, 1997; Becker and Bechstädt, 2006), the Pennsylvanian Paradox Basin from Utah, USA (Goldhammer *et al.*, 1991; Raup and Hite, 1992; Weber *et al.*, 1995), and also the modern Arabian Gulf (Kendall and Skipwith, 1969; Alsharhan *et al.*, 1995) (Figure 1.1). Each of these carbonate-evaporite basins required particular depositional, tectonic, climatic, and eustatic settings. The evaporites of the Pennsylvanian Paradox Basin, for example, were accumulated in a palaeo-tectonic depression (Weber *et al.*, 1995) and convergent tectonic setting (Warren, 2010), whereas the evaporites of the Late Permian Zechstein Basin are an example of basin-centre and slope evaporite deposition (Börner, 2004; Warren, 2006). On the other hand, the modern evaporites of the Arabian Gulf have accumulated in a supratidal sabkha setting at the margins of a shallow-dipping carbonate ramp (Kinsman and Park, 1976).

The Paradox Basin was developed during the Pennsylvanian to Early Permian at a time when the Earth was subject to the effects of major Gondwanan glacial to interglacial cyclicality. The deposition of the thick evaporite succession in the Paradox Basin was coincident with the main Pennsylvanian glaciation when an arid and dry climate was developed across the basin due to its proximity to the palaeo-equator (Baars and Stevenson, 1981). The accumulation of evaporites (anhydrite and salt) in the Paradox Basin is restricted to the basin centre, whereas the carbonates are accumulated at the shelf margin (Hite and Buckner, 1981). The correlation of the evaporite cycles at the basin centre with their lateral carbonate equivalents at the shelf margin has been conducted over the whole basin (Hite and Buckner, 1981). The deposition of the evaporites at the basin centre is coincident with subaerial exposure at the shelf margin that is defined as a sequence boundary type1 (Goldhammer *et al.*, 1991). Twenty-nine complete evaporite cycles are recorded at the basin centre and they have been correlated

to the carbonate equivalent cycles at the shelf margin (Peterson and Hite, 1969; Hite and Buckner, 1981). The deposition of the thick evaporite cycles with their lateral carbonate equivalents in the Pennsylvanian changes upward to carbonate-siliciclastic cycles in the Permian at which time a thick wedge of siliciclastic deposits commenced progradation into the basin from a mountain belt developed at its margins (Gianniny and Miskell-Gerhardt, 2009; Williams, 2009). The Paradox cycles provide a valuable case study because they consist of mixed carbonate-evaporite-siliciclastic cycles throughout the succession and the deposits were accumulated in a foreland basin. Additionally, the depositional architecture reflects the influences of tectonic-uplift, palaeoclimate, and eustatic sea-level changes.

The Zechstein Basin covered a large part of Central Europe and was developed during the Late Permian in an arid and dry climate (Benton *et al.*, 2002). Following the main Gondwanan glacial-interglacial cyclicity of the Early Permian, the climate of Central Europe changed to arid and semi-arid and then more humid conditions through later Permian and Triassic times (Benton *et al.*, 2002). The deposition of evaporites commenced as marginal gypsum wedges during sea-level falls that were laterally equivalent to subaerial exposure at the shelf margin (Tucker, 1991). Then during relative rises in sea-level, carbonates accumulated. Five main cycles are recorded from the basin, Z1-Z5 (Ziegler, 1990). The cycles can be regionally correlated over the whole basin. A thick carbonate and evaporite succession accumulated in the lower cycles (Z1-Z3), whereas in the upper cycles carbonate sedimentation was reduced or ceased due to the climate change from arid to humid (Wagner and Peryt, 1997). The Zechstein cycles are of significance as a case study because they are dominated by extensive carbonate-evaporite cycles which reflect the controls of palaeoclimate and eustatic sea-level changes.

The Miocene carbonate-evaporite cycles of the Fatha Formation accumulated in the Zagros foreland basin of the Kurdistan region, NE Iraq. This formation is composed of a cyclical succession of carbonate, evaporites and siliciclastics. Each cycle typically consists of calcareous mudstone, shallow-marine carbonates, evaporites with chicken-wire fabrics, and fluvial siliciclastic deposits. The nature and thickness of the cycles vary from basin margin to basin centre where a thicker succession and maximum cycle number accumulated. At the basin margin, 17-42 cycles are recorded in successions of 50-300 m thickness, whereas at the basin centre fifty cycles accumulated in a succession about 600 m thick (Tucker, 1999). These carbonate-evaporite cycles accumulated in an

arid and hot climate during the Miocene in this region, but a palaeoclimate which was also characterized by climatic fluctuations (Miller *et al.*, 2005).

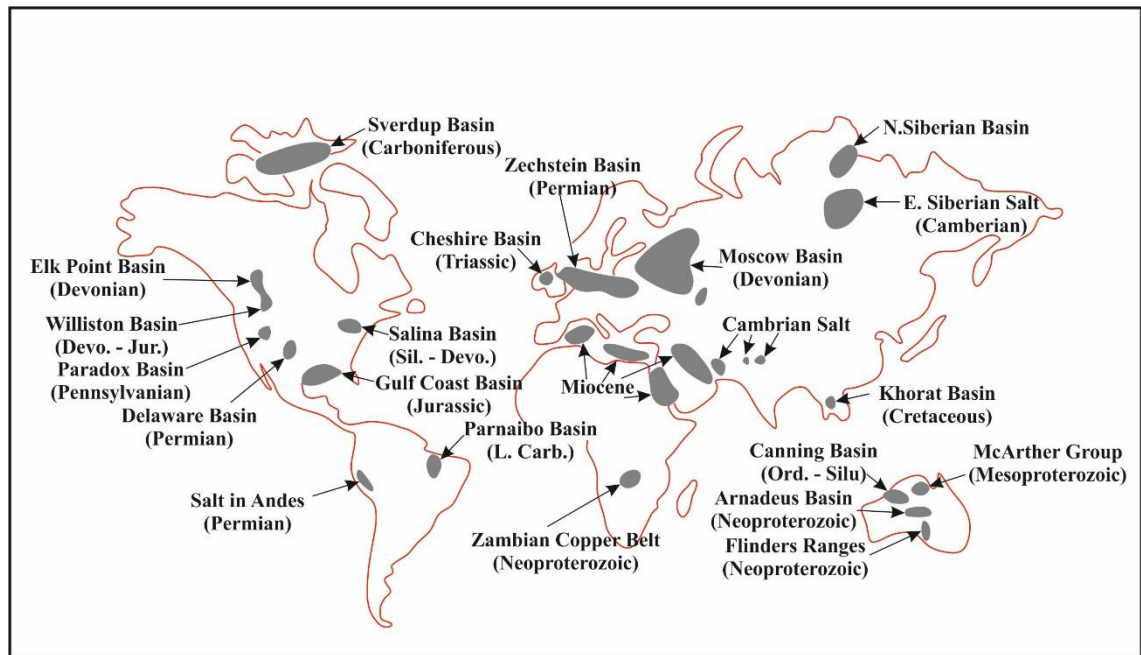


Figure 1-1 Map showing the distribution of major evaporite basins, including the Miocene, Paradox, and Zechstein evaporite basins (Kendall, 1992).

This study focuses primarily on the Miocene carbonate-evaporite cycles from the Fatha Formation at the periphery of the Zagros foreland basin, Kurdistan. The study includes an assessment of palaeodepositional processes and environments, palaeoclimate, sequence stratigraphy, and the accommodation history of the Zagros foreland basin, during the Miocene.

Previous sedimentological and sequence stratigraphical studies of the Fatha Formation are documented in a variety of research papers (Shawkat, 1979; Aqrawi, 1993; Tucker, 1999; Al-Juboury and McCann, 2008). However, no detailed study has previously been conducted to investigate the types and distributions of the cycles, with a detailed analysis regarding the sequence stratigraphic framework for the high-frequency cycles.

1.2 Aims and objectives of the study

The main aim of this thesis is to characterize the sedimentology and depositional architecture of carbonate-evaporite cyclical successions, as deposited in ramp settings. Variations in architecture will be explored in terms of the regional (tectonic) and global (glacio-eustatic and palaeoclimatic) controls that may have led to such variants.

The main element of this study is an investigation of the Fatha Formation in Kurdistan, predominantly composed of cycles of carbonate and evaporites (Aqrawi *et al.*, 2010). The project aims in relation to the formation are to interpret its sedimentology, in particular in the more proximal basin margin settings, and to establish the relationship between the carbonate and evaporite elements. The study also set out to develop a sequence stratigraphic model for the studied succession, providing a framework within which to explain their origin of Fatha Formation depositional cyclicities in terms of relative sea-level changes. The extensive exposure of these cycles (17-42) in Kurdistan makes this area an ideal study locale for characterizing the palaeoenvironments and their cyclical variation in a restricted basin during a period of known glacio-eustatic fluctuations.

Recently, after discoveries of oil and gas reserves in Kurdistan, including in Cenozoic reservoirs, the Early-Middle Miocene succession has been a target for study and a significant focus of attention. This study is therefore topical, given its focus on the outcrops of the Miocene Fatha Formation around Sulaimani Governorate and its presentation of Miocene lithostratigraphic and chronostratigraphic columns, depositional environments, and sequence stratigraphic architecture.

In addition to the focus on the Fatha Formation, this study aims to analyse and compare different carbonate-evaporite basins from the geologic record, in terms of their depositional context and development. Through analysis of the carbonate-evaporite cycles of the Paradox and Zechstein basins and comparison with the Fatha Formation, the aim is to establish general characteristics of cyclical carbonate-evaporite successions in ramp settings, and what are the variations in such depositional architectures and the explanations for any observed variations.

Given the aims outlined above, the following list provides a summary of project objectives:

1. Determine sedimentary facies of the Fatha Formation, sedimentary facies associations, lateral/vertical variations, microfacies and related sedimentary structures to reconstruct the depositional history and present a depositional model for the formation.
2. Present lithostratigraphic and chronostratigraphic columns of the Fatha Formation from the basin margin, as well as to evaluate thickness and facies variations from

proximal to basin centre locations, so characterizing lateral and vertical facies changes

3. Determine the platform configuration and geometry of the basin, by studying facies changes and compositions throughout the succession, contributing to a general depositional model of the basin
4. Determine the sequence stratigraphic division of the Fatha Formation, identifying the sequence boundaries, sequences, systems tracts, and parasequences.
5. Establish the stratigraphic architecture across the NE margin of the Zagros foreland basin. This will provide the framework for consideration of the eustatic and/or tectonic and sediment supply controls upon sequence development in the late stages of Neo-Tethys closure.
6. Determine the age of the formation and estimate the cycles' durations, by using the strontium isotope relative dating method.
7. Explore the use of Fischer plots in the evaluation of the major controls on the Fatha cyclicities and factors affecting deposition.
8. Carry out a literature-based comparative analysis of other examples of basins with a substantial record of carbonate-evaporitic cyclical sedimentation, with a focus on the depositional architectures and settings of the Paradox and Zechstein Basins.
9. Compare the Miocene carbonate-evaporite cycles of the Fatha Formation with the Paradox and Zechstein cycles in terms of depositional architectures, and the tectonic, palaeoclimatic, glacio-eustatic or other mechanisms that have determined their cyclical character. Then to propose a generalised model to account for the effects of various controls on the accumulation of mixed carbonate, evaporite, and siliciclastic successions.

1.3 Thesis structure

This PhD studentship is financially supported by the Ministry of Higher Education and Scientific Research of Kurdistan Regional Government (KRG). The fieldwork was conducted in Kurdistan Region, NE Iraq. Thin sections and strontium isotope analysis were conducted within the Earth and Environment School, University of Leeds, UK.

There are four principal topics in this thesis: (1) analysis of sedimentary lithofacies to enable the development of a depositional model for the carbonate-evaporite cycles of

the Fatha Formation in Kurdistan Region. (2) Analysis of a series of high-frequency cycles for the purpose of development of a sequence stratigraphic framework that can be used to define and evaluate the mechanisms responsible for cycle development. (3) Analysis of high-frequency carbonate-evaporite cycles of the Pennsylvanian-Permian of the Paradox and Zechstein basins for the purpose of comparison with cycles of the Fatha Formation to present a generalized model for mixed carbonate-evaporite-clastic cycles. (4) Finally, estimating these mechanisms that control cyclic-successions and generate high-frequency cycles.

This thesis is composed of seven chapters. This introductory chapter discusses the aims and objectives behind this PhD thesis. The organization of the remainder of the thesis outlined below.

- **Chapter 2:** This chapter discusses, in detail, the geological setting of the Zagros foreland Basin, including structure, tectonic, stratigraphy, palaeogeography, palaeoclimate, and regional correlation. As well as it introduces the study areas, and summarizes the previous research undertaken in the region.
- **Chapter 3:** This chapter discusses the sedimentary lithofacies types, their arrangement and the distribution of the Miocene carbonate-evaporite cycles of the Fatha Formation in Kurdistan Region. Additionally, it considers carbonate microfacies in detail, as well as fossil contents of the Fatha Formation. In addition, lateral and vertical facies changes of the cycles in the basin margin have been discussed. Moreover, depositional environments have been determined and a depositional model has been developed. The contents and results of this chapter have been prepared for publication in the journal 'Sedimentary Geology', (Abdullah, H., Collier, R.E.LI., and Mountney, N.P. 'Variations in carbonate-evaporite ramp facies trends: Late Burdigalian Fatha Formation, Kurdistan').

Chapter 4: In this chapter the high-frequency cycles of the Fatha Formation have been analysed to propose a sequence stratigraphic framework. Types of cycles and their spatial distributions have been described. In addition, lateral and vertical changes in cycle stacking patterns have been described and discussed. Determination of lateral extent and correlation of the cycles has been undertaken based on the presence of several marker beds. The significance of Fischer plots, cycle-sets, and systems tracts have been discussed. Lastly, the mechanisms responsible for the generation of the cycles have been evaluated. The contents and results of this chapter have been prepared

for publication in the journal 'Sedimentary Geology', (Abdullah, H., Collier, R.E.LI., and Mountney, N.P. 'Third-order accommodation space, parasequence stacking patterns, and mechanisms controlling shallowing-upward cycles: The Miocene shallowing-upward cycles, Fatha Formation, Kurdistan Region/NE Iraq').

- **Chapter 5:** In this chapter the carbonate-evaporite cycles of the Pennsylvanian-Permian of the Paradox and Zechstein basins have been reviewed and discussed in terms of their developments, palaeotectonics, palaeoclimates, stratigraphy, sequence stratigraphy, and cycle analysis. Additionally, the mechanisms that have controlled the cyclicities developed in each of these basins have been discussed. The cyclical arrangement of assemblages of lithofacies of each of these basins has been compared to that of the Fatha cycles.
- **Chapter 6:** This chapter discusses the main outcomes of this thesis. As well as, it evaluates the main controls on the architectures of the basins. In addition, limitations and difficulties of this study are discussed and a number of recommendations for future research is presented.
- **Chapter 7:** This chapter summarizes the main conclusions of this study.
- **Appendices:** In Appendix 1, nine stratigraphic logs of the Fatha Formation have been presented, including sample locations, lithology, microfacies, water depth, shallowing-upward cycles, and type of cycles. In Appendix 2, nine tables have been presented in which cycle numbers, cycle thicknesses, cumulative thicknesses, and cumulative departures of the cycles have been shown.

Chapter Two

Geological Settings

2.1 Introduction

The location of Kurdistan in North East Iraq, at the north-eastern margin of the Arabian Plate, as well as adjacent to the Zagros Mountains, means that it has been affected by tectonics throughout much of its geological development. Therefore, regional tectonic changes associated with movement of the Arabian Plate and local changes in Iraq as well, have each affected the stratigraphy and tectonic evolution of Kurdistan.

The most widely used regional tectonostratigraphic and sequence stratigraphic divisions of the accumulated successions on the Arabian Plate are those of Sharland *et al.* (2001) in which eleven tectonic megasequences (AP1-AP11) are documented (Figure 2.1).

During mid-Permian to Early Jurassic times (Tectonic Megasequence AP6) the Arabian Plate started to separate from the Sanandaj-Sirjan, central Iran and Afghan plates. As a result, the Neo-Tethys Ocean was developed and started to expand and subsidence of its passive margins continued through the Cretaceous (Sharland *et al.*, 2001).

During the Early-Late Jurassic (AP7), the Mediterranean Basin opened due to the separation of the Turkish plate as part of the expansion of the Neo-Tethys Ocean (Jassim and Goff, 2006; Aqrabi *et al.*, 2010). In the Late Jurassic to Late Cretaceous (AP8), the Indian Plate separated from the Arabian Plate and the Indian Ocean began to form. In the next megasequence (Late Cretaceous to late Paleogene, AP9), the Arabian Plate was affected by compression, which occurred as a result of opening of the Atlantic Ocean. At this stage, ophiolite was locally obducted across the north eastern margin of the plate. In the next megasequence (Early Paleogene to Latest Eocene, AP10), compression continued and the Neo-Tethys Ocean started to close due to Arabian Plate movement, and as a result subduction occurred between the Arabian and Iranian plates. Initiation of Red Sea rifting occurred in the Oligocene (Sharland *et al.*, 2001; Ziegler, 2001; Sharland *et al.*, 2004).

The last tectonic megasequence (Late Eocene to the Present, AP11) included the period when the Red Sea and Gulf of Aden opened and evolved from continental to oceanic extension. In addition, the Neo-Tethys Ocean closed during the Oligocene to Early Miocene as a result of collision that occurred between the Arabian and Eurasian plates (Sharland *et al.*, 2001). Due to the separation of the Arabian Plate from the African Plate and the opening of the Red Sea in the late Oligocene (Haq and Al-Qahtani, 2005), the Arabian Plate underwent tilting to the northeast (Sharland *et al.*, 2001; Ziegler, 2001; Sharland *et al.*, 2004).

The Miocene Fatha Formation is included within the last tectonic megasequence (Late Eocene to the Present, AP11) that is bounded by a Late Eocene regional unconformity surface at the base (Ziegler, 2001). This unconformity surface is identified in the studied areas at the top of the Late Eocene Pila Spi Formation. The deposition of the Miocene succession in the Kurdistan Region thus occurred in a position that could be influenced by the tectonic setting of the Arabian Plate, as well as the opening of the Red Sea and Gulf of Aden (Beydoun, 1991; Beydoun *et al.*, 1992; Sharland *et al.*, 2001; Ziegler, 2001). This possibility will be assessed in later chapters.

Geological time scale		Tectonic development	Tectonic megasequences		
Period / Epoch					
Pleistogene	Holocene	<p>Final closure of Neo-Tethys-Zagros folding and thrusting</p> <p>Red Sea rifting</p> <p>Yemen (Aden) Volcanics</p>	Ap11		
	Pleistocene				
Neogene	Pliocene				
	Miocene				
Paleogene	Eocene			<p>Cessation of ophiolite obduction</p> <p>Rapid subsidence</p>	Ap10
	Oligocene				
	Paleocene				
Cretaceous				<p>Ophiolite obduction and foredeeps on northeast margin, localized uplifts</p>	Ap9
				<p>Passive margins on northwest, northeast and southeast margins of Arabian Plate</p>	Ap8
Jurassic				<p>Yemen rifts, Indian Ocean rifting, Intra-shelf basins</p>	Ap7
				<p>Onset of Mediterranean rifting</p>	AP6
Triassic	<p>Back-arc rifting (north Arabia)</p>				
Permian	<p>Neo-Tethys opening- passive margin subsidence</p>				

Figure 2-1 Tectonic developments and megasequences of the Arabian Plate (Sharland *et al.*, 2001).

2.2 Tectonics of the area

Tectonically, Iraq has been divided into three main tectonic zones: the Stable Shelf, the Unstable Shelf and the geosynclinal areas (Buday, 1980). Subsequently, a new tectonic division was proposed for Iraq and seven tectonic zones were identified by (Numan, 1997). The seven tectonic zones were the Rutba-Jazira Zone, the Salman Zone, the Mesopotamian sagged basin, the suspended basin, the highly folded zones of the foreland basin, the imbrication zone of the foreland basin, and the subduction zones, from SW to NE direction. More recently, the tectonic divisions of Iraq were modified to distinguish three main zones, which have been termed the Stable Shelf, the Unstable Shelf and the Zagros Suture Zone (Jassim and Goff, 2006). The Stable Shelf covers most of the south and west of Iraq and extends towards Syria and Jordan to the west and Kuwait and Saudi Arabia to the south. The Unstable Shelf is characterized by surface folds parallel to the Zagros-Taurus belt and is subdivided into the Foothill Zone (also called the Low Folded Zone), the High Folded Zone and the Imbricated Zone. The Imbricated Zone includes both the Balambo-Tanjero and Northern (Ora) Thrust Zones, whereas the Zagros Suture Zone is subdivided into the Qulqula-Khuwakurk, Penjween-Walash and Shalair Zones (Jassim and Goff, 2006). Recently in 2010, all the previous divisions were compiled and five main tectonic elements were recognized. These tectonic elements are the Thrust Zone, the Folded Zone (the High and Low Folded zones), the Mesopotamian Zone, the Salman Zone and the Rutbah-Jezira Zone (Aqrabi *et al.*, 2010) (Figure 2.2). The Low Folded Zone is characterized by wide and low anticlines and wide synclines with Neogene sediments preserved in their cores. However, narrow deep synclines and high amplitude anticlines are the main characteristics of the High Folded Zone, which covers most of the Iraqi Kurdistan Region. Aqrabi *et al.*, (2010) terminology is used throughout the thesis.

Tectonically, the studied area, which lies in the south and south-east of the Kurdistan region, is mostly located in Low Folded Zone plus parts of the High Folded zone.

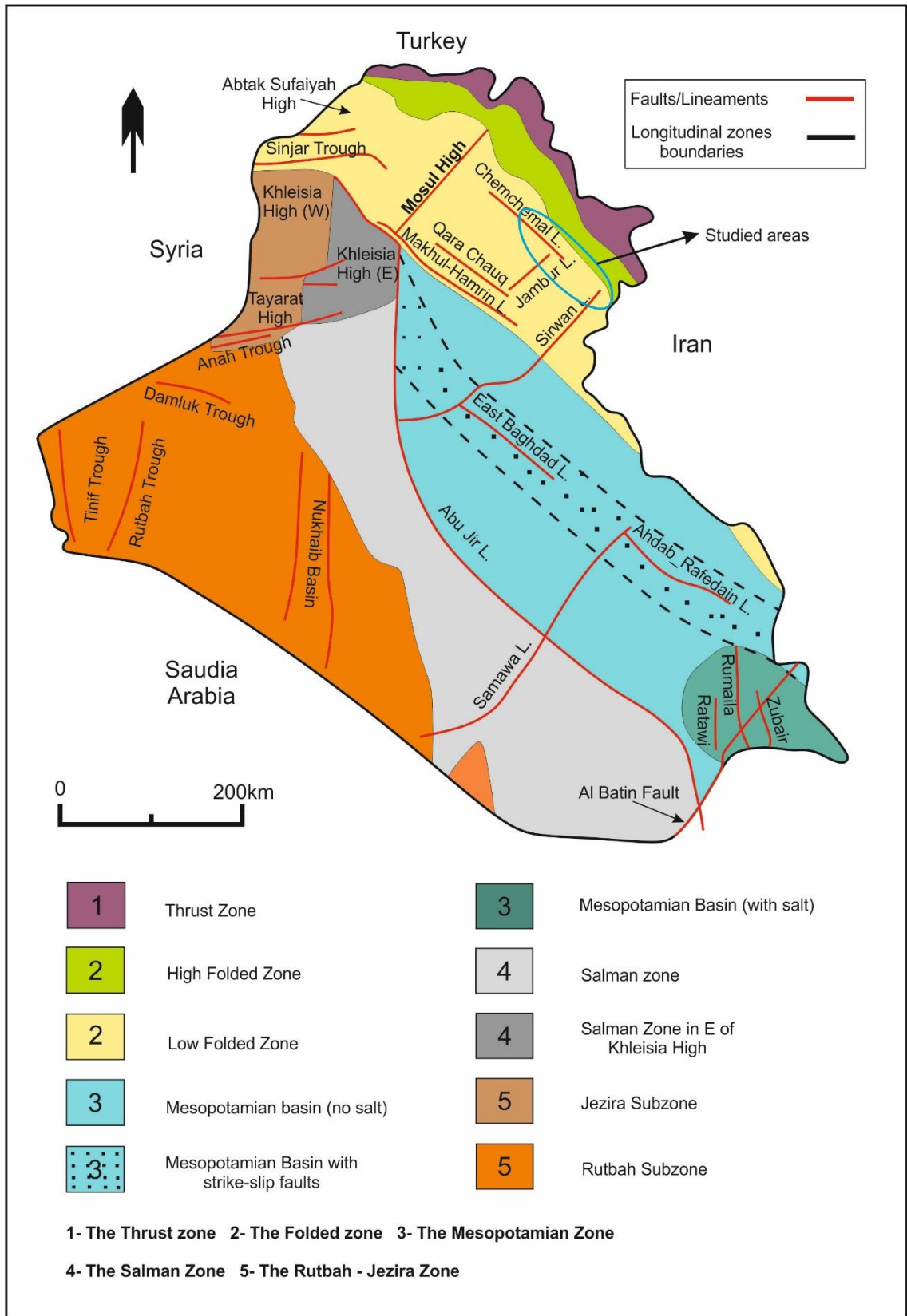


Figure 2-2 Structural elements of Iraq (Aqrabi *et al.*, 2010).

2.3 The Zagros foreland basin during the Cenozoic

The Zagros foreland basin includes the succession deposited since Zagros collision (Upper Eocene to Holocene). The basin is ~1800 km in length and 250 to 300 km in width (Beydoun *et al.*, 1992). It is known that a 7 to 14 km thickness of sediments accumulated along the NE margin of the Arabian Plate (Bahroudi and Koyi, 2004). The basin occupies much of Iraq along a NW-SE trend and extends into NE Syria and SW Iran. During the Miocene, the basin was split into six discrete sub-basins (Bahroudi and Koyi, 2004) and these were separated by palaeo-highs (Figure 2.4). Of these, the Sinjar and Kirkuk sub-basins were located in Iraq and were separated by the Mosul high (van Bellen *et al.*, 1959; Ziegler, 2001; Bahroudi and Koyi, 2004).

The Zagros foreland basin includes numerous supergiant oil and gas fields in high-amplitude structures generated by the Neogene convergence. The basin has been a key focal point for a number of evaporite and hydrocarbon studies, mainly due to its stratigraphic position and tendency to create seals above the much explored hydrocarbon reservoirs (Beydoun, 1991; Beydoun *et al.*, 1992; Aqrawi, 1993).

The development of the foreland basin resulted from the collision of the Arabian and Eurasia continental plates. The oceanic crust of the Arabian Plate was subducted under the Eurasian Plate during the Late Cretaceous and then the continent-continent collision occurred from the Late Eocene to the present day (Ziegler, 2001). As a result, the Zagros mountain range and the Zagros foreland basin were developed, with additional stresses from the opening of the Red Sea and Gulf of Aden (extension to the south-west) (Beydoun *et al.*, 1992; Sharland *et al.*, 2001).

2.4 Palaeogeography of Miocene

The Miocene period spanned deposition of the Euphrates, Jeribe, Fatha (Iraq), Gachsaran, Agha Jari (Iran), and Dam, Hofuf, and Hadruk (Saudi Arabia) formations, with massive evaporite and salt deposits (Figure 2.3). These deposits were accumulated within the Zagros foredeep and foreland that developed as a result of the strong compression between the Arabia and Eurasia (Ziegler, 2001) (Figure 2.3).

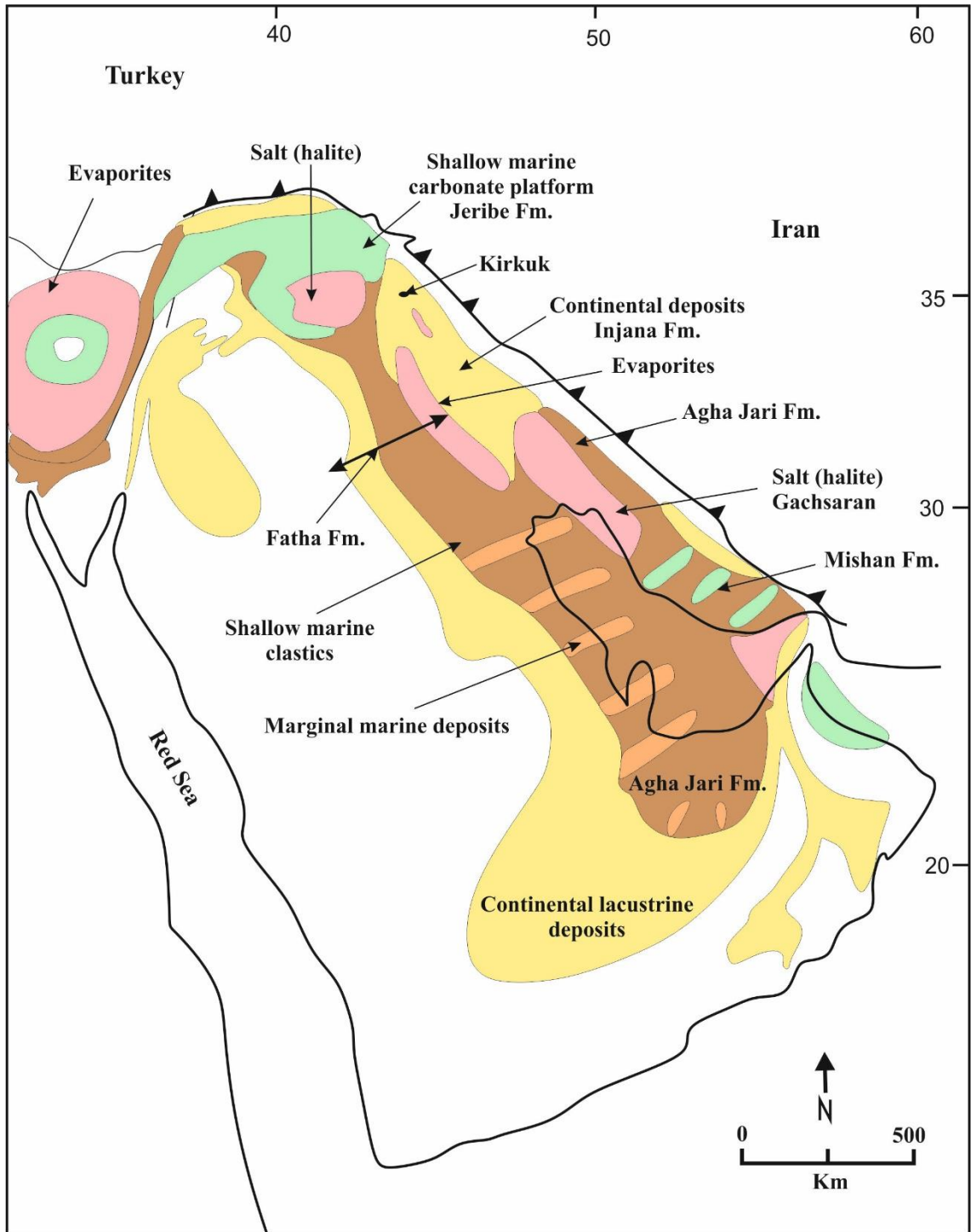


Figure 2-3 Palaeofacies map of the Miocene spanning deposition of the Jeribe, Fatha and Injana formations from Iraq and their time equivalents, the Gachsaran, Mishan and Agha Jari Formations in Iran (Ziegler, 2001).

Due to tectonic movements along the Zagros margin at the end of the Oligocene, the basin system became restricted that resulted in the deposition of the Basal Anhydrite. This is the first indicator of total desiccation of the Miocene basin (Aqrabi *et al.*, 2010). Along the northeastern part of the Zagros foreland basin, clastics and evaporites of the Fatha Formation (western part) and Gachsaran salt Formation (Iran) were deposited

(Sharland *et al.*, 2001; Ziegler, 2001; Aqrawi *et al.*, 2010). Around the Arabian Arch, continental to transitional-marine deposits of Hardukh and Dam formations, as well as lacustrine deposits of the Hofuf Formation, were accumulated. Large amount of conglomerate was incorporated into the Hofuf Formation as a result of uplift of the western part of the Arabian shield (Ziegler, 2001). A shallow sea with carbonate deposition covered the Gulf of Aden, and the Red Sea was periodically restricted that caused to the evaporite deposition during the Middle Miocene. Whereas, the Early Miocene deposits in the southern Red Sea is characterized by a deep-marine clastic unit rich with planktonic foraminifera (Ziegler, 2001). The Late Miocene sediments are characterized by transitional, shallow-marine unit with sabkha deposits.

In Iraq, the first restriction of the Miocene basin is marked by the deposition of the Basal Anhydrite that overlies Ibrahim Formation (Oligocene) and underlies the Serikagni Formation. The deposition of the anhydrite was restricted in the centre of the Mesopotamian and Sinjar sub-basins (Aqrawi *et al.*, 2010). The Serikagni Formation is calcareous and marly sediments that were deposited in the deeper parts of the basin and bordered by the shelf carbonate of the Euphrates Formation. These facies passed toward the end of the Lower Miocene into lagoonal evaporites of the Dhiban Formation (Buday, 1980). The distribution of the Dhiban Formation is similar to the distribution of the Basal Anhydrite in the basin centre (Al-Juboury *et al.*, 2007; Aqrawi *et al.*, 2010). A new transgression is marked by the deposition of the carbonate and evaporite deposits of the Jeribe Formation that has the same distribution of the previous carbonate deposits of the Euphrates Formation (Aqrawi *et al.*, 2010).

The deposition of the Middle Miocene deposits occurred during the Zagros orogeny. Evaporites and siliciclastics of the Fatha Formation were accumulated during the early stage of regional compression, whereas the overlying siliciclastics of the Injana and Mukdadiya formations were deposited during the convergent and suturing (Ziegler, 2001; Aqrawi *et al.*, 2010). The evaporite facies of the Fatha Formation is restricted in two depocentres (Zagros and Sinjar) in Iraq as shown in Figure (2.4). the evaporites are restricted in the basin centre and they bordered by carbonate and mudstone toward the margin (Goff *et al.*, 1995).

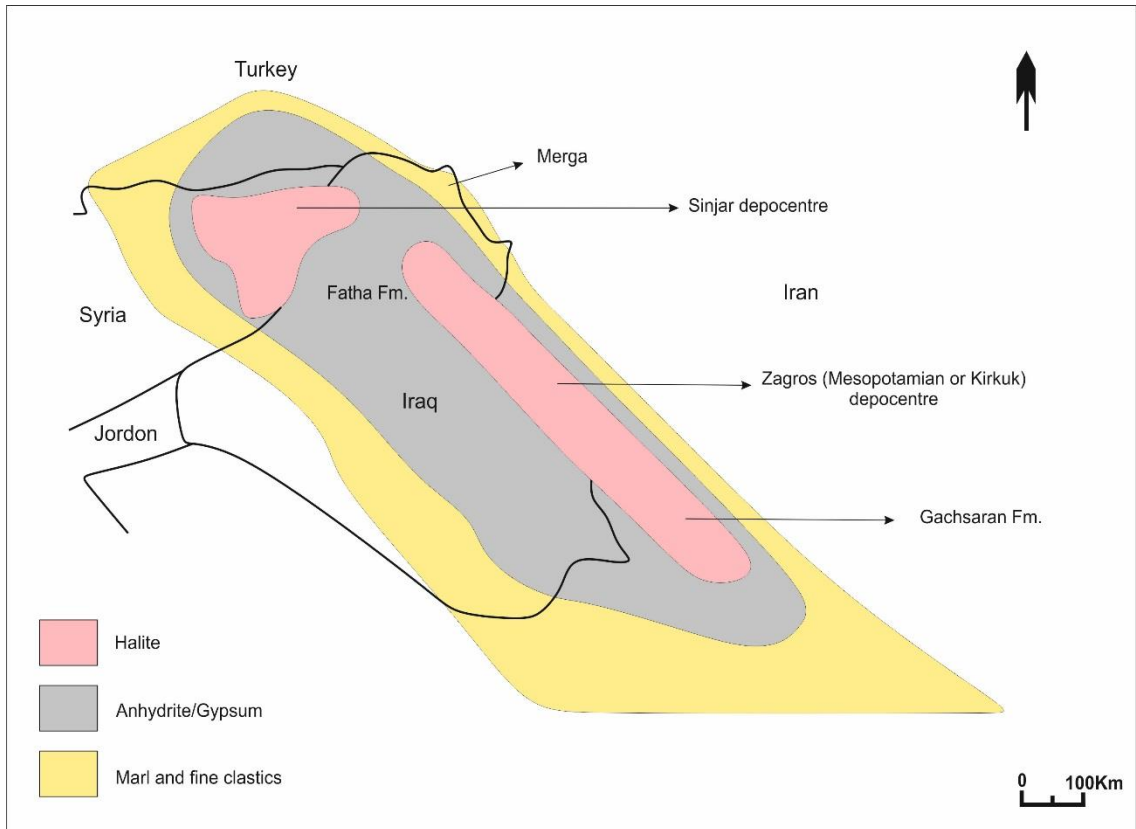


Figure 2-4 Palaeogeographic map and palaeofacies distributions of the Middle Miocene Fatha Formation (Goff *et al.*, 1995). Two main depocentres were developed in Iraq, including Sinjar sub-basin that extended to Syria and Zagros sub-basin that extended to Iran where Gachsaran Formation was deposited.

2.5 Regional Correlation

The stratigraphy of Iraq is affected by the major tectonic elements of the Middle East area, as well as by the structural elements inside Iraq. In addition, most stratigraphic units in Iraq extend towards other surrounding countries due to the trend of the Zagros Basin.

The palaeogeographic map of the stratigraphic units of the Miocene basin in Iraq and Arabia (Figure 2.8) show that the Miocene basin extended 2000 km from SW Iran into north-eastern and central Iraq and towards NE Syria and southern Turkey (Sharland *et al.*, 2001; Ziegler, 2001; Jassim and Goff, 2006; Aqrabi *et al.*, 2010). Importantly, deposition in this Miocene basin was diachronous, being older in the southwest and becoming younger to the northwest (Shawkat, 1979).

In Iran, the Late Oligocene to Early Miocene Asmari Limestone Formation (a significant hydrocarbon reservoir) is equivalent to the Iraqi Euphrates, Dhiban and Jeribe Formations, whereas the Euphrates Formation is laterally replaced by continental clastics of the Hadruk Formation in Saudi Arabia and the Ghar Formation in Kuwait and southern Iraq (Aqrabi *et al.*, 2010).

The Middle and Upper Miocene in Iran were previously represented by the Fars Group, which included the Lower, Middle and Upper Fars formations but are now represented by the Gachsaran, Mishan and Agha Jari formations, respectively (Sharland *et al.*, 2001). In Iraq, the Middle and Upper Miocene are represented by the Fatha (equivalent to the Gachsaran, previously Lower Fars) and Injana (equivalent to the Agha Jari, previously Upper Fars) formations, respectively. The Mishan (previously Middle Fars) Formation is not recognized in Iraq and it is included within the Injana Formation (Sharland *et al.*, 2001; Jassim and Goff, 2006; Al- Juboury *et al.*, 2010). The Fatha Formation extends towards the Syrian and Turkish borders, but also changes to the Dam Formation in Saudi Arabia (Jassim and Goff, 2006). In addition, the Injana Formation is equivalent to the Dibdibba Formation in Kuwait and southern Iraq and the Hofuf Formation in Saudi Arabia (James and Wynd, 1965).

2.6 Palaeoclimate

From research on sedimentary archives covering the last 65 million years, it is increasingly apparent that the Earth underwent a great climatic change from greenhouse to icehouse conditions. The greatest greenhouse phase peaked between 59 and 50 Ma, during the Mid-Palaeocene to Early Eocene, and declined until present day with a rapid cooling stage during the Early Oligocene, with the formation of ice caps at the poles (Zachos *et al.*, 2001; Zhao *et al.*, 2001). These interpretations are determined from stable oxygen isotope data from benthic foraminifera on a worldwide scale (Zachos *et al.*, 2001; Zhao *et al.*, 2001). Based upon oxygen isotopes, palaeoclimate and palaeotemperature can be determined (Zhao *et al.*, 2001), as the value of $\delta^{18}\text{O}$ will decrease during warm climates, and will increase during cool climates. After the rapid increase of $\delta^{18}\text{O}$ during the Oligocene and the formation of significant ice at the poles, the $\delta^{18}\text{O}$ value started to decrease, representing warmer conditions during the Miocene from about 17 to 14 Ma, which is known as the Miocene climatic warmth or the Miocene climatic optimum. However, two cooling phases are recorded during the Miocene climatic optimum from 17.2 to 16.8 and from 16.2 to 15.8 Ma, respectively (Zhao *et al.*, 2001).

In terms of palaeoclimate, the Lower to Middle Miocene units were deposited in an arid and warm climate, evidenced by deposition of the thick evaporites. From the significant deposition of evaporites and warm climate during deposition of the Fatha Formation, the formation might be correlated with the Miocene climatic warmth or optimum from 17-14 Ma (Zachos *et al.*, 2001; Zhao *et al.*, 2001).

2.7 Study areas

A thick Early-Middle Miocene succession is reported in Iraq, which extends from the marginal area in north Kurdistan Region toward the basin centre to the south west in central Iraq. The study area runs very close to the basin margin and is centred on the Sulaimani Governorate in the Kurdistan Region. Three main areas were selected: the Qishlagh-Sargrma, Garmyan and Darbandikhan areas (Figure 2.5).

The first study area is located along the Qishlagh-Sargrma Mountain with a NW-SE trend. The Sargrma Mountain is an asymmetrical double plunging anticline, of which the north-eastern limb is steeper than the south-western limb (Ghafur, 2012). This

structure extends to the south-east toward the Golan structure and to the north-west toward the Bazian structure. As a whole, the Qishlagh-Sargrma structure extends in length for more than 80 km and is 2 to 3 km in width. Three sections have been logged along this structure: the Takiya, Basara and Krbchna sections from NW to SE (Figure 2.5 and Table 2.1).

The second study area is around Garmyan, which is represented by the Aj Dagh and Qara-Wais anticlines. These anticlines are asymmetrical with double plunging folds, with a NW-SE trend and with en-echelon fold geometries (Kharajiany, 2008). They are parallel to the Qishlagh-Sargrma Mountain. The Aj Dagh anticline is located at the SE end of the structure, whereas the Qara-Wais anticline is at the NW end of the structure. The Aj Dagh section was logged along the Aj Dagh anticline, whereas the Mamlaha and Sangaw sections were logged along the Qara-Wais anticline (Figure 2.5 and Table 2.1). In addition, the outlying Kfri section was logged near Kfri town, 57 km SW of the Aj Dagh anticline.

The third study area is located around Darbandikhan town, next to the Darbandikhan Dam, along the NE limb of the Qaradagh anticline. The Darbandikhan section was logged next to the Darbandikhan Dam, whereas the Chnarah section was recorded near Chnarah village (Figure 2.5 and Table 2.1).

Takiya section. At latitude $35^{\circ} 39' 07.38''$ and longitude $44^{\circ} 57' 28.90''$, the Takiya section is located 2.5 km NW of Takiya town and 45 km NW of Sulaimani city, along the Qishlagh anticline. A number of gypsum quarries are present in this area of the Fatha Formation.

Basara section. At latitude $35^{\circ} 26' 40.30''$ and longitude $45^{\circ} 09' 25.84''$, the Basara section is situated along the SW limb of the Qaradagh anticline, near the outlet of the Basara gorge.

Krbchna section. At latitude $35^{\circ} 17' 53.65''$ and longitude $45^{\circ} 16' 22.31''$ and along the Sargrma Mountain, the Krbchna section is located 2km NW of Krbchna village, near the Sangaw-Qaradagh road. In this section, a 4.5m unit of Oligocene carbonate was also recorded.

Darbandikhan Dam section. At latitude $35^{\circ} 06' 43.01''$ and longitude $45^{\circ} 42' 12.07''$, this section is located at the Darbandikhan Dam near Darbandikhan town, 53km SE of Sulaimani city.

Chnarah section. At latitude 35° 08' 37.78" and longitude 45° 41' 24.05", this section is located near Chnarah village along the Darbandikhan-Sulaimani road, 45km SE of Sulaimani city.

Aj Dagh section. At latitude 35° 09' 31.87" and longitude 45° 17' 50.98", this section is located on the NW limb of the Aj Dagh anticline, near Hazar Kani village.

Sangaw section. At latitude 35° 16' 39.26" and longitude 45° 09' 49.63", the Sangaw section is located 1km SW of Sangaw town, along the Qara-Wais anticline.

Mamlaha section. At latitude 35° 22' 06.84" and longitude 45° 00' 27.72", this section is located near Mamlaha village and 19km NW of Sangaw town, along the Qara-Wais anticline.

Kfri section. At latitude 34° 42' 04.83" and longitude 44° 57' 53.07", the Kfri section is located along the Bawa Shaswar Dam, 1km NW of Kfri town and 69km S of Sangaw town. This area has undergone post-depositional thrust faulting and only the upper part of the Fatha Formation crops out.

Table 2-1 Geographical and structural locations of the studied sections.

Sections	Latitude N	Longitude E	Structure	Description
Takiya	35° 39' 07.38"	44° 57' 28.90"	Qishlagh	45 km NW Sulaimani
Basara	35° 26' 40.30"	45° 09' 25.84"	Qishlagh	26 km SW Sulaimani
Krbchna	35° 17' 53.65"	45° 16' 22.31"	Sargrma	32 km SW Sulaimani
Darbandikhan	35° 06' 43.01"	45° 42' 12.07"	Qaradagh	53 km SE Sulaimani
Chnarah	35° 08' 37.78"	45° 41' 24.05"	Darbandikhan	45 km SE Sulaimani
Aj Dagh	35° 09' 31.87"	45° 17' 50.98"	Aj Dagh	18 km SE Sangaw
Sangaw	35° 16' 39.26"	45° 09' 49.63"	Qara-Wais	1 km SW Sangaw
Mamlaha	35° 22' 06.84"	45° 00' 27.72"	Qara-Wais	19 km NW Sangaw
Kfri	34° 42' 04.83"	44° 57' 53.07"	Kfri	69km S Sangaw

2.8 Data collection

Nine sections were selected and logged around Sulaimani city from the Miocene Fatha Formation. These sections cover all the lithological cycles from the lower to upper part of the formation. All the geological features were documented during the logging, including lithological variations, thickness measurements, sedimentary structures, sedimentary textures and fossil content. Overall, 615 samples of calcareous mudstone, carbonate, and evaporite were collected from the studied sections (Table 2.2).

Table 2-2 Geographical locations, thicknesses and sample numbers of the studied sections.

No.	Sections	Thickness (m)	Elevation (m)	Samples
1	Basara	195	673	70
2	Takiya	245	954	85
3	Krbchna	116	1078	80
4	Darbandikhan	148	511	50
5	Chnarah	50	754	50
6	Aj Dagh	182	774	80
7	Sangaw	171	804	60
8	Mamlaha	300	582	130
9	Kfri	120	260	10
	Total	1527		615

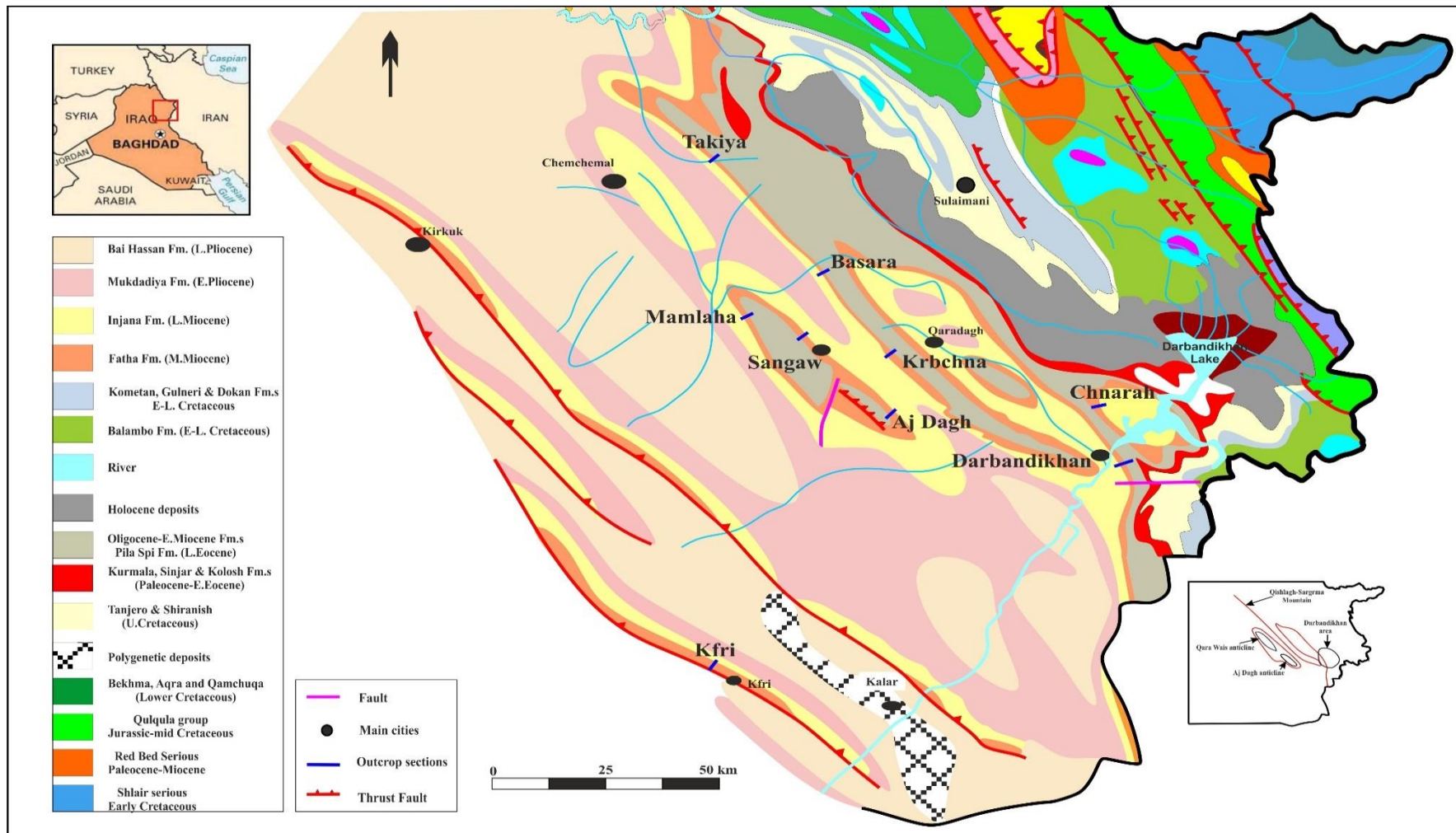


Figure 2-5 Location and geological map of the study area in Kurdistan, Sulaimani Government, NE Iraq. The Fatha Formation and the studied outcrop sections are illustrated.

2.9 The stratigraphy of the studied areas

A thick Miocene succession is preserved in the Zagros foreland basin, which covers most parts of Iraq and SW Iran. The base of the AP11 tectonic megasequence (Sharland *et al.*, 2001) is marked by a regional unconformity surface in the Late Eocene, which probably represents the first continent collision (Ziegler, 2001). The filling of the foreland basin was commenced along the narrow Zagros foredeep. After this became filled, sedimentation prograded south-eastwards along the axis of the foredeep, from Mesopotamia into the Arabian Gulf (Sharland *et al.*, 2001). By the end of the Pliocene, final Zagros closure took place, which caused extensive tectonic folding and thrusting of the earlier sediments.

The Miocene succession in Iraq is represented by the Ghar, Serikagni, Euphrates, Dhiban and Jeribe formations of the Lower Miocene, and the Fatha, Injana and Mukdadiya formations of Middle-Upper Miocene times (Figure 2.6 and Figure 2.7). The continuation of continental collision during the Early Miocene and flexural downwarping of the area led to the marine transgression and development of deep marine sediment of the Serikagni Formation and its shallow lateral equivalent, sediments of the Euphrates Formation (Aqrabi *et al.*, 2010). The short-term development of localized, restricted to enclosed basins arose from tectonic stability and led to the deposition of the Dhiban Formation (Al-Juboury *et al.*, 2007).

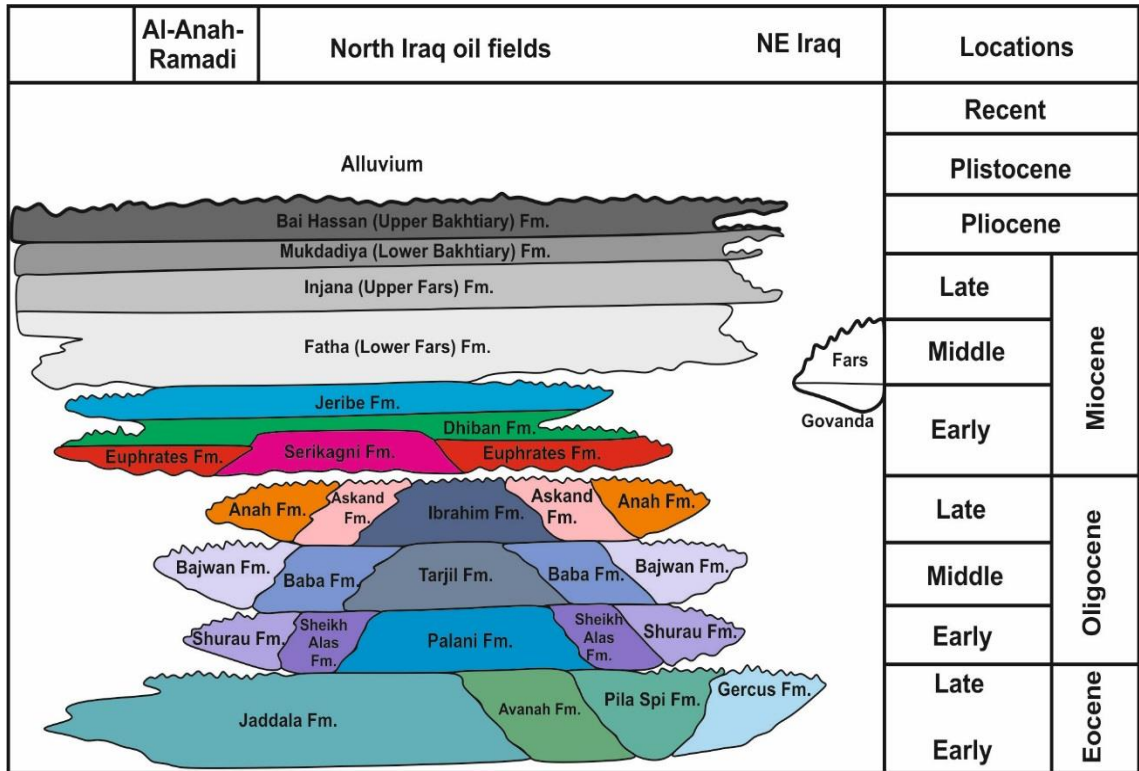


Figure 2-6 Chronostratigraphic column for NE Iraq during the Tertiary (van Bellen *et al.*, 1959).

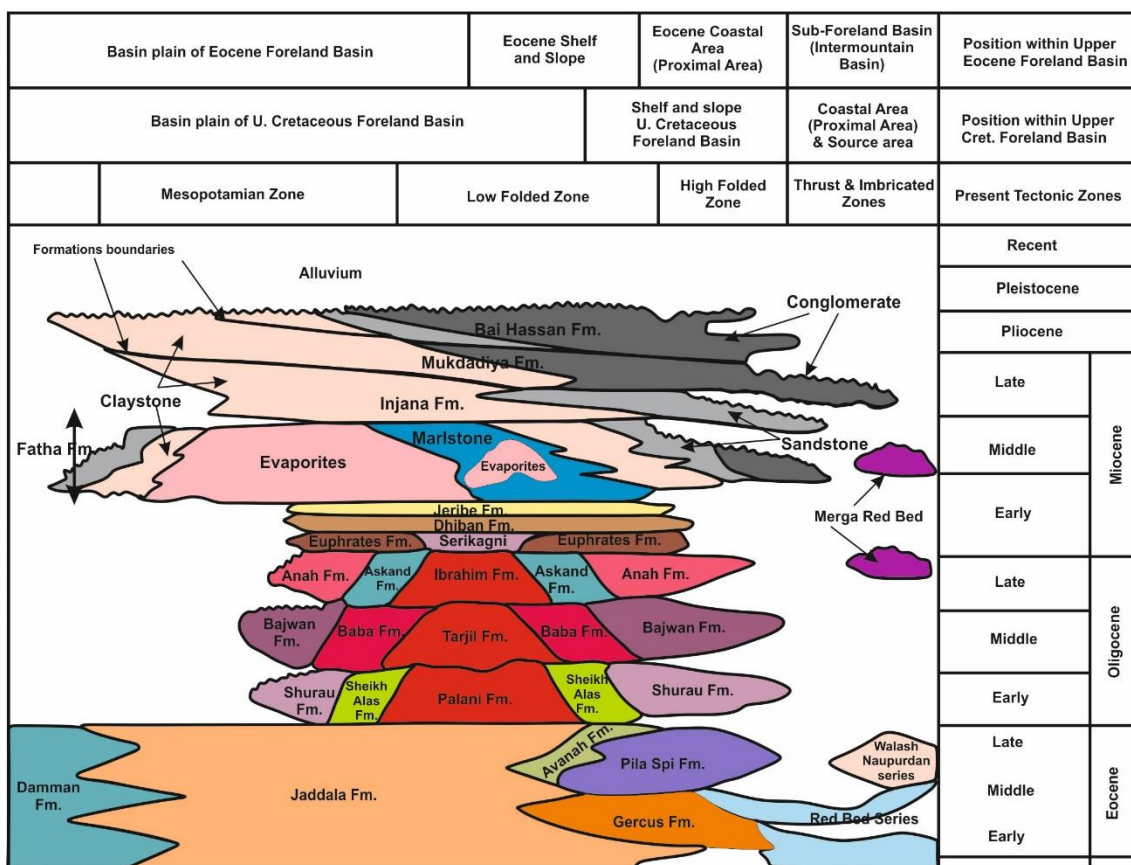


Figure 2-7 Chronostratigraphic column of north eastern Iraq from the Eocene to Recent (Karim, 2010).

A new transgression may have contributed to a deeper facies rich in planktonic foraminifera in the deep part of the basin, where the Jeribe Formation was deposited, and then the basin progressively infilled, changing to shallow open to variably restricted conditions, as also represented on the NE margin of the basin throughout the Jeribe Formation (Aqrawi *et al.*, 2010; Hussein 2016). As a result of the continuation of regional uplift and the uplift of hinterlands, relatively shallow semi-restricted to closed basins were then developed and led to the deposition of the Fatha Formation carbonate-evaporite cycles. Then, progradation of the Fatha facies began from the north-east toward the south-west. The continuation of progradation led to the eventual replacement of the carbonate-evaporite deposits by siliciclastic deposits and in the form of the deposition of fluvial deposits of the Injana, Mukdadiya and Bai Hassan Formations (Aqrawi *et al.*, 2010).

The deposition of the deep planktonic facies of the Serikagni Formation was restricted in the basin centre and there is no Serikagni facies recorded towards the basin margin, which is what is represented in the Kurdistan region. However, the lateral equivalents of

the Serikagni Formation, the Euphrates Formation, and the younger Dhiban and Jeribe formations have been identified in the Kurdistan region (Hussein, 2016).

The Basal Fars Conglomerate at the base of the Fatha Formation is recognized in Darbandikhan areas where a thick siliciclastic deposits, comprising red claystone, sandstone, conglomerate, and brecciated carbonate, is documented at the top of the Late Eocene Pila Spi Formation. The Early Miocene and Oligocene formations are not recorded in Darbandikhan and Chnarah sections. However, the Early Miocene formations, including Euphrates and Jeribe, as well as a thin Oligocene unit (4m thick), are documented between the Late Eocene Pila Spi and Fatha formations along the Qishlagh-Sargrma Mountain. In this area, the Basal Fars Conglomerate is located at the base of the Early Miocene formations. Toward the south-west of the studied areas, Azh Dagh and Qara-Wais anticlines, the Basal Fars Conglomerate becomes thin, and a thick Oligocene succession is documented. Further toward the basin centre, this surface and the associated clastics change to a conformable succession in the centre of the basin.

The stratigraphy of the studied areas can be summarised as follows, as described from the base of the succession to the top.

2.9.1 Late Eocene Pila Spi Formation

The Pila Spi Formation crops out extensively in the High Folded Zone in the Kurdistan region and its lithological composition shows no significant variations. It is characterized by well-bedded dolomitic carbonate, chalky in appearance, and includes the presence of chert nodules in the uppermost part (Buday, 1980). Benthic foraminifera comprising miliolids, chilostomellids and peneroplids are abundant, and they represent an inshore lagoonal facies (Buday, 1980). The lower boundary is gradational with the red mudstone facies of the underlying Gercus Formation, whereas the upper boundary is unconformable with overlying Oligocene or Miocene strata.

In the studied areas, the Pila Spi Formation is overlain by the Miocene Fatha Formation in the Darbandikhan and Chnarah sections where a thick siliciclastic unit (the Basal Fars Conglomerate) is recorded between them (Figure 2.8H). However, in the Qishlagh-Sargrma Mountain region, the formation is overlain by a thin Oligocene unit (4 m thick) (Figure 2.8 C, D, and G).

2.9.2 Oligocene formations

The Oligocene deposits in Iraq are composed of nine formations that have a relatively restricted area of distribution. The Oligocene basin was generally restricted to central Iraq near the city of Kirkuk where a thick and complete Oligocene succession is documented (van Bellen *et al.*, 1959). The Oligocene formations reduce in thickness or are absent toward the Kurdistan region. The Oligocene strata are predominately composed of carbonate and they were first defined as reef, back-reef, and fore-reef facies (van Bellen *et al.*, 1959; Buday, 1980). However, Ghafur (2012) argues that the formations accumulated in inner, middle and outer ramp platform settings.

In the studied areas, the Oligocene units are not recorded in the Darbandikhan and Chnarah sections, whereas a thin carbonate unit (4 m) that is rich in corals is documented at Sargrma Mountain, near Krbchna village (Figure 2.8G). The Oligocene formations become thicker toward the Azh Dagh and Qara Wais anticlines. Both underlying and overlying units are unconformably separated from the Oligocene strata.

2.9.3 Basal Fars Conglomerate

The Basal Fars Conglomerate was first defined by van Bellen *et al.* (1959) at the base of the Fatha Formation (previously Lower Fars). In the studied areas, this unit is composed of thick siliciclastic deposits that comprise conglomerate, sandstone, siltstone, and claystone, as well as carbonate conglomerate that channelized within palaeosols (Figure 2.8H). It is about 10 m thick in the Darbandikhan area at Qishlagh-Sargrma Mountain, occurring below the base of the Fatha and Euphrates Formations, respectively (Figure 2.8 A and C). This unit thins toward the Azh Dagh and Qara Wais areas where it is about 4 m thick.

2.9.4 Euphrates Formation

The Euphrates Formation is mainly composed of carbonate and contains beds of greenish marl, breccia, marly sand, and conglomerate (Buday, 1980). It is characterized by chalky, shelly, well-bedded recrystallized limestones, siliceous, oolitic, corraline, and coquinas (van Bellen *et al.*, 1959). Based on these variations in lithological composition, the formation was divided into three members: a basal cavernous and conglomeratic limestone, a shelly carbonate, and a marly and chalky carbonate (van Bellen *et al.*, 1959). The formation was deposited in shallow marine lagoons and reef

settings (Buday, 1980). The lower boundary is usually unconformable with the underlying Oligocene and Late Eocene formations, whereas in some areas, where the underlying unit is the Serikagni Formation, it is conformable (Buday, 1980). The upper boundary is conformable with the overlying Dhiban Formation.

In the studied areas, the formation is absent in the Darbandikhan and Chnarah sections (Figure 2.8H), whereas it is recorded for the first time along the Qishlagh-Sargrma Mountain in this study (Figure 2.8A). The formation is mainly composed of carbonate, and it is about 4 m thick (Figure 2.8C, E, and F). It comprises conglomeratic carbonate at the base and shelly carbonate at the top. It is composed of miliolid packstones and grainstones at the base, and oolitic grainstones at the top. *Borelis melo melo* as an index fossil for the Lower Miocene is identified in the carbonate unit (Figure 2.8B). The lower boundary is unconformable with the underlying Oligocene or Late Eocene formations or represents a flooding surface over the Basal Fars Conglomerate where present, whereas the upper boundary is conformable with the overlying Dhiban Formation. In the Aj Dagh area, the formation was first identified by Hussein (2016) (Figure 2.8E).

2.9.5 Dhiban Formation

The Dhiban Formation is composed of thick beds of gypsum that are interbedded with thin beds of marls, recrystallized limestone, and dolomite (Buday, 1980). It is 100 to 150 m in thickness in the subsurface. Fossils are lacking in the formation, and its age is determined based on its stratigraphic position, being underlain by the Serikagni or Euphrates Formations (Al-Juboury *et al.*, 2007).

In the studied areas, the formation is recorded in the Azh Dagh-Qara Wais Mountain area where it is only 1 m thick. It is underlain and overlain by the Euphrates and Jeribe formations, respectively. It is characterized by yellowish evaporitic carbonate. However, the formation is locally recognized for the first time in this study along the Qishlagh-Sargrma Mountain at the boundary of Euphrates and Jeribe formations. It is a thin (10cm) yellowish evaporitic carbonate.

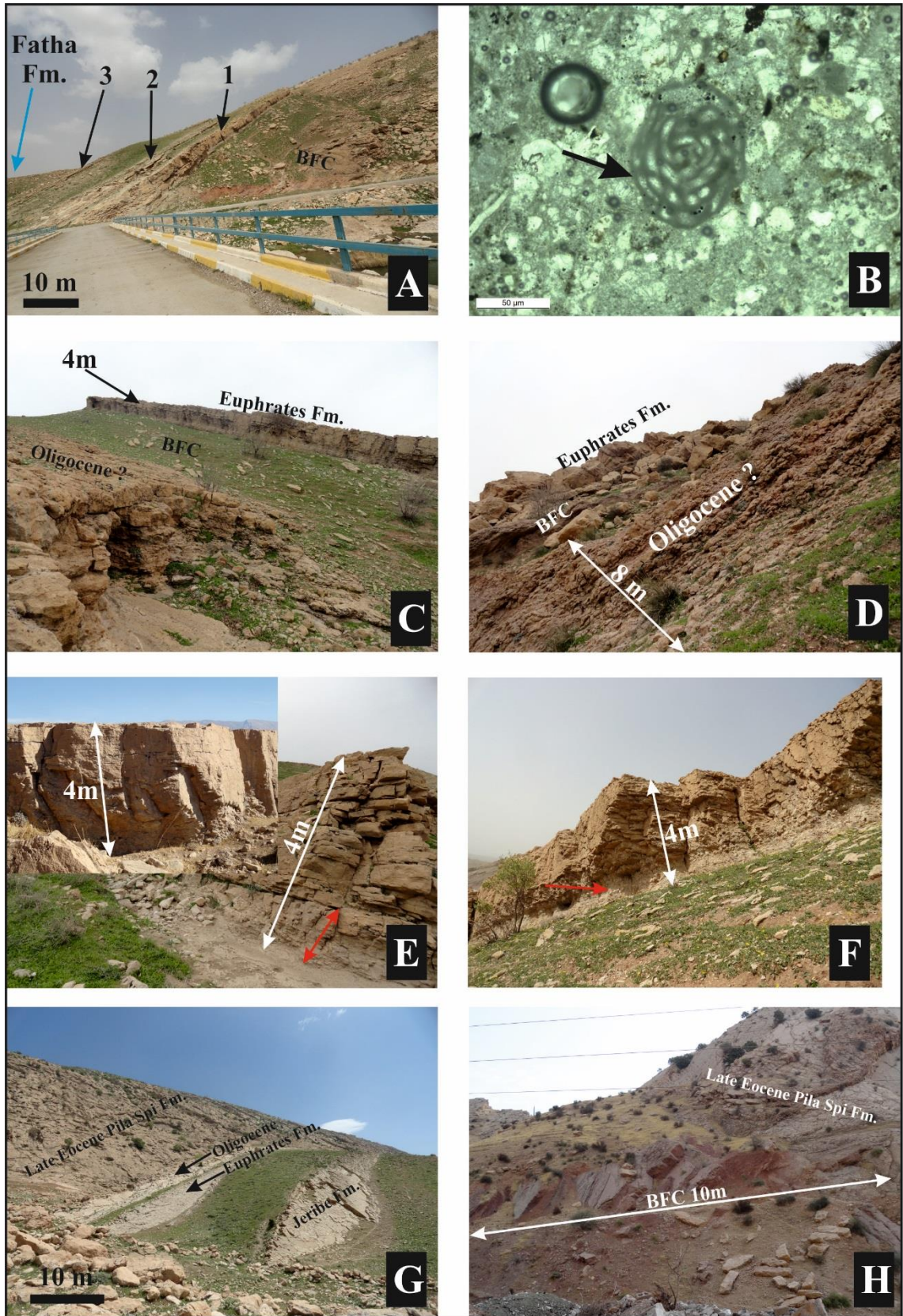


Figure 2-8 Field photographs of the Early Miocene Euphrates and Jeribe formations.

A: The lower boundary of the Euphrates Formation (1) that overlies the Basal Fars Conglomerate (BFC) and underlies the Jeribe Formation (2, 3) which is in turn overlain by the Fatha Formation; Basara section. **B:** Thin section photomicrograph of Euphrates Formation including the index fossil *Borelis melo melo*. **C:** The lower boundary of the Euphrates

Formation that is underlain by the BFC which in turn underlain by a possible Oligocene unit; Basara section. **D:** The same boundary in the Takiya section. **E:** The carbonate unit of the Euphrates Formation showing both lower brecciated (red arrow) and upper shelly carbonate members; as seen in the Azh Dagh and Mamlaha sections. **F:** The same carbonate unit of the Euphrates Formation, including both brecciated (red arrow) and shelly carbonate members in the Basara section. It is underlain by the BFC. **G:** The carbonate units of the Euphrates and Jeribe Formations in the Krbchna section. The Euphrates Formation is unconformably underlain by an Oligocene unit that is rich in corals. **H:** The BFC in the Darbandikhan section. It is underlain by the Late Eocene Pila Spi Formation and overlain by the Fatha Formation.

2.9.6 Jeribe Formation

The Jeribe Formation is composed of recrystallized and dolomitized carbonates that are interbedded with evaporite and dolomite. The lower boundary is conformable with the Dhiban Formation, whereas it is unconformable with the Serikagni Formation in the type area with an evidence of a conglomeratic bed at the base of the formation (Buday, 1980). The upper boundary is conformable with the Fatha Formation. The formation was deposited in lagoons and reef environments (van Bellen *et al.*, 1959).

In the studied areas, the Jeribe Formation is not recorded in the Darbandikhan and Chnarah sections (Figure 2.8H), whereas it is documented in all the other areas (Figure 2.8A and G). It is first recorded along the Qishlagh-Sargrma Mountain and it is underlain by the Euphrates Formation and overlain by the Fatha Formation. It is 8 to 10 m thick and comprises three cycles of carbonate, marl, and yellowish evaporitic carbonate. However, a very thin (10cm) yellowish gypsiferous carbonate bed has been locally documented at the boundary of Euphrates and Jeribe formations. This bed may represent Dhiban Formation that thins toward the margin of the basin.

2.9.7 Fatha Formation

The Fatha Formation (previously termed the Lower Fars Formation) was originally defined and described by Busk (1918), and later reviewed by van Bellen *et al.* (1959), in Iran, as part of the Fars Group. The Fars Group from Iran was divided into the Lower, Middle and Upper Fars Formations. Lithologically, the Lower Fars Formation (Fatha Formation) was also recognized in Iraq and was named after its Iranian equivalent (van Bellen *et al.*, 1959; Buday, 1980). Then, a new type section was described in Iraq on the south-western flank of Makhul Mountain, in Al-Fatha Gorge. This was used as the basis for the definition of the Fatha Formation by Al-Rawi *et al.* (1993). The type section of

the formation is divided into two members based on the absence or presence of red mudstone units. The lower member, which lacks the red clastic units, is 220m thick at the type section; the upper member, in which red clastic units are present, is 400m thick at the type section (Jassim and Goff, 2006).

In general, the Fatha Formation is characterized by widespread evaporites (gypsum, anhydrite and salt) facies, which are interbedded with carbonate, calcareous mudstone and red continental clastic units (Buday, 1980). It is a mixed carbonate-evaporite unit which shows a cyclic repetition of lithologies, comprising red claystone or sandstone, siltstone, mudstone, green marl (calcareous mudstone), gypsum, anhydrite, halite and thin beds of limestone (Jassim and Goff, 2006).

There are no adequate data that fully characterize the presence of halite in the formation. However, several halite beds were recorded in the central part of the basin in Iraq, in the middle part of the formation (van Bellen *et al.*, 1959), and the halite is apparently more extensively developed in the south-eastern part of the basin towards Iran (O'Brien, 1957). Moreover, salty water (brine) derived from the subsurface part of the Fatha Formation is used as an economic resource for salt production in Mamlaha village. In addition, several halite beds are recorded in boreholes in the Sinjar and Kirkuk areas in the north of Iraq (Al-Juboury and McCann, 2008).

Fossils are very rare in the formation; the only fossils that are recorded in the limestone beds are miliolids, ostracods, *Rotalia beccari*, *Elphidium sp.* and *Ostrea latimarginata* (considered to be an index fossil of the formation), which belong to the Middle Miocene (Buday, 1980). Recently, some fossil mollusc species have been studied and these have been ascribed to a late Lower Miocene (Burdigalian) age (Mahdi, 2007). In addition, ostracods from the Fatha Formation have been studied in terms of biostratigraphy, palaeogeography and as palaeoecological indicators by many authors (Khalaf, 1988; Abdol Rassul and Al-Sheikhly, 2001; Hawramy and Khalaf, 2013). A Middle Miocene age for the formation is indicated by all the mentioned authors.

Grabowski and Liu determined the age of the Fatha Formation, using strontium stable isotope dating, for both carbonate and evaporite units. They determined that the formation accumulated during the Burdigalian, or more specifically the Middle Burdigalian to Lower Langhian stages (18.5 to 15.6 Ma) (Grabowski and Liu, 2009; Grabowski and Liu, 2012).

The upper contact of the Fatha Formation is gradational and diachronous with the overlying Injana Formation (Buday, 1980; Jassim and Goff, 2006). In addition, the Fatha Formation is diachronous at a regional scale, being older toward the SE of the basin (SW Iran) but younger towards the NW of the basin (Iraq to Syria) (Shawkat, 1979). However, Al-Juboury and McCann (2008) consider the last anhydrite bed as the top of the Fatha Formation and define it as a sequence boundary with the overlying Injana Formation.

It has been suggested that the Fatha Formation was deposited in a relatively rapidly subsiding basin, which was separated by rising ridges from the open sea (van Bellen *et al.*, 1959; Buday, 1980). In addition, Ibrahim (1979) and Aqrabi (1993) concluded that the basin was supplied by some fluvial and aeolian detritus during deposition. The sedimentology and petrography of the formation have been widely studied by Hamid (1994) and Ameen and Karim (2007) who concluded that the formation was deposited in a semi-restricted lagoonal setting.

The clastic element, as a main unit, has been studied and a fluvial-dominated bird's foot deltaic environment has been inferred, which represents prodelta, delta front, distributary channels, natural levees and crevasse splay components (Al-Juboury *et al.*, 2001). In addition, Ameen and Karim (2007) state that the formation was deposited in a storm-affected evaporitic foreland basin by the presence of Skolithos traces, erosional surfaces, graded bedding, and hummocky cross stratification in the carbonate clastic units that indicate tempestite deposits.

The cyclicity of the formation has not been studied in detail in terms of sequence stratigraphy. Each cycle is composed of red claystone, marl and evaporites, from base to top, and might be accumulated during lowstand, transgressive and highstand system tracts, respectively (Ameen, 2006). This author attributed each lithological cycle to Milankovitch glacio-eustatic cycles. The cycles were related to eccentricity (ca. 100 kyr), which was modulated by precession (ca. 20kyr) and obliquity (ca. 41 kyr) variations in the orbit of the Earth around the sun. Thus, the repetition of warm and cold time intervals was interpreted to have caused the deposition of evaporites and red claystones, respectively. This will be explored in more detail in chapter 4.

The marl unit has been studied in terms of mineralogy and petrography (Al-Kawaz and Al-Juboury, 2006; Al-Juboury and Al-Kawaz, 2008). These authors observed two

different colours of the marl unit; red and green. In addition, the authors stated that the marl beds include quartz grains, carbonate fragments and clay minerals. These components from the marl beds with evaporitic associations have led to the conclusion that the marls were deposited in hypersaline and semi-restricted lagoonal environments.

In different studies, the formation was investigated in terms of petrography, mineralogy (including heavy and clay minerals) and provenance. These studies revealed that the provenance for the clastics in the formation were from ophiolite groups, with igneous and metamorphic rocks from the north-eastern margin of the Zagros Zone and mostly Cretaceous rocks from the High Folded Zone. This interpretation was reached because, during the Miocene, most of this highly folded and thrust area was uplifted and so sourced the Miocene sediments, which were deposited in arid to semi-arid climatic conditions (Al-Juboury *et al.*, 2001; Aghwan, 2004; Al-Kawaz and Al-Juboury, 2006; Jassim and Goff, 2006; Kassim, 2006; Al-Juboury, 2009; Al-Juboury *et al.*, 2009).

The high-frequency cycles of the Fatha Formation resulted from a rapid change in accommodation space in various palaeoenvironmental settings, ranging from open to restricted marine environments to continental sabkha and fluvial environments (Al-Juboury and McCann, 2008). The authors argued that the formation as a whole represents a transgressive – regressive third order sequence.

The preserved thickness of the formation changes from the basin centre towards the north-eastern part of the basin. Furthermore, the general components and thicknesses of limestones and evaporites vary in the same direction (Dunnington, 1958). In the Zagros Basin, in the Sinjar sub-basin and around Kirkuk, the formation reaches its maximum thickness (600 to 900 m), whereas along most anticlines around Sulaimani city the formation is 200 to 500 m thick (Jassim and Goff, 2006).

The depositional environments of the formation and the associated thick evaporites are controversial. Some authors concluded that the marl, limestone and evaporite units of the formation were deposited in subtidal, intertidal and sabkha supratidal settings, respectively (Shawkat and Tucker, 1978; Shawkat, 1979; Tucker, 1999). This interpretation was largely based upon the recognition of stromatolites and algal mats in the formation at Shaikh Ibrahim in NW Iraq. By contrast, other authors stated that the lack of sedimentary features typical of sabkha deposits (e.g. stromatolites and dolomites), is the main reason to infer that the evaporite was deposited in a marine to

restricted lagoonal environment, rather than including sabkha environments (Ajel, 2004). On the other hand, Aqrabi (1993) stated that subaqueous evaporite may have occurred together with subaerial sabkha evaporite in the Fatha Formation. This is a main question of this PhD study, to investigate the depositional environments of the evaporites and related deposits.

2.9.8 Injana Formation

The Injana Formation conformably overlies the Fatha Formation. It is composed mostly of red silty marlstones, claystone, siltstone, and sandstone. In addition, limestone, gypsum, and shale also occur in the lower part of the formation (van Bellen *et al.*, 1959). The lower boundary is mostly gradational with the Fatha Formation, whereas the upper boundary is defined by the first pebbly sandstone bed of the Mukdadiya Formation (Buday, 1980). In the studied areas, the Injana Formation is composed of cycles of red claystones and sandstones, and it shows a gradational transition from the underlying Fatha Formation.

Chapter Three

Variations in carbonate-evaporite ramp facies trends: Late Burdigalian Fatha Formation, Kurdistan

3.1 Introduction

Carbonate ramps were originally defined by Ahr (1973) as low-angle inclined platforms that extend toward the basin without any slope break. High-energy packstone and grainstone facies typically dominate the landward (inner) part of ramps; low-energy and mudstone and wackestone facies tend to dominate in the basinal (outer) parts of ramps (Ahr, 1973). Most high to moderate energy ramps are dominated by a strandplain complex or a barrier-lagoon shoreline, whereas low energy ramps tend to be dominated by tidal flats and lagoons (Tucker, 1992a). The Trucial Coast in the Arabian Gulf is an example of a modern carbonate ramp with barrier, lagoon and tidal flat elements.

Cyclic sequences on carbonate ramps are documented from different basins and many examples of high-frequency shallowing upward cycles are recorded (Ginsburg, 1975; Wilson, 1975; Grotzinger, 1986a; Grotzinger, 1986b; Goldhammer *et al.*, 1987b; Alsharhan and Kendall, 2003; Khalifa *et al.*, 2004). In arid climates, evaporites may be deposited along the intertidal and supratidal (sabkha) zones (e.g. the Arabian Gulf). However, evaporites are not associated with carbonate ramps in more humid climate settings, such as South Florida (Bosence and Wilson, 2003). Many shallowing-upward cycles record evidence for emergence in their upper part, whereby a mixed carbonate-evaporite cycle is produced; for example in the Trucial Coast in Abu Dhabi (Kinsman and Park, 1976; Kendall *et al.*, 2002; Warren, 2006). In addition, in the proximal (i.e. basin margin) areas, continental siliciclastic fluvial and aeolian deposits are commonly mixed with the carbonate-evaporite cycles.

Models of carbonate ramps tend to emphasize two-dimensional facies trends, from proximal to basinal (Burchette and Wright, 1992). However, changes in rates of deposition and environmental controls that vary both spatially across a ramp system and temporally due to changes in, for example, carbonate production, relative sea level and climate, lead to microfacies variations in the sedimentary succession (Flügel, 2004), thereby potentially preserving complex arrangements of lithofacies within multiple depositional cycles.

The Miocene Fatha Formation in Kurdistan region and its time-equivalents record an example of an ancient mixed carbonate-evaporite ramp which covered most of the northeast margin of the Arabian plate. This succession forms an important hydrocarbon seal system in Syria, Iraq and Iran (Aqrawi, 1993; Goff *et al.*, 1995). Between 17 and 42 depositional cycles of carbonate, evaporitic carbonate, evaporite and in some cases siliciclastic red claystone are preserved in the Fatha Formation; these cycles are variable in nature and thickness. At the margin of the Zagros foreland basin (Kurdistan area), the cycles of the lower part of the Fatha Formation comprise marl (carbonate mudstone), carbonate, evaporites and siliciclastic rocks upward throughout each of the cycles. However, in the upper part of the formation marine carbonate and evaporite deposits are volumetrically less significant, whereas alluvial clastic units are dominant. This regressive trend continues into the overlying alluvial Injana Formation, which is predominantly terrestrial (fluvial) in origin. Towards the centre of the basin, the lateral equivalent of the Fatha Formation cycles comprise marl, carbonate and evaporites, with the only occurrence of red clastic mudstone being as minor accumulations in the upper part of cycles in the upper member of the formation (Aqrawi *et al.*, 2010). The proportions and thicknesses of the units are variable from place to place; the number of cycles characterized by clastic deposits in their upper part increases toward the basin margin, whereas the number of cycles dominated solely by carbonate-evaporite units increases toward the basin centre.

The depositional environment of the formation, with its characteristic carbonate-evaporite cycles, has been the subject of debate. Some researchers concluded that the marl, limestone and evaporite units were deposited in subtidal, intertidal and sabkha supratidal settings, respectively (Shawkat and Tucker, 1978; Shawkat, 1979; Tucker, 1999). Evidence to support this interpretation includes the recognition of stromatolite carbonate algal-mat deposits and chicken-wire evaporite (anhydrite) in the formation at Shaikh Ibrahim, NW Iraq. However, others argued that the formation was deposited in a relatively rapidly subsiding basin, which was separated by from an adjacent open seaway tectonic barriers (van Bellen *et al.*, 1959; Buday, 1980). Furthermore, Ajel (2004) argued that the general paucity of sedimentary features indicative of sabkha environments, such as stromatolites and dolomites, suggests that the development of sabkha environments was not widespread across the region; an interpretation of a marine-connected, restricted lagoonal environment was favoured. Additionally, Aqrawi (1993) stated that subaqueous evaporite might be occurred together with subaerial

sabkha evaporite in the Fatha Formation. Moreover, another related study proposed a model for a semi-restricted lagoon setting for the depositional environment (Hamid, 1994). A further study argued that the formation accumulated in a storm-affected evaporitic basin that was subject to freshwater influxes (Ameen and Karim, 2007). Furthermore, other studies have documented a stratigraphic equivalent to the Fatha Formation, the Gachsaran Formation in Iran, which is also characterized by shallowing-upward cycles capped by evaporites that are interpreted to have accumulated in supratidal and sabkha environments (James and Wynd, 1965; Gill and Ala, 1972; Pirouz *et al.*, 2011). Thus, the origin and environmental significance of the preserved cycles of the Fatha Formation remain contentious.

The aim of this chapter is to determine the depositional environments of the mixed carbonate-evaporite cycles of the Fatha Formation and to present a model with which to account for the variation in the expected facies trends of ramp systems more generally. Specific objectives are as follows: (i) to document the sedimentary facies and determine their depositional palaeoenvironments; (ii) to demonstrate variations in the style of preserved carbonate-evaporite cycles and ramp facies trends; and (iii) to present a depositional model for the formation.

This study is timely and of broad appeal for the following reasons: (i) it presents the evaluation and correlation of the carbonate-evaporite cycles across a regional area which can be correlated into the adjacent countries of Iran and Syria, and therefore assists in constraining regional palaeogeography in relation to plate tectonic configuration across the wider region; (ii) the carbonate-evaporite succession creates a significant hydrocarbon system (currently a secondary target in Kurdistan) in which the carbonates make a good potential reservoir, sealed by the extensive evaporites, and (iii) economically, the evaporites offer an important local source for the extraction of gypsum and sulphur.

In the current study, detailed sedimentary logs, lateral/vertical facies variations and detailed sedimentary facies and microfacies studies have been analysed for the Fatha Formation for the purpose of interpreting the depositional settings. Detailed sedimentary logs for all the sections, including age, thickness measurement, sample locations, water depth, lithology and facies descriptions, are illustrated. Detailed descriptions and interpretations of the carbonate microfacies are illustrated in Table 3.1 and 3.2. In

addition, detailed thin-section photomicrographs and field photographs for all the sedimentary facies are included.

3.2 Methods

Measured vertical sections were recorded from exposures of the Fatha Formation in the Qishlagh, Sargrma, Darbandikhan, Aj Dagh, Sangaw, Qara-Wais and Bawa Shaswar anticlines (see Chapter Two, Fig. 2.5; Table 2.1). Nine complete sections totalling 1527 m in thickness were recorded from the well-developed Miocene succession in the Kurdistan region (see Chapter Two, Table 2.2). The 9 sedimentary logs (see Appendix 1) were measured to characterize lateral and vertical variations in lithofacies and associated sedimentary structures. In total, 615 samples were collected from the studied sections from different lithological units. From these samples, 300 thin sections were studied from the carbonate units for analysis of petrography; twenty additional thin sections were studied from the calcareous mudstone and evaporite units. Carbonate microfacies were interpreted using the Dunham classification (Dunham, 1962) with the modifications of Embry and Klovan (Embry and Klovan, 1971). Microfossils were extracted from 50 samples of the calcareous mudstone unit using the H₂O₂ method (Boltovskoy and Wright, 1976), as the following:

- a) The dried field samples were broken into pieces less than a centimetre in diameter.
- b) The samples were transferred in to a 250ml beaker in the fumehood.
- c) The H₂O₂ solution was diluted to 20% using distilled water.
- d) The rock samples were submerged in the H₂O₂ solution left to break down for 2-4hr.
- e) The samples were then washed through a 63µm diameter sieve.
- f) The samples were then gently rinsed in the sieve until the water run clear.
- g) A filter paper was folded and put in a funnel. The sample was transferred to the funnel, which was placed in a beaker to drain and dry.
- h) The samples were dried in an oven at approximately 40°C.
- i) The samples were ready to be sorted or picked and identified.
- j) The selected fossils were coated with gold and platinum alloys and imaged with the scanning electron microscope at the University of Leeds, UK.

3.3 Divisions of the Fatha Formation

The main division of the formation was based on analysis of the section in the area around Kirkuk by van Bellen *et al.* (1959) and it was divided into four informal units, from bottom to top : (i) The Transition Beds that rest on the Basal Fars Conglomerate and are composed of anhydrite with thin carbonate and mudstone, (ii) The Saliferous Beds consisting of anhydrite and salt with mudstone, siltstone and less frequent carbonate beds, (iii) The Seepage Beds that are composed of anhydrite beds with mudstone, siltstone and carbonates, and (iv) The Upper Red Beds that are composed of red mudstone and siltstone with less frequent carbonate and anhydrite. This division is easily recognized in Kirkuk area. However, it is not identified in other areas.

Research groups in the general directorate of geological survey and mineral investigation (Al-Mubarak and Youkhana, 1977; Taufiq and Domas, 1977) divided the formation regionally into two main members, based on the lack and presence of red clastics, which are the lower member (without red clastic) and upper member (with red clastic), respectively. The lower member is composed of marls, carbonates and anhydrites; the upper member is composed of the same rhythmic alternation as the lower part but with the additional presence of red clastics. Based on the current study close to the basin margin, the formation can be divided into these two units that are used throughout the study, as discussed below.

3.3.1 The lower evaporite-dominated part

This unit is mainly composed of cycles of calcareous mudstone (marl), carbonate, evaporite (gypsum) and red clastic beds and is 100 to 200 m thick (Figure 3.1A). This unit rests on the Basal Fars Conglomerate in the Darbandikhan area and the Jeribe Formation in the other areas. The basal part of this unit starts with red claystone in the most marginal parts of the studied areas, like Basara, Sargrma, Takiya and Darbandikhan. In the Garmian area, the basal part starts with alternations of thin evaporite and thin calcareous mudstone beds.

3.3.2 The upper clastic-dominated unit

This unit is 100 to 150 m thick and is mainly composed of alternations of thin beds of calcareous mudstone and carbonate with thick red clastic unit (red claystone, siltstone and sandstone, 2-8m thick) and thin less frequent evaporite beds (Figure 3.1B). The

clastic unit is mostly composed of medium grain size sandstone beds including different sedimentary structures, such as different types of ripple marks, cross bedding and different types of bioturbation (*Skolithos* and *Rhizolithos* traces). Toward the top of this unit, the proportion of units of inferred marine origin decreases. These are replaced by units of fluvial origin of the Injana Formation.

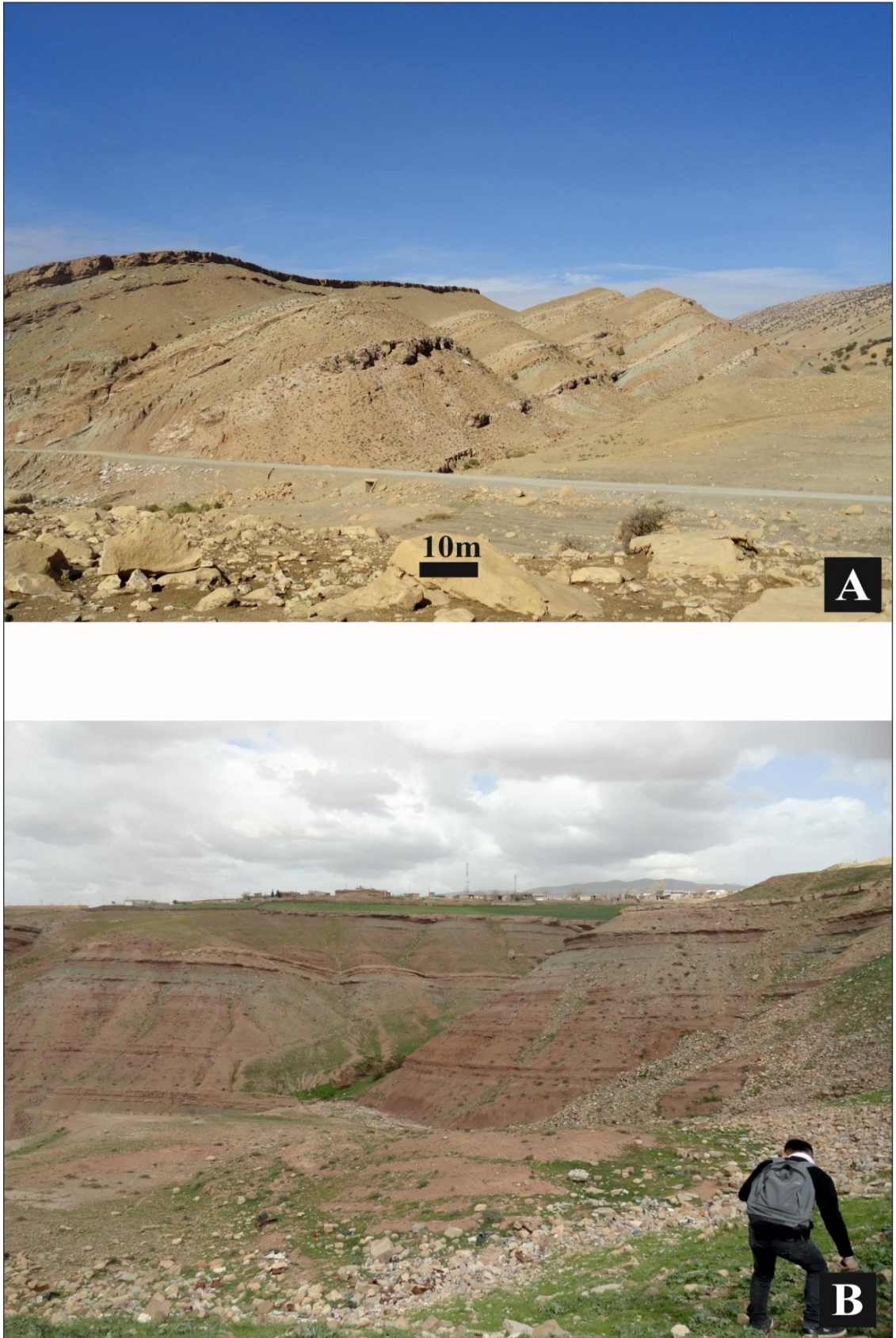


Figure 3-1 Field photographs of the Fatha cycles of the lower evaporite (A) and upper clastic-dominated (B) units from Basara and Sangaw sections, respectively.

3.4 Sedimentary facies

The characterization of sedimentary lithofacies is the main tool for determining palaeodepositional environments. Detailed microfacies analysis and the detection of fossil assemblage allow the recognition of depositional settings. In addition, sedimentary structures and lateral and vertical variations of the lithofacies aid the determination of hydrodynamics and depositional settings. In this section, the results of the sedimentary facies analysis are presented in detail, key features of each facies or microfacies being summarized. Different fossil associations have been recognized from the calcareous mudstone units. Twenty-one carbonate microfacies have been interpreted and illustrated in Tables (3.1 and 3.2).

3.4.1 Calcareous mudstone facies (CM)

Description

The calcareous mudstone facies comprises 13 to 24% of the succession, from the most distal to proximal parts of the studied areas. It is characterized by bluish to green and yellowish colours (Figure 3.10E), fine-grained textures, and is generally structureless, though millimetric planar laminations and bioturbation are locally visible. The thickness of the unit varies from 0.1 to 4.5 m.

Petrographically, different minerals, rock fragments and microfossils are identified in the samples in a fine muddy matrix (Figure 3.10A-D). The minerals observed are quartz, chert, calcite, ferrous dolomite and plagioclase. Quartz is very common in all of the samples, comprising 10-30% of the facies. The quartz content increases toward the top of each individual cycle, which is also evidenced in the field by lithological change to a silty carbonate in some cycles. The quartz grains occur in small sizes (50-100 μm) and have irregular shapes, with low interference colours. They also contain small inclusions. Carbonate minerals are common in the unit and occur in different types such as detritus, chemical and microfossil remains. The detritus carbonate mineral is composed of calcite grains, while the chemical carbonate mineral is composed of dolomite. The calcite minerals are the most common carbonate minerals and exhibited laminar twinning. However, the dolomite grains are much less abundant and appear in turquoise colours. In addition, the plagioclase feldspar minerals aren't common and, when they appear, they occur in irregular shapes with laminar twinning.

The main fossils of the unit include rotaliids (*Ammonia*, *Neorotalia*, *Pararotalia*, *Elphidium* and *Rotalia*) (Figure 3.7A-F), ostracods (Figure 3.8A-F), bryozoans (Figure 3.9D-F), oysters, bivalves, miliolids (Figure 3.9A-B) and gastropods (Figure 3.9 C). The sizes of observed *Ammonia* and *Rotalia* are variable. For example, in the base of an individual unit they are typically smaller than 200 µm and have low abundance, whereas in the top of the unit, they range between 400 and 800 µm in size and have high abundance. Moreover, the sizes of ostracods vary from 400 to 800 µm, and their morphologies show variations from smooth to moderate/high ornamentations. Miliolids and gastropods are also recorded in the samples and associated with rotaliid group.

The percentages of the fossil components vary in the cycles. In some cycles and especially at the base of the individual units, fossils are absent. Petrographically, the calcareous mudstone unit includes detrital quartz grains (10%), grains of feldspar minerals (2%) and ferrous dolomite grains (5%). The percentage of the detrital quartz grains increases toward the top of the individual units to 30% (Figure 3.10C-D). Lithological variations include the presence of more marl-prone carbonate in some cycles. Planar laminations and bioturbation are common in the units. In the studied sections planktonic foraminifer are not recorded, though such forms are recorded from similar facies in the basin centre (Shawkat, 1979). In general, the calcareous mudstone units from the lower part of the succession include rotaliid group foraminifera, miliolids and ostracods within muddy matrices. However, toward the upper part of the succession, normal marine bryozoans and oysters are seen. *Skolithos* ichnofabrics are abundant in the upper part of the succession (Figure 3.11C).

Interpretation

The association of rotaliids with ostracods and miliolids has been found from different parts of modern hypersaline lagoons on the both sides of the Red Sea and Gulf of Suez, Egypt by a number of researchers (Abou-Ouf *et al.*, 1988; Gheith and Auf, 1996; Hariri, 2008; Mohamed *et al.*, 2013). Modern rotaliids live in hypersaline lagoons on the eastern coast of the Red Sea at water depths of less than 20 m (Yusuf, 1984; Hariri, 2008). Furthermore, rotaliids indicate and have an affinity with abnormal environmental conditions of saline lagoons and pools (Murray, 1973; Mohamed *et al.*, 2013). The genus *Ammonia* lives in a wide range of settings from normal marine to hypersaline lagoon, from 0 to 50 m water depth, in warm water (0 to 30°C). *Elphidium* lives in brackish to hypersaline marsh and lagoon settings (0 to 70 ‰), in water depths of 0 to

50 m (Murray, 1991). The variable size of *Ammonia* likely relates to salinity variations (Bradshaw, 1961). With decreasing salinity, the size of *Ammonia* increases.

Ostracods occur in fresh, brackish and marine waters and also live in hypersaline waters (Scholle and Ulmer-Scholle, 2003). Sizes and morphologies of the ostracods from the calcareous mudstone units are variable. The percentages of these fossils, including both the smooth and noded forms, are fluctuating in the cycles. A negative relation between ornamentation of ostracods with salinity was previously documented (Bate, 1971; Keen, 1977; Garbett and Maddocks, 1979; Bodergat, 1983; De Deckker, 2002). However, some authors concluded a positive relation between ostracod ornamentation and water salinity (Sandberg, 1964; Vesper, 1975; Van Harten, 2000). On the other hand, Bodergat (2008) states that the calcium content of the water, granulometry of the substrate, nutrient inputs and pH of the water have to be taken into account to conclude whether there is a relationship between ornamentations and salinities. However, Kilenyi (1972) and Van Harten (1975) stated that there is no critical relation between salinity and ostracod ornamentation. Moreover, Keen (1977) believes that the ornamentation variations are related to CaCO₃ content of the water. Studying the relationship between the size of ostracods and water salinity is also a critical subject and it is believed that there is a negative relation between the size of the carapaces and salinity (Van Harten, 1975).

Bryozoans are colonial and filter-feeding marine benthos organisms. Generally, bryozoans live in normal marine water with salinity approximately 35‰, any salinity fluctuations causing bryozoans to decline (Boersma, 1978; Haq and Boersma, 1998). The *Skolithos* ichnofacies is common in very shallow coastal environments (Seilacher, 1967) and also occurs in brackish water settings (Curran, 1985).

Overall, the calcareous mudstone units are interpreted to have been deposited in low-energy muddy hypersaline lagoonal to shallow, normal marine conditions from their lower to upper parts of the succession respectively. This is evidenced by the presence of abundant rotaliids, ostracods and miliolids, lacking high-energy sedimentary structures, the muddy matrix, planar laminations and bioturbations in the lower part, and the increase of normal marine bryozoans, oysters and bioturbation in the upper part of the succession (Figure 3.2).

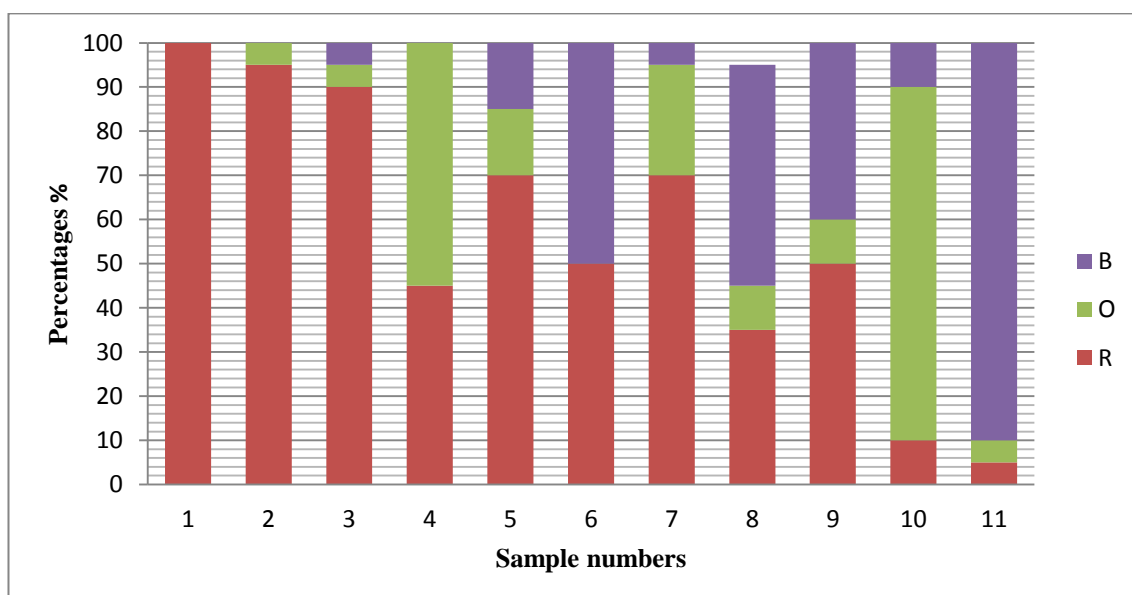


Figure 3-2 A column diagram showing percentages of the extracted fossils from the calcareous mudstone unit from the Mamlaha section. **B:** bryozoas, **O:** ostracods and **R:** rotaliids. The samples are stratigraphically ordered. The percentage of rotaliids is relatively high at the lower part of the succession. However, it becomes low toward the upper part where bryozoan, oyster and bivalve are high.

3.4.2 Carbonate microfacies

The carbonate units range from 0.10 to 5.0 metres thick and comprise 5 to 15.5% of the total succession, from the most distal to proximal parts of the studied areas. They include different textures and structures which vary from fine carbonate units of mudstone and wackestone at the base to packstone, grainstone and rudstone textures at the top. Stromatolite or algal mat structures are present at the top of some carbonate units, as are a varied range of sedimentary structures, including planar and wavy laminations, trough cross-bedding, ripple marks and bioturbation.

Based on the sedimentary structures, facies associations, skeletal and non-skeletal components and diagenetic processes, 21 carbonate microfacies are distinguished, which themselves can be assigned into six microfacies associations: skeletal (SK1-7), mollusc dominated (M1-3), non-skeletal (NS1-7), algal mat (AG1-2), dolomite (D1) and sandy carbonate (S1) (Tables 3.1 and 3.2).

Table 3-1 Microfacies associations and divisions of the carbonate members.

Group Name	Microfacies
Skeletal Microfacies (SK)	1 Mudstone (SK1)
	2 Ostracods wackestone (SK2)
	3 Rotaliids-ostracods wackestone (SK3)
	4 Rotaliids wackestone/packstone (SK4)
	5 Miliolids wackestone (SK5)
	6 Strongly-micritized bioclastic packstone (SK6)
	7 Echinoids wackestone/packstone (SK7)
Molluscs Microfacies (M)	8 Bioclastic gastropods-bivalve packstone (M1)
	9 Bioclastic oyster-barnacles floatstone (M2)
	10 Bivalve float/rudstone (M3)
Non-skeletal Microfacies (NS)	11 Bioclastic peloidal grainstone (NS1)
	12 Faecal pellets grainstone (NS2)
	13 Peloidal-oidal grainstone (NS3)
	14 Bioclastic ooidal grainstone (NS4)
	15 Ooidal grainstone/packstone (NS5)
	16 Coated grains rudstone (NS6)
	17 Intraclasts packstone (NS7)
Algal mats (AG)	18 Microbial laminites (AG1)
	19 Stromatolites (AG2)
Dolomite (D)	20 Dolo-mudstone (D1)
Sandy carbonate (S)	21 Bioclastic calc-arenite (S1)

3.3.1.1 Skeletal microfacies (SK)

This group comprises of different microfacies, based on different skeletal associations and textures. The SK includes rotaliids, miliolids, ostracods and echinoids as the major bioclasts as well as molluscs as minor bioclasts. The bioclasts include both perforated bioclasts (rotaliids, echinoids and bryozoas) and porcelaneous imperforated foraminifera (miliolids, *Peneroplis* and *Borelis*). The microfacies of this group are mostly making up the base of the carbonate units in most of the cycles, except the non-fossiliferous mudstone sub-microfacies, which occurs at the top. The sediments are mostly of well-bedded, white, clean, and fine-grained textures of mudstone and wackestone, with few packstone textures. Very fine laminations and bioturbations are common sedimentary structures in this group. This group of microfacies makes up the lower part of the carbonate units and is comprised of about 15% of the total carbonate microfacies of the succession. It comprises of seven different associations of benthic foraminifera

(rotaliids and miliolids), ostracods and echinoids as the main constituents in different percentages, and textures of mudstone, wackestone and packstone (SK1-SK7).

A. Mudstone microfacies (SK1)

Description

This microfacies included both non-fossiliferous and bioclastic mudstone microfacies, which are characterised by having a very fine texture. Three different sub-microfacies were found within this microfacies, namely Bioturbated mudstone (SK1a), Quartz mudstone (SK1b), and Non-fossiliferous mudstone (SK1c) sub-microfacies.

The SK1a sub-microfacies were common at the base of the carbonate units and was characterised by bioturbated homogenous micritic matrix (Figure 3.12A). Ostracods and miliolids were seen in this microfacies at less than 5% in a muddy matrix (Figure 3.12A). The mud matrix was highly bioturbated, with some unidentified micritized faunas. The rocks were well bedded, very fine with structureless/non-laminated textures. This microfacies was recorded at the base of the carbonate units and it was interbedded with bioclastic wackestone and packstone microfacies.

The SK1b sub-microfacies were characterised by a high percentage of quartz and chert grains (20-30% at average) in muddy to micro-sparitic matrices (Figure 3.12B). The associated bioclasts were oyster shells, ostracods, miliolids and echinoid plates and spines. Bioturbations and pseudomorphs after evaporites weren't available, while micro patches of sparite occurred in some samples. This facies is recorded at the top of the carbonate units in few cycles, with planar and wavy laminated sedimentary structures.

The SK1c sub-microfacies were characterised by laminated fine grain textures without any bioclasts. Quartz and calcite pseudomorphs after both gypsum and anhydrite were very common, represented by lenticular (Figure 3.12D) and lath (Figure 3.12E) crystals for both gypsum and anhydrite, respectively. In addition, large nodular evaporites were common and were dissolved and formed large vugs, 1-3mm in size (Figure 3.12C). Small detritus quartz grains also occurred at an average of 10%. This microfacies was recorded at the middle and top of the carbonate units from Mamlaha and Takiya sections. Occasionally, the sub-microfacies were alternating with very thin laminae of karst subaerial exposures, about 5mm thick (Figure 3.12G-H), and then grading up to stromatolites and algal bindstones at the top of the cycles. Dissolution, dolomitization and cementation were the main diagenetic processes.

Interpretation

Paucity of foraminifera in diversity and abundance, high percentage of muds, no evidences of subaerial exposures and interbedding with lagoonal microfacies (wackestone and packstone) in the SK1a sub-microfacies are evidences for a restricted hypersaline lagoonal depositional environment in the inner ramp. High percentages of terrigenous materials and low abundance of fossils in the SK1b sub-microfacies are indicative of mixed siliciclastic-carbonate rocks in near-coast environments in the inner ramp (Flügel, 2004). Planar and wavy laminations with a high percentage of detritus quartz indicate a medium/high energy setting in near-coast environments. Authigenic evaporite pseudomorphs and fine structureless mud in the SK1c sub-microfacies indicate deposition in a hypersaline lagoon during arid climate. The presence of the evaporite pseudomorphs without any subaerial exposure indicates that the evaporite crystals were probably grown subaqueously because of strong brine refluxes (Becker and Bechstädt, 2006). However, subaerial exposure couplets and interbedding of the sub-microfacies with stromatolites and algal mats from the Takiya section indicate evaporitic tidal-flat mud in an arid climate. Algal laminites commonly interbed with fenestrate mudstone (Nagy *et al.*, 2005). Gypsum-pseudomorphs indicate brine concentrations, with prolonged exposure in supratidal settings (Wright, 1986), and they are features of arid intertidal sediments (Lasemi *et al.*, 2012). These features are characteristic of tidal-flats in the inner ramp.

B. Ostracods wackestone microfacies (SK2)

Description

The major bioclast component present in this microfacies was the ostracods, as they comprised around 10% of the total bioclasts. The ostracods were 300-500µm in size (Figure 3.12F). The associated bioclasts were miliolids and rovaliids. Quartz and chert grains occurred in a lime mud or micro sparitic matrix. Calcite and quartz pseudomorphs after evaporites were also present. Bioturbations and organic matters occurred in the facies. This facies was common and it was seen in most of the sections at the base of the carbonate units.

Interpretation

The abundance of the ostracods was declining from the calcareous mudstone to the carbonate units, in which they occurred in wackestone texture and were associated with rotaliids and miliolids. Reducing ostracods, as well as foraminifera assemblages, from the carbonate units and the associated foraminifera indicate a low energy and hypersaline restricted lagoon. In addition, calcite and quartz pseudomorphs, after gypsum/anhydrite crystals, and bioturbations infer to that restriction in an arid climate. Pseudomorphs after evaporites indicate hypersalinity in the depositional environment (Paszkowski and Szyd³ak, 1986).

C. Rotaliids-ostracods wackestone microfacies (SK3)

Description

This microfacies includes both rotaliids and ostracods as the major components. These bioclasts were dispersed in a lime mud matrix and they comprised about 10% of the facies (Figure 3.13B). The bioclasts were 300-600 µm in size. Quartz, chert, organic matters and pseudomorphs after evaporites were seen in this facies. Miliolids were also present as a minor component. This facies was common and it was recorded in most of the studied sections, such as Takiya and Mamlaha, at the base of the carbonate units. Cementation was the main diagenetic process, which included both ferro and non-ferro calcite cements.

Interpretation

The abundance of lime mud with small benthic foraminifera and ostracods indicate low energy settings. Presence of quartz and chert grains indicates that the depositional environment was shallow and influx of the detritus grains was near. The evaporite pseudomorphs indicate an arid climate. Presence of rotaliids and ostracods in a wackestone texture in a muddy matrix with evaporite pseudomorphs indicate low energy hypersaline shallow lagoon in an arid inner ramp.

D. Rotaliids wackestone/packstone (SK4)

Description

Rotaliids were the main components of this facies (10-30%) in a muddy matrix. They were 400-500µm in diameter. The associated bioclasts were miliolids and echinoids, in

the wackestone texture (Figure 3.13C-D), and miliolids, ostracods and fragments of barnacles, in the packstone texture. Quartz and chert grains were observed in both textures, with impregnated grains with organic matters. In addition, quartz pseudomorphs after anhydrite are available and the original cleavages of the previous anhydrite were preserved. Bioturbations were also common. This facies was common and it was seen in most of the sections, such as Mamlaha, Takiya and Basara. Cementation, dissolution and silicification were the common diagenetic processes in this microfacies.

Interpretation

Rotaliids are hyaline perforate benthic foraminifera and occur in very shallow agitated water at 0-40m depth (Geel, 2000). The representative genera of this group in the carbonate microfacies are *Ammonia*, *Rotalia*, *Neorotalia*, *Pararotalia* and *Elphidium*. The genus *Ammonia* lives in a normal marine to hypersaline lagoon environment at 0-50m water depth and 0-30°C temperature, whereas *Elphidium* occurs in brackish to hypersaline marshes and lagoons at 0-7% salinity and water depth of 0-50m (Murray, 1991). An association of rotaliids (*Ammonia*) and miliolids from a modern hypersaline lagoon in Brazil was recorded (Debenay *et al.*, 2001). In addition, rotaliids and miliolids were recorded separately in two different modern hypersaline lagoons in the Red sea (Hariri, 2008). The author concluded that the water depth of the lagoons was the main factor affecting the distribution of the benthic foraminifera, as the rotaliids live in the deeper (2-14m depth) hypersaline lagoon than miliolids (2m depth).

The associations of the rotaliids group with ostracods, miliolids, *Peneroplis* and *Borelis* in the carbonate wackestone and packstone textures in a muddy matrix indicate low energy hypersaline condition in the inner ramp. This was also evidenced by evaporite pseudomorphs within the microfacies.

E. Miliolids wackestone (SK5)

Description

The SK5 microfacies were very common in most of the studied sections at the base of the carbonate units. Miliolids made the main bioclast component in this facies, about 10-20%, and were 100-300µm in size (Figure 3.13E). The miliolid group observed included different genera, such as *Triloculina*, *Quinloculina*, *Dentritina*, *Peneroplis* and

Borelis, which were scattered in a muddy matrix. This facies was characterised by highly bioturbations and micritizations. It was difficult to recognise the micritized bioclasts. The associated bioclasts were ostracods and rotaliids, which had the same size as the miliolids. This facies was associated with peloidal microfacies on most of the cycles. Micritization of the bioclasts was the main diagenetic process. However, cementation was also common. The lithofacies was of fine to medium texture with bioturbations and organic matters.

Interpretation

Miliolids are a large group of imperforate porcelaneous foraminifera and live in low-turbulence and very shallow waters, from subsaline to hypersaline environments. They are generally used as an indicator of restricted lagoon and hypersaline (Geel, 2000). In addition, miliolids occur in lagoons and shallow nearshore environments down to about 50m (Flügel, 2004). Where they are abundant, they indicate a connection to open ocean (Chassefiere *et al.*, 1969), fore-reefs and shallow lagoons (Schlanger, 1963). In the current study, the wackestone microfacies with miliolids occurred mostly at the base of the carbonate units and were characterised by the presence of different forms of miliolina groups such as *Triloculina*, *Quinloculina*, *Dentritina*, *Peneroplis* and *Borelis*. *Peneroplis*, *Quinqueloculina* and *Triloculina* occur at water salinities of 3.5-5.3%, 3.2-6.5% and 3.2-5.5%, respectively (Murray, 1991). Thus, miliolids wackestone microfacies represent very shallow hypersaline lagoon in the inner ramp and bioturbation and muddy matrix indicate low energy and high nutrition environments.

F. Strongly micritized bioclastic packstone (SK6)

Description

This microfacies is documented from Takiya and Basara sections and is comprised of 2% of the total carbonate microfacies of the succession. It is characterized by intense bioturbation and micritization. The matrix comprises of bioturbated muds and most of the bioclasts are difficult to recognize due to the micritization. However, several miliolids and ostracods were recognized (Figure 3.13F-G). Fenestrate pores are seen between the grains (Figure 3.13F). Micritization and is the main diagenetic process. Quartz grains and evaporite pseudomorphs are absent.

Interpretation

Highly micritized bioclasts and benthic foraminifera such as miliolids and ostracods indicate low energy and well oxygenated conditions (Flügel, 2004). The presence of shallow water foraminifera and low energy mud matrices with fenestrate pores indicate a low energy intertidal setting.

G. Echinoid wackestone/packstone (SK7)

Description

This microfacies is comprised of about 2% of the total carbonate microfacies of the succession. Echinoid fragments of both spines and plates (10 to 20%) are the main bioclasts in a muddy matrix (Figure 3.13H). The echinoid plates are 500 µm to 2 mm in size; echinoid spines are <300 µm. The associated bioclasts in wackestone and packstone textures are miliolids (2%), ostracods (2%) and rotaliids (5%). Detrital quartz and chert grains (5%) occur in this facies. Moreover, cementation of the echinoid spines and plates is the main diagenetic process.

Interpretation

The high percentage of echinoid spines and plates indicates normal marine salinity for the depositional setting (Strasser *et al.*, 1995). The presence of an associated benthic foraminiferal assemblage of miliolids and rotaliids, and ostracods indicates a shallow lagoon but with connection to open marine conditions on the inner ramp.

3.3.1.2 Mollusc microfacies (M)

The microfacies of this group were classified, based on the existence of different mollusc types (Table 3.1). The molluscs reported were bivalves (pelecypods and cephalopods), oysters and gastropods. Barnacles from Arthropods group were also accounted in this group because of their close association with the molluscs. The minor associated bioclasts in this group were miliolids, rotaliids, ostracods, red algae and serpulid tube worm. The lithofacies were characterised by a coarse to a very coarse texture and well to massive bedded fossiliferous carbonate rocks. The molluscs were visible and reached a maximum size of 3.0cm, while the smallest molluscs were 400µm in diameter. However, this group was characterised by several sedimentary structures such as planar and wavy laminations, ripple marks and slight cross-beddings. The microfacies of this group were associated with each other and they were mostly

interbedded with marl. Oriented bivalves and bioclasts were very common in most of the microfacies. Moreover, compaction, dissolution and cementation were very common. Moldic was the main type of porosity within this facies by dissolution of the shell fragments.

A. Bioclastic gastropod-bivalve packstone (M1)

Description

This facies is comprised of about 5% of the total carbonate microfacies of the succession and is seen in the Aj Dagħ and Sangaw sections; gastropods and bivalves are the main component (50 to 60%) (Figure 3.14A-B). The major associated bioclasts are of echinoids and bryozoans and the minor associated bioclasts are miliolids, rotaliids and serpulid worm tubes in a micrite matrix. The bivalve shells have been subjected to micritization and dissolution. Micritic intraclasts, detrital quartz and chert grains are also seen. This lithofacies is characterized as a very coarse (coarse sand size), massive fossiliferous carbonate. Micritic envelopes around the bioclasts are abundant. Cementation and dissolution of the shell fragments are the main diagenetic processes.

Interpretation

The presence of gastropods, together with the microfaunal assemblage, indicates deposition in shallow lagoonal to intertidal settings (Flügel, 2004). The micritic matrix indicates deposition in a low-energy environment. This facies was thus probably deposited in a low energy and very shallow lagoonal setting.

B. Bioclastic oyster-barnacle floatstone (M2)

Description

This facies is comprised of about 5% of the total carbonate microfacies of the succession. It is characterized by abundant barnacles and oysters (20%) which are greater than 2mm in size (Figure 3.14C-D) and associated with bivalves (5%), benthic foraminifera (2%), serpulid tube worms (1%), echinoids (2%), gastropods (2%) and ostracods (2%) in a micrite matrix. The oysters and bivalves have large and complete valves (Figure 3.14E-F). *Ostrea* is the only genus that is recognized within the oysters. The oysters and bivalves are in situ forms and have complete valves, whereas the

barnacles are attached to the oysters and bivalves. Micritic intraclasts, and quartz and chert grains are also abundant. Micritic envelopes around the barnacle and oyster shells are also abundant and the bivalve shells are filled by fine-grained peloidal micrite. The rock is characterized by a very coarse carbonate texture with large oyster and barnacles. This facies is very common and recorded in all of the sections, with 30 to 50 cm-thick carbonate beds. Dissolution and micritization are the main diagenetic processes.

Interpretation

The genus *Ostrea* live in a salinity less than normal marine, typically about 23‰ (Hudson, 1963). Barnacles live in intertidal environments (Flügel, 2004; Ghosh and Sarkar, 2013). Floatstone textures and the associated bioclasts of oysters, barnacles and bivalves in a muddy matrix, together with bioturbation and common micritic envelopes, indicate low to moderate energy conditions. The abundance of the oysters indicates deposition in less than 50 m depth of brackish, nutrient-rich and poorly oxygenated water (Gertsch *et al.*, 2010). In addition, *Ostrea* live in marine water between depths of 0 and 35m (Keen and Coan, 1974). The occurrence of barnacles with the oysters suggests deposition in intertidal to sublittoral waters (Schmitt, 1957) and the presence of micritic intraclasts, quartz and chert grains indicate that the depositional environment was relatively close to the shoreline. The presence of micritic intraclasts suggests syn-depositional erosion of partially lithified sediment and is a common feature of shallow subtidal and peritidal carbonates (Flügel, 2004). The oysters and bivalves acted as a substrate for the barnacles' attachment. Micritic envelopes and infilled bivalves indicate early marine diagenesis. The association of barnacles and oysters with abundant micritic intraclasts suggests deposition in normal marine to low salinity waters in very shallow lagoonal to intertidal settings.

C. Bivalve floatstone/rudstone (M3)

Description

This facies is the most common microfacies in this group and is seen in all the studied sections that composed of about 5% of the total carbonate microfacies of the succession. Bivalve shells are the main component of this facies (80 to 90%). The rudstone microfacies is characterized by very coarse, fossiliferous carbonate, rich in bivalves, in which the bivalves reach up to 15 mm in size (Figure 3.14G-H). The bivalves are well

preserved and many of the bivalves are intact. The associated carbonate components are miliolids, rotaliids, ostracods, gastropods, barnacles, oysters and red algae in sparite matrices. The floatstone microfacies are characterized by scattered bivalve shells in a mud or micro-sparite matrix, with some associated bioclasts comprising echinoid spines and miliolids. In addition, dissolved evaporite rosettes and detrital quartz grains occur in the floatstone texture. Weak planar laminations and ripple marks are seen in the rudstone microfacies. Evidence for dissolution and micritization is very common. The dissolved bivalve shells formed moldic porosity and sometimes are filled with evaporite minerals and calcite crystals. In addition, micritic envelopes, micro-borings, peloidal micrite and detrital quartz grains are very common in this facies. This microfacies is associated with the oyster-barnacle floatstone microfacies where it makes up the top of a carbonate unit.

Interpretation

The presence of large bivalves in a rudstone texture indicates wave-agitated, nearshore environments (Flügel, 2004). The lack of mud and presence of ripple marks indicate deposition and winnowing above the fair-weather wave base (Flügel, 2004). The preservation of large and complete bivalves in combination with oysters indicates in situ accumulation of skeletal materials. However, the floatstone textures with evaporite rosettes indicate lower energy environmental settings.

3.3.1.3 Non-skeletal microfacies

This group of microfacies included non-skeletal and coated grains and micritic intraclasts. The NS microfacies were very common in the formation in all the studied sections. It was characterised by different textures of packstone, grainstone and rudstone. The microfacies were classified based on the type of grains and textures into peloids, ooids and intraclasts (Table 3.1). The rocks of this group are recognised by coarse and fine grains. In ooid microfacies, the rocks were characterised by a coarse texture with the presence of different sedimentary structures such as stylolites, planar laminations, ripple marks, trough cross beddings and cross beddings. However, the peloid microfacies were characterised by a fine to medium texture and grey to dark grey carbonate rocks that contained very fine planar laminations, graded beddings and bioturbations.

The microfacies of the NS group were associated with each other and with skeletal microfacies (SK1-SK7) in most of the cycles. The peloidal microfacies were mostly making up the middle of the cycles and graded up gradationally to ooidal microfacies at the top of the cycles.

A. Bioclastic peloidal grainstone (NS1)

Description

This facies was very common in the formation and it was seen in all of the studied sections. The peloids comprise 50-60% of facies components. They were 200-500 μ m in size. Based on the associated bioclasts, three bioclastic peloidal grainstone sub-microfacies were recognised: 1) Bivalve-peloidal grainstone (NS1a), 2) ostracods-peloidal grainstone (NS1b), and 3) Bioclastic-peloidal grainstone (NS1c) sub-microfacies.

The main components of the NS1a sub-microfacies are peloids and bivalves. The bivalves are 2mm in sizes and make 10-20% of the facies (Figure 3.15A). The peloids are 100-200 μ m in size and make up 70-80% of the facies. The peloids and bivalves are dispersed in a sparitic matrix. This facies was recorded in Sangaw and Mamlaha sections in a laminated massive carbonate unit. Micritic envelopes around the bivalves, peloidal micrite and bioturbations were very common. Occasionally, the bivalves and peloids were oriented.

The NS1b sub-microfacies were characterised by presence of poorly sorted and oriented ostracod fragments in a sparitic matrix (Figure 3.15B). The ostracods reached 500 μ m in diameter and formed 20-30% of the facies. Peloids were also available and were <250 μ m in size and constituted 60-70% of the facies. The grainstone texture of the oriented ostracods and peloids changed to a mudstone texture and an irregular boundary separated the two texture types (Figure 3.15C). The sub-microfacies was recorded in Takiya and Basara sections in a thin carbonate unit within the calcareous mudstone units.

Different associated bioclasts are available in the NS1c sub-microfacies, which are echinoids, miliolids, rotaliids, bryozoas, oysters, barnacles and ooids that are dispersed in a sparitic matrix (Figure 3.15D). In some samples, the original structures of the bioclasts/ooids were preserved and transitional changes were visible in others (Figure

3.15F). The peloids were 200-600µm in size and constituted 30-40% of the facies. The major bioclasts were echinoid plates which were partially or totally micritized and were >500µm in diameter and formed 30-40% of the facies. The ooids were radial in shape and <250 µm in size and constituted around 10% of the facies (Figure 3.15E). In some samples, the grains were oriented and formed moderately sorted textures. These sub-microfacies were recorded in Krbchna section in the upper part of the formation.

Interpretation

The peloids resulted from partial or total micritization of bioclasts and ooids. This type of peloid resembles the Bahamite peloids in the modern Bahama Banks (Flügel, 2004). However, those peloids which originated from micritizing ooids have also been called *pseudopeloids* (Flügel, 2004). High abundance of bivalve shells and peloids and poorly sorted fabric in the NS1a sub-microfacies suggests moderately energy conditions in the shallow lagoon. The abundance of peloids, micritic envelopes and peloidal micrite and lack of mud indicate algal origins and relatively moderate energy.

The predominance of ostracods, the poor sorting and lack of mud in the NS1b sub-microfacies are suggestive of a shallow lagoon environment. The irregular boundary and facies changes suggest storm deposit between the fair-weather wave base and storm wave base.

The peloids in the NS1c sub-microfacies were probably resulted from micritization of the pre-existing bioclasts/ooids as some of these bioclasts/ooids were partially or totally micritized. The peloids which were originated by micritizing bioclasts resemble the Bahamite peloids in the modern Bahama Banks, while the peloids originated from micritizing ooids are called pseudopeloids (Flügel, 2004). The bioclasts indicate normal marine salinity by presence of high percentage of echinoids (Strasser *et al.*, 1995). The absence of mud, the moderately sorted grain sizes, presence of small foraminifera, grainstone texture and highly diversity of different groups of fauna indicate that the facies was deposited in very shallow settings within fair-weather wave base. Moreover, the absence of mud and the grainstone texture indicate moderate/high energy conditions. Imbrications and orientations of the grains in some samples suggest possible proximity to wave ripples and relatively shallower positions.

B. Faecal pellet grainstone microfacies (NS2)

Description

This facies is comprised of about 2% of the total carbonate microfacies of the succession and is recorded from the Takiya, Basara and Darbandikhan sections. Faecal pellets are characterized by dark, rounded to elongate shapes and medium to well sorted grains (Figure 3.16A). The pellets are less than 300 µm in size and make up 80 to 90% of the rock. Bioclasts are very rare in this facies; however, a few miliolids and *Dentritina* are noted. Rarely, large micritic intraclasts up to 4 millimetres are seen, with large pelleted grains up to 1.5 mm in size. In addition, coarse graded bedding together with planar laminations rarely occurs. Authigenic evaporite minerals also occur. This facies occurs in three sequential cycles in the upper part of the formation; each cycle commences with a calcareous mudstone unit at its base, passing up to a fine calc-arenite microfacies, then to the laminated faecal pellet grainstone microfacies (Figure 3.15G-H). Each of the three cycles is capped by the red continental facies.

Interpretation

Pellets are ovoid to ellipsoidal grains of muddy carbonate sediments and range from few hundred microns up to several millimetres in size. Faecal pellets may be produced by gastropods, worms and shrimps. They commonly form in a wide range of shallow water environments and are preserved in lower energy muddy depositional settings. They dominantly form in subtidal and lower intertidal coastal settings in low-energy zones with a reduced sedimentation rate (Flügel, 2004). Laminated structures in fine to medium sand sized pellets indicate moderate to high energy subtidal to intertidal, lagoonal to back-shoal settings. The pellet preservation indicates very low sedimentation rates and early cementation (Tucker and Wright, 1990). The laminated structure of the pellets in the current study is interpreted to indicate low energy conditions in a lagoon with low sedimentation rates and early cementation. Associated miliolids and *Dentritina* species lead to the inference of a restricted lagoon. Well preserved planar laminations indicate a lack of bioturbation by organisms.

C. Peloidal-oidal grainstone (NS3)

Description

This facies is common in most of the studied sections and is comprised of approximately 3% of the total carbonate microfacies of the succession. It is characterized by micritized and concentric ooids with dark faecal pellets (Figure 3.16B). The faecal pellets form 50% and the ooids form 40% of the microfacies in a sparitic matrix. The ooids are 200 to 600 μm in size and are moderately sorted. Some of the ooids are concentric normal ooids; however, the other ooids are micritic and superficial ooids. The nuclei of the ooids are faecal pellets but most of the ooids' nuclei are dissolved and form a good secondary porosity in the rock. The faecal pellets are smaller than the ooids (100 to 400 μm) and are dark and rounded, and elongate or rod-shaped. Bioclasts and detrital quartz grains are very rare. The rocks of this microfacies is characterized by medium to coarse sand-grade carbonates and are associated with the NS1, NS4 and NS5 microfacies in most of the sections. This facies comprises the middle of the carbonate units of most of the cycles. Stylolitization, cementation, dissolution and micritization are the main diagenetic processes.

Interpretation

The association of this facies with bioclastic ooidal and ooidal grainstone microfacies, the presence of pellets, the lack of mud, the presence of ooids and the poor to moderate sorting indicate moderate energy conditions in the shoreface zone or at the edges of sand shoals, above the fair-weather wave base on the inner ramp.

D. Bioclastic ooidal and ooidal packstone and grainstone (NS4-NS5)

Description

This microfacies is comprised of approximately 10% of the total carbonate microfacies of the succession and is recorded in all the studied sections as outlined in Table 2. Generally, two variations of the bioclastic and ooidal grainstone microfacies were identified based on the type of matrix; mud (NS4) and sparite (NS5) matrices. The bioclastic-ooidal packstone and grainstone (NS4) microfacies are characterized by an abundant muddy matrix with different bioclasts (10%) and normal ooids (80 to 90%), together with varied sedimentary structures; cross bedding (Figure 3.17E-G) and trough cross bedding. In addition, micritic envelopes around the ooids and bioclasts are very common, envelopes which show irregular contacts between the micrite and the ooid/bioclast surfaces (Figure 3.16C). These irregular contacts represent micro-borings

on the surfaces of the ooids/bioclasts. Meniscus cements are occasionally available between the grains (Figure 3.16D).

The ooids (NS4) are mostly between 300 and 500 μm (Figure 3.16E and 3.18A-B). They are rounded to ellipsoidal in shape and exhibit medium to good sorting. In addition, they are mostly normal ooids (on average 90%) with a few micritized, distorted (Carozzi, 1961b) and superficial ooids (10%). However, rarely, the ooidal microfacies includes up to 80 to 90% of distorted, superficial, and micritized ooids. The ooids have concentric laminae with only a few micritized ooids and they occur in a sparitic matrix. The distorted ooids (Figure 3.16G) are flattened and joined together in pairs or chains (zig zag). Foraminifera (Figure 3.16E), quartz (Figure 3.18A), chert, pellets and molluscs make up the nuclei of the ooids, which are mostly dissolved and form good secondary porosities. However, the nuclei of some ooids are filled with micritic cements (Figure 3.16E). Ooid aggregates (Figure 3.16F) are also seen and these are >2 mm in size and include different coated grains and bioclasts. Dissolution, micritization, cementation, and pressure solution in the form of stylolites are the main diagenetic processes. In addition, micro-stylolites are also seen where thin sections cut the ooids along the stylolite surfaces. Meniscus, peloidal and micritic cements are the main diagenetic cements in the facies. Partial micritization occurs along the cortices or nuclei of the ooids. However, in some samples total micritization has occurred. The meniscus cements bridge the ooids and any bioclasts (Figure 3.16H). Micritic cements filled the nuclei of the ooids and peloids that are mostly 20 to 40 μm in size are dispersed in the sparitic matrix. The rocks of this microfacies are characterized by coarse to very coarse carbonates with varied sedimentary structures including planar laminations, wavy laminations, ripple marks (Figure 3.17C-D), trough cross-bedding (Figure 3.17A-B), together with post-depositional horizontal and vertical stylolites (Figure 3.17H). This microfacies is common close to the top of the carbonate units of most of the cycles and is associated with microfacies NS1 and NS3 in most of the sections.

The ooidal packstone microfacies are not common and are only seen in two cycles in the Mamlaha and Takiya sections. It is characterized by the presence of ooids (50 to 60%, on average) with bivalve shells in a muddy matrix.

Interpretation

Modern ooids are commonly deposited in marine and non-marine settings at water depth of 1 to 5 metres, up to a maximum 10 to 15 metres, in subtropical and tropical waters at temperature usually between 18 and 20° C (Rameil, 2005), in intertidal and upper subtidal environments (Flugel, 2004). They form in high energy wave-agitated and lower energy marginal settings. Ooids are common in the studied succession and form packstone and grainstone textures, but the grainstone textures are more common. The ooids are of different types (concentric, micritized and distorted), with different types of cortices (normal and superficial), and matrices (mud and sparite). These criteria indicate differing depositional settings for the ooids but normal concentric ooids in sparite matrices are the most abundant. Locally, in some samples the ooids are superficial in type and form packstone and grainstone textures in muddy matrices (NS4). These criteria indicate a more quiet and protected environment. However, most of the ooids from the studied succession are rounded in shape, normal and concentric in type and from 300 to 500 µm in size (NS5). These features indicate shallow marine and high energy conditions, in which the ooids were influenced by wave and current action (Flugel, 2004). Field observations of cross bedding, trough cross-bedding, planar laminations and ripple marks also indicate deposition above the fair-weather wave base. Medium to well-sorted grains and grainstone textures of the ooids are typical of being winnowed under wave current action. Meniscus cements between the ooids and bioclasts indicate very early diagenetic cementation and meteoric, vadose freshwater diagenesis and subaerial exposure (Inden and Moore, 1983; Strasser, 1986; Strasser *et al.*, 1995; Flugel, 2004). Peloidal cements and micritic envelopes indicate early marine cementation. The presence of micritic envelopes with micro-borings and coated grains indicate constant wave action at or above wave base and occur in current-washed sand shoals of inner ramp environments (Flugel, 2004). The association of the ooids with peloids and benthic foraminifera, the marine-phreatic and meteoric cements, and the observed sedimentary structures are, together, indicators that the ooidal microfacies accumulated along sand shoals or beaches.

E. Coated grain rudstone (NS6)

Description

This facies is recorded in the Takiya section in the middle part of a carbonate unit and is comprised of about 2.5% of the total carbonate microfacies of the succession. This microfacies includes 50% bioclastic coated grains, 10% serpulid tube worms,

gastropods and bivalve shells (20%) in a sparitic matrix. The other grains are intraclasts. The coated grains are irregular and compacted in shape and about 1 to 3 mm in size (Figure 3.18C-E). They have thin concentric laminae with dissolved and micritized nuclei. Bioturbation, peloidal micrite and micrite envelopes are abundant in this facies. The serpulid tube worms are elongate in shape and about 1 to 2 mm in length. The rocks of this microfacies are very coarse carbonate rocks in which the coated grains are very visible in the field samples. This facies is associated with mudstone, algal laminites and stromatolitic microfacies. Dissolution, micritization and cementation are the common diagenetic processes.

Interpretation

The abundance of large coated grains in sparitic matrix indicates moderate energy in a nearshore shallow lagoon of an inner ramp (Flügel, 2004).

F. Intraclast packstone (NS7)

Description

This microfacies is very common in most of the studied areas such as the Mamlaha, Darbandikhan, Krbchna and Chnarah sections and is comprised of about 2.5% of the total carbonate microfacies of the succession. The micritic intraclasts (20 to 30%) are characterized by being poorly sorted, semi-oriented, irregular in shape and of various sizes (Figure 3.18F-H). In some samples, intraclasts range from 100 to 1000 μm in size; in others from 100 to 500 μm . In the former type, the intraclasts are associated with gastropods, barnacles, and oysters with a few benthic foraminifera and quartz grains. However, in the second type; the intraclasts are mainly associated with benthic foraminifera such as miliolids and with ostracods. Fenestrate pores are seen between the grains. Quartz grains are absent. Micritization is the main diagenetic process. Evaporite pseudomorphs are absent.

Interpretation

Intraclasts originate from the syn-depositional erosion of partially lithified sediment and are a common feature of shallow subtidal and peritidal carbonates (Flügel, 2004). Moreover, fenestrate pores indicate deposition in intertidal settings. The presence of larger intraclasts with the associated bioclasts and quartz grains indicate a shallower

setting than the smaller intraclasts with benthic foraminifera. Thus, the intraclast packstone microfacies were deposited in very shallow lagoonal to intertidal settings in the inner ramp depositional environment.

3.3.1.4 Algal mats

This group of microfacies was common in the formation and making up the top of the carbonate units in the cycles. The rocks of this group were characterised by being thin (10-30cm) and dark grey in colour with wavy and planar laminations and dome structures. This group of microfacies was associated with dissolved micro nodular evaporites and calcite/quartz pseudomorphs after evaporites. Calcite and quartz lenticular crystals are pseudomorphs after gypsum, while lath and acicular crystals are pseudomorphs after anhydrite. In some cases, a half of the lenticular crystals were cemented by calcite while the other half was cemented by quartz mineral. In addition, the original cleavages of the gypsum were preserved after replacing by quartz grains. Two types of algal mats were recognised based on the algal structures: microbial algal bindstone microfacies (AG1) and stromatolites (AG2).

A. Microbial algal bindstone (AG1)

Description

This facies is recognized based on visible laminations which include very small peloids (10-30 mm) due to algal activity (Figure 3.19B-C). It is recorded in most of the studied sections at the top of some of the carbonate units of the cycles, comprising 5% of the total carbonate microfacies of the succession. It is characterized by dark grey, fine-grained carbonate rocks with planar laminations (Figure 3.19D-F). Calcite and quartz pseudomorphs after gypsum and anhydrite are very common in this facies, as are fenestrate pore. This facies is associated with stromatolites in the Takiya section, but in the Mamlaha section they form thin carbonate units 0.2 to 0.3 m thick below the evaporite units. This facies in the Takiya section is associated with thin, vuggy carbonates, which represent a short period of exposure at the top of this facies, at the base of evaporate units.

Interpretation

This type of rock is a common facies in arid intertidal to supratidal depositional settings; for example, it occurs in the arid Trucial Coast (Kinsman and Park, 1976). Laminated algal bindstone with authigenic evaporitic minerals, fenestrate structures and associations with stromatolites and chicken-wire evaporites indicate upper intertidal settings in an arid climate (Kendall *et al.*, 2002; Flugel, 2004). The short-lived subaerial exposure above the associated stromatolite with this facies is consistent with an intertidal setting.

B. Stromatolites (AG2)

Description

The stromatolite microfacies are recorded at the top of the carbonate unit and comprised of about 5% of the total carbonate microfacies of the succession. Two types of stromatolites are recorded in the current study: the first one (AG2a) is a domal fenestrate algal bindstone and is interbedded with mudstone microfacies in the Takiya section (Figure 3.20A). The rocks of this facies are characterized by fine, dark grey carbonate rocks with visible dome structures and laminations. The fenestrate pores become larger toward the top (Figure 3.20B-D). In addition, the laminations are cut by a subaerial erosion surface at the top. This type of stromatolite overlies the laminated quartz mudstone microfacies (SK1-3) in a thick carbonate unit. The thickness of the stromatolite is 10 cm.

The second type (AG2b) is wavy-laminated, with interbedded couplets of muddy and sparite laminae (Figure 3.20F), and with lenticular (Figure 3.20H) and acicular (Figure 3.20G) evaporitic minerals which indicate authigenic evaporitic minerals, as seen in the Mamlaha section. It includes micritized ooids and acicular evaporite crystals in the muddy laminae. This type of stromatolite occurs in a cycle which begins with a calcareous mudstone unit at the base and passes up to the stromatolite (0.1 m thick) and then the overlying evaporite unit (Figure 3.20E).

Interpretation

Ancient and modern analogues indicate that stromatolites usually grow in the intertidal to supratidal zones, and also the subtidal zone (Tucker and Wright, 1990). They grow in the subtidal zone when the activity of the grazers and burrowers is reduced, at a maximum depth of 4 to 5 metres. However, intertidal to supratidal stromatolites are

characterized by desiccation features, high salinity, and high temperatures which are unfavourable for animal grazer activities (Kinsman and Park, 1976; Hoffman, 1976b; Tucker and Wright, 1990). Modern flat-laminated structures of stromatolitic and microbial origins occur in lower intertidal settings in arid climates in the Persian Gulf and Shark Bay (Kinsman and Park, 1976; Hoffman, 1976b; Flugel, 2004). Fenestrate structures, subaerial exposure, authigenic evaporitic minerals and associations with algal mats and nodular evaporites at the top of the carbonate units all indicate intertidal settings in an arid climate (AG2a). The same facies of stromatolites and algal laminites was observed in the Fatha Formation in the basin centre (Shawkat and Tucker, 1978; Shawkat, 1979). Moreover, fenestrate mudstones, stromatolites and microbial laminites are recorded from the Oligocene-Miocene Asmari Formation in Iran by many authors (Amirshahkarami *et al.*, 2007; Vaziri-Moghaddam *et al.*, 2010; Amirshahkarami, 2013). The second type of stromatolite (AG2b), with no evidence of subaerial exposure, is interpreted to have been deposited in a low energy restricted lagoon.

Table 3-2 Descriptions and interpretations of the carbonate microfacies.

microfacies	Description	Physical structures and geometries	Interpretation
1- Skeletal microfacies group (15% of the total carbonate microfacies)			
Mudstone (SK1)	SK1a: Bioturbated mudstone sub-microfacies: lime mud matrix, ostracods and miliolids.	Highly bioturbated mud and very fine texture, non-laminated and structureless.	Low-energy restricted hypersaline lagoon. Inner ramp.
	SK1b: Quartz mudstone sub-microfacies: Mud to micro sparite matrix. 20-30% of quartz and chert grains with oysters, ostracods, miliolids and echinoid plates and spines.	Thin beds of 10-40cm with planar and wavy laminations.	Mixed siliciclastic-carbonate coastal environment. Inner ramp.
	SK1c: Non-fossiliferous mudstone sub-microfacies: lime mud matrix, evaporite pseudomorphs, dissolved large vugs of nodular evaporite and quartz and chert grains (10%).	Thin, very fine textures and structureless. Exposure couplets and planar laminations.	Hypersaline restricted lagoon. Intertidal. Inner ramp.
Ostracods wackestone (SK2)	Mud and local micro sparite matrix. Major component: ostracods (10%). Minor component: miliolids and rotaliids. Quartz and chert grains and evaporite pseudomorphs.	20-50cm thick beds. Bioturbations.	Low energy hypersaline restricted lagoon. Inner ramp.
Rotaliids-ostracods wackestone (SK3)	Lime mud matrix, rotaliids and ostracods (10%) and miliolids. Quartz, chert and evaporite pseudomorphs.	20-50cm thick beds. Bioturbations.	Low energy hypersaline restricted lagoon. Inner ramp.
Rotaliids wackestone/packstone (SK4)	Lime mud and local micro sparite matrix. Rotaliids (10-30%), ostracods, miliolids and few barnacles. Quartz, chert and evaporite pseudomorphs.	Medium beds 20-40cm thick. Bioturbations.	Low energy hypersaline restricted lagoon. Inner ramp.

Miliolids wackestone (SK5)	Lime mud matrix, miliolids (10%), ostracods and rotaliids. Micritised unidentified bioclasts.	20-50cm thick beds. Bioturbations and micritisation.	Low energy restricted lagoon. Inner ramp.
Strongly micritised bioclastic packstone (SK6)	Bioturbated mud matrix, unidentified micritised bioclasts with few ostracods and miliolids.	10-30cm thick beds with highly bioturbations.	Low energy and well oxygenated lagoon to intertidal. Inner ramp.
Echinoids wackestone/packstone (SK7)	Mud matrix, echinoid spine and plates, oysters, bryozoas, bivalves, miliolids, ostracods and rotaliids. Quartz and chert grains.	10-20cm thick beds. With local bioturbated mud.	Low energy open lagoon. Inner ramp.
2- Mollusc microfacies group (25% of the total carbonate microfacies)			
Bioclastic gastropods-bivalves packstone (M1)	Micrite matrix. 50-60% gastropods and bivalves. Minor component: echinoids, bryozoas, miliolids, rotaliids and serpulids. Quartz and chert grains.	Coarse carbonate facies and 50-60cm thick beds. Bioturbations, micritic envelopes and micritic intraclasts.	Low energy shallow lagoon. Inner ramp.
Oyster-barnacles floatstone (M2)	Mud and local sparite matrix. Oysters, bivalves, barnacles, serpulids, echinoids and bryozoas. Quartz and chert grains.	40-50cm thick and coarse carbonate with bioturbations. Micritic intraclasts and micritic envelopes.	Low energy and low salinity conditions. Shallow lagoon to intertidal settings. Inner ramp.
Bivalve floatstone/rudstone (M3)	Mud and sparite matrices. Bivalves, rotaliids, miliolids, ostracods, gastropods, barnacles, oysters and local red algae. Local echinoids and evaporite rosettes. Quartz grains.	Very coarse 20-50cm thick carbonate. Local planar laminations and ripple marks.	High energy and wave-agitated skeletal shoreline.
3- Non-skeletal microfacies group (30% of the total carbonate microfacies)			
Bioclastic peloidal grainstone (NS1)	NS1-1: bivalve peloidal grainstone: sparite matrix. Bivalves (10-20%) and peloids (70-80%). Few miliolids, rotaliids, lithoclasts, quartz, chert,	Coarse and thick bed (50-60cm) of oriented and laminated carbonate bed. Bioturbations.	Moderate energy shallow lagoon. Inner ramp.

	gastropods and barnacles.		
	NS1-2: Ostracods peloidal grainstone: sparite matrix. Ostracods (20-30%) and peloids (60-70%).	20-40cm thick beds. Oriented and poor sorting grains.	Moderate energy shallow lagoon. Inner ramp.
	NS1-3: Bioclastic peloidal grainstone: sparite matrix. Peloids, echinoids, rotaliids, miliolids, ostracods, ooids, gastropods, oysters, barnacles and bryozoas.	Thick beds (40-50cm) of coarse carbonate. Oriented and moderately sorting.	Moderate energy in shallow lagoon with open marine connection. Inner ramp.
Faecal pellets grainstone (NS2)	Sparite matrix. Pellets (80-90%). Few miliolids. Local evaporite pseudomorphs.	Thin bed (10-15cm). Planar laminations. Well sorting.	Low energy restricted lagoon with low sedimentation rate.
Peloidal ooidal grainstone (NS3)	Sparite matrix. Peloids/pellets (50%), ooids (40%) and rare bioclasts.	20-40cm thick beds and coarse. Slightly cross beddings. Bad sorting.	Moderate energy, edges of sand shoals and shoreface zone.
Bioclastic ooidal grainstone (NS4)	Mud matrix. Ooids (50-60%). Micritic and superficial ooids. Bivalves, miliolids, rotaliids and gastropods. Ooid aggregates and intraclasts. Meniscus, peloidal and micritic cements and micritic envelopes and micro borings.	Beds of 30-50cm thick and coarse carbonate. Laminations cross beddings and trough cross beddings. Stylolites.	Moderate energy, edges of sand shoals and beaches. Inner ramp.
Ooidal grainstone (NS5)	Sparite matrix. Normal and concentric ooids (80-90%). Foraminifera, quartz, chert and pellets nuclei of the ooids. Meniscus, peloidal and micritic cements and micritic envelopes.	Beds of 30-50cm thick and coarse carbonate. Laminations cross beddings, trough cross beddings and ripple marks. Stylolites.	High energy sand shoals and beaches. Inner ramp.
Coated grains rudstone (NS6)	Sparite matrix. Coated grains (50%), serpulids, gastropods, bivalves and intraclasts. Peloidal micrite and micritic envelopes.	Very coarse carbonate of 30cm thick. Bioturbations and laminations.	Moderate energy shallow lagoon. Inner ramp.

Intraclasts packstone (NS7)	Mud matrix, intraclasts (50%), gastropod, barnacles, oysters, miliolids and oyster. Quartz grains.	Medium to coarse carbonate bed (around 40cm thick). Fenestrate pores.	Very shallow lagoon to intertidal settings. Inner ramp.
4- Algal mat microfacies group (10% of the total carbonate microfacies)			
Algal bindstone (AG1)	Algal laminites. Fenestrate pores, evaporite pseudomorphs and quartz.	Beds of 10-30cm thick. Dark grey and fine carbonate. Planar laminations. Exposure surfaces.	Intertidal zone. Inner ramp.
Stromatolites (AG2)	AG2a: domal fenestrate algal bindstone. Evaporite pseudomorphs. Fenestrate pores. Exposure couplets.	10cm thick beds. Domal and wavy laminations. Exposure surfaces.	Intertidal zone. Inner ramp.
	AG2b: Wavy laminated of interbedding couplets of muds and sparite laminae. Evaporite pseudomorphs. Ooids and acicular evaporite crystals.	10cm thick bed. Wavy laminations.	Restricted lagoon.
5- Dolo-mudstone microfacies group (5% of the total carbonate microfacies)			
Dolomudstone (D1)	10-20µm dolomite crystals (90-95%).	High porosity rock.	Intertidal zone. Inner ramp.
6- Sandy-carbonate microfacies group (15% of the total carbonate microfacies)			
Bioclastic calc-arenite (S1)	Mud and sparite matrices. Quartz, feldspar minerals, lithoclasts, miliolids, rotaliids, ostracods, barnacles, bivalves, echinoids and oyster.	10cm-1m thick beds. Laminations, cross beddings, ripple marks, flute casts and load casts. Graded beddings and bioturbations.	Marginal marine and coast environments. Inner ramp.

3.3.1.5 Dolo-mudstone microfacies (D1)

Description

The dolo-mudstone microfacies are characterized by fine dolomite crystals which are approximately 10 to 20 μm in size, with high porosities (Figure 3.19A). This facies is recorded at the top of the carbonate units from the Takiya and Mamlaha sections and is associated with the evaporite units. It is comprised of about 5% of the total carbonate microfacies of the succession.

Interpretation

The association of dolomite with nodular evaporites and chicken-wire structures is very common in the modern upper intertidal and lower supratidal zone of the arid Trucial Coast (Alsharhan and Kendall, 2003). Fine grained dolomite and associated evaporites in the Fatha Formation are interpreted to indicate the upper intertidal zone.

3.3.1.6 Sandy carbonate, bioclastic calc-arenite microfacies (S1)

Description

This facies is characterized by mixed siliciclastic and carbonate components and is comprised of about 15% of the total carbonate microfacies of the succession. The grain sizes vary from fine sand to coarse sand and are associated with different bioclasts such as miliolids, rotaliids (Figure 3.21C), ostracods (Figure 3.21D), barnacles, bivalves, echinoids (Figure 3.21A), and oysters. Quartz (Figure 3.21E) and chert grains, feldspar minerals (Figure 3.21E), lithoclasts, bioclasts and organic matters are the main components of the facies. The thickest unit of this facies is recorded from the more proximal locations represented by the Basara and Darbandikhan sections. Toward the more distal, southwest area of the basin, this facies is not preserved. The thickness of this facies reaches a maximum in the Basara section of about 3.5m. However, it is just 0.1 to 0.3 m thick in the Mamlaha section. Toward the Darbandikhan section (proximal area) the facies becomes more abundant. The rocks of this facies are characterized by a grey-dark grey to greenish colour with micro planar laminations (Figure 3.21G), cross bedding, graded bedding (Figure 3.21F), and borings (Figure 3.21B). Additional sedimentary structures are flute casts, load casts, asymmetrical mega-ripple marks and planar laminations. The amplitudes of the preserved ripple forms are up to 10 cm.

Interpretation

The sandy calcarenite microfacies with these sedimentary structures such as planar laminations, cross bedding and ripple marks indicate deposition above the fair-weather wave base in an area influenced by wave action in a marginal inner ramp setting (Thrana and Talbot, 2006). The predominance of quartz, chert, feldspar minerals and lithoclasts with different bioclasts indicates mixed carbonate-siliciclastic facies near the shore line and source areas. The presence of high amplitude mega-ripples indicates high energy wave agitated, very shallow environments near the coastline.

3.4.3 Evaporite facies

Evaporites are an important component within the Fatha Formation, being associated with the carbonates and calcareous mudstones within the cycles, and comprising 15 to 43% of the total succession, from the most distal to proximal parts of the studied area. The thickest evaporite succession was deposited toward the basin. The thickness of the unit in the cycles is between 1 and 10 metres. The lower boundary of each evaporite with underlying units has been observed in detail. In a few cycles the boundary consists of interbedding of several thin beds of gypsum and bluish grey calcareous mudstones as a transitional zone between the calcareous mudstone and gypsum, whereas in most cycles, the boundary is at the top of an underlying calcareous mudstone or carbonate, without the transitional zone. In the formation, two main evaporitic facies are recorded, laminated (LE) (Figure 3.23) and nodular gypsum (NE) (Figure 3.22A-D), but as a whole, nodular gypsum (comprising chicken-wire, CH and enterolithic, EN textures) is more dominant.

3.4.3.1 Nodular evaporites (NE)

Description

The NE is a thick evaporitic body (1.0-10.0m) with nodular appearance and makes up the top of the calcareous mudstone and carbonate units. The nodules display variations in size (few millimetres to 10cm) and shape, usually irregular and occasionally elongated and spheroidal. The colour is generally milky white with patchy bluish grey tones. The matrix around the nodules is composed of bluish grey carbonate mudstone. In some places, the nodules coalesce to form contorted folded layers of enterolithic evaporites (EN). The lower boundary of evaporite with its underlying units has been

observed in detail. In a few cycles, the lower boundary with the underlying calcareous mudstone consists of several interbedding thin beds of gypsum and bluish grey calcareous mudstones as a transitional zone between them (Figure 3.22D). In other cycles, the boundary consists of either calcareous mudstone or carbonate without the transitional zone. The main evaporitic mineral in the outcrops is gypsum (Figure 3.22F), while both halite and anhydrite minerals were recorded from the bore well in the basin centre (Al-Juboury and McCann, 2008). Petrographically, the nodular gypsum forms a chicken-wire structure between the gypsum mineral and mudstone and forms an irregular tight folding in enterolithic evaporites. In some cases, dolomite crystals are associated with the nodular evaporites (Figure 3.22E).

Interpretation

The depositional setting of the evaporites is controversial because of the presence of huge amount of chicken-wire structure. However, not all nodular evaporites are deposited in sabkha settings because it might have been formed during burial diagenesis (Machel and Burton, 1991). The sabkha nodules must associate with intertidal stromatolites, algal laminites, dolomites, fenestrate pores, tepee structures and mud cracks. In addition, they interfinger with hypersaline lagoonal deposits, intertidal and subtidal deposits (Warren and Kendall, 1985; Warren, 1989). Therefore, the depositional settings of the calcareous mudstone and carbonate units are a very important tool for determining the depositional environment of the evaporites. The nodular evaporites are typical facies of the supratidal portion of a coastal sabkha, which grow in highly saturated water pores of the capillary zone (Warren, 2006). The distribution and presence of evaporite in the cycles varies in different parts of the basin. In the most proximal areas, close to the hinterlands, evaporite is lacked and the cycles are more clastic-dominated, for example, in Chnarah section. However, toward the basin centre, the evaporite is frequently increased in number and thickness. The Fatha succession comprises of approximately 15-43% of evaporite in the studied sections, while this ratio is increasing toward the basin centre. In addition, different evaporite facies are documented from the basin centre, for example; massive evaporite, selenite and satin-spar, nodular evaporite (chicken-wire structure), laminated evaporite and halite (Al-Juboury and McCann, 2008).

Two depocentres, Sinjar (NW Iraq) and Kirkuk (middle of Iraq), were developed during the Fatha deposition in Iraq and were extended to Syria and Iran, respectively (Aqrawi

et al., 2010). In addition, six syn-tectonic sedimentary sub-basins were recognised along the Zagros foreland basin during the Gachsaran deposition (Bahroudi and Koyi, 2004) and these sub-basins were separated by palaeo highs. The Fatha Formation and its equivalent Gachsaran Formation in Iran were deposited in these sub-basins. The study area is situated at the margin of the Kirkuk depocentre.

Based on the evaporite facies and carbonate microfacies, it can be interpreted that the evaporite was deposited in different settings subaerially and subaqueously. The evaporite was deposited subaqueously in a restricted saline basin and subaerially in a supratidal sabkha setting around the basin margin. The position of the evaporite nodules at the top of the cycles, interfingering with intertidal stromatolite/algal mats, hypersaline lagoonal and shallow coastal deposits lead to the conclusion that the evaporites nodules were deposited in supratidal sabkha setting in an arid climate.

3.4.3.2 Laminated evaporites (LE)

The laminated evaporite (LE) occurs at the top of the calcareous mudstone/carbonate units and was documented just in a cycle from the studied areas (Figure 3.23). This facies is about 1m thick in all the studied areas and consists of thin laminae of gypsum and carbonate. Individual evaporite/carbonate laminae range in thickness from a few millimetres to 1cm (Figure 3.23C-D). The laminae are planar or wavy laminated between gypsum minerals and mudstone (Figure 3.23G-H). Under the microscope, the laminated evaporite facies consists of thin layers of carbonate mudstone, alternating with granular gypsum laminae (Figure 3.22G-H). The gypsum laminae consist of layers of granular gypsum of silt to fine sand sizes. This facies is about 1m thick in the whole areas and extended laterally along more than 100 km in length and can be used as a marker bed for correlation. However, individual laminae are not traceable laterally.

Interpretation

Laminated evaporites have been discussed by many researchers. Some authors considered a detrital origin for the lamination (Garrison *et al.*, 1978), while others favour reworking of gypsum during storms (Hardie and Eugster, 1971). Kendall (1978b) interpreted these laminae as storm deposits which formed during flooding of an evaporitic tidal-flat.

In the margin of the Miocene evaporitic basin in the current study, the LE was documented in just one cycle that extended along the whole areas for more than 100km wide. The large covering area of the LE leads to the conclusion that this facies was formed during flooding of the sea upon the evaporitic supratidal setting. The sea water covered the supratidal sabkha and laminated evaporite was deposited in the flooding depressions and pools. The laminated evaporite was also recorded from the Fatha Formation in the other parts of the Zagros foreland basin in Iraq and Iran (Shawkat and Tucker, 1978; Tucker, 1999; Aqrabi *et al.*, 2010). Moreover, the same facies was documented from different part of the world, for instance: Holocene evaporite sequences in the Gulf of Suez, Egypt (Aref *et al.*, 1997), coastal hypersaline pools of the Red Sea (Kushnir, 1981), the Messinian evaporite of the Mediterranean basin (Ogniben, 1955; Hardie and Eugster, 1971; Garrison *et al.*, 1978).

3.4.4 Red clastic facies (RC)

Description

This facies is makes up the top of the cycles and comprises 40-78% of the total succession, from the most distal to proximal parts of the studied areas. It is comprised of red claystone (Figure 3.24A), red or greyish siltstone, and green or red sandstone. The thickness of the unit varies from 0.5 to 6 metres in the lower part of the Fatha Formation and from 2 to 8 metres in the upper part of the succession. Typical grain size varies from the lower to the upper parts of the formation, siltstone and sandstone increasing toward the upper part. The claystone and siltstone are characterized by a red colour with fine laminations and rare cross bedding in the latter (Figure 3.24B-C). The sandstone is characterized by planar laminations, wavy laminations (Figure 3.25A), cross bedding (Figure 3.25B-C), ripple marks (Figure 3.25D-F), flute casts (Figure 3.25G) and load casts (Figure 3.25H). Bioturbation in the form of vertical, horizontal and inclined burrows increases in the upper part of siltstone and fine sandstone beds; recognized ichnofacies include *Skolithos* (Figure 3.24E-G) and *Rhyzolithos* (Figure 3.24H).

Generally, different clastic lithofacies may be differentiated: red claystone (C); laminated red siltstone (LS); cross bedded sandstone (CS); trough cross bedded sandstone (TS); rippled sandstone (RS); massive sandstone (MS); *Rhyzolithos*-rich sandstone (RhS) and highly bioturbated mottled mudstone-siltstone (HM).

Interpretation

The red claystone (C) and laminated red siltstone (LS) lithofacies were deposited in continental areas, for which sediment was sourced from the adjacent hinterlands of the Zagros Mountains; deposits represent the distal parts of alluvial fans. The sandstone lithofacies (CS, TS and RS) were deposited in higher energy fluvial parts of the system, and are most commonly developed in the upper part of the succession. The highly bioturbated mudstone-siltstone lithofacies (HM) that comprises sandstone with *Skolithos* and *Rhyncholithos* (RhS), and which is present in the clastic parts of cycles in the uppermost part of the succession, may indicate palaeosol development influenced by a more humid climate (Seilacher, 1967), possibly on floodplains between the fluvial channels.

3.5 Fatha Formation cyclicity

The Miocene Fatha Formation in the Kurdistan region is represented by repeated carbonate-evaporite cycles, the study of which has been enabled by the detailed analysis of widespread outcrops arranged in a NW-SE orientation across the foreland of the Zagros Mountains. The nature of the cyclicity of the carbonate-evaporite units is clearly observed across the Zagros foreland basin (James and Wynd, 1965). Each cycle is defined by a marine flooding surface at its boundary. The arrangement of lithofacies within each cycle is indicative of upward shallowing and progradation.

Cycles in the marginal parts of the basin are characterized internally by bluish-grey to greenish calcareous mudstone at their base. This passes up into shallow marine carbonate deposits that are themselves capped by nodular evaporite deposits. In the proximal areas (studied areas), continental red siliciclastic units prograded basinward to form the uppermost parts of some of the cycles.

In the studied area, completely developed cycles comprise four major units: calcareous mudstone (13 to 24%), carbonate (5 to 15%), evaporite (15 to 43%) and continental red clastic (40 to 78%) units, from base to top of each cycle (Figure 3.4). However, towards the basin centre, to the southwest, the preserved facies expression of cycles is more varied and demonstrates that the basin was repeatedly evaporative, such that it accumulated thick gypsum, anhydrite and halite deposits (Aqrabi *et al.*, 2010).

The cycles from the lower member of the basin centre succession (which lacks the red siliciclastic deposits) include calcareous mudstones, carbonates and evaporites (Al-

Mubarak and Youkhana, 1977; Taufiq and Domas, 1977). The evaporite facies change from nodular to laminated (bedded) evaporites or salt at the top of the cycles (Tucker, 1999). In the upper member of the formation in the basin centre (characterized by the presence of red siliciclastic deposits), the evaporites are nodular and capped by red claystone unit.

Overall, the analysis of the microfacies demonstrates that the Fatha Formation in the studied area represents a shallow marginal and shoaling upwards marine to continental succession, both at the scale of individual cycles and at the scale of the entire formation. The number of preserved cycles increases from the basin margin towards its centre. About to 12 to 40 cycles were identified in the study sites (Figure 3.4). However, in the Chnarah section, the site closest to the basin margin, a reduced number of cycles (10 to 12 cycles) were identified and these were without evaporites (Figures 3.4 and 3.5).

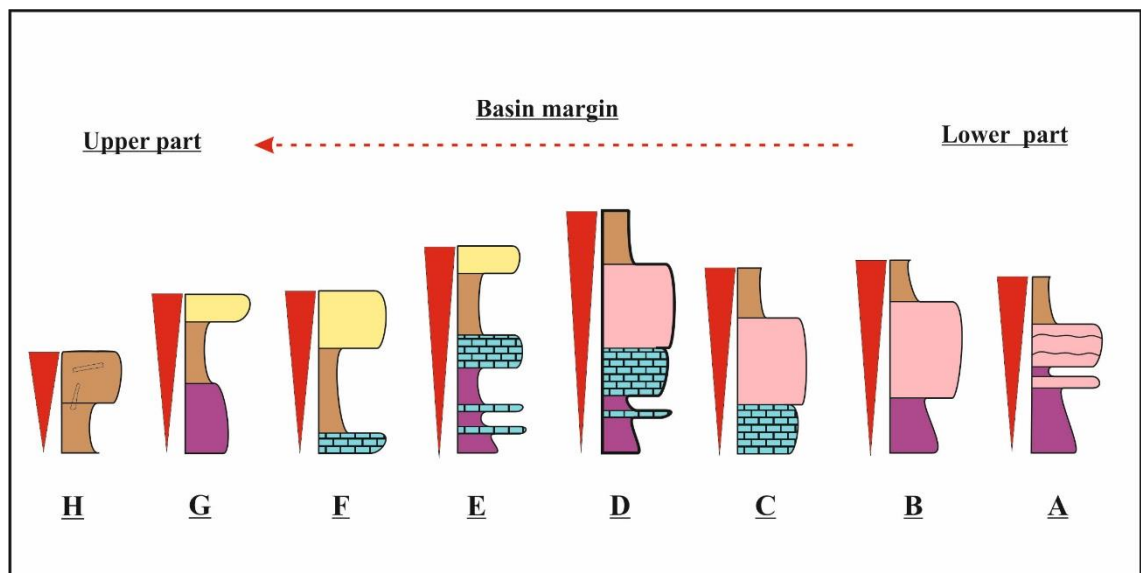


Figure 3-3 Variations of the carbonate-evaporite cycles of the Fatha Formation from the lower to upper parts of the succession. The cycles, as well as the marine deposits, become thinner toward upper part, and the evaporite deposits are ceasing.

Significantly, in all the studied sections, the nature of cyclicity changes from the lower to the upper part of the succession in terms of both preserved thickness and internal facies composition. Notably, the proportion, preserved thickness and grain size of the red continental clastic units that define the uppermost parts of the cycles increase toward the upper part of the formation, whereas the proportion of marine deposits decreases (Figures 3.3 to 3.5). The red continental clastic units vary as a percentage of the total formation from the sites closest to the basin margin (78%) to the sites closest to the basin centre (40%). Thus, the facies trend of the formation changes from marine

dominance in the lower part, to a transitional zone in the upper part, and then to fluvial dominance in the Injana Formation that overlies the Fatha Formation. In general, the preserved trend is that of a basinal shallowing-upward and associated progradation of a shoreline from the basin margin towards its centre. This is observed clearly both within each individual cycle and across the multiple vertically to progradationally stacked cycles of the entire formation.

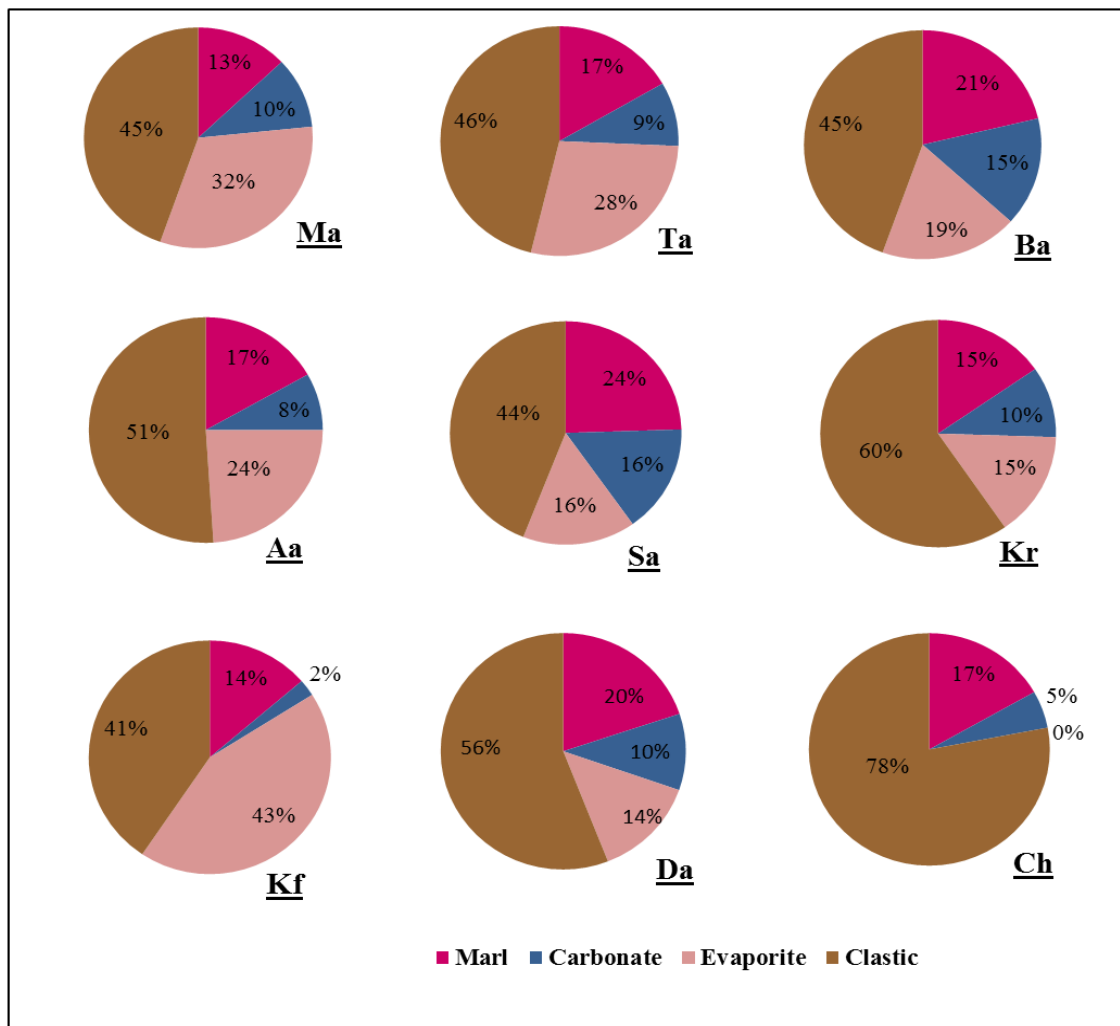


Figure 3-4 Two dimensional pie diagrams showing the percentages of the sedimentary facies, which are making the cycles from all the studied sections. The percentages of evaporite deposits are increasing toward the basin centre. In contrast, the percentages of clastic deposits are decreasing. Ma: Mamlaha; Ba: Basara; Ta: Takiya; Aj: Azh-Dagh; Sa: Sangaw; Da: Darbandikhan Dam; Kr: Krbchna; Kf: Kfri and Ch: Chnarah sections.



Figure 3-5 Bar diagrams between cycle numbers and thickness of the cycles from all the studied sections; Ma: Mamlaha; Ba: Basara; Ta: Takiya; Aj: Azh-Dagh; Sa: Sangaw; Da: Darbandikhan Dam; Kr: Krbchna; Kf: Kfri and Ch: Chnarah sections.

3.6 Variations in carbonate-evaporite ramp models

The Fatha Formation was deposited as a mixed carbonate-evaporite succession with a secondary siliciclastic supply derived from basin margin areas. Based on detailed microfacies analysis, several related and more detailed environmental settings have been recognized: open lagoon, hypersaline to restricted lagoon, shallow lagoon, sand shoals and beaches, intertidal flat, tidal flat, supratidal sabkha, supratidal ponds, alluvial coastal plain, channels and alluvial plains with palaeosols. These represent different hydrodynamic conditions ranging from low-to-moderate to high wave energies and from quiet to storm-affected shorelines and coastal plains. Siliciclastic supply from the hinterland to the basin progressively increased over time, as recorded by the increasing proportion of continental facies in higher parts of the formation. These variations are expressed in the cyclical nature, as well as in the overall progradational nature of the formation.

- i. **Lateral variations.** Lateral variations within the sedimentary units are revealed by the microfacies analysis. Although the carbonate and evaporite units are laterally traceable for tens of kilometres between the studied sections, microfacies analysis reveals local lateral variations within the sedimentary basin for about 10 to 15km lateral scale. For this purpose, the carbonate microfacies are analysed in detail to detect lateral variations.
- ii. **Change in water depth over time.** Evidence for changes in water depth is observed throughout the succession, notably in the calcareous mudstone and carbonate units. Variations in the microfacies succession of the calcareous mudstone units are expressed chiefly by changing fossil content: the rotaliids group tends to decline in abundance from the lower to upper part of the formation; conversely, the percentage of bryozoans, bivalves and oysters increases toward the upper part (Figure 3.2). Ostracods vary in percentage terms in the cycles and include both smooth and nodulose forms. Based on the fossil percentages represented graphically through the succession in the Mamlaha area (Figure 3.2), it can be demonstrated that the water depth that prevailed at the time of accumulation of the calcareous mudstone units changed from relatively deep in the lower part of the formation to relatively shallow in the upper part, as demonstrated by the gradual decline of rotaliids and the increase of bryozoans, bivalves and oysters (Figure 3.2). Variation in water depths represented by the

carbonate units may also be inferred through the succession. Overall, these changed from mainly hypersaline to restricted deeper lagoons in the lower part to shallower lagoons and coastal settings in the upper part of the succession.

- iii. **Change in salinity over time.** The abundance of rotaliids and miliolids at the lower part of the succession, and declining them through the succession are possibly indicative of salinity variations through time. Rotaliids and miliolids are indicative of hypersaline restricted lagoons and are documented from a number of modern hypersaline lagoons (Abou-Ouf *et al.*, 1988; Hariri, 2008; Mohamed *et al.*, 2013). This group of microfossils are declining through the succession, and stenohaline fauna (bryozoan), normal marine fauna (oyster) and brackish water ichnofacies (*Skolithos*) become abundant toward the upper part of the formation (Figure 3.2).
- iv. **Carbonate thickness over time.** The carbonate units vary in thickness and frequency towards the upper part of the succession. The maximum preserved thickness of carbonate units (5 m) is recorded in the lower to middle part of the succession. By contrast, carbonate units are only 0.1 to 0.2 m thick in the upper part.
- v. **Increasing siliciclastic input over time.** Siliciclastic units increase in thickness, grain size and frequency upwards within the succession, with different types of ichnofossil such as *Skolithos* and *Rhyzolithos*, and sedimentary structures becoming more common. Red claystone (RC) is present in every cycles from the lower part of the succession; while towards the upper part, higher energy siltstone and sandstone components increase.

In general, the facies changes observed record a transition from a fully marine carbonate-evaporite setting in the lower part, to a transitional between marine to fluvial settings in the upper part, and then to fluvial deposits of the Late Miocene Injana Formation. These variations are also recorded from the Miocene equivalent units in Iran from Gachsaran Formation of supratidal sabkha origin (equivalent to the Fatha Formation), to the Agha Jari Formation of fluvial origin (equivalent to the Injana Formation) (Pirouz *et al.*, 2011).

3.7 Discussion

The mixed carbonate-evaporite ramp deposits in the proximal areas of the Mesopotamian Basin were evidently subject to dramatic and frequent variations in depositional settings toward the top of the formation where siliciclastic deposits predominate. This variation is clearly observed from the lower to upper part of the succession. It records the progradation into the basin of siliciclastic detritus of continental origin. This significantly affected carbonate production and evaporate precipitation.

Each cycle from the lower part of the succession typically passes from a calcareous mudstone unit at its base, to a shallowing-up carbonate package, and then to massive nodular evaporite that is itself capped by a red continental clastic units in many examples. This facies trend changes toward the upper part of the succession in which the marine deposits are reduced in thickness.

Based on the results of this study, each cycle is shown to represent a regressive trend from calcareous mudstone at its base, grading up to shallow marine carbonates, and then to sabkha evaporites. The red clastic deposits prograded toward the basin and capped the evaporites at the top of each cycle. A new depositional model has been presented for the Fatha Formation for first time in this study and is illustrated in Figure 3.6. The depositional model has been constructed based on the outcomes, including the interpretations of the sedimentary facies and lateral/vertical variations of the cycles, of this study. Moreover, the lateral/vertical variations of the cycles has been shown in the model from marginal to basinal part of the basin. The sedimentary facies has been summarized as the following:

The calcareous mudstone units (CM) at the base of the cycles were deposited in a low energy hypersaline lagoonal environment, as evidenced by hypersaline benthic foraminifera (rotaliids and miliolids) and ostracods. However, this depositional setting became gradually shallower through time toward the upper part of the succession, in which normal marine water and stenohaline organisms (bryozoa), oysters and brackish water ichnofacies (*Skolithos*) became more abundant.

The carbonate sediments were deposited in a variety of environments along the basin margin including both low and high energy hydrodynamic settings. The detailed

microfacies thus represent lateral variations in the extent and morphology of the lagoonal complexes developed on the basin margin. The length scale of these variations was less than the spacing of the measured sections, as it is not consistently possible to trace individual microfacies from one section in any one cycle to the equivalent cycle in an adjacent section. This lateral variation in lagoonal and nearshore environments at a scale of tens of kilometres is represented in cartoon form in Figure (3.6).

The skeletal mudstone, wackestone and packstone microfacies (SK1-SK7) at the base of the carbonate units represent deposits of still-restricted hypersaline environments as evidenced by the presence of restricted foraminifera (rotaliids and miliolids) and ostracods with evaporite pseudomorphs that indicate hypersalinity. The mollusc microfacies (M1-M3) represent very shallow water systems developed in shallow lagoons to intertidal or skeletal shoal settings. The deposition of skeletal peloidal and pelleted grainstone microfacies (NS1-NS2) occurred in moderate energy shallow lagoons. Sand shoals separated the restricted lagoons from the open ocean where non-skeletal microfacies (NS3-NS5) were deposited, including peloidal, and ooidal packstone and grainstone microfacies. Along parts of the shoreline in protected embayments, algal bindstone and stromatolites (AG1-AG2) were deposited in the intertidal zone of restricted lagoons.

The evaporite sediments at the top of the carbonates represent a regressive facies and were deposited in a variety of environments. The main abundant evaporite facies is nodular; including chicken-wire (CH) and enterolithic (EN) evaporites resulting from subaerial deposition in a coastal sabkha. Such nodular evaporites originate from repeated arid and high rainfall episodes when the original gypsum crystals formed within the capillary groundwater zone undergo repeated hydration and dehydration (Schreiber and Tabakh, 2000). Laminated evaporites (LE) were subaqueously deposited during flooding over the tidal flat. These emergent evaporites present at the basin margin contrast markedly with subaqueous evaporites identified previously from basin-centre settings, where laminated selenite evaporites and halite were deposited (Al-Juboury and McCann, 2008).

The initial accumulation of siliciclastic deposits derived from the hinterlands during the Miocene occurred during deposition of the Fatha Formation when the red clastic units started to prograde south-westward into the basin. The south-westward progradation and shoreline migration into the basin through time is represented by the overall variation in

thickness of the preserved succession from the basin margin to its centre: a thinner succession comprising fewer cycles is recorded at the basin margin. In addition, siliciclastic-dominated cycles are preserved around the basin margin and evaporite-dominated cycles were best developed in the basin centre. The presence of climatically wet hinterlands and significant fluvial activity around the basin margin and its late-stage progradation towards the basin centre eventually resulted in a progressive termination of evaporite deposition, from a basin-margin to a basin-centre setting over time.

A number of factors acted to influence sedimentation rates and the position of the shoreline through time. Marine-marginal sabkha deposits can prograde with a thickness of 1m by 1km of shoreline migration per thousand years (Schreiber and Hsü, 1980). Progradation may lead to a seaward thickening succession of peritidal facies (Hardie, 1986). Furthermore, reduced evaporite deposition and increased fluvial activity from the basin margin through time – illustrated by coastal progradation – may also have been driven by an overall climate change from relatively arid to relatively more humid. Overall, progradation of the siliciclastic wedge progressively replaced carbonate-evaporite sedimentation in the basin and changed the system to an overfilled fluvial basin by the late stages of Fatha deposition, after which fluvial facies of the overlying Injana Formation became dominant.

Tectonics, sediment supply and relative sea level determined accommodation in the basin and collectively acted to determine the overall progradational (i.e. regressive) geometry of the formation. The position of the Miocene foreland basin meant that it was subjected to collisional forces between the Arabian and Eurasian plates. Increasing siliciclastic supply would have resulted from erosion of the uplifted areas of the developing fold and thrust belt. Indeed, the shallowing-upward trend of the Fatha Formation is typical of foreland-basin fills, indicating the significance of tectonic setting on basin stratigraphy (Baars and Stevenson, 1982; Sami and James, 1994; Brown, 2002). A high rate of sediment supply outpaced the generated accommodation space across the basin.

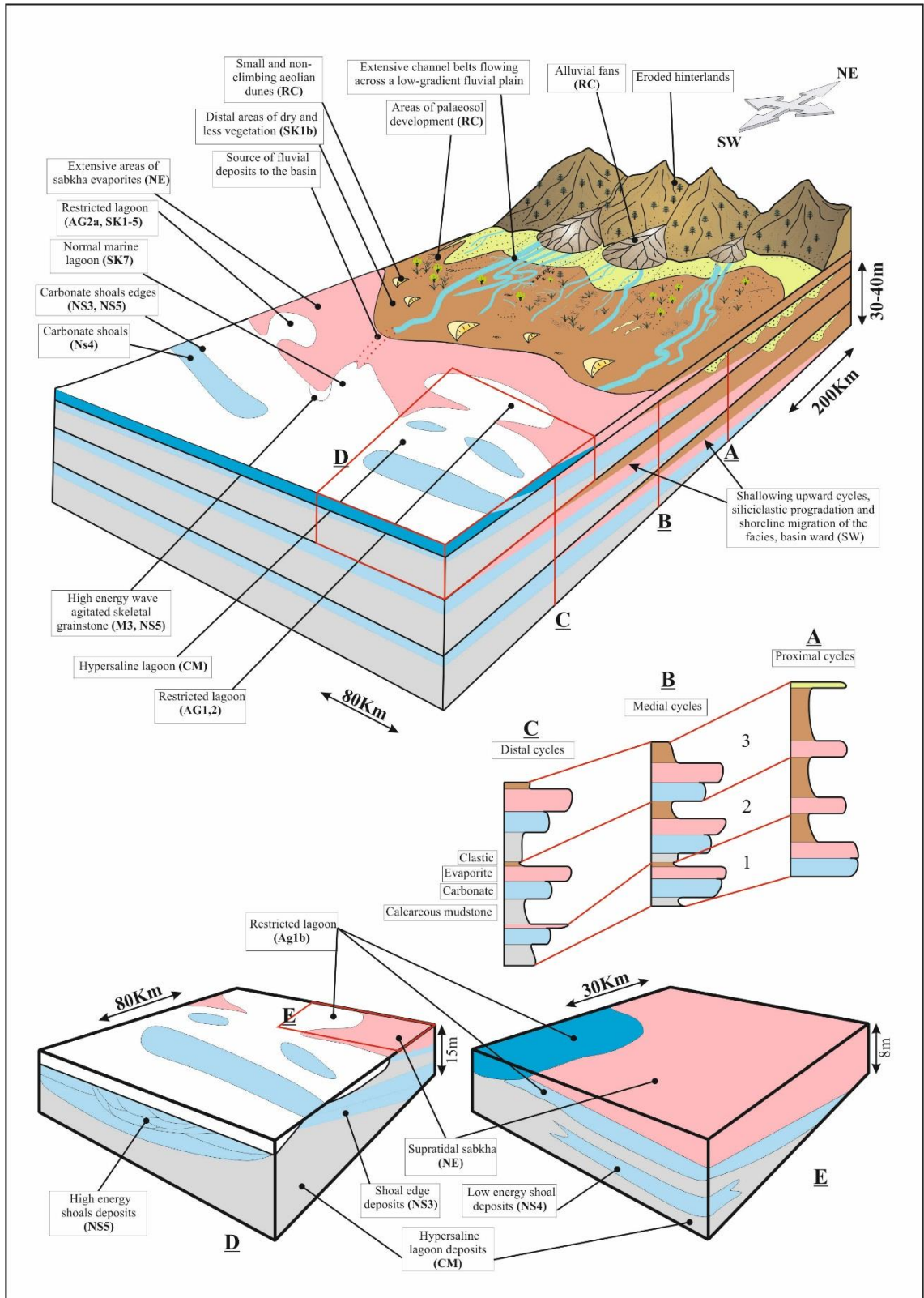


Figure 3-6 The depositional model of the Fatha Formation showing different depositional environments on a gently ramp platform. The model is presenting the progradation and migration of the Miocene shoreline along three vertical sections A, B, and C. In addition, D and E block diagrams are maximized to show detailed depositional settings of two cycles and to represent the lateral variation possible within these.

3.8 Conclusion

Deposition of the Miocene carbonate-evaporite cycles in the Kurdistan region from the Zagros foreland basin are interpreted to have accumulated in a very low angle ramp setting in which only inner ramp facies are recognized in the carbonate phase of each cycle. The carbonate ramp is recognized on the basis of lateral and vertical variations of the facies from relatively more offshore deposits of calcareous mudstone to shoreline and sabkha deposits closer to the basin margin. The main lithofacies divisions are calcareous mudstones, carbonates, evaporites and red siliciclastics. These facies are arranged in a number of cycles, each of which records a shallow upward trend. Cycles are capped by flooding surfaces. Each preserved depositional cycle has a facies arrangement which in its lower part is indicative of low-energy calcareous mudstone accumulation, and which passes up to moderate- to high energy shallow marine carbonates, which are in turn overlain by nodular evaporites and, in some cases, are capped by a red siliciclastic unit at the top of the cycle. Different carbonate environmental settings are recognized along the basin margin. Shoreline deposits range from high energy rippled and cross bedded carbonate grainstones to low energy stromatolite facies of protected embayments in a complex and laterally extensive lagoonal system. The vertical and lateral variations of the microfacies in an individual cycle and between the cycles have features in common. These features include microfacies variations in an upward shallowing trend within each cycle.

The succession overall records a progradational shallowing upward succession. The preserved facies trend through the succession can be regarded as being due to a combination of variations in sea level, salinity, climate, carbonate-evaporite production, siliciclastic supply, tectonic subsidence rate and tidal flat progradation. The cycles can be traced and correlated regionally along the NW-SE trend of the foreland basin. The overall up-succession variation in facies was driven by increasing siliciclastic supply from the uplifting Zagros Mountains due to the collision between the Arabian and Iranian plates. As a result, a siliciclastic alluvial depositional system advanced into the basin causing regression of the shoreline. This may have been due to a progressive increase in relief or, additionally, to an increasingly humid/wet orographic climate response that could have been induced by the tectonic growth of the Zagros Mountains.

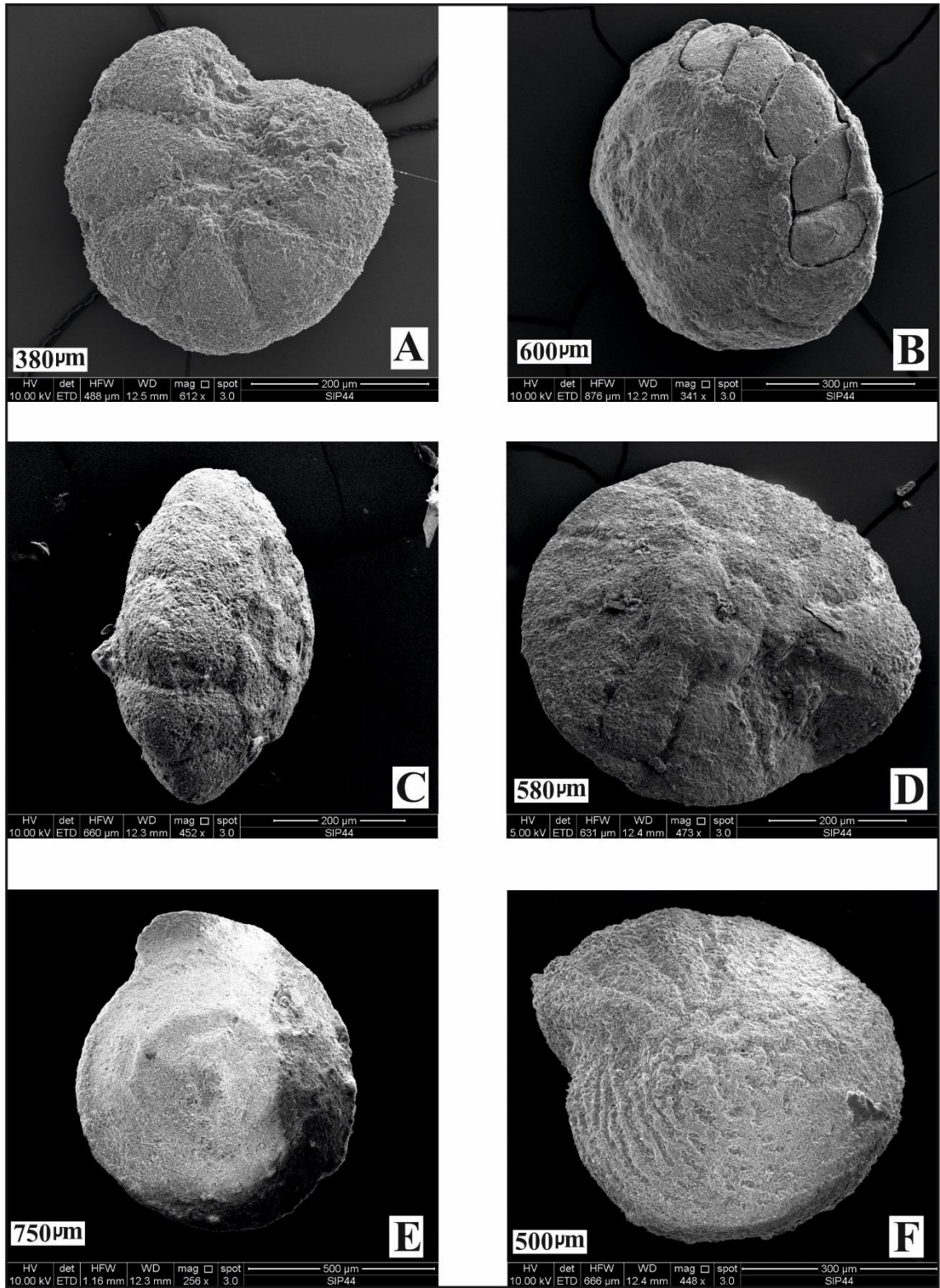


Figure 3-7 Scanning electron photomicrographs of the rotaliids foraminifera from the calcareous mudstone units of the Fatha Formation.

A to E: Different species of *Ammonia* from different areas. F: An *Elphidium* species from Mamlaha section.

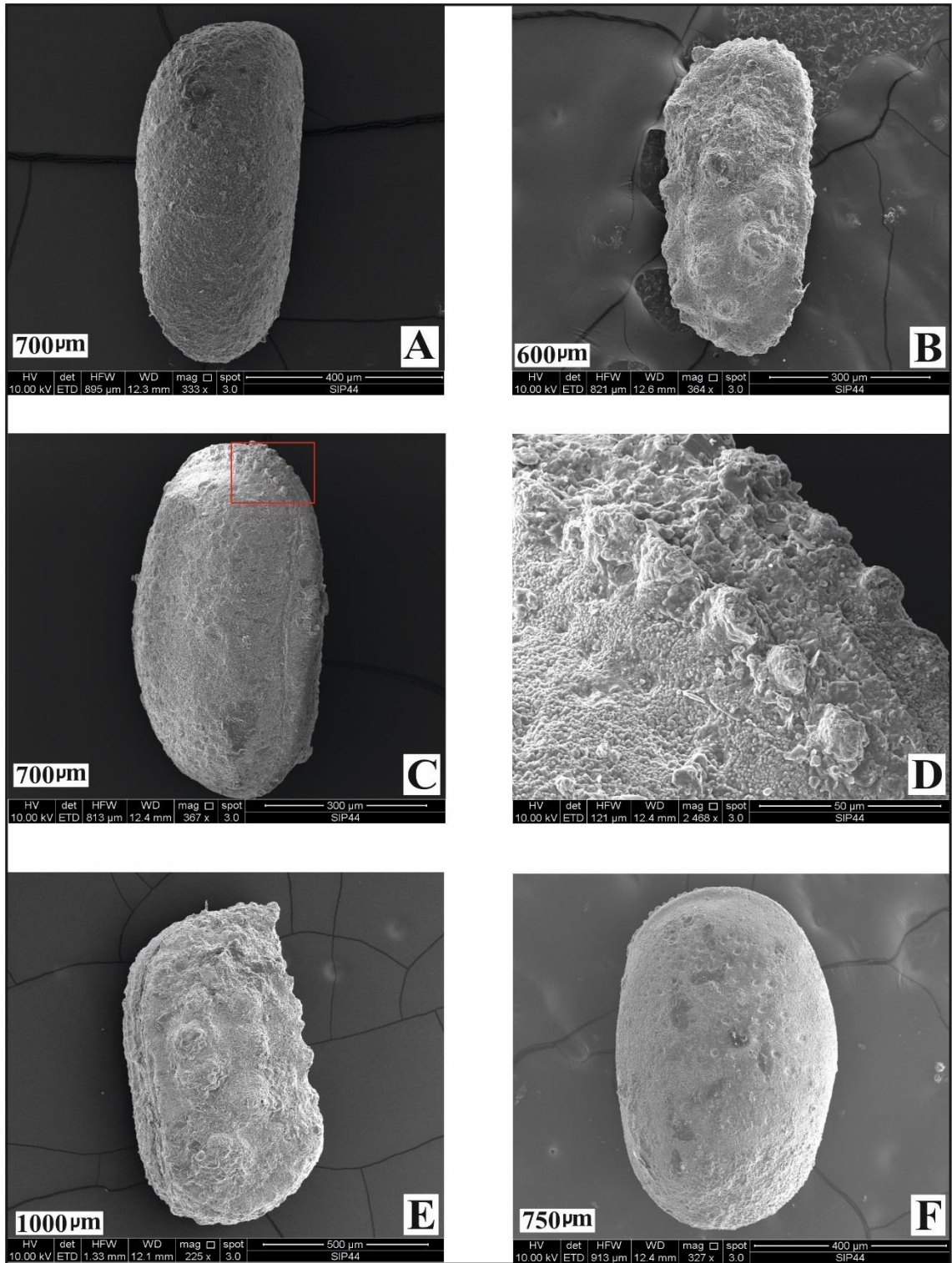


Figure 3-8 Scanning electron photomicrographs of the ostracod specimens from calcareous mudstone units of the Fatha Formation.

A: A smooth ornamented ostracod specimen (700µm) from Mamlaha section. B: A highly ornamented ostracod specimen (600µm) from Basara section. C: A moderate ornamented ostracod specimen (700µm) from Mamlaha section. D: A closer view of the ornamentation of the previous sample (red square) from Takiya section. E: A highly ornamented ostracod specimen (1000µm) from Mamlaha section. F: A moderate ornamented ostracod specimen (750µm) from Sangaw section.

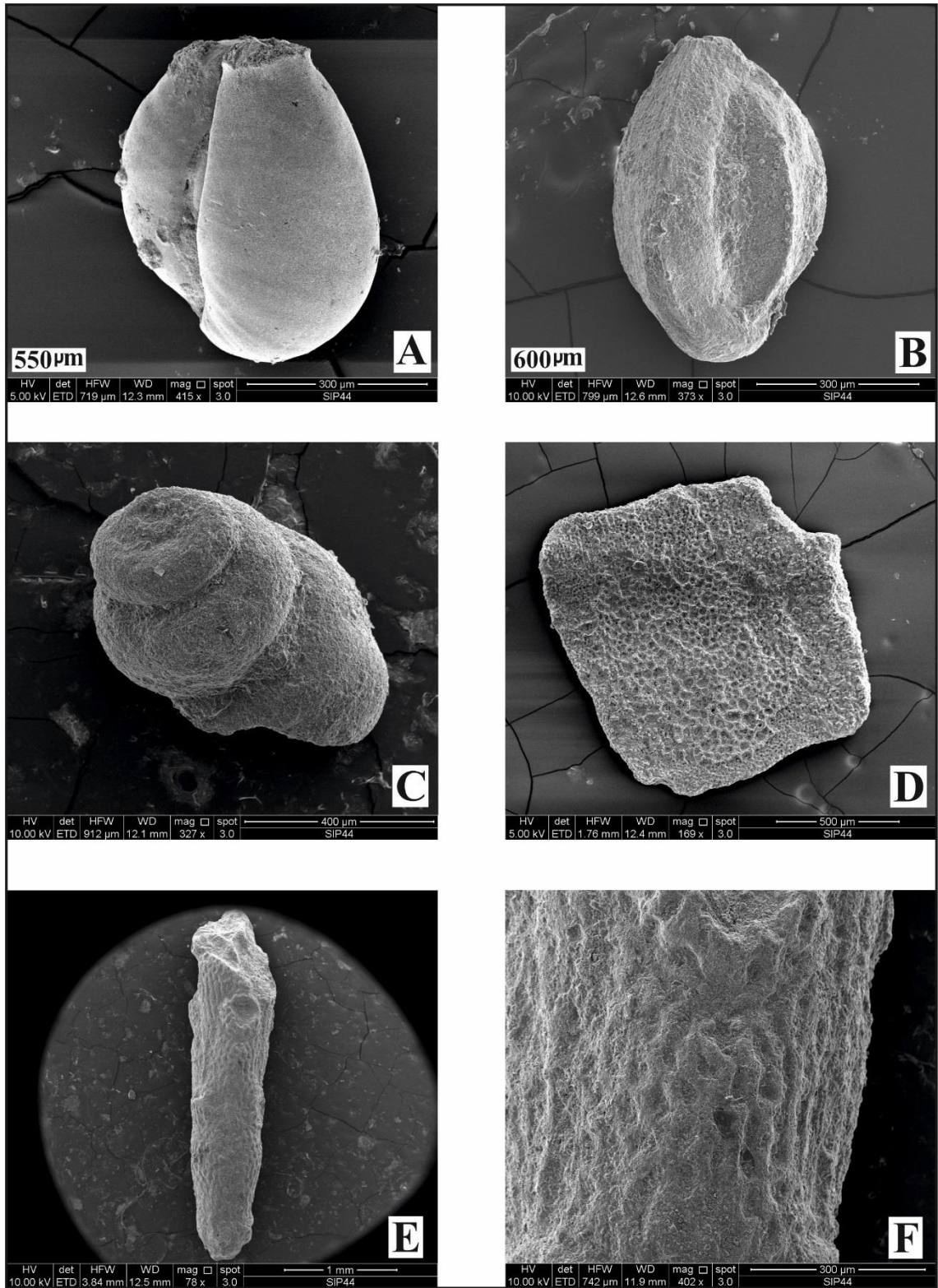


Figure 3-9 Scanning electron photomicrographs of extracted microfossils from the calcareous mudstone units of the Fatha Formation.

A and B: Miliolid specimens (550 and 600µm) from Mamlaha and Basara sections, respectively. C: A gastropod specimen from Mamlaha section. D, E, and F: Bryozoa specimens from the upper unit of the succession.

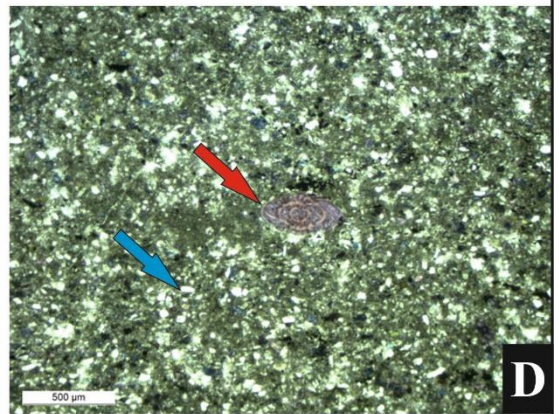
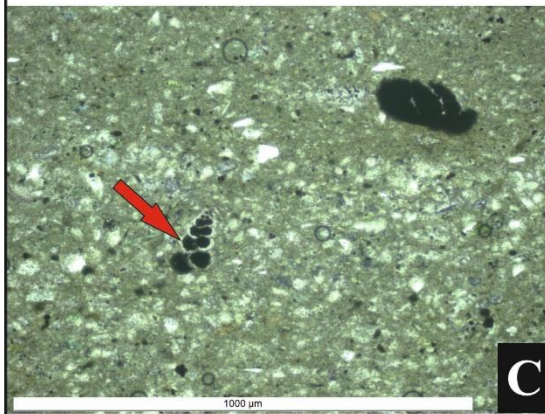
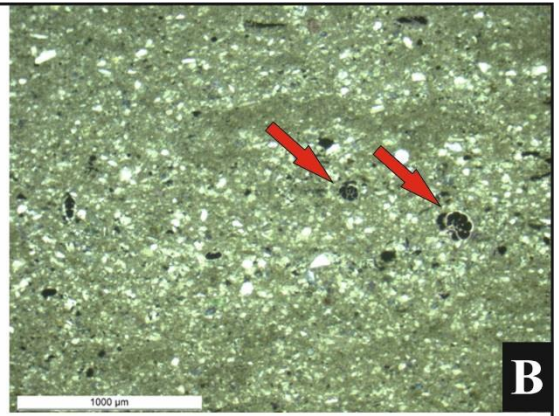
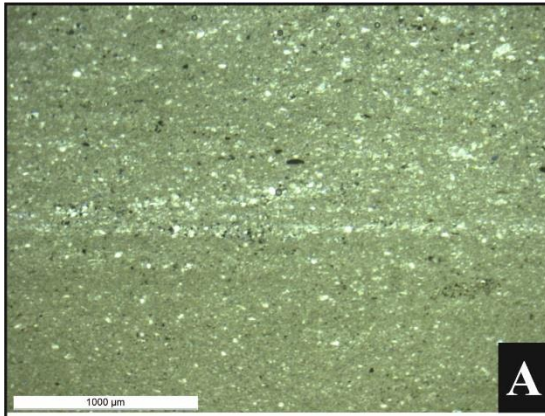


Figure 3-10 Thin section photomicrographs of calcareous mudstone unit (CM)

A: A photomicrograph of calcareous mudstone (marl) facies (CM). The sample was taken at the base of an individual unit in which fossils are very small and quartz grains are rare. Unstained thin section from Mamlaha section.

B: A photomicrograph of calcareous mudstone (marl) facies (CM). The sample was taken nearly at the middle part of an individual unit in which the fossils (rotaliids, the red arrows) and quartz grains (the white grains) are moderately abundant and increasing in sizes. Unstained thin section from Mamlaha.

C: A photomicrograph of calcareous mudstone (marl) facies (CM). The sample was taken at the middle part of an individual unit where the fossils (the red arrow) and quartz grains (the white grains) are increasing. Unstained thin section from Mamlaha.

D: A photomicrograph of calcareous mudstone (marl) facies (CM). The sample was taken from the top of the unit where the fossils (the red arrow), quartz grains (the white grains) and feldspar minerals (the blue arrow) are very abundant and large in sizes. Unstained thin section from Mamlaha.

E: A field photograph of the Fatha cycles. The cycles grade up from greenish to bluish-grey calcareous mudstone unit (CM) at the base to a thin shallow carbonate and then to nodular evaporites (NE). The cycle capes by red clastic unit (RC) at the top of the cycles. The photo was taken from Basara section.

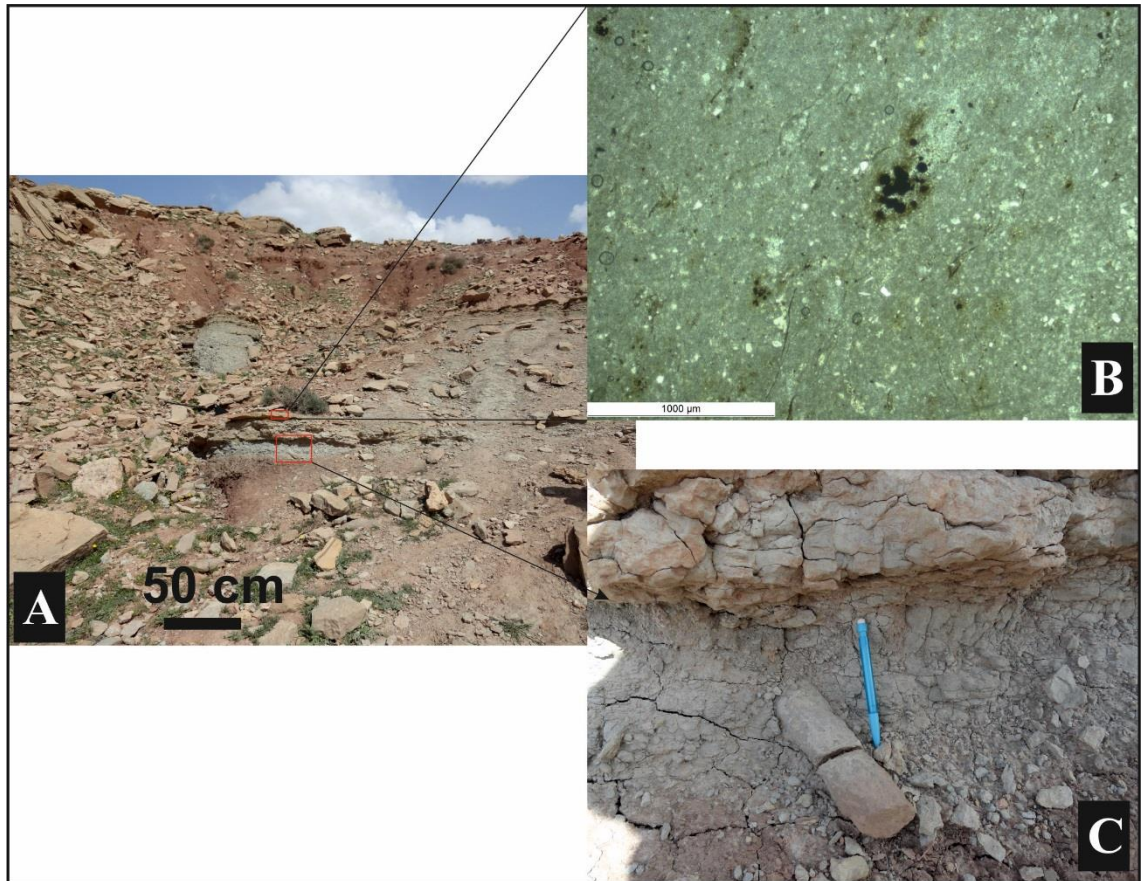


Figure 3-11 Field photographs and thin section photomicrograph of a thin cycle at the upper part of the succession.

- A:** A field photograph of cycles at the upper siliciclastic-dominated part of the formation in Sangaw section. The cycle passes up from thin greenish-grey calcareous mudstone (10cm) at the base with trace fossils (C) to a thin bed of carbonate bed (5cm thick) and then caps by red claystone unit.
- B:** A photomicrograph of quartz mudstone sub-microfacies (SK1b) of the thin carbonate bed of the cycle.
- C:** A field photograph and closer view of the calcareous mudstone unit which includes trace fossil.

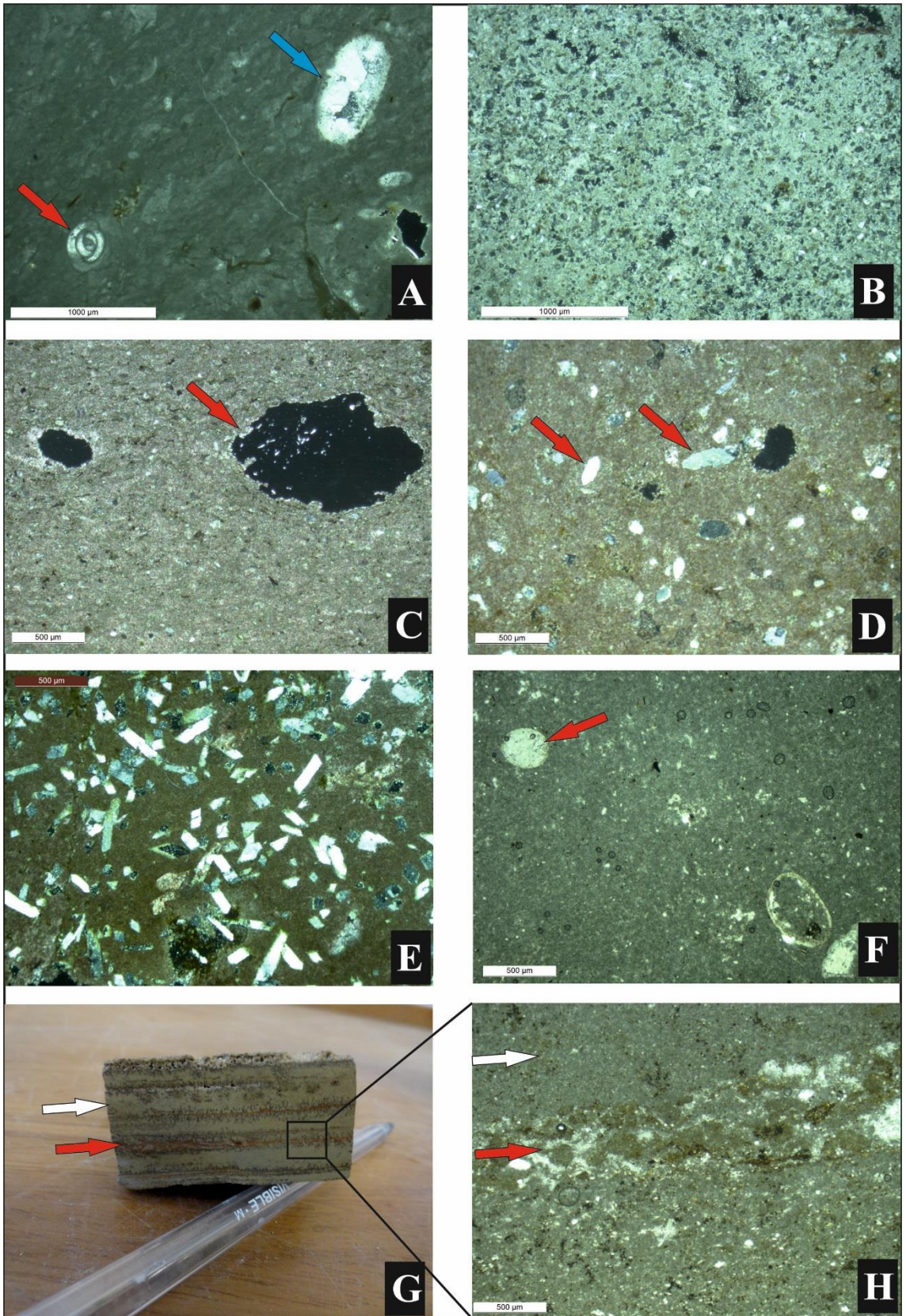


Figure 3-12 Thin section photomicrographs of carbonate mudstone microfacies (SK1).

- A:** A photomicrograph of bioturbated mudstone sub-microfacies (SK1a) with a micritized ostracod (the blue arrow) and a miliolid (the red arrow) within a bioturbated muddy matrix. Unstained thin section from Mamlaha.
- B:** A photomicrograph of quartz mudstone carbonate sub-microfacies (SK1b). Micro sparite matrix with abundant quartz and feldspar grains. Unstained thin section from Sangaw.
- C:** A photomicrograph of non-fossiliferous mudstone carbonate sub-microfacies (SK1c). Muddy matrix with dissolved nodular evaporites (the arrow). Stained thin section from Mamlaha.
- D:** A photomicrograph of non-fossiliferous mudstone carbonate sub-microfacies (SK1c). Muddy matrix with lenticular pseudomorphs after evaporite (the arrows) which indicate original gypsum minerals. Stained thin section from Mamlaha.
- E:** A photomicrograph of non-fossiliferous mudstone carbonate sub-microfacies (SK1c). Quartz and calcite pseudomorphs after evaporite include both lenticular and lath shaped crystals. Stained thin section from Mamlaha.
- F:** A photomicrograph of ostracod wackestone carbonate microfacies (SK2). Muddy matrix with ostracods (the arrows). Unstained thin section from Basara.
- G and H:** A photograph of a carbonate sample (G) with thin section representative (H) non-fossiliferous mudstone carbonate sub-microfacies (SK1c). Interlaminations of the mudstone sub-microfacies (SK1c) (the white arrows) with karst exposure laminae (the red arrows). The sample was taken from Takiya section.

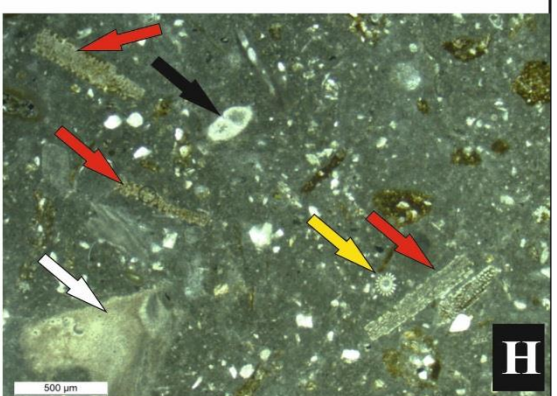
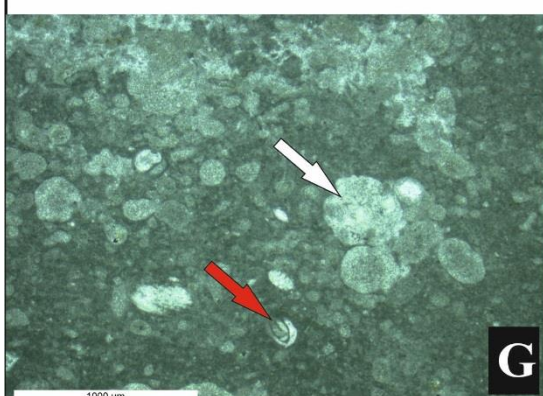
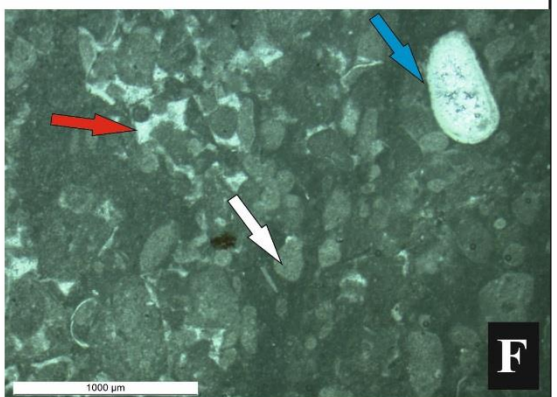
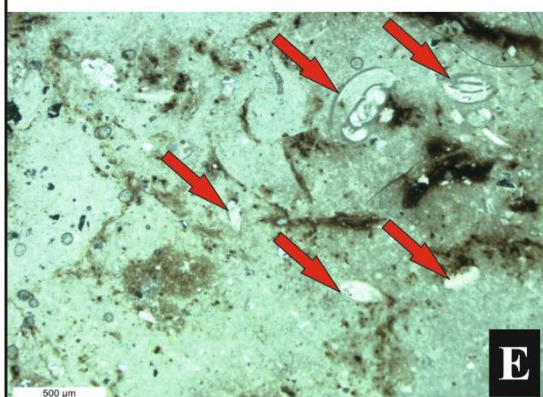
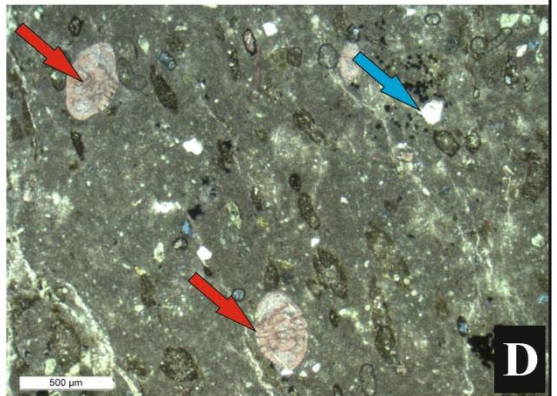
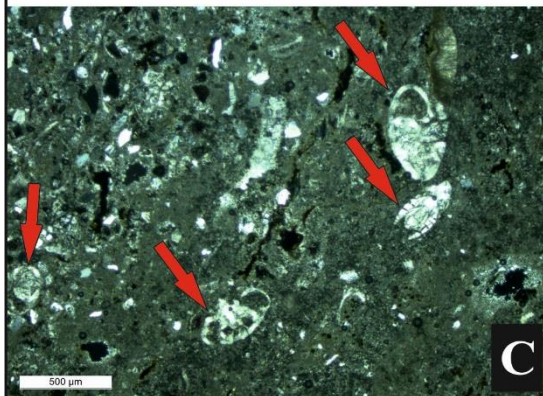
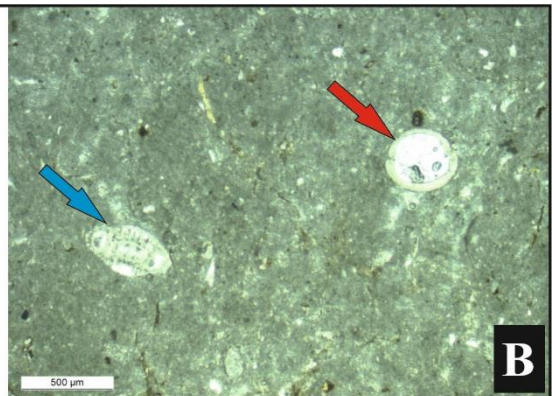
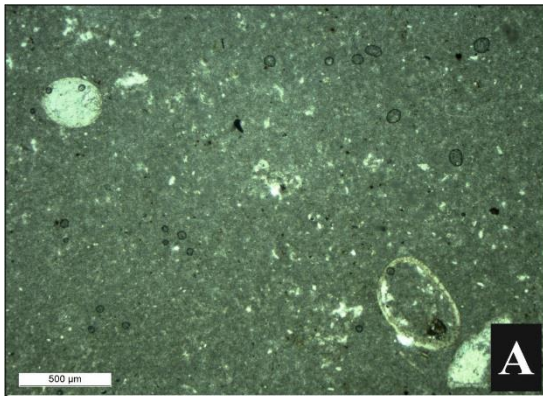


Figure 3-13 Thin section photomicrographs of carbonate microfacies.

- A:** A photomicrograph ostracod wackestone carbonate microfacies (SK2). Muddy matrix with ostracods (the arrows). Unstained thin section from Sangaw.
- B:** A photomicrograph of rotaliid-ostracod wackestone carbonate microfacies (SK3). Muddy matrix with an ostracod (the red arrow) and rotaliid (the blue arrow). The white grains are quartz. Unstained thin section from Basara.
- C:** A photomicrograph of rotaliid wackestone carbonate microfacies (SK4). Muddy matrix with dispersed rotaliids (the red arrows) and quartz grains (the blue arrows). Stained thin section from Mamlaha.
- D:** A photomicrograph of rotaliid packstone carbonate microfacies (SK4). Muddy matrix with rotaliids (the arrows) and quartz grains (the white grains). Unstained thin section from Basara.
- E:** A photomicrograph of miliolid wackestone carbonate microfacies (SK5). Muddy matrix with miliolids (the arrows). Unstained thin section from Mamlaha.
- F:** A photomicrograph of highly micritized skeletal packstone carbonate microfacies (SK6). Muddy matrix with unrecognised micritized bioclasts (the white arrow) and a miliolid (the red arrow). Unstained thin section from Mamlaha.
- G:** A photomicrograph of highly micritized skeletal packstone carbonate microfacies (SK6). Muddy matrix with unrecognised micritized bioclasts (the white arrow), an ostracod (the blue arrow) and fenestrate pores between the grains (the red arrow) which are filled with calcite cements. Unstained thin section from Mamlaha.
- H:** A photomicrograph of echinoid packstone carbonate microfacies (SK7). Muddy matrix with echinoid plates (the red arrows), echinoid spines (the yellow arrow), rotaliids (the black arrow) and oyster shell (the white arrow). The white grains are quartz. Unstained thin section from Basara.

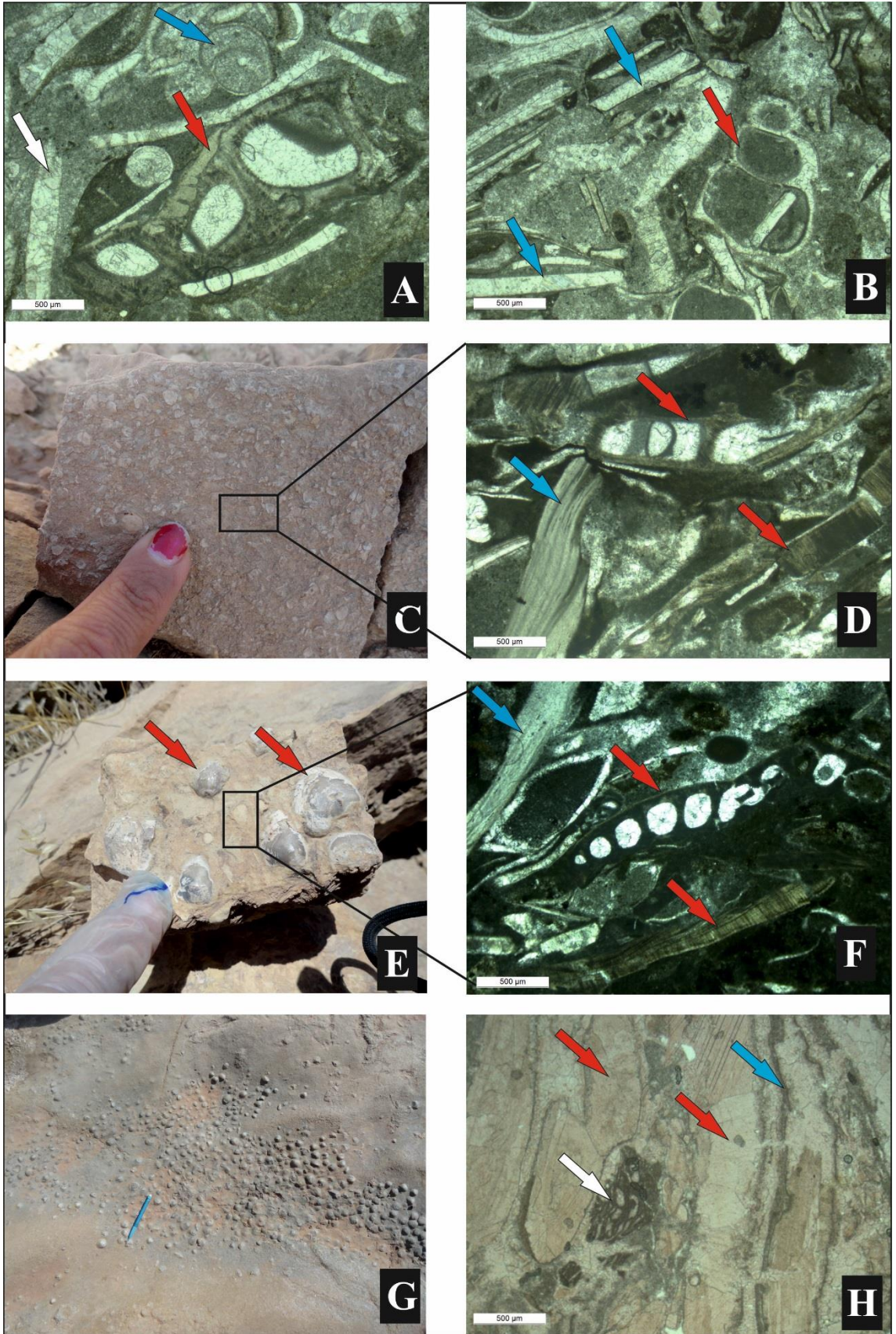


Figure 3-14 Field samples with their representatives thin section photomicrographs of carbonate microfacies.

- A:** A photomicrograph of bioclastic gastropod-bivalve packstone carbonate microfacies (M1). Muddy to micro sparite matrix with bivalve shells (the white arrows) and a gastropod (the blue arrow) with a barnacle shell (the red arrow). Unstained thin section from Aj Dagh.
- B:** A photomicrograph of bioclastic gastropod-bivalve packstone carbonate microfacies (M1). Muddy-micro sparite matrix with bivalve shells (the blue arrows) and a gastropod (the red arrow). Unstained thin section from Aj Dagh.
- C:** A field sample photograph of a carbonate bed from Krbchna section which riches with barnacles and oysters.
- D:** A photomicrograph of bioclastic oyster-barnacle rudstone microfacies (M2) which is indicated from the previous photo. The microfacies include barnacle shells (the red arrows) and an oyster shell (the blue arrow) within muddy matrix. Unstained thin section from Krbchna.
- E:** A field sample photograph of a carbonate unit with bivalves (the arrows). The photo was taken from Mamlaha section.
- F:** A photomicrograph of bioclastic oyster-barnacle rudstone microfacies (M2) from the previous photo. The microfacies includes barnacle shells (the red arrows) and an oyster shell (the blue arrow) within muddy matrix. Bivalve shells are also present (not included in the photo).
- G:** A field photograph of a carbonate bed which riches with bivalves. The photo was taken from Sangaw section.
- H:** A photomicrograph of bivalve rudstone carbonate microfacies (M3). Sparite matrix with bivalve shells (the red arrows), red algae (the white arrow) and micritic envelopes (the blue arrow). Stained thin section from Mamlaha.

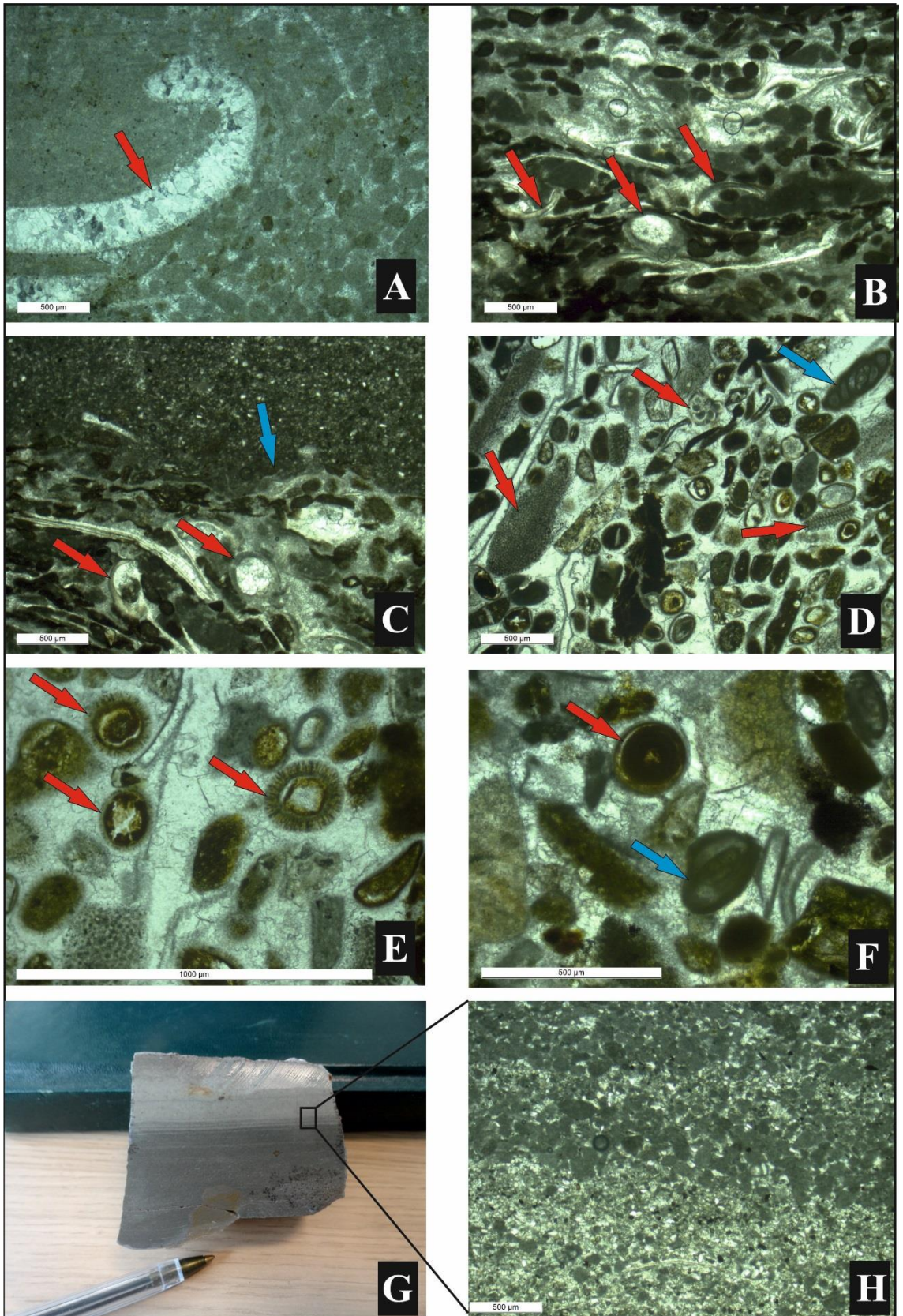


Figure 3-15 Thin section photomicrographs of non-skeletal microfacies (NS1-NS2).

- A:** A photomicrograph of bivalve-peloidal grainstone carbonate sub-microfacies (NS1a). Sparite matrix with bivalve shell (the arrow) and peloids. Unstained thin section from Sangaw.
- B:** A photomicrograph of ostracod-peloidal grainstone carbonate sub-microfacies (NS1b). Sparite matrix with ostracods (the arrows) and peloids (the black grains). Unstained thin section from Basara.
- C:** A photomicrograph of ostracod-peloidal grainstone carbonate sub-microfacies (NS1b). Sparite matrix between the ostracods (the red arrows) and peloids (the black grains). An erosional boundary (the blue arrow) between the ostracods peloidal grainstone and mudstone microfacies indicates storm deposits. Unstained thin section from Basara.
- D:** A photomicrograph of bioclastic peloidal grainstone carbonate sub-microfacies (NS1c). Sparite matrix with echinoid plates (the red arrows) and a miliolid (the blue arrow). The black grains are peloids and the bioclasts are partially micritized. Unstained thin section from Krbchna.
- E:** A photomicrograph of bioclastic peloidal packstone-grainstone carbonate sub-microfacies (NS1c). Closer view of radial ooids grains with partial micritization within sparite matrix. Unstained thin section from Krbchna.
- F:** A photomicrograph of bioclastic peloidal grainstone carbonate sub-microfacies (NS1c). Closer view of partial micritized grains of an ooid (the red arrow) and a miliolid (the blue arrow). Unstained thin section from Krbchna section.
- G:** A field sample of planar laminated faecal pellet grainstone carbonate microfacies (NS2). The facies is composed of planar laminations. Unstained thin section from Basara.
- H:** A photomicrograph of planar laminated pellet grainstone carbonate microfacies (NS2) of the previous sample. Unstained thin section from Basara.

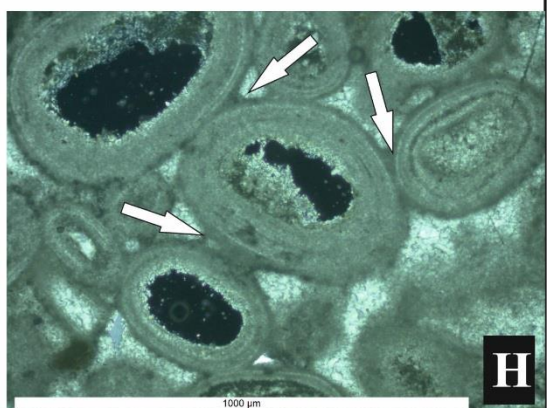
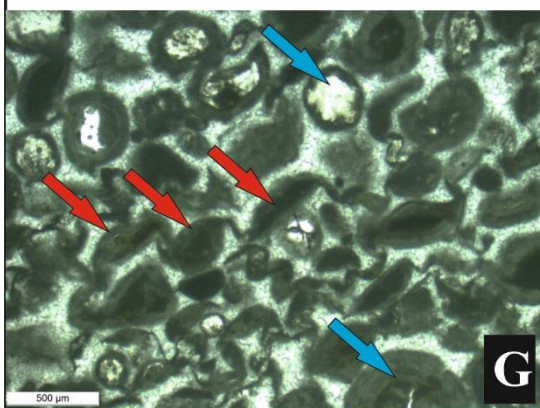
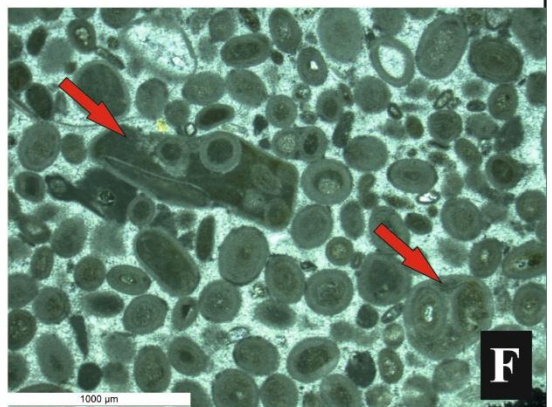
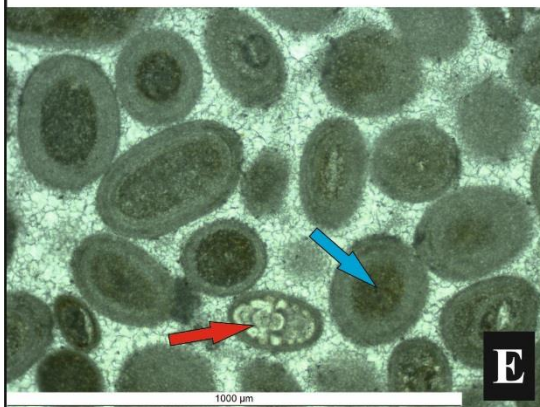
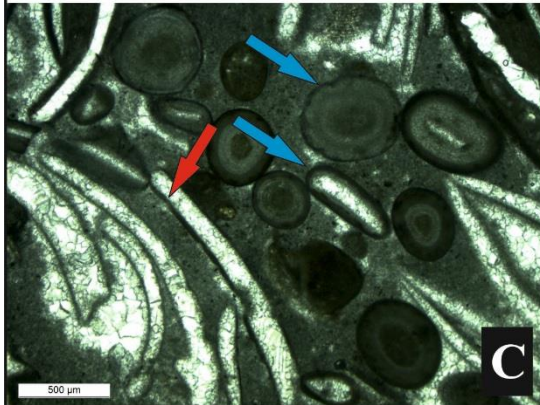
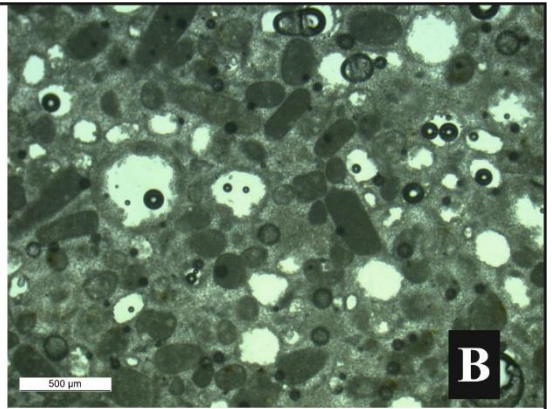
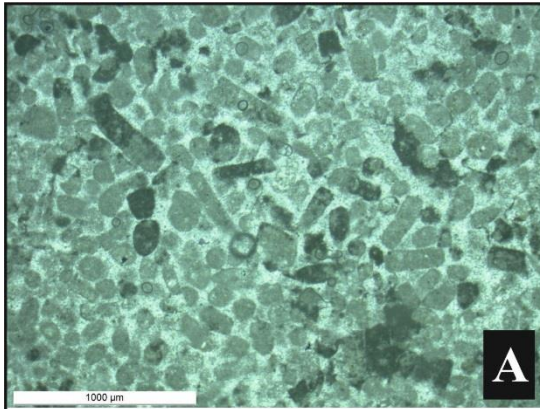


Figure 3-16 Thin section photomicrographs of non-skeletal microfacies (NS2-NS5).

- A.** A photomicrograph of faecal pellet grainstone carbonate microfacies (NS2). The pellet grains are both elongated and rounded shaped within sparite matrix. Unstained thin section from Mamlaha.
- B.** A photomicrograph of peloidal-oidal grainstone carbonate microfacies (NS3). The black grains are pellets and the dissolved grains are ooids within sparite matrix. Unstained thin section from Mamlaha.
- C.** A photomicrograph of bioclastic ooidal packstone-grainstone carbonate microfacies (NS5). Muddy matrix with bivalves shells (the red arrow) and ooids. The ooids are partially micritized. The micro borings and micritic envelopes around the grains are common (the blue arrows). Unstained thin section from Aj Dagh.
- D.** A photomicrograph of bioclastic ooidal packstone-grainstone carbonate microfacies (NS5). Closer view of the previous thin section showing micritized ooids (the white arrow) and bivalve shells (the red arrows). Meniscus cement between the grains is bridged the grains together (the blue arrow). Unstained thin section from Aj Dagh.
- E.** A photomicrograph of ooidal packstone-grainstone carbonate microfacies (NS4). The ooids are normal concentric within sparite matrix. The ooids are filled with micritic cement as nucleus (the blue arrow) and rotaliids nuclei (the red arrow) as well. Unstained thin section from Darbandikhan.
- F.** A photomicrograph of ooidal packstone-grainstone carbonate microfacies (NS4). The ooids are normal concentric with micritic cement nucleus. Ooids aggregates are common (the arrows). Unstained thin section from Sangaw.
- G.** A photomicrograph of ooidal grainstone carbonate microfacies (NS4). The ooids are distorted (the red arrows) and some ooids are normal (the blue arrows). Unstained thin section from Sangaw.
- H.** A photomicrograph of ooidal packstone-grainstone carbonate microfacies (NS4). Closer view of Meniscus cement between the ooids grains (the arrows). Unstained thin section from Sangaw.

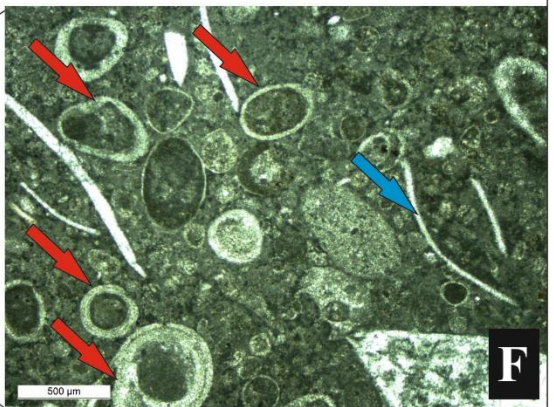


Figure 3-17 Field photographs of non-skeletal microfacies (NS4-NS5)

- A:** A field photograph of a carbonate unit showing erosional surface (the red arrows) between deposits of lagoon-intertidal setting (the lower facies) and bioclastic ooidal grainstone (the upper facies). The ooidal facies is characterised by trough cross beddings (NS4).
- B:** A field photograph of the previous carbonate unit and closer view of the trough cross beddings within the bioclastic ooidal grainstone microfacies (NS4).
- C and D:** Field photographs of carbonate beds with symmetrical ripple marks of ooidal grainstone microfacies (NS4) from Chnarah and Darbandikhan sections respectively.
- E:** A field photograph of a massive carbonate bed which is slightly cross laminated which represents bad sorting bioclastic ooidal grainstone microfacies (NS5). The photo was taken from Takiya section.
- F:** Thin section photomicrograph of the previous photo which represents bad sorting bioclastic ooidal grainstone microfacies (NS5). The ooids (the red arrows) are of different sizes and shapes and associated with bivalve shells (the blue arrow).
- G:** A field photograph and closer view of the carbonate bed in photo (E). The ooids and the bivalve shells are visible at the surface of the bed.
- H:** A field photograph of a carbonate unit which represent ooidal grainstone microfacies (NS4). The carbonate unit is slightly cross bedded with vertical and horizontal stylolites. The photo is taken from Darweshan village near the Basara gorge.

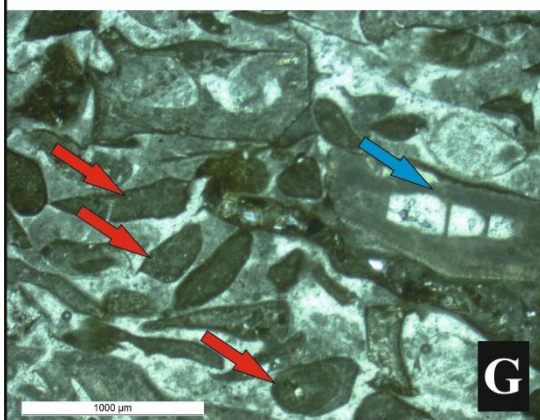
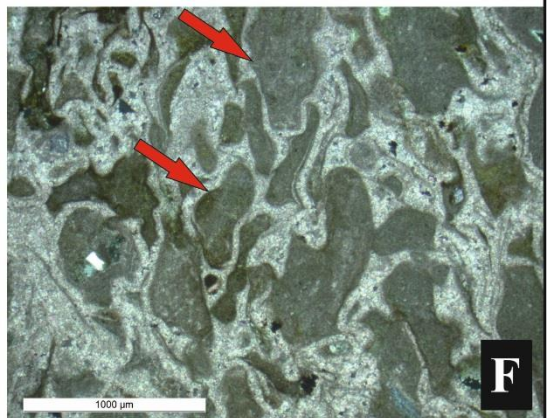
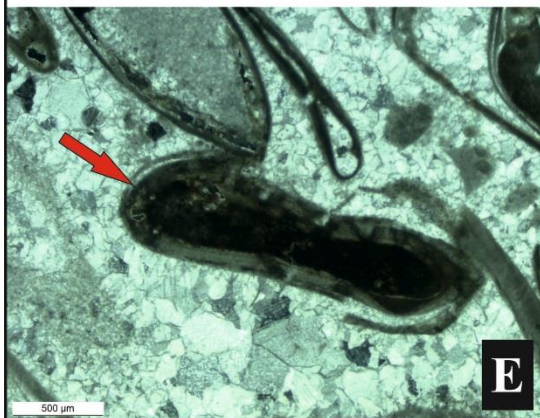
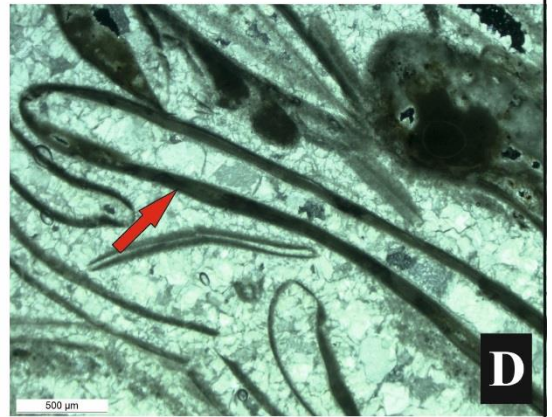
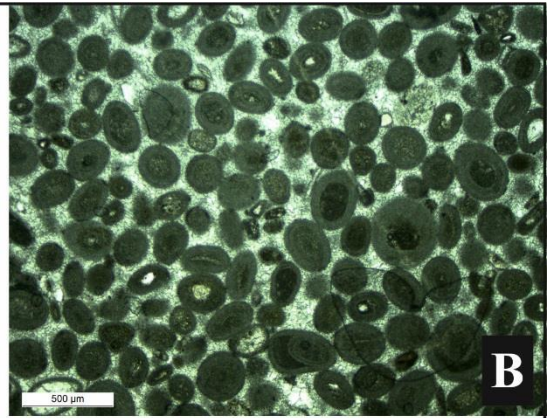
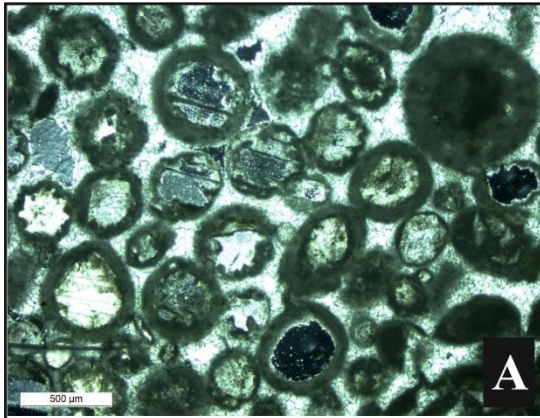


Figure 3-18 Thin section photomicrographs of non-skeletal microfacies (NS5-NS7).

- A:** A photomicrograph of ooidal packstone-grainstone carbonate microfacies (NS4). The nucleus of the ooids are quartz and some ooids nuclei are dissolved. Unstained thin section from Takiya.
- B:** A photomicrograph of ooidal packstone-grainstone carbonate microfacies (NS4). The ooids are normal concentric and filled with micritic cement within sparite matrix. Unstained thin section from Sangaw.
- C:** A photomicrograph of coated grain rudstone carbonate microfacies (NS6). The grains are filled with micritic cement and coated by concentric laminae (the arrow). Unstained thin section from Takiya.
- D:** A photomicrograph of coated grain rudstone carbonate microfacies (NS6). A skeletal shell coated by concentric laminae (the arrows) within a sparite matrix. Unstained thin section from Takiya.
- E:** A photomicrograph of coated grain rudstone carbonate microfacies (NS6). The grains are rounded by micritic cement and coated by concentric laminae. A serpulid tube worm is filled with micritic cement (the arrow). Unstained thin section from Takiya.
- F:** A photomicrograph of intraclast packstone carbonate microfacies (NS7). The intraclasts are irregular micritic grains (the arrows) dispersed within a sparite matrix. Unstained thin section from Darbandikhan.
- G:** A photomicrograph of intraclast packstone carbonate microfacies (NS7). The micritic intraclasts (the red arrows) are dispersed within a muddy matrix with barnacle shells (the blue arrow). Unstained thin section from Darbandikhan.
- H:** A photomicrograph of intraclast packstone carbonate microfacies (NS7). The intraclasts (the arrows) are micritic irregular grains within muddy matrix. Unstained thin section from Darbandikhan.

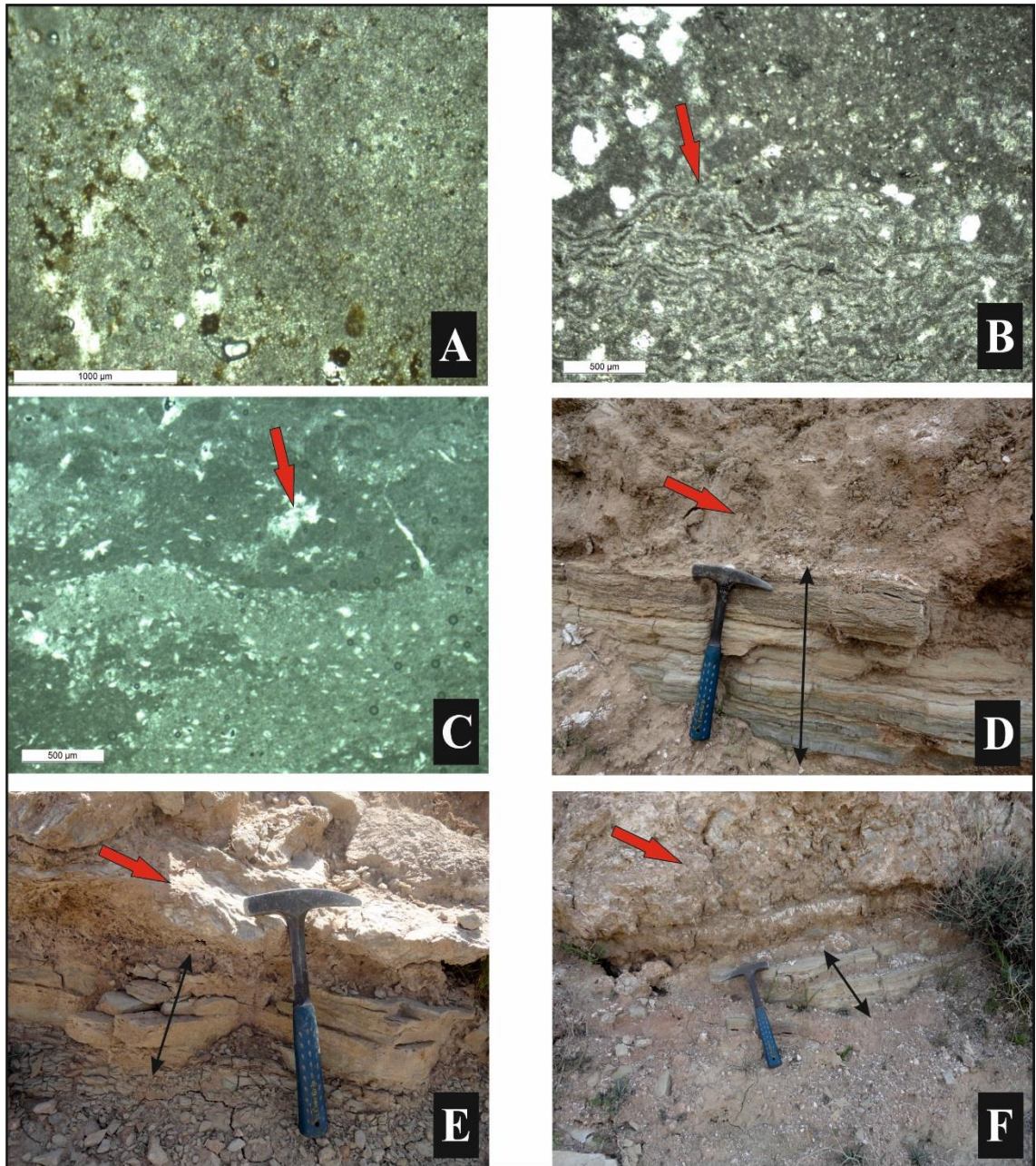


Figure 3-19 Thin section and field photographs of algal bindstone and dolo-mudstone microfacies (AG1 & D1).

- A:** A photomicrograph of dolo-mudstone carbonate microfacies (**D1**). Small dolomite grains form this microfacies. Unstained thin section from Takiya.
- B:** A photomicrograph of wavy laminated algal laminites (**AG1**). Stained thin section from Mamlaha.
- C:** A photomicrograph of wavy laminated algal laminites (**AG1**). The white grains are lenticular pseudomorphs after evaporites. Unstained thin section from Mamlaha.
- D-F:** Field photographs of wavy laminated algal laminites. The carbonate units are about 10-30cm thick and are overlaid by nodular evaporite (the red arrows). The photos were taken from Basara, Aj Dagh, and Krbchna sections, respectively.

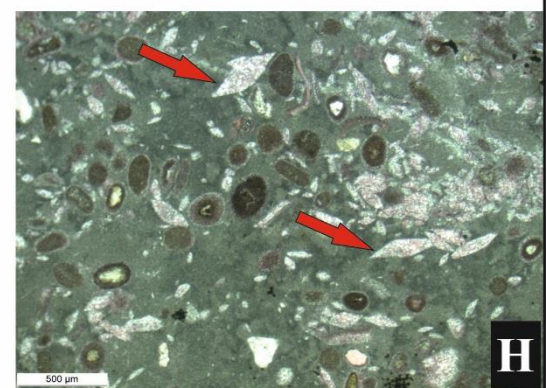
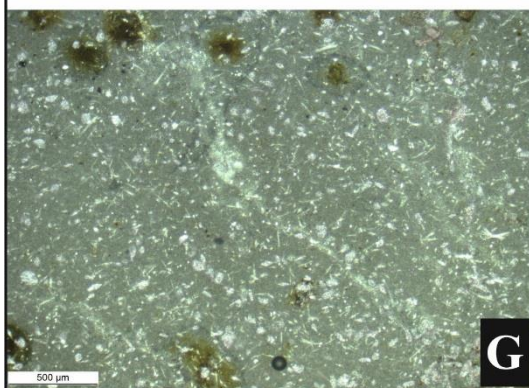
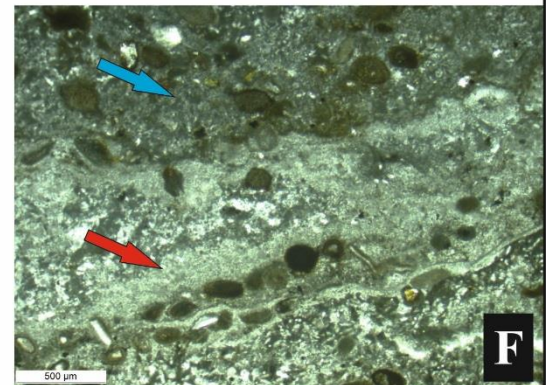
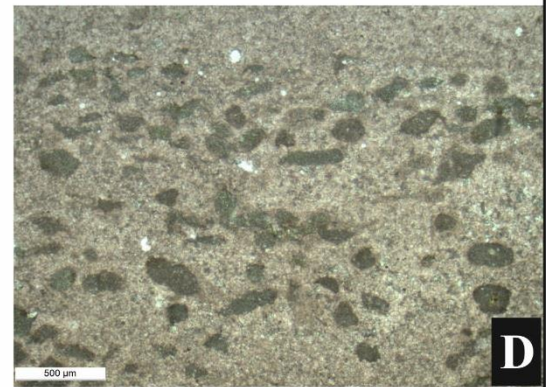
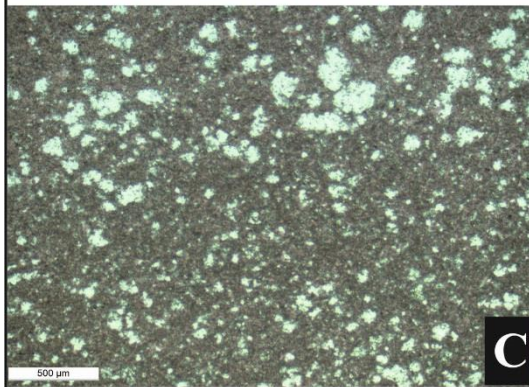
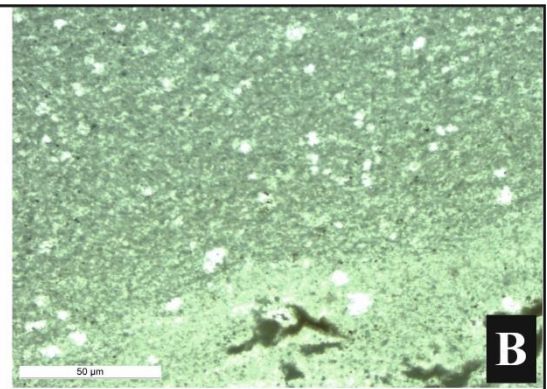
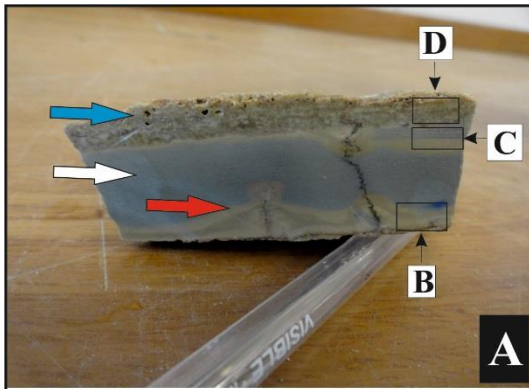


Figure 3-20 Field and thin section photographs of stromatolite microfacies (AG2).

- A.** A field sample of wavy laminated stromatolite (AG2a) (the red arrow) which interlaminated with algal laminites (AG1) (the white arrow). The algal laminites are cut by erosional exposure (the blue arrow). The sample was taken from Takiya.
- B.** Unstained photomicrograph of wavy laminated stromatolite (AG2a) which is indicated in the previous photo. The photo represents a part of an erosional exposure at the base of the stromatolite from the previous laminae and stromatolite laminae. The small white grains are fenestrate pores.
- C.** A stained photomicrograph of laminated algal mats (AG1) which is indicated in the stromatolite sample in (A). The algal laminae include fenestrate pores (the white grains) which are increasing in sizes toward the top.
- D.** A stained photomicrograph of erosional exposure at the top of the algal mat from the photo sample (A). The aerial exposure includes micritized grains (the dark grains) within a coarse sparite matrix.
- E.** A field photograph of wavy laminated stromatolite (AG2b). The stromatolite bed is about 10cm thick and is overlain by nodular evaporite. The photo was taken from Mamlaha.
- F.** Unstained photomicrograph of wavy laminated stromatolite microfacies (AG2b) which indicated in the previous photo. The stromatolite includes interlaminations of muddy (the blue arrow) and sparite (the red arrow) laminae. Micritized peloids (the black grains) and the white grains (evaporite pseudomorph) are also included. The photo was taken from Mamlaha.
- G.** A stained photomicrograph of wavy laminated stromatolite microfacies (AG2b). The photo represents the muddy laminae with acicular crystals. The position of the sample is indicated in the first photo.
- H.** A stained photomicrograph of wavy laminated stromatolite microfacies (AG2b). The muddy laminae of the stromatolite with lenticular pseudomorphs after evaporites (the arrows). The position of the sample is indicated in the first photo.

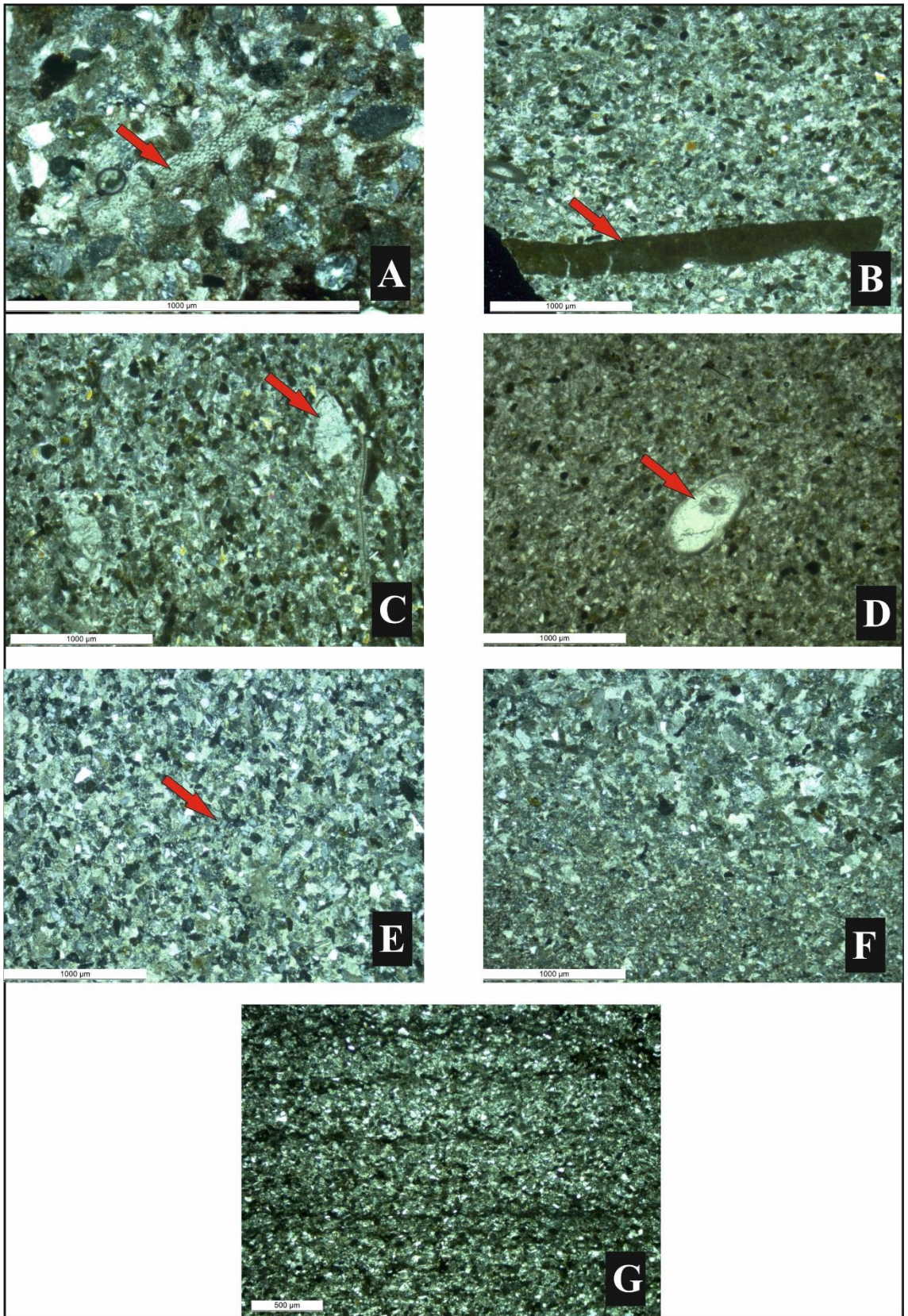


Figure 3-21 Thin section photomicrographs of sandy carbonate microfacies (S1).

- A:** A photomicrograph of sandy carbonate microfacies (**S1**). The microfacies represent bioclastic calc-arenite microfacies. The grains are quartz, chert, feldspar and echinoid plates (the arrow). Unstained thin section from Krbchna.
- B:** A photomicrograph of sandy carbonate microfacies (**S1**). The microfacies represent bioclastic calc-arenite microfacies. The grains are quartz, chert, micritized grains and feldspar with micro borings (the arrow). Unstained thin section from Basara.
- C:** A photomicrograph of sandy carbonate microfacies (**S1**). The microfacies represent bioclastic calc-arenite microfacies. The grains are quartz, chert, micritized grains and feldspar with rotaliids (the arrow). Unstained thin section from Darbandikhan.
- D:** A photomicrograph of sandy carbonate microfacies (**S1**). The microfacies represent bioclastic calc-arenite microfacies. The grains are quartz, chert, micritized grains and feldspar with ostracods (the arrow). Unstained thin section from Darbandikhan.
- E:** A photomicrograph of sandy carbonate microfacies (**S1**). The sample includes quartz, chert and feldspar (the arrow) grains. Unstained thin section from Basara.
- F:** A photomicrograph of sandy carbonate microfacies (**S1**) with graded beddings. Unstained thin section from Aj Dagh.
- G:** A photomicrograph of sandy carbonate microfacies (**S1**) includes planar laminations. Unstained thin section from Basara.

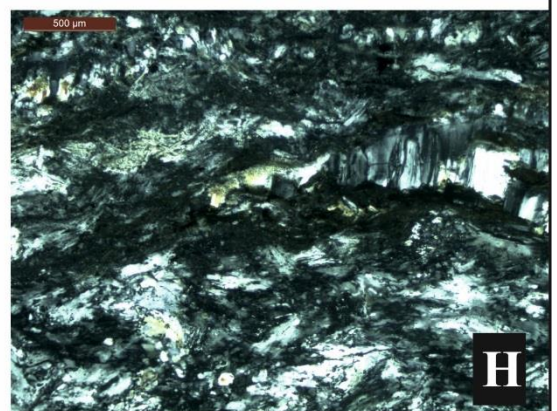
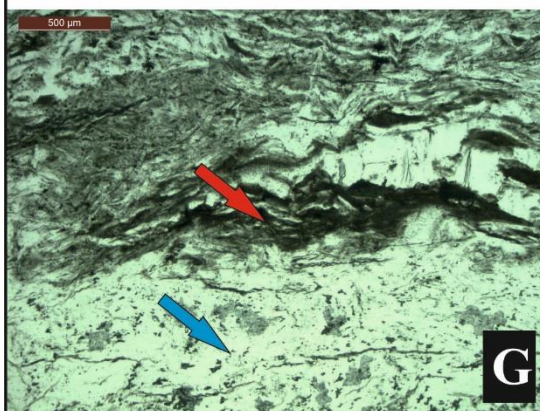
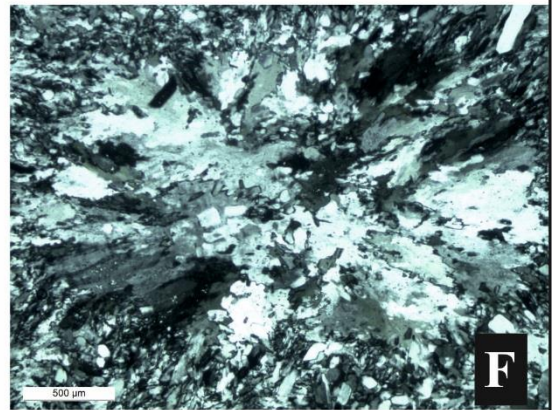
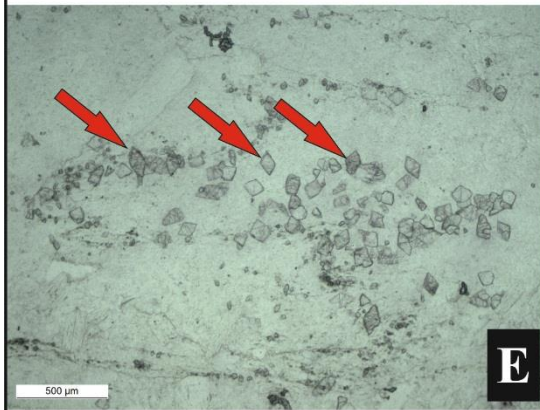
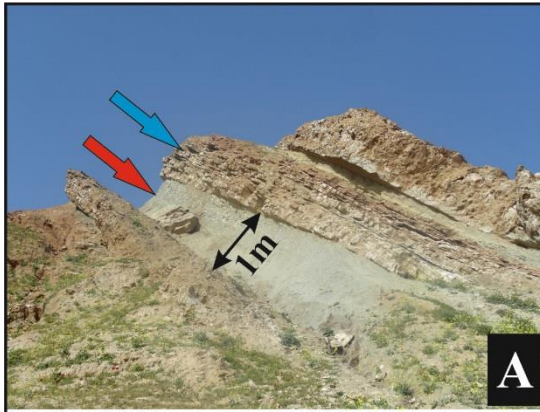


Figure 3-22 Field and thin section photographs of evaporites (NE & LE).

A: A field photograph showing multiple cycles of calcareous mudstone (**CM**) and nodular evaporites (**NE**) in Kfri section. These cycles are preserved from the lower carbonate-evaporitic-dominated part and they are mostly composed of calcareous mudstone (the red arrow) and nodular evaporites (the blue arrow).

B: A field photograph of a thick nodular evaporite (**NE**) from Aj Dagħ section.

C: A field photograph of a thick nodular evaporite (**NE**) from Sangaw section.

D: A field photograph of thin nodular evaporites (**NE**), which are interbedded with thin calcareous mudstone (**CM**) beds in Sangaw section.

E: A photomicrograph of nodular evaporite (**NE**) in plane polarised light. The gypsum grains appear colourless under plane polarised light. The gypsum is associated with dolomite crystals (the arrows). Unstained thin section from Mamlaha.

F: A photomicrograph of nodular evaporites (**NE**) in cross polarised light. The grains are gypsum minerals which are formed an evaporite rosette. Unstained thin section from Mamlaha.

G: A photomicrograph of laminated evaporite (**LE**) in plane polarised light. The laminations are formed between gypsum laminae (the blue arrow) and mudstone laminae (the red arrow). Unstained thin section from Mamlaha.

H: The same photomicrograph of the previous photo in cross polarised light.



Figure 3-23 Field photographs of laminated evaporites (LE).

A: A field photograph of laminated evaporites (LE) between gypsum laminae (the white laminae) and mudstone laminae (the grey laminae). The photo was taken from Mamlaha section.

B: A field photograph of laminated evaporites (LE) between gypsum laminae (the white laminae) and mudstone laminae (the grey laminae). The photo was taken from Darbandikhan section.

C: A field photograph of laminated evaporites (LE) (1m thick) (the blue arrow). The laminated evaporite is mostly underlain by an enterolithic evaporite bed (EN) (10cm) (the red arrow). Both evaporites are separated by a thin calcareous mudstone (CM) bed (10cm) (the white arrow) in between. The photo was taken from Mamlaha section.

D: A field photograph of laminated evaporites (LE) (the blue arrow). The same cycle as (C) was seen in Sangaw section where the laminated evaporite (1m) (the blue arrow) is underlain by an enterolithic evaporite bed (EN) (10cm). Both evaporites are separated by a thin calcareous mudstone (CM) bed (5cm) (the white arrow) in between. These two sections are 18km apart.

E and F: Field photographs of laminated evaporites (LE) from Basara and Krbchna sections, respectively (the arrows). The cycles are passing up from calcareous mudstone (CM) unit at the base to a thin enterolithic evaporite bed (10cm) then to a thin calcareous mudstone bed (10cm) and pass up to the laminated evaporites (LE) (1m) and cap by red claystone unit. The laminated evaporite is traceable between two sections (20km apart).

G and H: Field photographs of laminated evaporites (LE) from Darbandikhan and Sangaw sections, respectively. The evaporites consist of wavy laminated gypsum (white laminae) and carbonate mudstone (dark laminae).

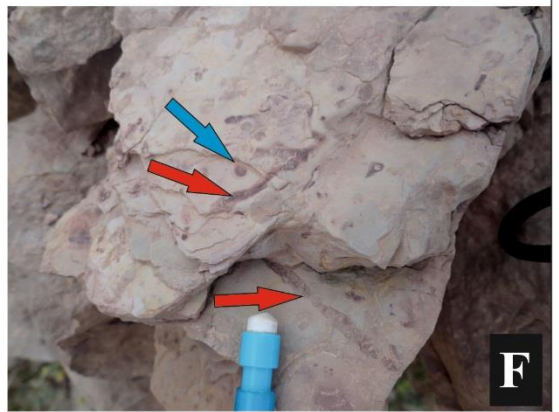
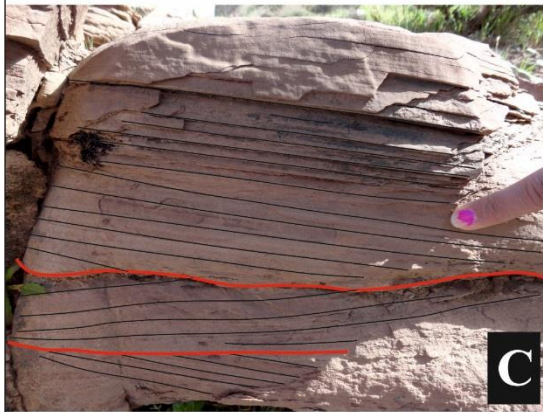


Figure 3-24 Field photographs of red clastic unit (RC).

- A:** A field photograph of a cycle in Mamlaha section. The cycle is capped by red claystone (RC) at the top of a nodular evaporite (NE) unit (the white bed).
- B:** A field photograph of red claystone (RC) beds from the lower carbonate-evaporitic-dominated part in Sangaw section.
- C:** Field photographs of a thin cross bedded sandstone (CS) bed from the lower carbonate-evaporitic-dominated part in Aj Dagh section. The sets of the cross beddings are separated by erosional scours (the red lines).
- D:** A field photograph of fine planar laminated red claystone (RC). The photo was taken from Sangaw section.
- E:** A field photograph of a highly bioturbated bluish-red mudstone-siltstone bed (HM). This facies is very common at the upper most part of the succession and interbedded with red claystone (RC). The photo was taken from Aj Dagh section.
- F:** A field photograph and closer view of *Skolithos* ichnofacies from highly bioturbated bluish-red mudstone-siltstone (HM). The ichnofacies include both horizontal (the red arrows) and vertical (the blue arrow). The photo was taken from Sangaw section.
- G:** A field photograph of interbeddings of highly bioturbated bluish-red mudstone-siltstone (HM) with red claystone (RC). The photo was taken from Sangaw section.
- H:** Field photographs of plants roots from a sandstone bed at the upper siliciclastic-dominated part of the succession. The photo was taken from Mamlaha section.

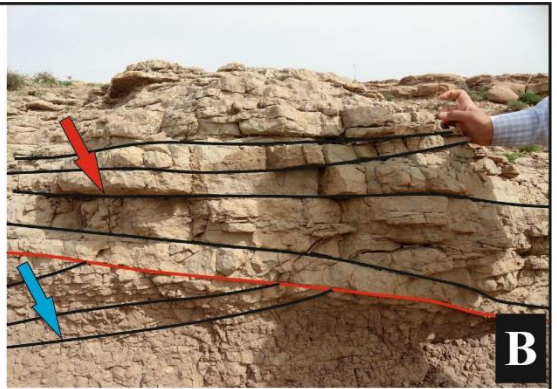


Figure 3-25 Field photographs of siliciclastic sandstone (RC).

- A. A field photograph of a thick and massive green sandstone bed from the upper siliciclastic-dominated part in Kfri section. The sandstone bed includes planar and wavy laminations.
- B. A field photograph of a channel of cross-bedded sandstone (CS) (the red arrow) within red claystone (RC) beds (the blue arrow). The two sets of the cross beddings are separated by an erosional scour (the red line). The photo was taken from the upper siliciclastic-dominated part in Aj Dagh section.
- C. A field photograph of a green sandstone bed with cross beddings (CS). Four sets of cross beddings (the black lines) are formed which are separated by gutter scours (the red lines). The photo was taken from Kfri section from the upper siliciclastic-dominated part.
- D. A field photograph of a greenish sandstone bed with wave asymmetrical ripple marks (RS) at the surface. The photo was taken from Chnarah section from the upper siliciclastic-dominated part.
- E. A field photograph of a reddish sandstone bed with wave asymmetrical ripple marks (RS) at the surface. The photo was taken in Mamlaha section from the upper siliciclastic-dominated part.
- F. A field photograph of a greenish sandstone with current ripple marks (RS). The photo was taken in Takiya section from the upper siliciclastic-dominated part.
- G. A field photograph of a thick sandstone unit. The sandstone beds are dark grey in colour with planar laminations; flutes cast (the directed photo) on the base of a sandstone bed and load casts (photo H, the arrow). The photo was taken in Basara section from the lower carbonate-evaporitic-dominated part.
- H. A field photograph and closer view of a part of the previous photo showing load casts. The load casts were developed by differential sinking of still soft sandstone in to less dense sediment below.

Chapter Four

Sequence Stratigraphy of the Fatha Formation

4.1 Introduction

Sequence stratigraphy has gradually evolved since the fundamental recognition by James Hutton in the late 1700's that an unconformity surface represents a time gap. It is worth mentioning that sequence stratigraphy began as a more formal stratigraphic discipline in 1949 when the term *sequence* was proposed as a stratigraphic unit bounded by regional unconformities (Sloss, 1949), and subsequently the concept of sequences was further developed (Sloss, 1963).

Nowadays, sequence stratigraphy is used as a framework within which interactions between basin fill processes, tectonics and eustasy may be analysed. In all types of sedimentary basins, depositional stacking patterns and stratal geometries are used to divide the stratigraphic succession into unconformity bounded sequences, based upon the commonly applied definitions (Mitchum and Van Wagoner, 1991). Local and global driving forces on sedimentary basin architecture can then be estimated in terms of the balance between accommodation space and sediment supply.

Different sequence stratigraphic models have been proposed for siliciclastic and carbonate successions (Van Wagoner *et al.*, 1990; Handford and Loucks, 1993; Sarg, 2001). This recognizes that sedimentation and sediment supply differ in siliciclastic and carbonate deposits. In contrast to siliciclastic deposits, where the sediments come from the hinterland under the effects of tectonics and climate and respond to sea-level changes, carbonate deposits are formed in situ and are controlled by depositional environment, temperature, climate, nutrients and biotic evolution as well as tectonics and sea level (Flugel, 2004). Moreover, carbonate platforms and ramps differ significantly in their microfacies ranges, in which the former have a wide range of microfacies which change markedly across breaks in slope, while the latter tend to display gradational changes in microfacies (Flugel, 2004). As previously outlined, carbonate ramps are recognized as being developed on low-angle, inclined slopes that extend basinwards without any slope break, and where high-energy packstones and grainstones are typical landward facies (inner ramp), changing to low-energy muddy facies toward the basin (outer ramp). In some cases, high-frequency cyclicity is

preserved in carbonate ramps that reflect variations in the controls on carbonate productivity and hence stacking patterns. These high-frequency cycles reflect the product of changes in sedimentation that may occur across different hierarchical orders. The changes in sedimentation are the result of either local or random sedimentary process or regular processes of global sea-level and climate change that control the cyclicity through astronomical forcing of palaeoclimate variations (Fischer, 1964; Arthur and Garrison, 1986; Fischer, 1986; Berger, 1988; Tucker and Garland, 2010).

The Miocene Fatha Formation is composed of high-frequency carbonate-evaporite cycles which extend approximately 2000km across NW Syria, Iraq and SW Iran (as outlined in Chapter 2). The cycles exhibit shallowing-upward trends and are traceable for tens of kilometres, distances only being limited by the continuity of outcrop. In more proximal locations, each individual cycle includes a calcareous mudstone which passes up to a shallow water carbonate facies, and which typically then grades up to nodular evaporites above. Fluvial siliciclastic deposits derived from the Zagros hinterlands overlie the evaporites in most cycles. In the basin centre, each cycle is composed of thin calcareous mudstones interbedded with thick evaporite or of calcareous mudstone, carbonate and evaporite. Variations in thickness of the whole succession and in the individual cycles and cycle numbers are observed over the entire basin (Figures 3.4 and 3.5, Chapter Three). In general, each cycle may be interpreted to represent a regressive or shallowing-upward trend which passes up from the mudstone and carbonate mudstone/wackestone to carbonate packstone/grainstone, and then to evaporite and fluvial deposits (as detailed in Chapter 3).

The sequence stratigraphic correlation of sedimentary facies and the carbonate-evaporite cycles in the Fatha Formation allows variations in cycle thickness and cycle character across the basin, and hence the controls thereon, to be analysed. This is the principal aim of this chapter. Whilst the sedimentology of the succession has been studied in Iraq and the Kurdistan region previously (Shawkat, 1979; Aqrabi, 1993; Ajel, 2004), as well as in Iran (Gill and Ala, 1972), sequence stratigraphic studies regarding the nature and reasons for the cyclicity have not been carried out in detail until now.

The main aim of this chapter is to characterize the environmental context and variations in environmental conditions that controlled the architecture of the Miocene Fatha Formation carbonate-evaporite cycles at the scale of the whole formation and at the

scale of the individual cycles. To achieve this, the following objectives were set, listed in the order in which they are dealt with in this study:

- 1- To use the excellent and extensive outcrops of the Fatha Formation to identify cycles and bounding surfaces (as presented in chapter 3).
- 2- To determine the total time elapsed for deposition of the Fatha Formation by using the strontium isotope relative dating method and so allow estimation of the time duration of individual cycles.
- 3- To review and critically assess sequence stratigraphic methods, identifying approaches and definitions appropriate to the characterisation and interpretation of the Fatha Formation.
- 4- To identify parasequence types and their distribution within the Fatha Formation.
- 5- To use parasequence stacking patterns and representations of these in the form of Fischer Plots to analyze the long-term changes in accommodation space and hence establish larger scale systems tracts and the sequence-scale architecture of the Fatha Formation.
- 6- To discuss the sequence stratigraphic variables that may have controlled the observed cyclicity.

4.2 Methods

The Fatha Formation was studied in the north-eastern marginal areas of the Zagros Basin through characterization of a number of surface sections (Figure 1.2). As mentioned previously, the succession includes a number of high frequency carbonate-evaporite-clastic cycles that are continuous across the entire basin. The lateral and vertical sedimentary facies variation within the formation, as presented in Chapter 3, forms the framework for determining the architecture of the formation at a variety of scales, and for considering the impact of sea level variations through time and other environmental controls upon stacking patterns. Because the studied areas are marginal and basinal facies were not studied directly, previous studies were used as the basis for correlating the marginal to the basinal facies, notably after the publications of (Tucker, 1999; Al-Juboury and McCann, 2008; Aqrabi *et al.*, 2010). Consideration of the rocks that underlie and overlie the Fatha Formation, which are represented by the Euphrates and Jeribe Formations from the Early Miocene and the Injana Formation from the Late Miocene, respectively, has allowed characterisation of the nature of key stratal surfaces and bounding conformities or unconformities.

4.2.1 Strontium isotope $^{87}\text{Sr}/^{86}\text{Sr}$ method

The Fatha Formation includes large benthic foraminifera but largely comprises unfossiliferous rocks, including the thick evaporites, which makes an accurate biostratigraphic age determination impossible. However, a Middle Miocene age has been determined by using the biostratigraphy of ostracod species (Khalaf, 1988; Abdol Rassul and Al-Sheikhly, 2001; Hawramy and Khalaf, 2013). Also, a late lower Miocene (Burdigalian) age has been estimated by using index fossils of mollusc species (Mahdi, 2007).

The most accurate methods for determining the age of rocks and sediments are radiometric dating methods, which determine ages numerically. Other relative dating methods are then tied to absolute radiometric dating records. Among these methods, the strontium isotope ratio $\text{Sr}^{87}/\text{Sr}^{86}$ method has been used for determination of the age of Oligocene-Miocene rocks in the Kurdistan region (Grabowski and Liu, 2009; Grabowski and Liu, 2012). A duration from the middle Burdigalian to lower Langhian (Bur.3 to Lang.1) was determined for the Fatha Formation, of between 18.5 and 15.6 Ma. To further assess the age of the Fatha Formation, in this study twenty two samples of either carbonate or evaporite were chosen for isotopic measurements, including four samples of bivalve and oyster shells (see Appendix 1, for sample positions in the measured Mamlaha section). Before the isotope measurements were carried out, thin sections were made for each of the samples and the samples were carefully examined under a polarized microscope for evidence of preservation, diagenesis and recrystallization. Approximately 50 μg of carbonate or evaporite powder (including for the shell samples) was collected for $^{87}\text{Sr}/^{86}\text{Sr}$ measurement at the University of Leeds. The McArthur procedure was used for the leaching method (McArthur *et al.*, 2000). In this method, the sample powders were submerged into 0.9ml 18M Ω water and then 0.2ml of 0.4M acetic acid was added and centrifuged for 5 minutes. After that, up to 1ml of the leached solution was removed, leaving the remaining insoluble residue. Then, 1ml of 1.7M acetic acid was added to the insoluble residue to achieve total dissolution before the liquid was evaporated until dry, at 80°C for 1 hour. From this process, a white carbonate/evaporite residue was obtained and this was re-dissolved in 1.5ml of 2.5 M HCl solution and then centrifuged. After that, the solution was taken to the separation columns and strontium was separated via the standard chromatography method using Eichrom Sr-resin. The purified solution was dried at 80°C and then the

Sr-extract was re-dissolved in ultrapure weak HCl acid and then added onto tungsten wire with softly dried TaCl₅ ionization cocktail. Finally, the ⁸⁷Sr/⁸⁶Sr ratio was measured on a Thermo-Finnegan Triton-series thermal ionization mass spectrometer (TIMS). The measured ⁸⁷Sr/⁸⁶Sr ratio was corrected and used for calculating the age by using the LOWESS 5 database (McArthur *et al.*, 2000). The Sr⁸⁷/Sr⁸⁶ ratios and numerical ages obtained are shown in Table 4.1.

Table 4-1 Sr⁸⁷/Sr⁸⁶ ratios and inferred numerical ages of the carbonate and evaporite samples from the Fatha Formation, sampled in Mamlaha section.

No.	Sample type	Sample ID	Sr ⁸⁷ /Sr ⁸⁶	Error	Correction	Normalized to NBS 987 STD	Age (Ma) (LOWESS 5)
1	Shell	M19	0.708615	-/+ 7	-31x10 ⁻⁶	0.708584	17.99
2	Evaporite	G	0.708581	+/- 5	+8x10 ⁻⁶	0.708589	17.71
3	Carbonate	M21	0.708631	-/+ 26	-31x10 ⁻⁶	0.708600	17.70
4	Carbonate	M28	0.708249	+/- 5	No need	0.708249	22.96
5	Carbonate	M29	0.708673	+/- 23	No need	0.708642	17.15
6	Carbonate	M30	0.708847	-/+ 72	-31x10 ⁻⁶	0.708816	13.20
7	Carbonate	M31	0.708604	+/- 7	No need	0.708604	17.06
8	Carbonate	M32	0.708629	-/+ 5	-31x10 ⁻⁶	0.708598	17.70
9	Carbonate	M43	0.708728	-/+ 6	-31x10 ⁻⁶	0.708697	16.40
10	Evaporite	M43B	0.708718	+/- 39	-31x10 ⁻⁶	0.708687	16.55
11	Evaporite	M51C	0.70867	+/- 8	+8x10 ⁻⁶	0.708678	16.65
12	Evaporite	M52	0.708683	+/- 11	+8x10 ⁻⁶	0.708691	16.45
13	Shell	M57	0.708695	+/- 21	No need	0.708695	16.40
14	Evaporite	M57C	0.708682	+/- 3	+8x10 ⁻⁶	0.708690	16.44
15	Shell	M68	0.708717	-/+ 6	No need	0.708717	16.15
16	Evaporite	M70	0.708622	+/- 26	+8x10 ⁻⁶	0.708630	17.30
17	Carbonate	M75	0.70877	-/+ 5	-31x10 ⁻⁶	0.708739	15.81
18	Shell	M83	0.708796	-/+ 10	-31x10 ⁻⁶	0.708765	15.45
19	Carbonate	M107	0.708694	-/+ 5	-31x10 ⁻⁶	0.708663	16.85
20	Evaporite	PX	0.708644	+/- 7	+8x10 ⁻⁶	0.708652	17.00
21	Carbonate	M114	0.708662	+/- 4	No need	0.708662	16.83
22	Carbonate	M115	0.708668	+/- 4	No need	0.708668	16.81

4.2.2 Age of the Fatha Formation from strontium isotope dating

The strontium isotope ratio, Sr⁸⁷/Sr⁸⁶, was measured for the carbonates, evaporites and preserved shells of bivalves and oysters from the Fatha Formation. Two of the carbonate samples have anomalous results outside the range (22.97 and 13.20 Ma) and

are not plotted on the curve (Figure 4.1 and Table 4.1). The other samples have been plotted with the LOWESS 5 record of variation in Miocene sea water $\text{Sr}^{87}/\text{Sr}^{86}$. For determination of the age range of the Fatha succession, the minimum and maximum points, which were 15.45 and 18 Ma, were taken. Therefore, a duration from the late Burdigalian to early Langhian was estimated to be approximately 2.55my. This approximately confirms the previously published age range. A maximum 40 cycles were identified in the studied section of the Mamlaha area and encompassed by the 22 samples that were analysed. Hence, by dividing the total duration of 2.55my by the number of cycles, a maximum of 40, the average duration of each cycle is estimated to have been ~60ky. However, as shown in Figure 4.1 the inferred ages of cycles are not all in sequence. The numbered cycles denote the stratigraphic order of the samples cycles in the Mamlaha section (see Appendix 1, Mamlaha section). The fact that the stratigraphic order is not replicated in the records set against an approximately linear increase in $\text{Sr}^{87}/\text{Sr}^{86}$ ratio through time implies that there are errors, probably arising from sample contamination or isotope remobilisation, beyond the counting errors associated with the laboratory method itself. Where samples may contain unrecognized, detrital (isotopically old) carbonate, an age greater than the real age of the sample will result. Thus, for example, samples 16 and 19-22 may include some detrital material.

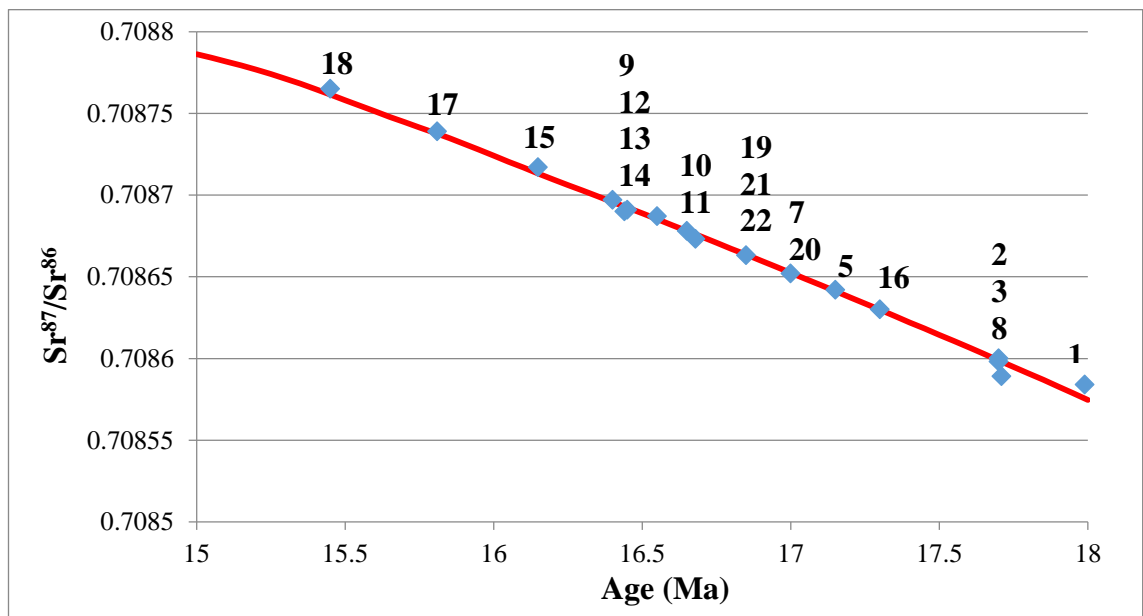


Figure 4-1 Comparison of Miocene strontium-isotope ratios ($\text{Sr}^{87}/\text{Sr}^{86}$) from the Fatha Formation (blue rectangles) with the Lowess 5 Miocene strontium-isotope ratio $\text{Sr}^{87}/\text{Sr}^{86}$ curve (red line). The value of Miocene sea water $\text{Sr}^{87}/\text{Sr}^{86}$ has increased through time and the $\text{Sr}^{87}/\text{Sr}^{86}$ values of the Miocene Fatha Formation have matched the curve.

4.3 Review of sequence stratigraphy methods

Sequence stratigraphy is a discipline in the field of sedimentary geology which has served to integrate stratigraphy and sedimentology to help understand facies changes and facies relationships in response to base level and other environmental changes (Embry, 2009). Thus, sequence stratigraphy is used alongside other geological disciplines to interpret the mechanisms that control the evolution of the fills of sedimentary basins, such as sea-level and climate changes, subsidence, sediment supply, tectonics and basin physiography (Van Wagoner *et al.*, 1988). Moreover, sequence stratigraphy is a field of research that is still being developed with ongoing debates regarding its application (Embry, 2001; Neal and Abreu, 2009; Abreu *et al.*, 2014).

Sequence stratigraphy has been defined as ‘*the study of rock relationships within a time-stratigraphic framework of repetitive, genetically related strata bounded by surfaces of erosion or no deposition, or their correlative conformities*’ (Posamentier *et al.*, 1988; Van Wagoner, 1995) or ‘*the recognition and correlation of stratigraphic surfaces which represent changes in depositional trends in sedimentary rocks. Such changes were generated by the interplay of sedimentation, erosion and oscillating base level and are now determined by sedimentological analysis and geometric relationships*’ (Embry, 2001).

Sequence stratigraphy allows a stratigraphic succession to be divided into time-equivalent sequences that in turn consist of systems tracts. Each system tract may contain smaller units that are known as parasequences.

4.3.1 Sequence

The fundamental unit of sequence stratigraphy is the sequence, which was originally defined by Sloss (1963) as *an unconformity bounded unit* and revived by Exxon researchers in their development of the discipline in the late 1970s and early 1980s and its application to seismic interpretation, when they added the concept of the correlative conformity to the unconformity bounded unit. The sequence thus became ‘*a relatively conformable succession of genetically related strata bounded by unconformities or their correlative conformities*’ (Mitchum *et al.*, 1977).

The first definition of a depositional sequence was published in AAPG Memoir 26 (Payton, 1977) and SEPM Special Publication 42 (Wilgus *et al.*, 1988). The

depositional sequence was defined as a unit bounded by unconformities and correlative surfaces in the margin and basin respectively, and included the Lowstand System Tract (LST), Transgressive System Tract (TST) and Highstand System Tract (HST). Two types of depositional sequence were defined based on the nature of the unconformity bounded surfaces (Vail and Todd, 1981). A type 1 sequence boundary represents a significant episode of subaerial exposure along the basin edge, shelf margin and upper slope, and a correlative conformity in the basin centre. This resultant sequences include the Lowstand System Tract (LST), Transgressive System Tract (TST) and Highstand System Tract (HST) (Figure 4.2). A type 2 sequence boundary represents a relatively minor subaerial exposure, which does not reach the shelf edge and bounds a sequence that includes a Transgressive System Tract (TST), Highstand System Tract (HST) and Shelf Margin System Tract (SMST).

4.3.2 System Tract

Sequences are subdivided into different smaller units termed “system tracts” (Posamentier and Vail, 1988; Van Wagoner *et al.*, 1988), a concept that was originally defined by Brown and Fisher (1977) as a *‘linkage of contemporaneous depositional systems’*. System tracts *“are defined by their position within the sequence and by the stacking patterns of parasequence sets and parasequences ”* (Van Wagoner *et al.*, 1988). A new definition of a system tract was proposed by Embry *et al.* (2007) as *‘a component unit of a sequence which is bound by sequence stratigraphic surfaces’*. Thus, each specific component of system tracts is defined based on its own sequence stratigraphic boundaries and correlative conformities.

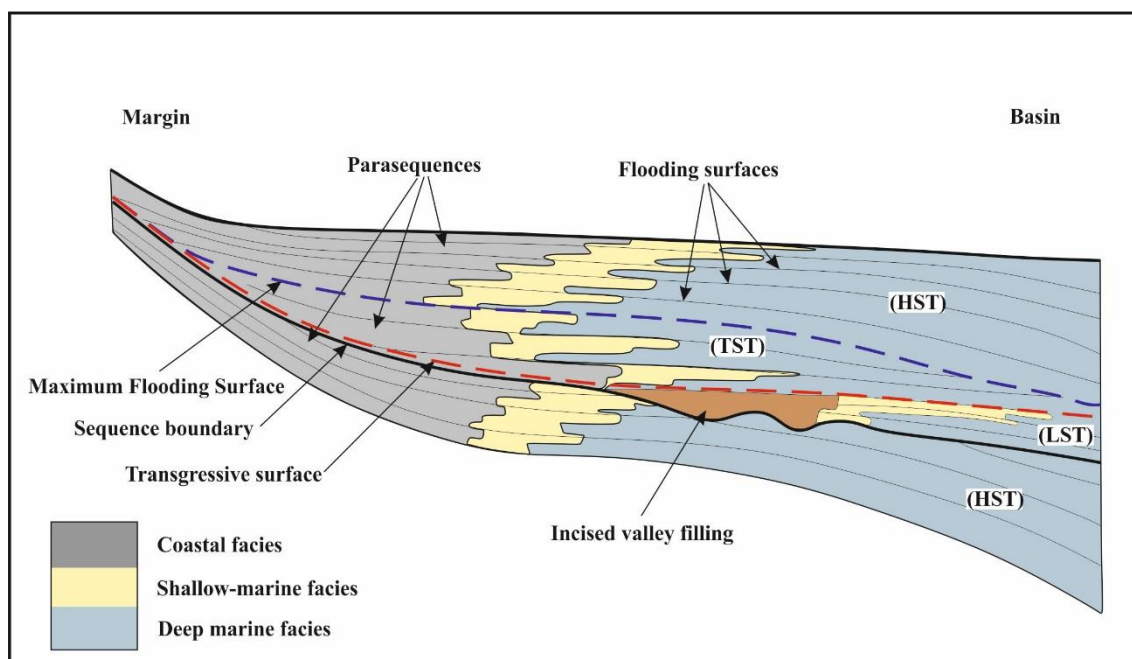


Figure 4-2 A general sequence stratigraphy model, including type-1 sequence boundary, systems tracts, and parasequences. LST: Lowstand System Tract, TST: Transgressive System Tract, and HST: Highstand System Tract (Van Wagoner, 1995).

4.3.3 Parasequences and their bounding surfaces

The further subdivision of system tracts into smaller units bounded by marine flooding surfaces (FS) generates *parasequences*, originally defined as ‘*a relatively conformable succession of beds or bedsets bound by marine-flooding surfaces*’ by Van Wagoner *et al.* (1988). The bounding surfaces of parasequences were defined as ‘*a surface separating younger from older strata across which there is an abrupt increase in water depth*’ (Van Wagoner *et al.*, 1988). Further information was added to define marine flooding surfaces and parasequences and they were defined as a unit of shallowing-upward beds bounded by transgressive surfaces and facies which mark transgression (Van Wagoner *et al.*, 1990). Parasequence stacking patterns, including aggradation, retrogradation and progradation, are first defined by Mitchum and Van Wagoner (1991) (Figure 4.2). Catuneanu (2006) recommends using parasequence concepts for the interpretation of prograding successions from marginal to shallow marine environments, where indications of abrupt marine transgression and deepening can be found.

Spence and Tucker (2007) proposed an alternative definition for a parasequence based upon detailed microfacies variation in a carbonate peritidal cycle as ‘*a regionally significant meter-scale sedimentary package characterized by a succession of facies*

that may shallow-up, deepen-up then shallow-up, aggrade, or reflect constant water depth. Bounding surfaces between each parasequence are sharp and defined by abrupt changes between genetic relays, genetic assemblages, paleowater depth and/or facies. Bounding surfaces need not always correspond to flooding surfaces'. In this definition, the flooding surfaces can occur within a parasequence or at the parasequence boundaries. The problem with this approach is that it introduces subjectivity in interpretation as it allows alternative picks of the parasequence boundaries. The approach followed in this study is to pick the resolvable flooding surface as the parasequence boundary and, where possible, to distinguish the transgressive and regressive elements in each cycle. As detailed in the following sections, most of the recorded cycles comprise a shallowing-up or regressive trend separated from the next cycle by a flooding surface.

In general, a parasequence can be attributed to a number of mechanisms, including a rapid change in subsidence or a high-frequency eustatically controlled relative sea-level rise or an autocyclic shift in depositional location in siliciclastic successions, such as a lateral shift in the position of a delta lobe through time (Mitchum and Van Wagoner, 1991).

4.4 Sequence stratigraphic model of high-frequency carbonate-evaporite cycles and mechanisms of their origins

Deposition of evaporite occurs when evaporation exceeds inflow at times of increased aridity in different environmental settings, from subaerial supratidal to subaqueous saline, as seen, for example, in the Zechstein, Paradox and Delaware Basins (Tucker, 1991; Sarg, 2001). Thick basin centre evaporites have been deposited in isolated basins, where these have been separated from the world's oceans by barriers, so reducing open circulation. Evaporites will not deposit or will be rare in open basins with open circulation and without barriers (Sarg, 2001). In most cases, carbonate is deposited around the basin margins when there is open connection and free circulation with the ocean (Tucker, 1991).

A number of sequence stratigraphic models for carbonate-evaporite cycles have been proposed for both ramp and rimmed platform profiles. For example, Tucker (1991) developed a sequence stratigraphic model for a carbonate-evaporite rimmed profile and applied it to the Zechstein Basin in NE England. Based on this model, during

incomplete drawdown, sequences start with a lowstand gypsum wedge at the basin margin, which pass laterally into gypsum-carbonate laminites in the basin centre, and then shift upwards to early TST sabkha/lagoonal gypsum. Then, during the late TST and HST, carbonate would be deposited. Deposition of evaporite may occur during the late HST in the upper most part of the sequence. However, during complete drawdown, i.e. when sea-level falls below the barrier, the basin is filled by a thick halite during the late lowstand. Then, the sequence passes up to the evaporite and carbonate of the TST and HST, respectively. Different sequence stratigraphic models have been proposed for the Zechstein cycles (Strohmenger *et al.*, 1996a; Wagner and Peryt, 1997; Becker and Bechstädt, 2006) and Paradox cycles (Weber *et al.*, 1995; Williams, 2009), and the origins in these cyclical architectures have been evaluated (Goldhammer *et al.*, 1991; Goldhammer *et al.*, 1994; Geluk, 2000a). This will be returned to as the focus of the comparative study outlined in Chapter 5.

Handford and Loucks (1993) proposed different sequence stratigraphic models for a variety of carbonate platforms in different climatic situations. They proposed a model for arid carbonate-evaporite ramps and stated that carbonate and evaporite are best developed during transgressive and highstand conditions, respectively. In addition, according to Sarg (2001), evaporite precipitation may occur in all the system tracts, depending upon the climatic and palaeo-oceanographic conditions of the basin but the best developed thick evaporite successions occur during the sea-level lowstands.

Small-scale shallowing-upward cycles have been described in a number of carbonate successions (Ginsburg, 1975; Wilson, 1975; Hardie, 1986; Grotzinger, 1986a; Grotzinger, 1986b; Goldhammer *et al.*, 1987a; Mitchum and Van Wagoner, 1991; Osleger, 1991; Strasser *et al.*, 1995). These shallowing-upward cycles are laterally and vertically variable. Microfacies analysis may highlight variations in an individual cycle when traced laterally and between cycles vertically (Tucker and Wright, 1990). Microfacies analysis and sequence stratigraphical investigations have been undertaken for peritidal shallowing-upward cycles in carbonate-dominated successions, including those representing subtidal, intertidal and supratidal settings (Read and Goldhammer, 1988; Montanez and Osleger, 1993). In some cases, these shallowing-upward cycles terminate with evaporite deposition during arid climate episodes, and numerous modern and ancient carbonate-evaporite cycles have been recorded (Alsharhan and Kendall, 2003; Nagy *et al.*, 2005). The supratidal evaporites are deposited in arid supratidal

sabkha and associated with shallow marine carbonate deposits of hypersaline lagoons and intertidal environments (Kendall and Patrick, 1969; Kinsman and Park, 1976).

There have been a number of reviews of the origins of cyclicity (Crevello, 1991; Osleger, 1991; Montanez and Osleger, 1993; Sami and James, 1994; Bosence *et al.*, 2009). A number of mechanisms have been invoked to interpret the origin of these cycles, namely variations in subsidence, tectonics, sedimentary processes, sediment supply and eustatic controls (Tucker and Wright, 1990). Each mechanism may control cyclicity alone or in combination.

Eustatic variation has been a widespread explanation for cyclicity through sea level changes related to the three Milankovitch cycles of precession (~20 kyr), obliquity (~40 kyr) and eccentricity (~100 kyr). When eustasy is the main control on cyclicity, the cycles should be traceable regionally along any extensive platform, and even globally, whereas poorly correlated cycles would suggest a local tectonic or autogenic origin (Tucker and Wright, 1990). In addition, cycles characterised by regular changes in accommodation, cycle type, stacking patterns and thickness all imply a eustatic control (Bosence *et al.*, 2009).

Tectonic mechanisms have a major role in the development of a basin fill stratigraphy and configuration (Miall, 2010). Syn-sedimentary faults during deposition of a cyclic succession result in the generation of differential subsidence or uplift (Bosence *et al.*, 2009), which in turn control accommodation creation. In this case, cycles which are laterally non-continuous with variable thickness would be generated (Tucker and Garland, 2010).

The tidal-flat progradation model of Ginsburg was developed to explain the origin of tidal-flat progradation (Ginsburg, 1975). A number of shallowing-upward cycles may be generated by progradation of tidal-flat facies belts across a platform. Subtidal or shallow lagoons are places of high carbonate production, and they may feed sediments to tidal-flat belts of nearly zero production, by current, wave and storm reworking. In the model, the high carbonate production in subtidal and shallow lagoons causes progradation of the tidal-flat belts basinward that in turn kills carbonate production and stops progradation. As a result, the next cycle will start with a new transgression. This process generates a number of shallowing-upward cycles that are capped by fine-grained deposits (Read *et al.*, 1991; Flugel, 2004) (Figure 4.3). Autogenic sedimentary

processes, including tidal-flat progradation, may thus generate laterally impersistent shallowing-upward cycles (Tucker and Garland, 2010). In addition, variability in cycles thickness, section thickness and stacking patterns are also indicative of such autogenic origins (Bosence *et al.*, 2009).

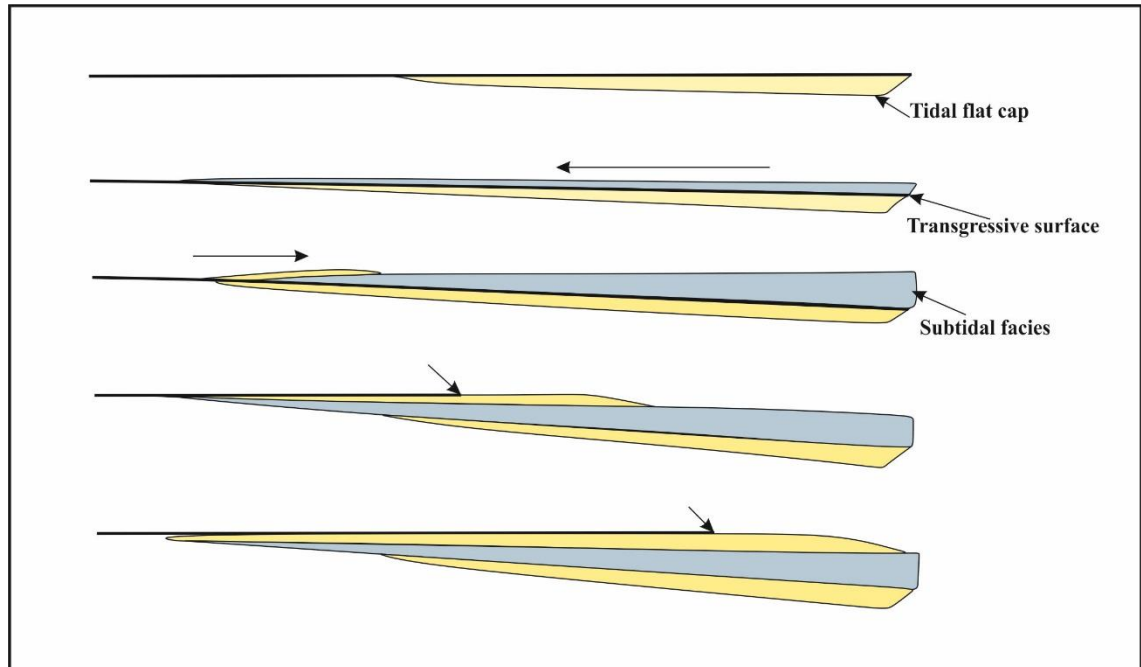


Figure 4-3 Tidal flat progradational model on a carbonate ramp. Each cycle terminates with a disconformity surface (heavy line) and is capped by tidal flat deposits. Subtidal deposits onlap the disconformity surface toward the margin, and then tidal flat deposits start to prograde toward the basin and continue to extend completely across the platform (Read *et al.*, 1991).

4.5 Review of vertical facies variations within the Fatha Formation

Each cycle of the Fatha Formation typically passes up from calcareous mudstone to shallow water carbonate and then grades up to nodular evaporite. The red alluvial unit that was sourced from the marginal hinterlands then caps each cycle, before a flooding surface marks the start of the next parasequence. During fieldwork investigations and microfacies studies (Chapter Three), vertical facies variations were observed and interpreted. For the purposes of this chapter, the vertical facies associations seen in each sedimentary facies are summarised as follows:

4.5.1 Vertical facies variations within the calcareous mudstone unit

The calcareous mudstone unit in the lower part of each cycle was investigated during fieldwork. The vertical facies variations included changes in colour, thickness and lithology. In each individual calcareous mudstone unit, a vertical change in lithology was observed from pure calcareous mudstone to marly carbonate at the top. In addition, this variation was also observed through thin section examination, in which quartz percentages increase toward the top. Furthermore, vertical variations were also observed within the extracted microfossils from different parts of each individual unit. For this purpose, samples were taken from the base, middle and upper parts of each individual unit. The extracted microfossils (rotaliids, miliolids and ostracods) from the base of an individual calcareous mudstone unit are very small, mostly 100µm in size, with low abundance and diversity. Toward the middle part of the unit, the extracted microfossils are moderately sized (200µm), with moderate abundance and diversity. However, toward the top of the unit, the extracted microfossils are large (300µm) in size with high abundance and diversity.

These variations in facies vertically reflect changes in water depth and salinity. There is a negative relation between size and water depth, as well as salinity (Bradshaw, 1961; Van Harten, 1975). The calcareous mudstone unit from an individual cycle becomes shallower toward the top. In addition, the percentage of bivalves, oysters and bryozoans increases with siliciclastic input.

4.5.2 Vertical facies variations within the carbonate unit

The carbonate members are the major sedimentary facies in the Fatha cycles and include different microfacies that represent different environmental settings (Chapter Three). Based upon the observed carbonate microfacies (Chapter three), seven facies associations were recognized within the cycles as illustrated in Table (4.2), as follows:

1- Ooid capped carbonate microfacies (OCCM)

This facies association passes up vertically from carbonate skeletal mudstone to wackestone/packstone microfacies (SK1-SK7) with evaporite pseudomorphs, to ooidal grainstone microfacies (NS4-NS5) at the top.

2- Peloid-oid capped carbonate microfacies (POCCM)

This facies association passes up from skeletal wackestone-packstone (SK2-SK7) to peloidal-oidal grainstone microfacies (NS3) and then grades up to ooidal grainstone microfacies (NS4-NS5) at the top. In some cases, the ooidal grainstone microfacies is modified by meteoric water diagenesis and capped by the red claystone units.

3- Stromatolite-algal mat capped carbonate microfacies (SACCM)

The carbonates of this cycle pass up from carbonate skeletal wackestone-packstone microfacies (SK2-SK7) to carbonate mudstone microfacies with subaerial laminae (SK1c) and then grade up to algal mats (AG1) and stromatolites (AG2) at the top with evaporite pseudomorphs, fenestrate pores and subaerial exposure laminae. This type of cycle is capped by nodular evaporites and then by the red claystone units. In a few cases, the carbonate constitutes a thin algal mat (AG1) or stromatolite (AG2) carbonate microfacies with evaporite pseudomorphs and fenestrate pores. This cycle is common throughout the succession.

4- Bivalve-barnacle-oyster capped carbonate microfacies (BBOCCM)

This cycle motif passes up from carbonate grainstone to floatstone/rudstone microfacies rich in bivalves, barnacles and oysters (M2-M3). The bivalves have complete valves and are in situ, while the oysters are commonly attached to the bivalves. This cycle is common throughout the succession.

5- Carbonate mudstone capped carbonate microfacies (CMCCM)

The carbonate of this cycle is composed of a thin carbonate mudstone microfacies unit (SK1b) and is capped by the red claystone unit. This cycle is common at the upper part of the succession.

6- Laminated pellet grainstone capped carbonate microfacies (LPCCM)

This cycle comprises multiple interbedded layers of thin calcareous mudstones and thin laminated pelletal grainstone microfacies (NS2) and then are capped by the red claystone units. This cycle is common at the upper part of the succession.

7- Bioclastic peloidal grainstone capped carbonate microfacies (BPCCM)

This type of cycle is composed of the bioclastic peloidal grainstone microfacies (NS1c) and it is overlain by the red claystone unit. This cycle is common in the upper part of the succession. In general, these vertical variations in the carbonate units represent shallowing-upward trends. The shallowing-upward changes within the carbonate microfacies are from mudstone to skeletal wackestone microfacies at the base, up into skeletal packstone microfacies and then these pass up into non-skeletal grainstone or mollusc rudstones or algal mats/stromatolites at the top. This means that the water depth of the carbonate units are diminishing toward the top.

Table 4-2 Shallowing-upward facies changes within the carbonate microfacies of the Fatha Formation.

Carbonate Cap	Characteristics	Occurrence
OCCM	Carbonates represent restricted to semi-restricted hypersaline conditions at the base and shallow lagoons and sand shoals at the top. They show increases in circulation and hydrodynamics, and diversity of organism, and decreases in salinity upward through the cycles. The thickness of the carbonates is about 1-3 metres.	Common in all the studied areas. Particularly abundant in the lower part of the succession.
POCCM	Carbonates represent restricted to semi-restricted hypersaline conditions at the base, then shallow lagoon and sand shoals at the top. They show increases in circulation, hydrodynamics and diversity of organisms, and decreases in salinity upward through the cycles. Thickness is about 2-4 metres.	Common in all the studied areas. It is abundant in the middle part of the succession.
SACCM	Carbonates are thin (10-30cm). Generally, they comprise intertidal algal bindstone or intertidal stromatolite, while occasionally they represent restricted hypersaline lagoon and shallow lagoon conditions at the base and intertidal algal bindstone and stromatolite conditions at the top. In a few cases, they just comprise a thin carbonate (20cm) of restricted stromatolite facies.	Very common and abundant throughout the succession. They were recorded in all the studied areas.
BBOCCM	Carbonates represent shallow lagoonal conditions at the base intertidal conditions at the top. They show increase in faunal diversity and circulation. Thickness is about 10-50 cm.	Very common and abundant in both parts of the succession.

CMCCM	The carbonates are thin (10-20cm) and represent mixed coastal carbonate-siliciclastic shallow lagoon conditions.	Very common in the upper part of the succession.
LPCCM	The carbonates are thin (10-20cm) and they are interpreted as shallow lagoon deposits in the basal parts and intertidal towards their tops.	Common in the Takiya and Basara sections in the lower part of the succession.
BPCCM	The carbonates are thin (20-50cm) and they are interpreted as shallow normal water lagoon toward the base and intertidal toward the top. They show increase in faunal diversity and circulation upward through the cycle.	Common in all the studied areas and particularly abundant in the upper part of the succession.

4.5.3 Vertical facies variations within evaporite unit

The vertical facies variations within the evaporite were also observed. The carbonate unit is vertically overlain by thick evaporite. The evaporite is mostly composed of nodular, while it is vertically passing to laminated evaporite and salt, in some cycles.

This trend in the evaporite unit also represents shallowing-upward trend that is part of the regressive cycles.

4.5.4 Vertical facies variations within red clastic unit

Vertical facies trend within the clastic unit was clearly observed throughout the succession or individual cycles. Siliciclastic deposits become abundant toward the upper succession in which sandstone is increasing. Furthermore, in each individual cycle, the clastic unit is passing up from claystone to siltstone and then to sandstone. In addition, the thickness of the unit is increasing toward the upper succession. There are several cycles of claystone and sandstone at the upper succession. This trend continues and becomes fully siliciclastic in the Injana Formation.

Overall, a shallowing-upward trend was observed from the largest scale of the whole succession of the Fatha Formation to the smallest individual bed or unit within the cycles. There is a regressive or shallowing-upward trend throughout the succession, in which marine deposits become missing toward the top of the succession. Furthermore, the succession constitutes a number of regressive cycles; each cycle represents a shallowing-upward trend from calcareous mudstone to shallow water carbonate and then evaporite and fluvial deposits. Shallowing-upward trend is one of the most observed features, not only in individual cycles and succession but rather in an individual sedimentary unit. It was observed in all the sedimentary facies such as calcareous mudstone, carbonate, evaporite and red clastic units.

4.6 High-frequency cycles of the Fatha Formation

A number of carbonate-evaporite shallowing-upward cycles are preserved from the Zagros foreland basin that extended along the margin of the Arabian Plate. At the basin margin, each cycle records an upward transition from calcareous mudstone (marl) at the base, which, as just detailed, grades up to or is interbedded with the shallow marine carbonate that changes from mudstone/wackestone at the base, to packstone/grainstone

or algal mat/stromatolite at the top. Occasionally, thin carbonate units (10-20cm thick) are interbedded with the calcareous mudstone unit. The carbonate unit then typically grades up to a thick nodular evaporite unit (1-10m) and this is capped by a red alluvial unit, at the top of the cycle (Figures 4.4 and 4.5). The red alluvial unit was sourced from the uplifted areas around the margin. However, in the basin centre, the majority of the cycles in the lower part of the succession are composed of interbedded thin calcareous mudstone or carbonate at the base, grading up to a thick evaporite (1-20m). However, toward the upper part of the succession, the cycles are composed of interbeddings of calcareous mudstone, carbonate and evaporite, from base to top respectively. The red alluvial to fluvial unit appears at the top of the cycles in the uppermost part of the succession. Occasionally, laminated evaporite (bedded evaporite) and salt cap the cycles in the basin centre (Tucker, 1999; Al-Juboury and McCann, 2008).

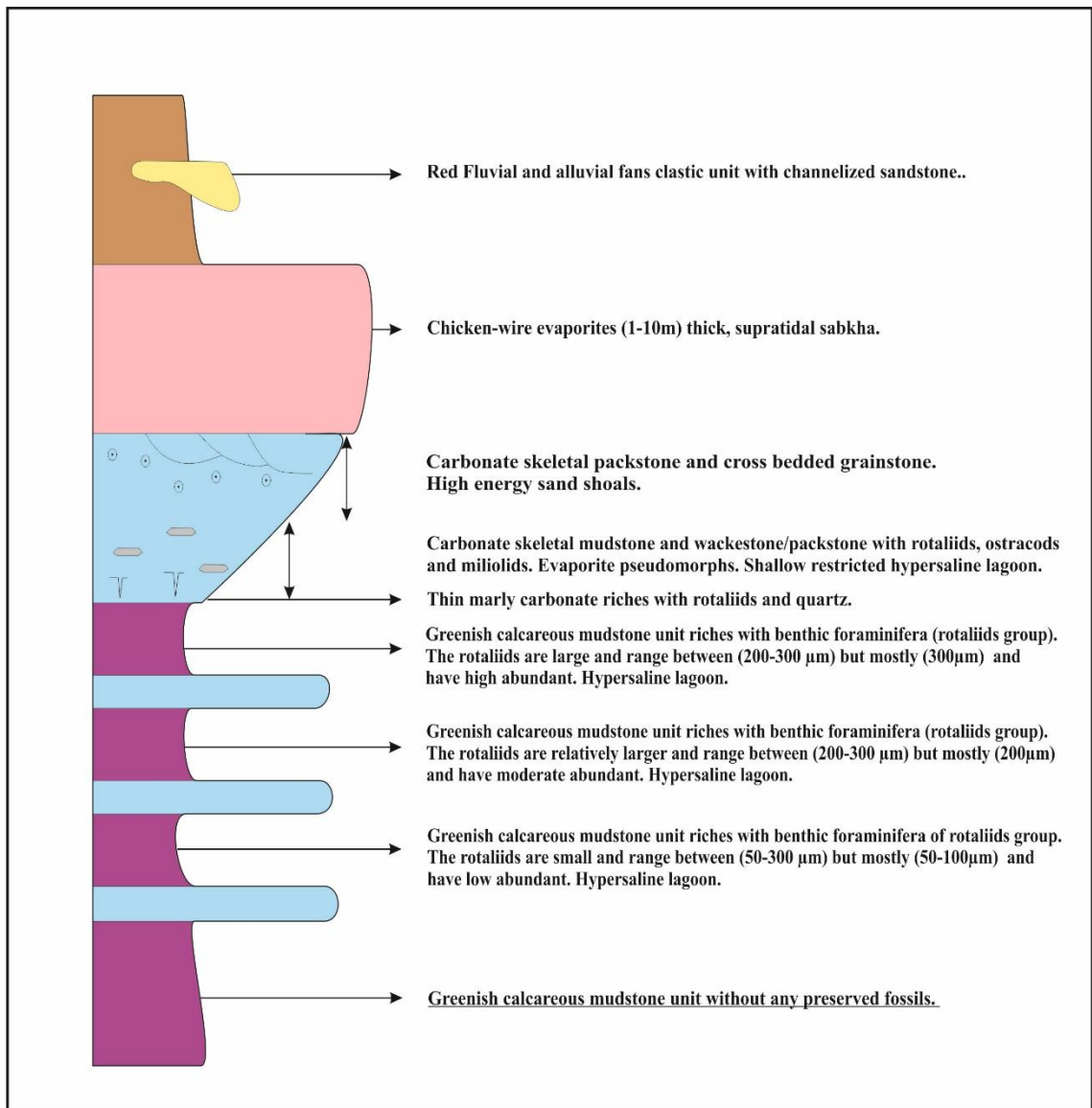


Figure 4-4 A representative schematic log of vertical facies variations of a high-frequency shallowing-upward cycle of the Fatha Formation. The facies variations form a high-frequency shallowing-upward package that is repeated throughout the succession.

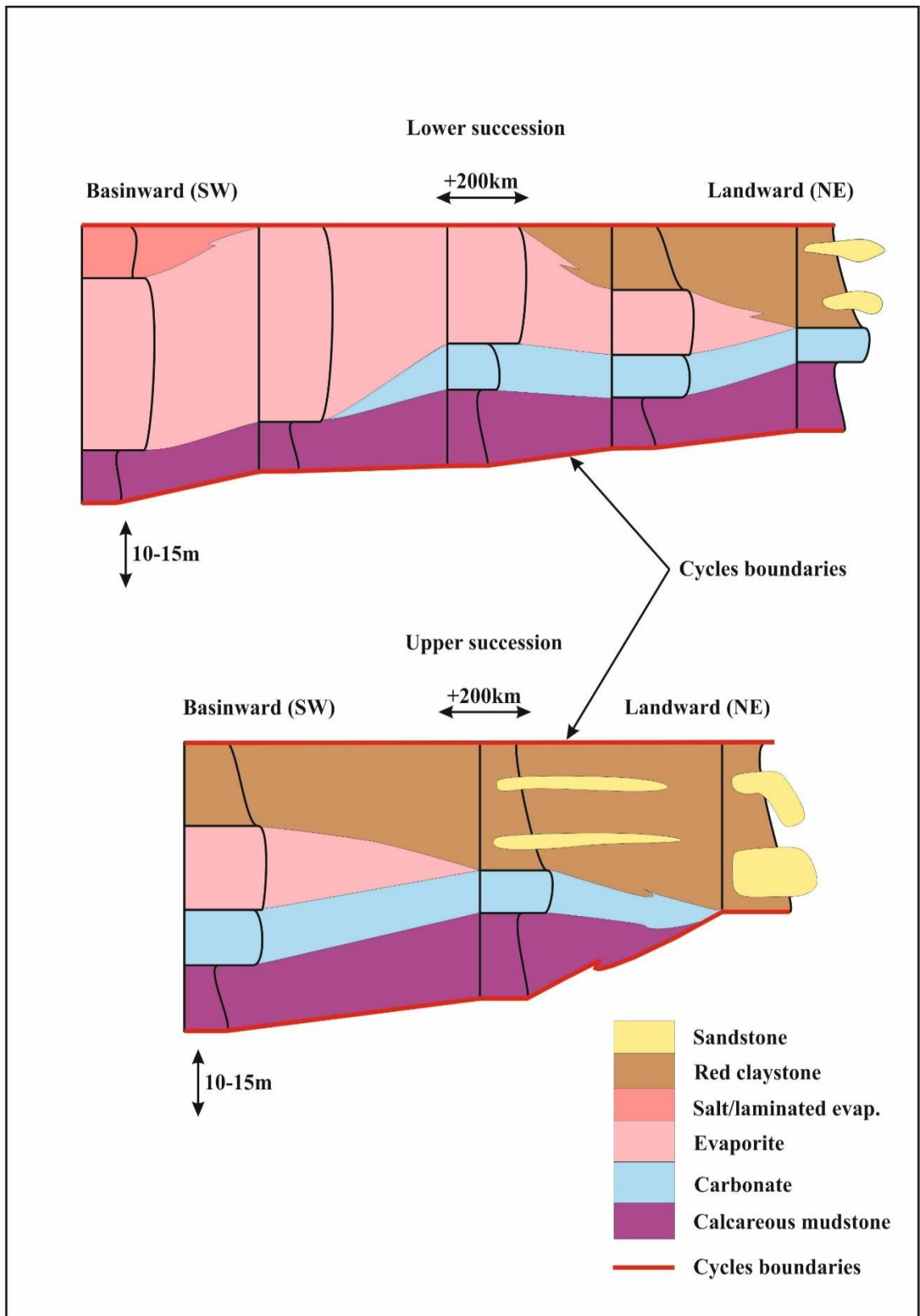


Figure 4-5 Lithostratigraphic correlation of the shallowing-upward parasequences from basin margin to basin centre in the lower and upper part of the succession. The evaporite thickens toward the basin centre (Al-Juboury and McCann, 2008) and the fluvial unit progrades toward the basin.

The calcareous mudstone and carbonate units become thinner toward the basin centre, whereas the evaporites becomes thicker. The proportion of the red alluvial/fluvial input increases toward the top of the succession and caps the basin centre cycles in the upper part of the succession (the Upper Member as defined in Figure 4.10). Moreover, salt is also documented at the top of the evaporite in some cycles in the basin centre. The salt was not documented from outcrops because it was dissolved out or probably was not deposited in marginal locations. Laminated evaporite (bedded evaporite), interpreted as subaqueously deposited evaporite, was recorded in one cycle only from the studied outcrops but in multiple cycles from the basin centre (Tucker, 1999). The thicknesses of the cycles and of the succession as a whole decrease from the basin centre to the basin margin. The succession was documented to be 400-650m thick in the basin centre (Al-Juboury and McCann, 2008); however, at the studied areas on the basin margin the thickness was around 50-300m thick. In addition, the maximum number of cycles, 55 cycles, is preserved in the basin centre (Tucker, 1999), whereas 30-40 cycles were recorded at the basin margin. Furthermore, the thickness of the cycles varies from lower to upper parts, and a number of thick cycles were preserved in the lower part. In contrast to the lower part, the cycles in the upper part become thinner.

4.7 Correlation panels and lateral facies changes

During fieldwork, several thick carbonate units were chosen and followed for more than 20km. These carbonate units were traced between the logged sections. In addition, the laminated evaporite was also followed between the sections for more than 10km. Based on these correlatable carbonate and evaporite units, all cycles have been correlated across the whole area, “hung from” these initially correlated units. As a result, two correlation panels have been constructed along two different trends. The first is along the Qishlagh-Sargrma-Darbandikhan Mountains, including the Takiya, Basara, Krbchna, Darbandikhan and Chnarah sections (Figure 4.6). The second follows the Aj Dagh-Qara-Wais anticlines, and includes the Aj Dagh, Sangaw, Mamlaha and Kfri sections (Figure 4.7). The correlated cycles from these two panels show consistent lateral and vertical facies changes. These changes include an overall vertical shallowing-up trend from evaporite-dominated cycles in the lower part, to siliciclastic-dominated cycles in the upper part. In addition, the thickness of the cycles is greater in the lower part of the succession than the upper part. However, the thickness of the succession and the number of cycles increases toward the SW of the studied area, where

the succession is about 320m thick and includes 40 cycles. In addition, the thickness of the succession becomes very thin (50m) in the most proximal areas (e.g. Chnarah), where it also becomes more siliciclastic-dominated. Hence, variations from the lower part to the upper part of the succession are clearly observed. The cycles within the lower part have been correlated between the sections. Some sections have a higher number of cycles when they were correlated laterally. The cycles from the Takiya and Basara sections for example, have a higher number of cycles distinguished in the lower part than the Krbchna section, and the Krbchna section has a higher number of identified cycles than in the Darbandikhan area. Lastly, the Chnarah section has the minimum number of cycles. This suggests that some cycles may have limited expression and have been missed between the sections, or more probably that they onlap onto underlying surfaces and pinch out between sections.

Cycle correlations based on sedimentary facies reveal that most of the cycles can be traced between the sections for distances of more than 50km. However, samples collected from a number of individual cycles reveal that any particular microfacies within an individual cycle cannot be traced for a distance greater than 20 km. This constrains the lateral continuity of cycles but the lateral variability of microfacies.

The high-frequency cycles of the Fatha Formation have previously been described as high-frequency sequences bounded by type 2 sequence boundaries in two studies (Tucker, 1999; Ameen, 2006), but with no any identified subaerial exposure. In contrast, in another study, the cycles are interpreted as high-frequency parasequences that are bounded by flooding surfaces (Al-Juboury and McCann, 2008). In this study, the key stratigraphic surface recognized in each cycle is the flooding surface representing a rapid transgression where calcareous mudstones overlie pre-existing red alluvial claystones. Above the flooding surface and carbonate mudstones, the cycle typically grades up to shallow water carbonate and then passes up to evaporite. A red alluvial/fluvial unit then progrades over the evaporite toward the basin. Therefore, each cycle is typically capped by the red fluvial unit at the top, and each cycle represents a regressive and shallowing-upward trend, which progrades toward the basin. The next cycle starts with a new flooding surface. Importantly, there is no any indicator of subaerial exposure or sea-level fall identified and observed at the top of the evaporite. This study therefore follows standard sequence stratigraphic terminology (Van Wagoner

et al., 1988), such that the Fatha Formation cycles are termed parasequences, being conformable packages of beds bound by marine flooding surfaces.

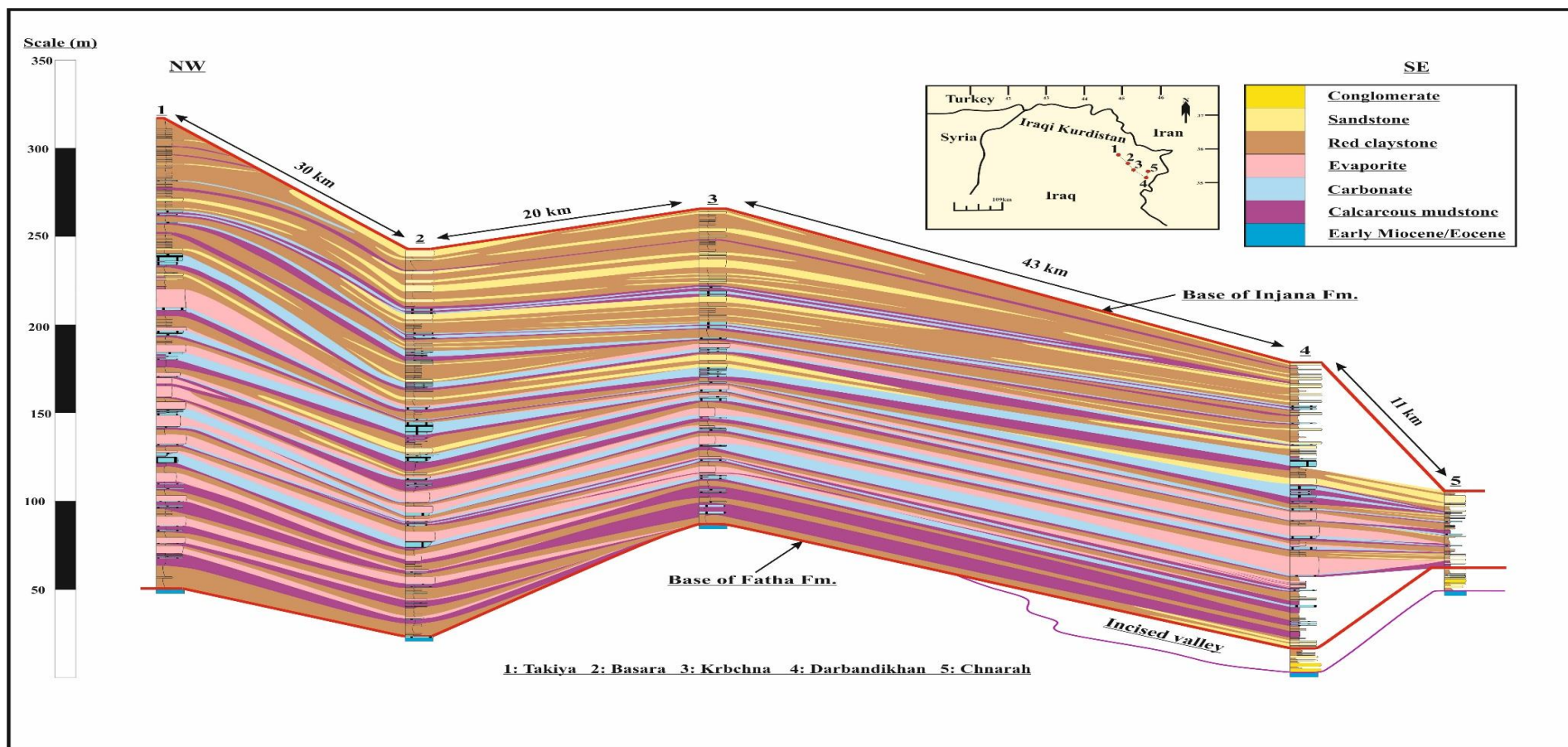


Figure 4-6 Lateral and vertical correlations of the studied cycles along the Qishlagh-Sargrma-Darbandikhan Mountains. The cycles are traceable for tens of kilometres but the microfacies within the individual cycles vary laterally. A higher number of siliciclastic-dominated cycles are recorded along these sections.

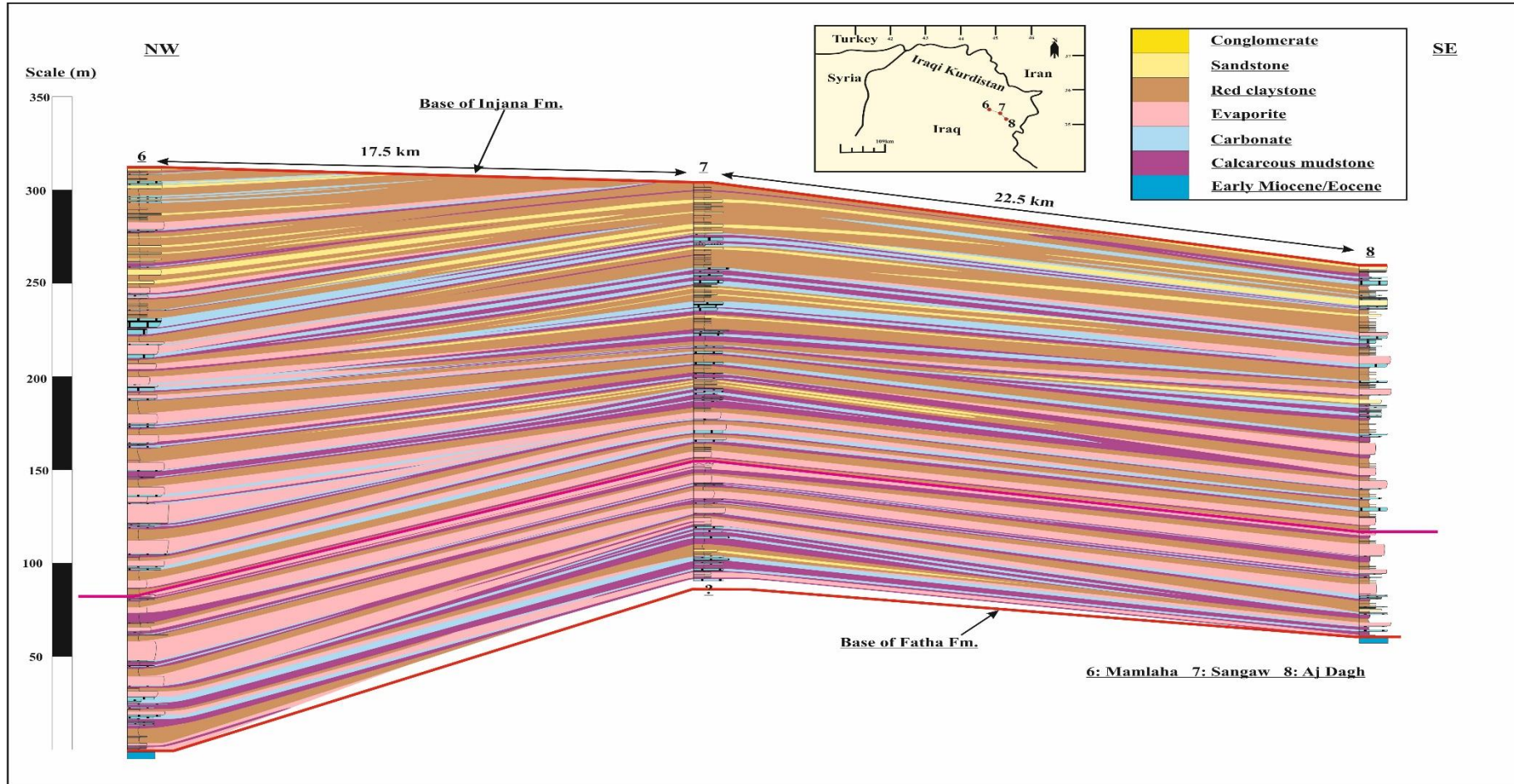


Figure 4-7 Lateral and vertical correlations of the studied cycles along the Aj Dagh-Qara-Wais anticlines. The cycles are traceable for tens of kilometres but the microfacies within the individual cycles vary laterally. A higher number of evaporite-dominated cycles are recorded in the thicker successions.

4.8 Types of parasequences

A variety of internal architectures of parasequences is observed, as outlined below. The distribution of these variants is then considered in terms of their lateral and vertical position in the Fatha Formation. This intra-parasequence variation is then considered together at the scale of the log correlation panels, to characterize the detailed spatial and temporal variation in parasequences through the formation (Figure 4.8 and Table 4.3).

4.8.1 Type A

This type of parasequence is represented by a calcareous mudstone unit overlying the basal flooding surface, which passes up to a thin bed of enterolithic evaporite (5cm) and then passes up again to a thin calcareous mudstone (5cm) and finally to a ca. 1m thick bed of laminated evaporites at the top. It is then capped by the red clastic unit (Figure 4.8). Occasionally, thin carbonate beds (10cm thick) are interbedded within the calcareous mudstone units. During field work, the laminated evaporite could be traced from the Takiya to Krbchna sections, a distance of approximately 70 km (Figure 4.9A-B). As described previously, the laminated evaporite has therefore been used as a marker bed for correlation, because of its lateral continuity and consistent stratigraphic position in all of the sections where it is seen. As a result, it was inferred that the cycles at the base of the succession onlap the sequence boundary toward the margin. In other words, the laminated evaporite is recorded at a relatively high stratigraphic position in the Mamlaha, Sangaw and Aj Dagh sections compared to the Darbandikhan area, and it is missing in the Chnarah section (the most proximal area). This type of parasequence is only recorded from one cycle in the measured sections. However, it has been described as a common signature in the basin centre (Figure 4.10), where nodular evaporites are capped by either halite or laminated evaporites in multiple cycles (Tucker, 1999).

4.8.2 Type B

Type B parasequences grade up from a calcareous mudstone unit (0.5-1.5m) to thick nodular evaporites (3-5m) and these are then capped by a red clastic unit (Figures 4.8 and 4.9C). This type of cycle is not common in the marginal areas and it was only documented in 2-3 cycles. However, it is a common cycle style of the Lower Member in the basin centre (Figure 4.10), but where it is not capped by the red clastic unit.

4.8.3 Type C

Type C parasequences pass up from a shallow water carbonate unit above the basal flooding surface to thick nodular evaporites and these are then capped by a red clastic unit (Figures 4.8 and 4.9D). This type is not common in the marginal area but it is common of the Lower Member in the basin centre (Figure 4.10), but where it is not capped by the red clastic unit.

4.8.4 Type D

Type D parasequences pass up from calcareous mudstone units above the basal flooding surface to a thick shallow water carbonate unit (1-3m) and then grade up to a thick nodular evaporite (1-10m) which is generally capped by a red clastic unit (Figures 4.8 and 4.9E-F). Occasionally, the calcareous mudstone unit at the base of the cycle is interbedded with thin carbonate beds (10cm). The carbonate unit constitutes different microfacies that shallow up from carbonate mudstone/wackestone to packstone/grainstone or algal mats/stromatolite at the top. The majority of the cycles in the lower part of the formation are composed of this type. However, in a few cycles, the red clastic unit is missing and the cycle is overlain by a flooding surface and the calcareous mudstone unit of the next cycle.

4.8.5 Type E

This type of parasequence is very common in the marginal areas, in which evaporites are missing (Figures 4.8 and 4.11A-B). This type also becomes more common toward the upper part of the succession and most of the cycles from the Darbandikhan area near Birke village and the Chnarah section are of this type of cycle. The cycles pass up from a calcareous mudstone unit at the base to shallow water carbonates (0.2-3m in thickness) and are then capped by a red clastic unit.

4.8.6 Type F

Type F parasequences pass up from shallow water carbonate rocks above the basal flooding surface to red claystone or sandstone beds at the top (Figures 4.8 and 4.11C). This cycle is very common in the upper clastic-dominated part of the formation toward the basin margin. The carbonate unit is mostly composed of grainstone textures.

4.8.7 Type G

This is a common parasequence type in the upper clastic-dominated part, toward the marginal areas. Above the basal flooding surface, a shallow marine silty calcareous mudstone unit passes up into red clastic or sandstone beds. The sandstone beds are enriched with *Rhyzolithos* ichnofacies (Figures 4.8 and 4.11D).

4.8.8 Type H

This type is also common in the uppermost part of the succession. Above each flooding surface, subaqueous highly bioturbated and mottled bluish-red mixtures of silt and marl are observed, and these contain various horizontal ichnofacies and vertical *Skolithos* (Figures 4.8 and 4.11E-F). These deposits pass up into red claystone beds in the upper part of the parasequence.

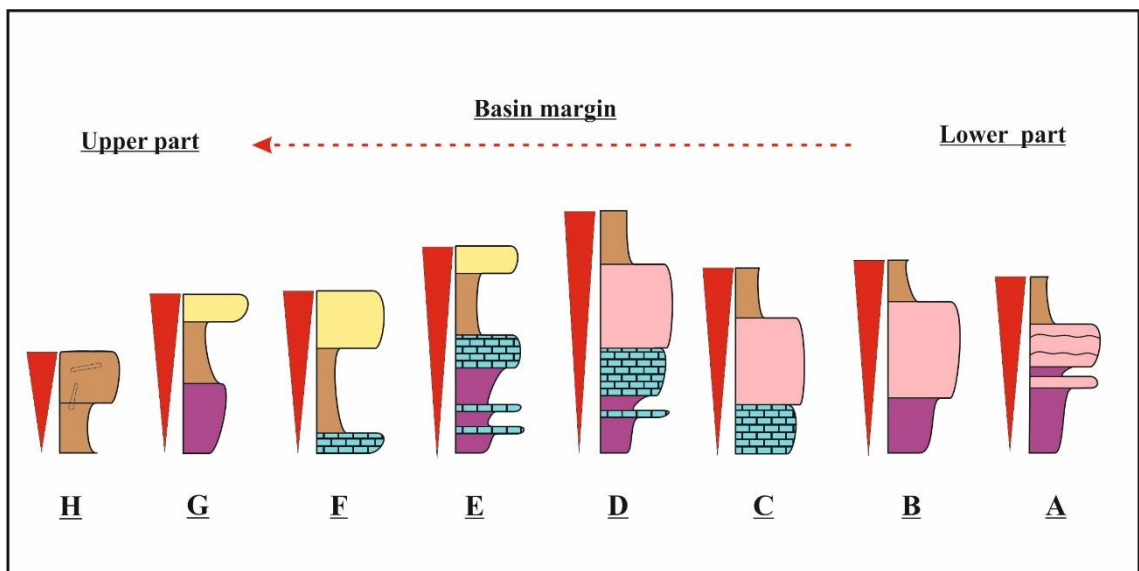


Figure 4-8 Types of parasequences and their distribution from the lower carbonate-evaporite-dominated part to the upper siliciclastic-dominated part.

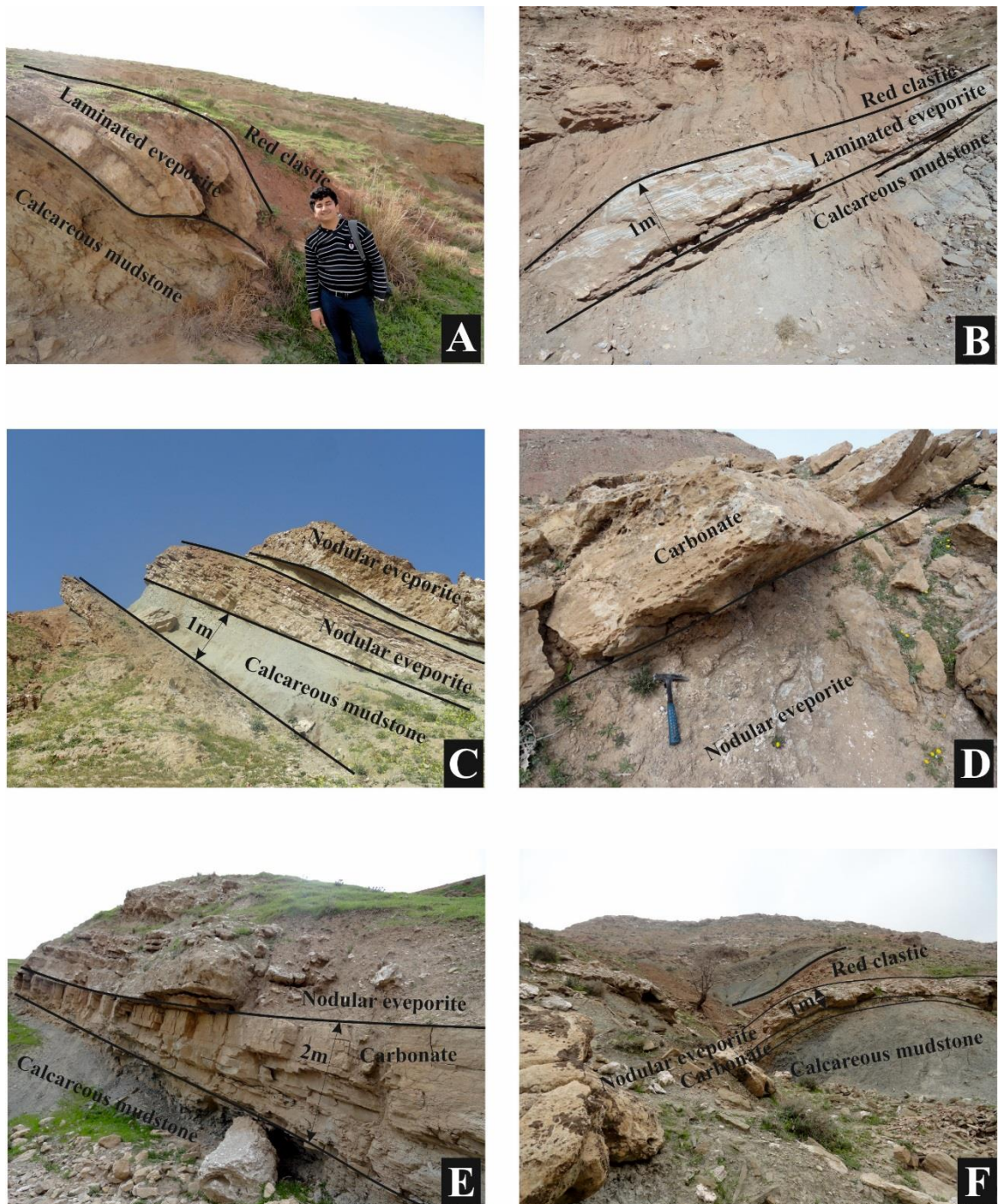


Figure 4-9 Field photographs of parasequence types in the lower part of the succession.

A and B: Parasequences of type A with calcareous mudstone at the base, shallowing up to laminated evaporite, followed by a red alluvial unit, from the Mamlaha and Basara sections, respectively. C: Parasequences of type B with calcareous mudstone at the base, shallowing up to nodular evaporite; Kfri section. D: A parasequence of type C, with nodular evaporite of the previous parasequence followed by a carbonate unit of the next and then shallowing up to nodular evaporite; from the Mamlaha section. E and F: Parasequences of type D with calcareous mudstone at the base, shallowing up to carbonate and then continuing the regressive trend to nodular evaporite and then a red alluvial/fluvial unit; from the Mamlaha and Basara sections, respectively.

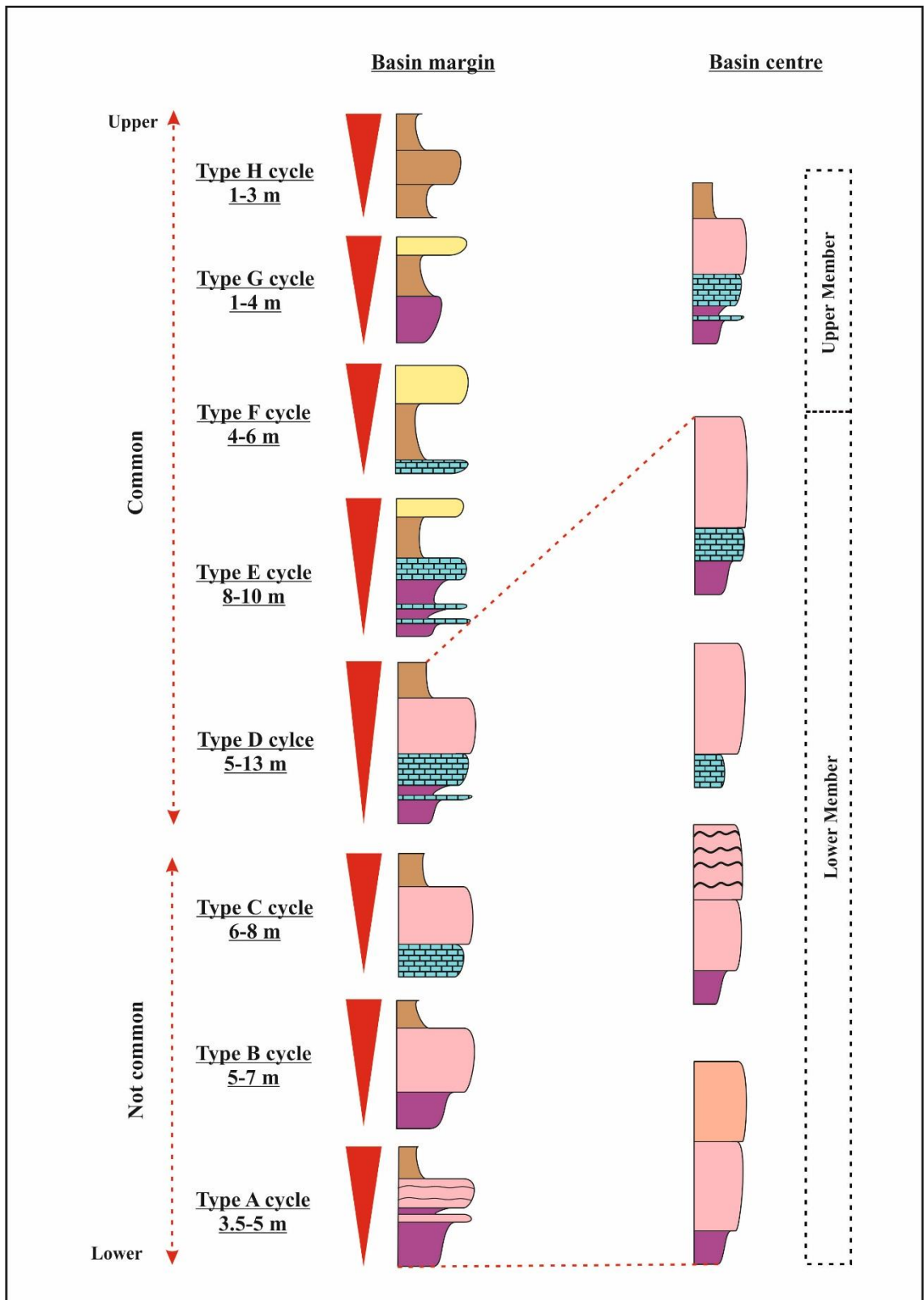


Figure 4-10 Representative logs of the shallowing-upward cycles or parasequences, type of cycles, their thickness ranges and distributions from the lower to upper parts of the succession and from the basin margin to basin centre. Overall, the cycles vary from evaporite-dominated in the lower part to siliciclastic-dominated in the upper part. Basin centre parasequence styles are after (Tucker, 1999).

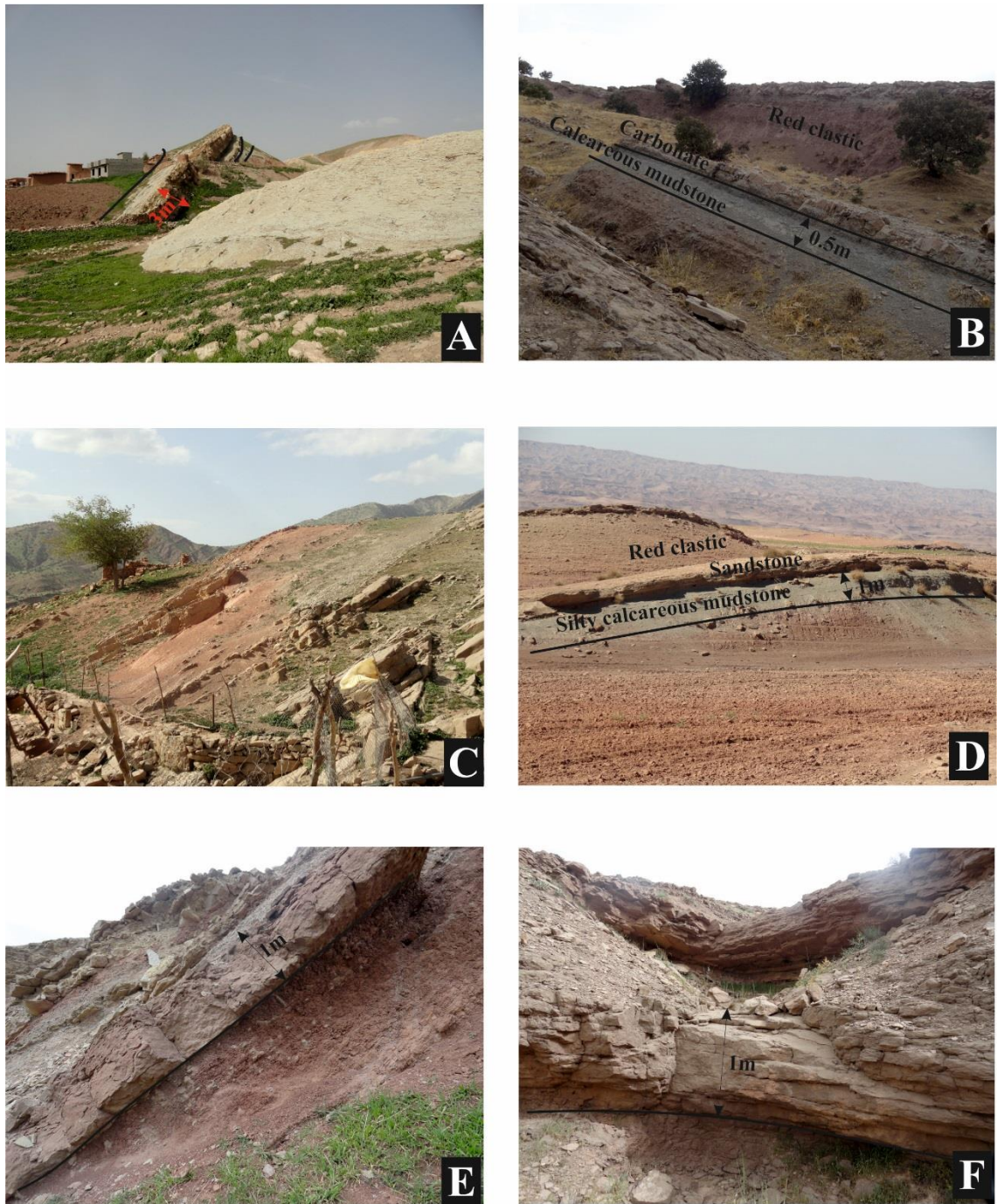


Figure 4-11 Field photographs of cycle (parasequence) types in the upper part of the succession.

A and B: Cycles of type E with calcareous mudstone at the base, shallowing up to carbonate and then followed by a red fluvial unit; from the Mamlaha and Chnarah sections, respectively. C: Cycles of type F with shallow marine carbonate at the base, shallowing up to red fluvial/alluvial units: from the Krbchna section. D: Cycles of type G with silty calcareous mudstone at the base, shallowing up to thin sandstone beds with *Rhyzolithos* ichnofacies; from the Mamlaha section. E and F: Cycles of type H with highly bioturbated mixed bluish-red siltstone at the base, shallowing up to red claystones; from the Takiya and Sangaw sections, respectively.

Table 4-3 Types, characteristics, occurrences of the cycles of the Fatha Formation.

Cycle-type	Characteristics	Occurrence (basin margin)	Occurrence (basin centre)
Type A	It is passing up from calcareous mudstone to laminated evaporite (1m) and then grades up to red clastic unit. Occasionally, thin carbonate (10-20cm) and enterolithic evaporite (5cm) are interbeddings with the calcareous mudstone. The thickness of the cycle is about 3.5-5m.	It is not common and it was just documented in one cycle in all the studied areas in the lower part.	It is common and it was documented in a multiple cycles in the lower member (without the red clastic unit).
Type B	It is grading up from calcareous mudstone unit at the base to thick nodular evaporite and then it is capped by red clastic unit. The thickness of the cycle is about 5-7m.	It is not common and it was just recorded in 2-3 cycles in the lower part.	It is the most common type in the lower member (without the red clastic).
Type C	The cycle is composed of interbeddings of calcareous mudstone at the base and thick nodular evaporite at the top. Then, the red clastic unit caps the cycle. The thickness of the cycle is about 6-8m.	It is not common and it was just recorded in 2-3 cycles in the lower part.	It is common in the lower member of the succession (without the red clastic).
Type D	The cycles are passing up from calcareous mudstone at the base to carbonate and then grades up to thick nodular evaporite and it is capped by red clastic unit. It is the thickest type 5-13m.	This is the most common type in the lower part of the succession.	It is common in the middle part (without the red clastic) and in the upper member (with the red clastic).

Type E The cycles are passing up from calcareous mudstone at the base to carbonate and then grades up to red clastic unit. Thickness of the cycles is about 8-10m. It is common type in the upper part of the succession. It is not common.

Type F It is passing up from shallow carbonate at the base to red clastic unit at the top. Thickness of the cycles is about 4-6m. It is common in the upper part of the succession. It is not common.

Type G It is passing up from silty calcareous mudstone at the base to red clastic unit at the top. Thickness of the cycle is about 1-4m. It is not common and it was just recorded in 2-3 cycles. It is not common.

Type H It is passing up from highly intensive bioturbated and mottled bluish-red mixtures of silt and marl at the base to red clastic unit. It is thin and is about 1-3m. It is very common in the upper most part of the succession. It is not common.

4.9 Parasequences and Fischer plots - methods

Examination of cycle thicknesses and variations in vertical facies trends help to constrain variations in accommodation space and relative sea-level changes, and Fischer plots are particularly useful visualisation tools for this purpose. Fischer plots were developed to present data on cyclic successions, with cycle number or a time dimension on the horizontal scale being plotted against cumulative departure from mean cycle thickness on the vertical scale (Fischer, 1964; Goldhammer *et al.*, 1987a; Read and Goldhammer, 1988). This type of plot was first introduced by Fischer in 1964 and used for the characterisation of peritidal carbonate cycles, in which a constant rate of subsidence and similar duration for each cycle were assumed. The vertical lines on the plots represent the thickness of each cycle, whereas the average thickness is represented by the diagonal lines on the plots (e.g. Figure 4.12). The subsidence rate (neglecting unknown compaction effects) is determined from the total thickness of the cyclic succession divided by total time duration of the succession. Whether chronostratigraphic constraints are available or not, original Fischer plots simply use cycle number on the horizontal scale, and so assume a constant time interval for each cycle. Sadler *et al.* (1993), for example, preferred this approach. In peritidal carbonate cycles (Fischer, 1964) and in regressive carbonate cycles (Tucker, 1999), it is the recognition that each cycle shallows upward to sea level that allows the Fischer plot to represent changes in accommodation through time, when averaged over the total duration of the stratigraphic interval being characterized.

Positive slopes on Fischer plots are produced by upward increases in the cycle thicknesses, when these are greater than the average thickness. However, thin cycles, which are less than the average thickness, generate falling slopes. The heavy line along the top of the cycles that is rising and falling thus reflects changes in accommodation space available to the depositional system. The conceptual basis behind these changes in the slope on the plots is exemplified by sets of thin cycles being represented by a downward slope, and these having been formed during decelerating accommodation space generation. Whereas, stacks of thick cycles are formed during a net accommodation space increase.

An alternative to the assumption that cycles are of equal time duration is to make the assumption that the sedimentation rate is constant from one cycle to the next. This is

achieved using the “modified Fischer plot” of Tucker (1999). In this, cumulative departure from mean cycle thickness is again plotted on the vertical scale with the thickness of each cycle plotted as a vertical line, but with the stratigraphic thickness of each cycle represented on the horizontal axis.

Assuming that background tectonic subsidence, if varying, was varying on a longer time scale than the high frequency parasequences, then a positive slope on the plot can be interpreted as an increase in accommodation space which was generated during relative sea-level rise. The high accommodation space was filled by thick carbonate and evaporite cycles. However, the falling parts on the plots are still positive and indicate decreasing accommodation space at the upper part that was generated during sea-level highstand. The decelerating accommodation creation on the falling parts of the plots are evidenced by decreases in cycle thicknesses.

Systematic vertical changes in cycle (parasequence) thickness and cycle type give a valuable data set for distinguishing the components of larger scale sequences, i.e. system tracts, through the variations in accommodation space that may have produced them (Mitchum and Van Wagoner, 1991). In addition, differences in stacking patterns give high resolution information for correlating and identifying the system tracts on broad platforms (Montanez and Osleger, 1993). Moreover, the Fischer plot is a useful tool for determining the origin of the parasequences by allowing examination of the regularity of the cycle thicknesses. Where the cyclicity was produced by orbital forcing, then one would expect regular patterns, and the Fischer plot may show a bundling of the cycles. In contrast, if the cyclicity was accumulated by autocyclic sedimentary processes, then a random pattern of cycle thickness would be expected on the Fischer plots (Tucker and Garland, 2010). Furthermore, the Fischer plot becomes more useful still where it is incorporated with facies analysis and vertical facies changes of the parasequences, as in this study. In this case, it can be used to examine and contrast the facies variations on the rising (high accommodation space) and falling (low accommodation space) slopes of the Fischer plot.

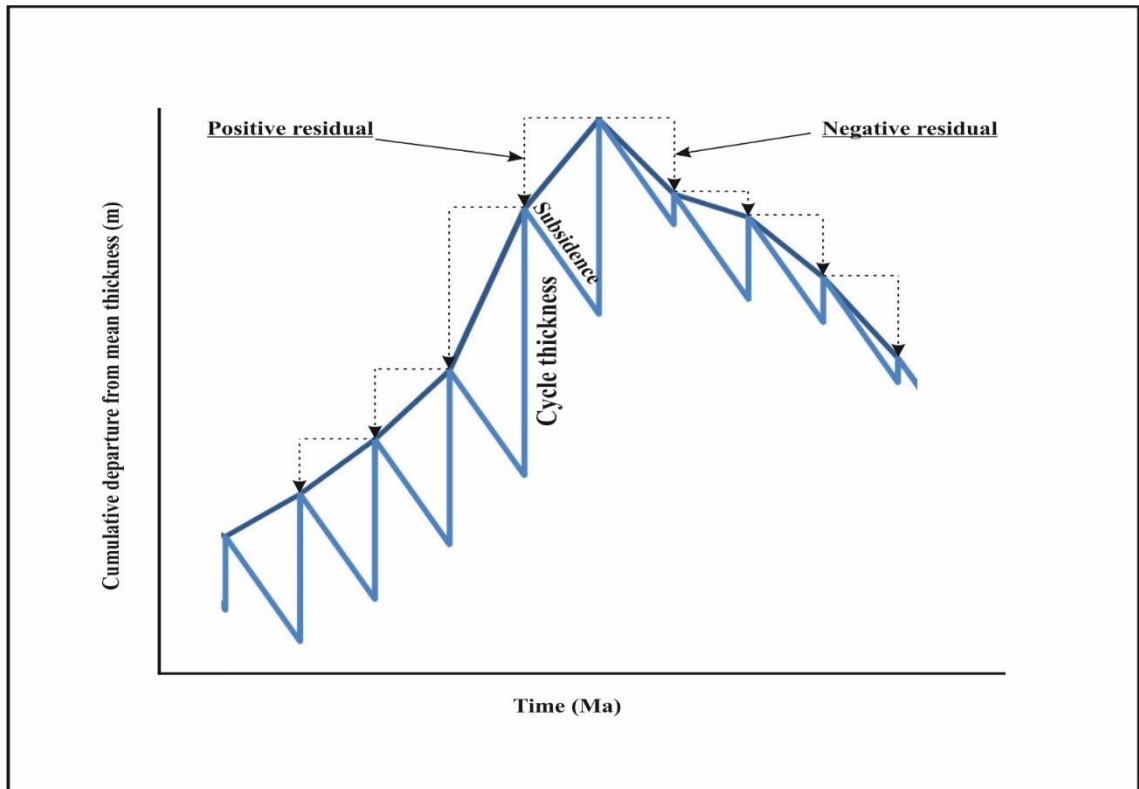


Figure 4-12 Standard curve of Fischer plot constructed between cumulative departure from mean cycle thickness and cycle number (Sadler *et al.*, 1993).

4.9.1 Results of Fischer plot analysis

The thick succession of mixed carbonate-evaporite-clastic cycles from the Fatha Formation shows dramatic variations in metre-scale cyclicities, dominant lithofacies and vertical facies trends. These are represented in Figures 4.13-4.21.

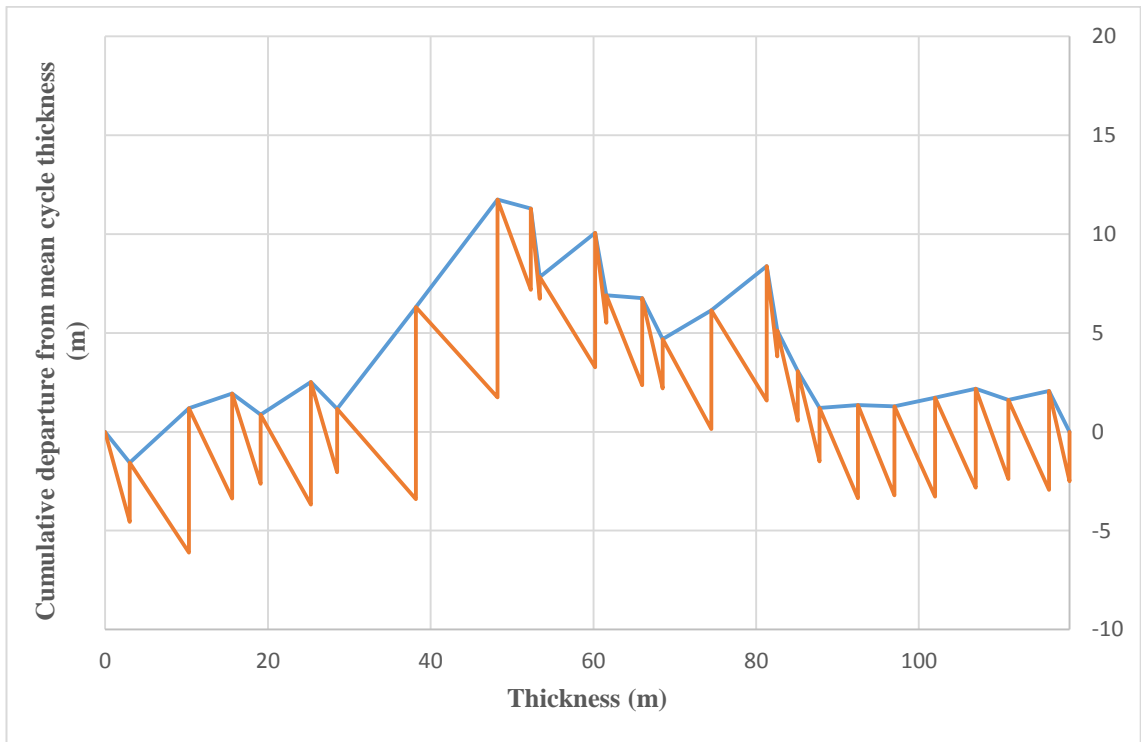
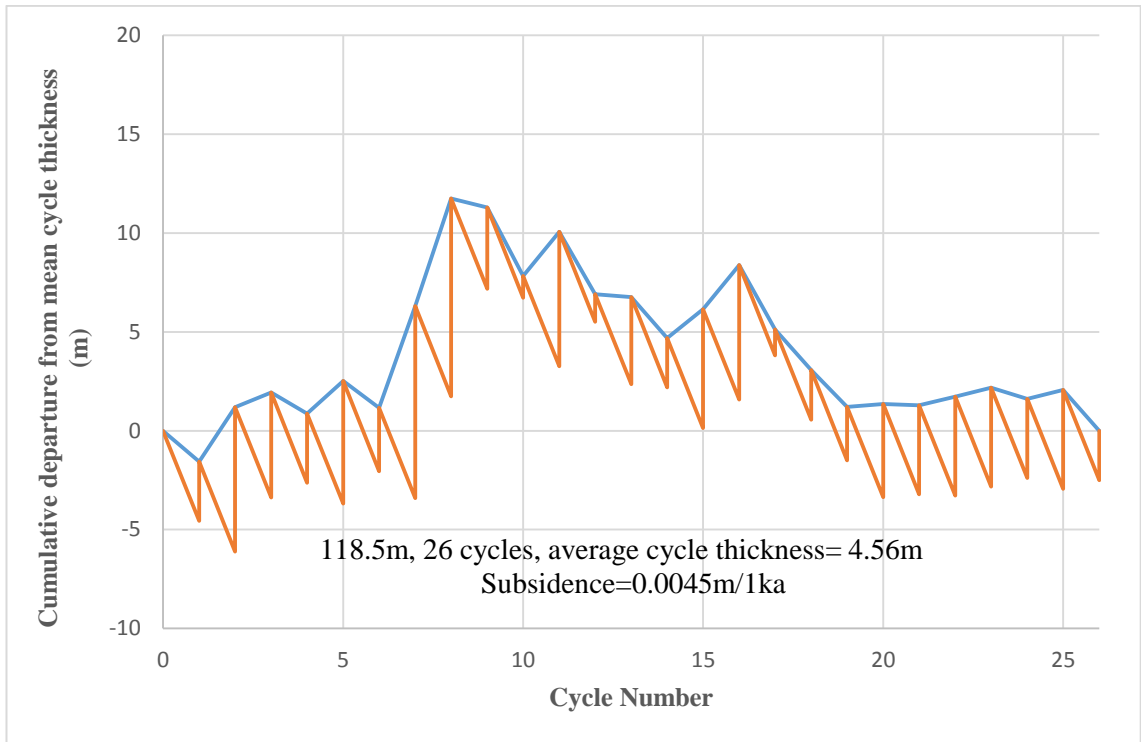


Figure 4-13 Fischer plot of the carbonate-evaporite cycles of the Fatha Formation from Kfri section. The plots represent the standard Fischer plot as constructed between cumulative departure of mean cycle thickness and cycle number (upper plot), as well as revised Fischer plot as presented between cumulative departure of mean cycle thickness and cycle thickness (lower plot).

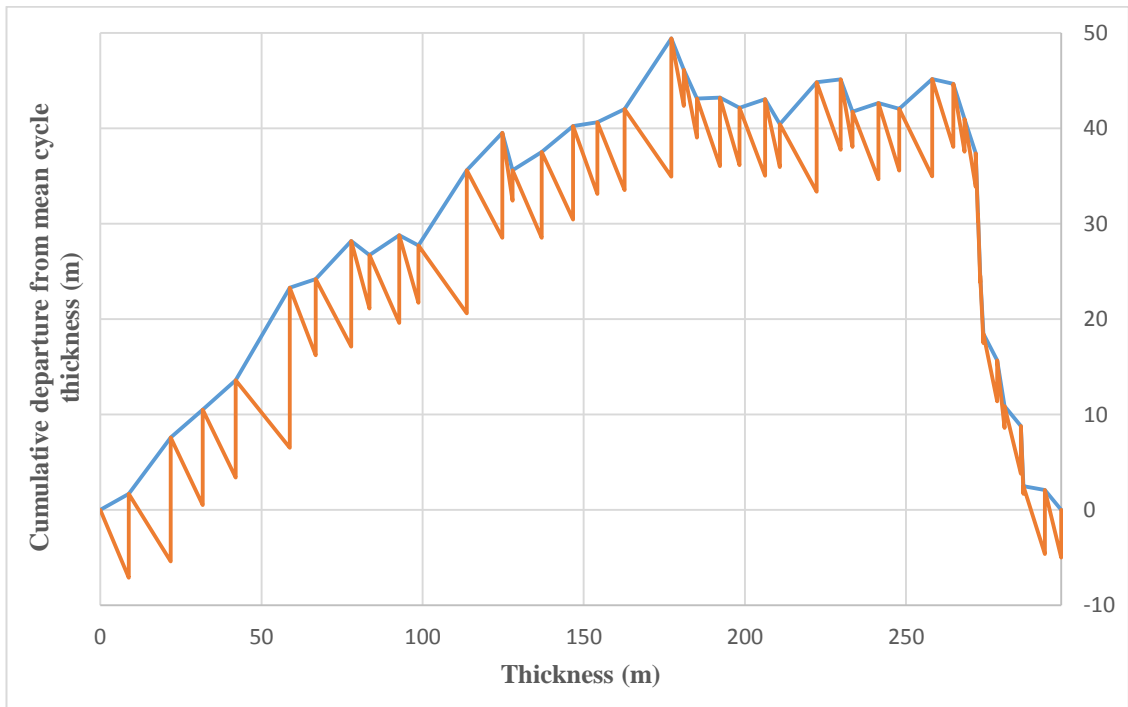
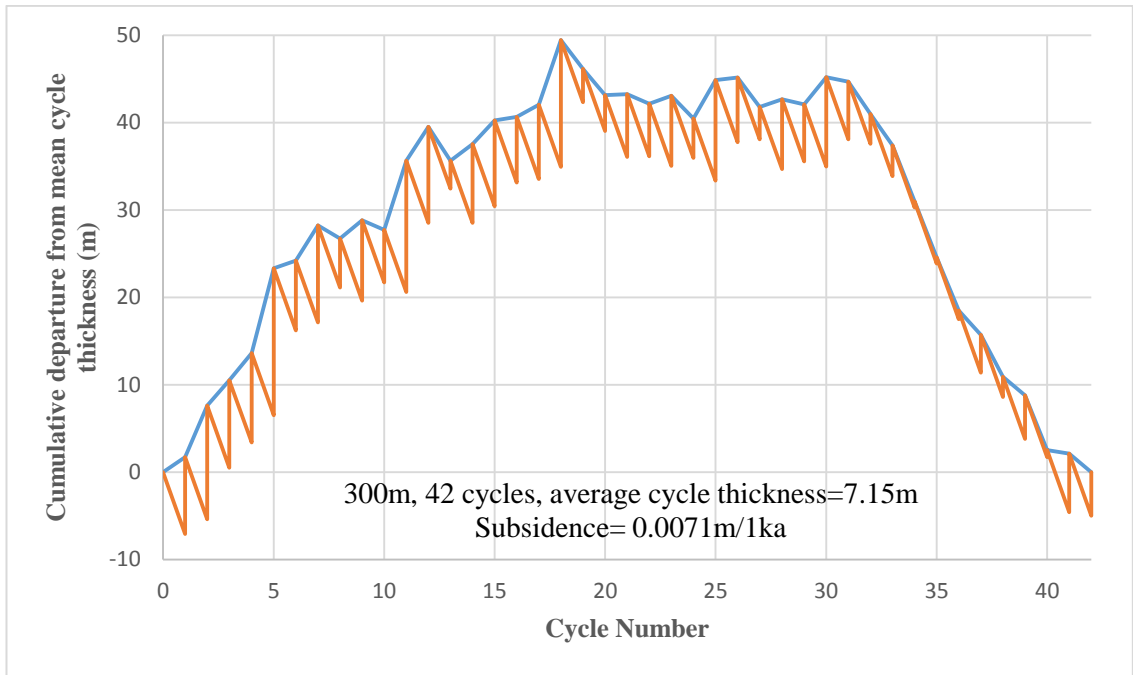


Figure 4-14 Fischer plot of the carbonate-evaporite cycles of the Fatha Formation from Mamlaha section. The plots represent the standard Fischer plot as constructed between cumulative departure of mean cycle thickness and cycle number (upper plot), as well as revised Fischer plot as presented between cumulative departure of mean cycle thickness and cycle thickness (lower plot).

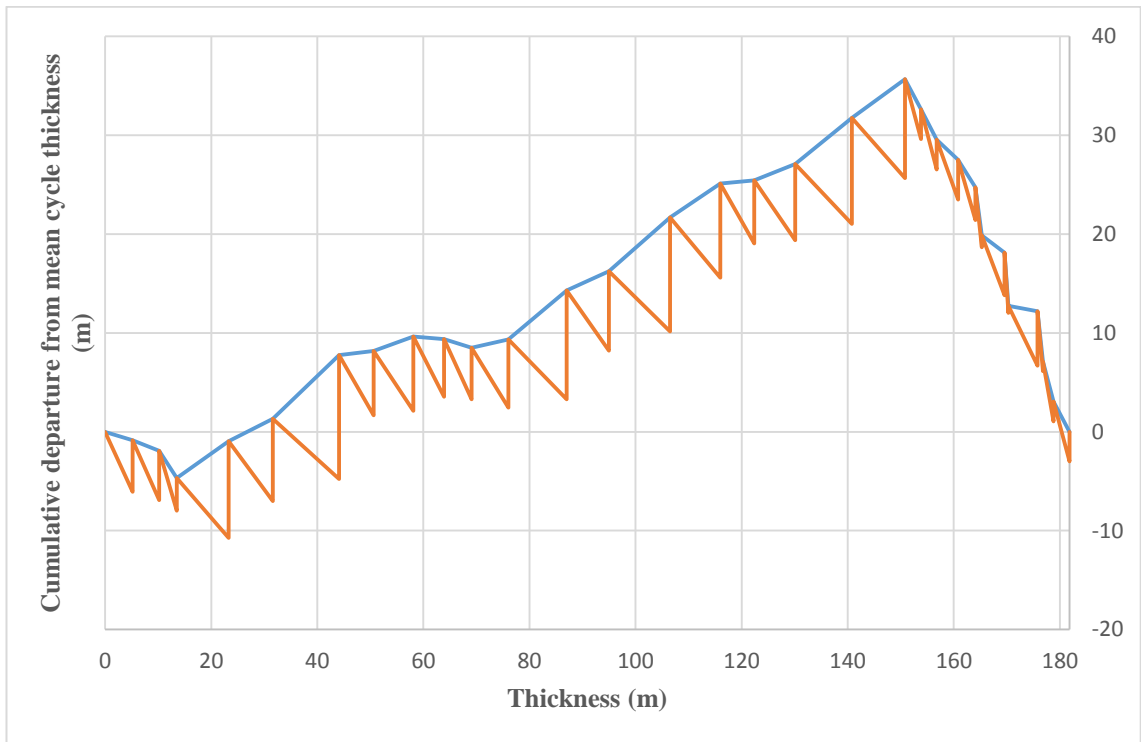
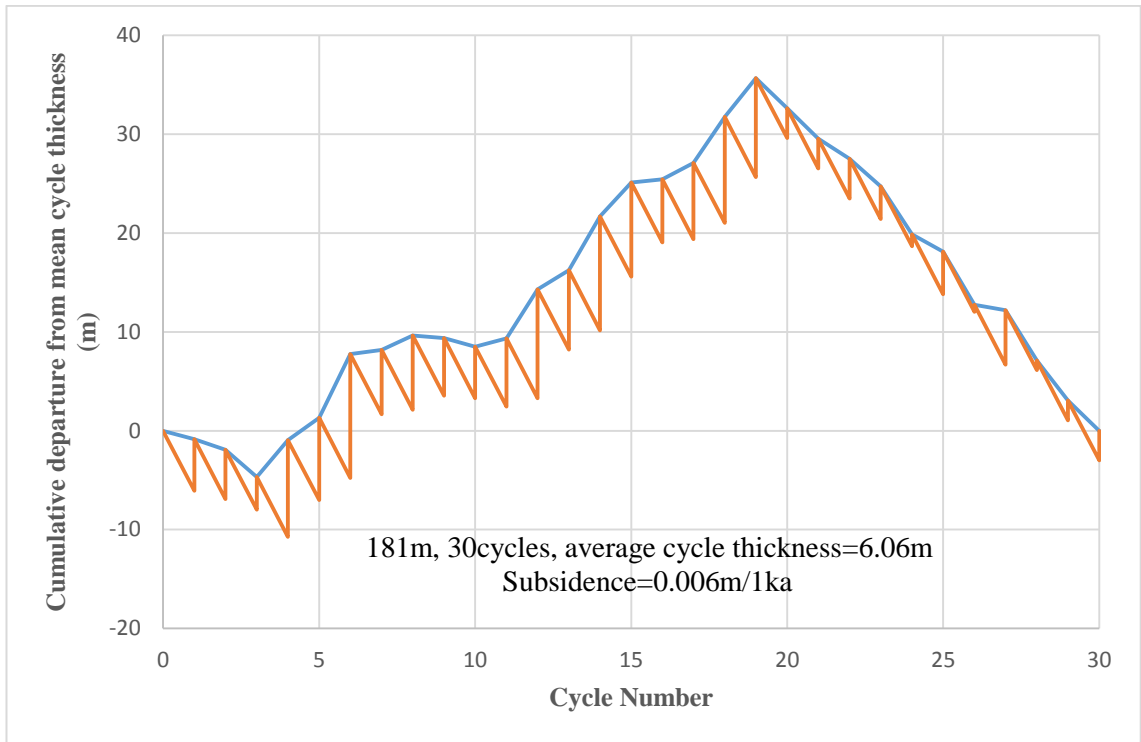


Figure 4-15 Fischer plot of the carbonate-evaporite cycles of the Fatha Formation from Aj Dagh section. The plots represent the standard Fischer plot as constructed between cumulative departure of mean cycle thickness and cycle number (upper plot), as well as revised Fischer plot as presented between cumulative departure of mean cycle thickness and cycle thickness (lower plot).

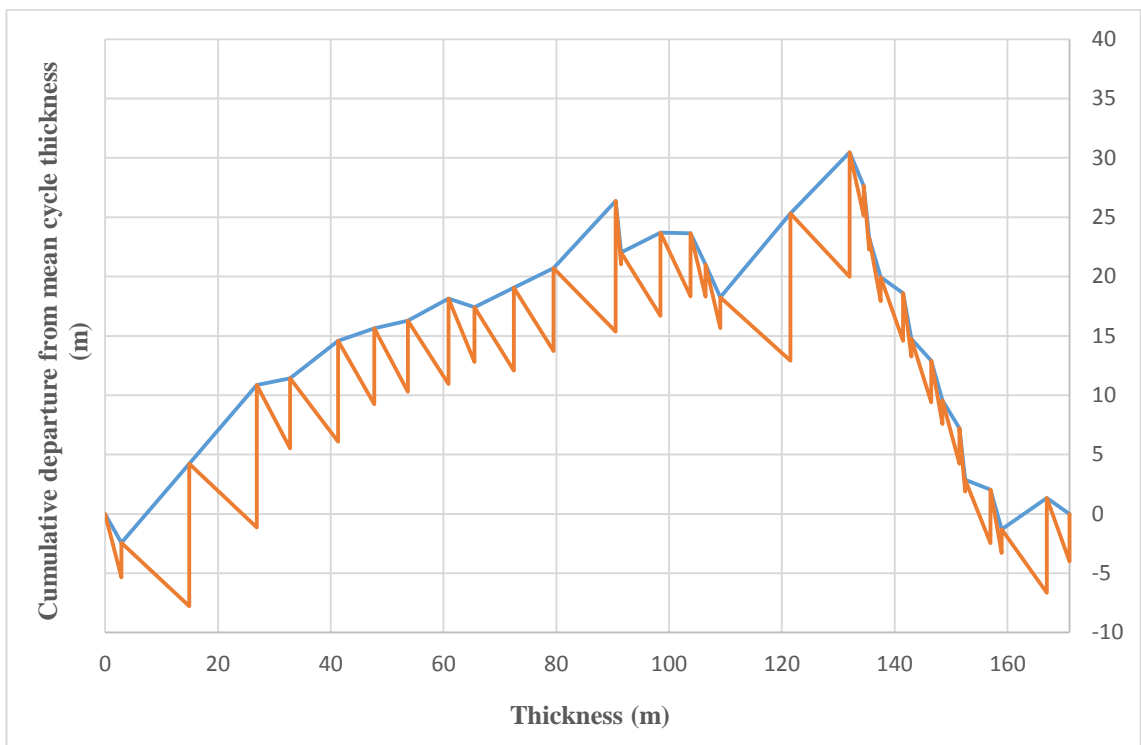
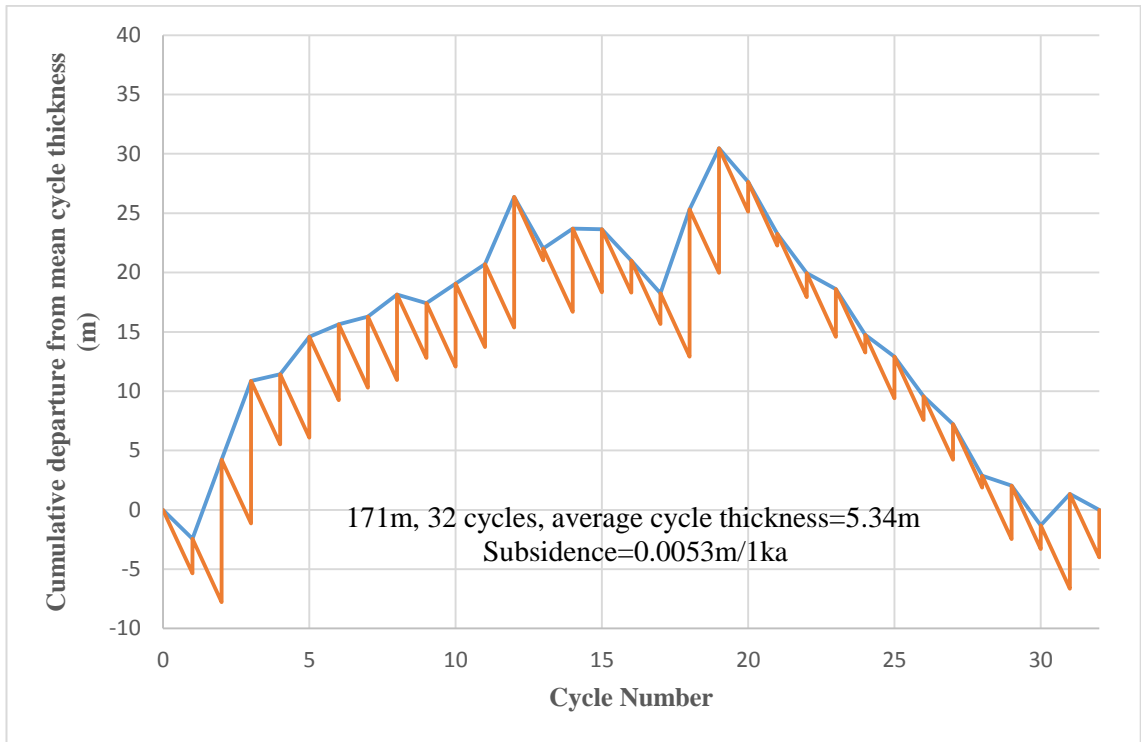


Figure 4-16 Fischer plot of the carbonate-evaporite cycles of the Fatha Formation from Sangaw section. The plots represent the standard Fischer plot as constructed between cumulative departure of mean cycle thickness and cycle number (upper plot), as well as revised Fischer plot as presented between cumulative departure of mean cycle thickness and cycle thickness (lower plot).

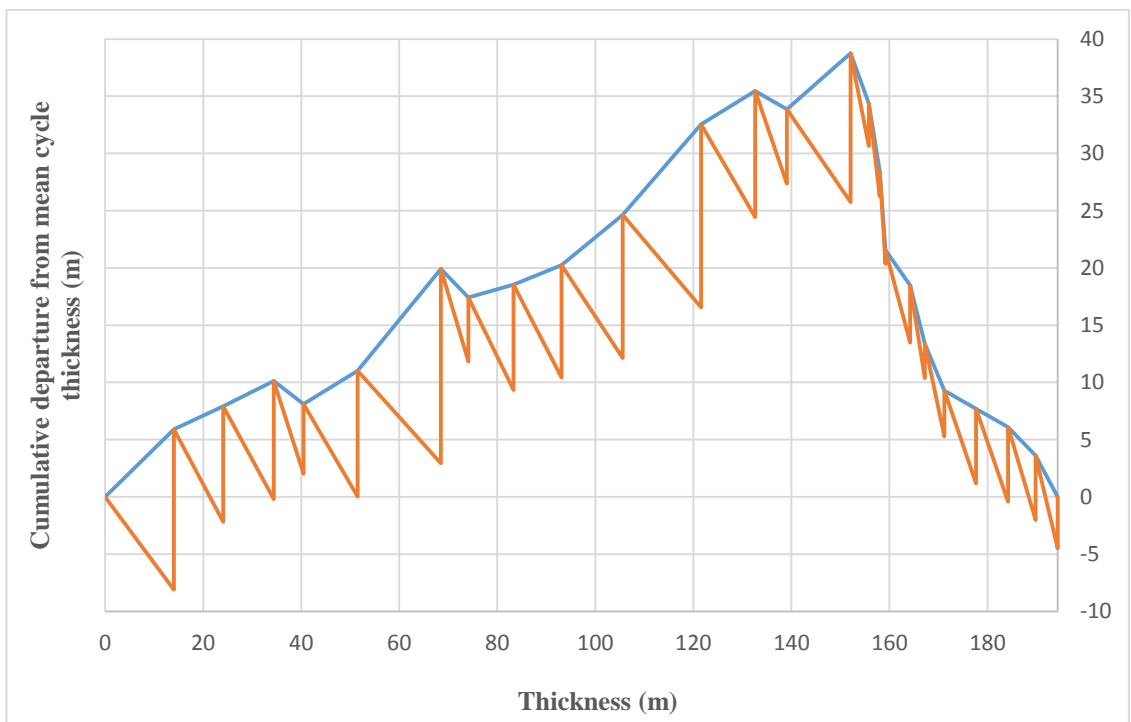
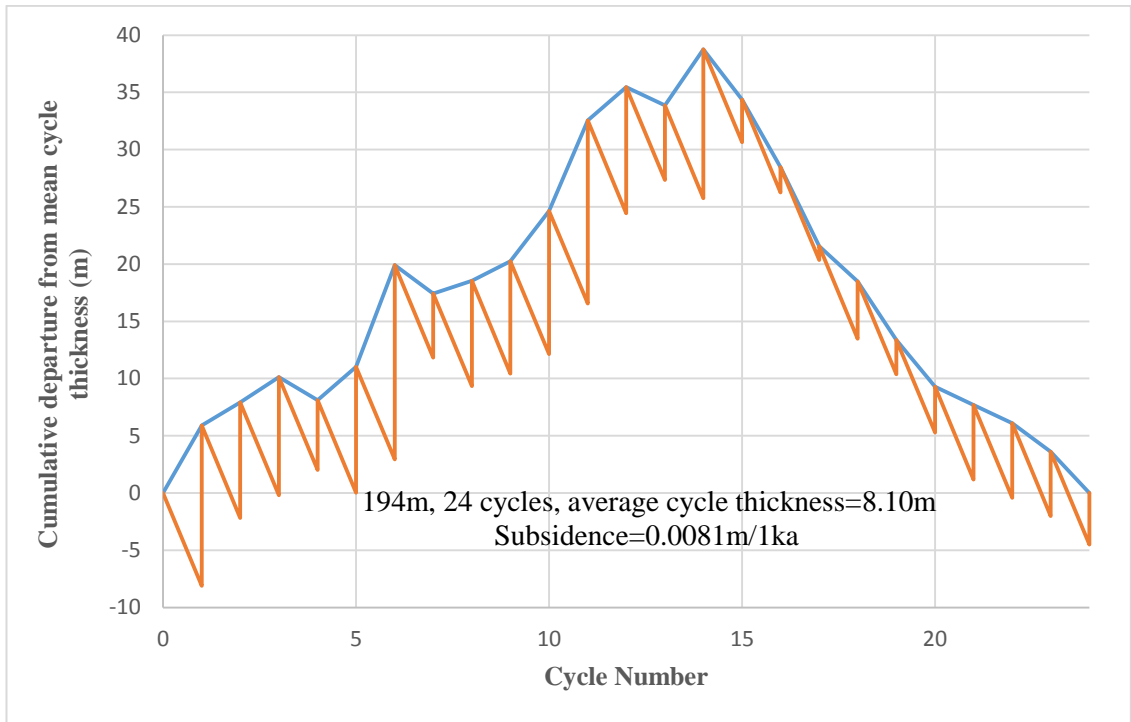


Figure 4-17 Fischer plot of the carbonate-evaporite cycles of the Fatha Formation from Basara section. The plots represent the standard Fischer plot as constructed between cumulative departure of mean cycle thickness and cycle number (upper plot), as well as revised Fischer plot as presented between cumulative departure of mean cycle thickness and cycle thickness (lower plot).

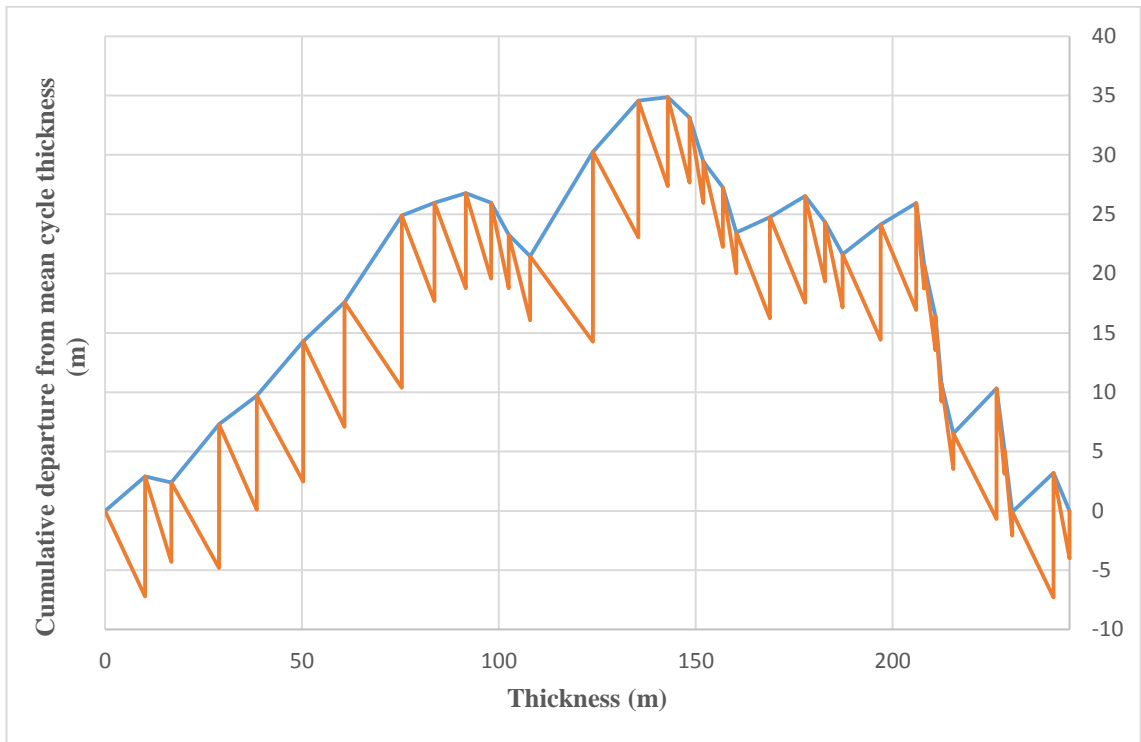
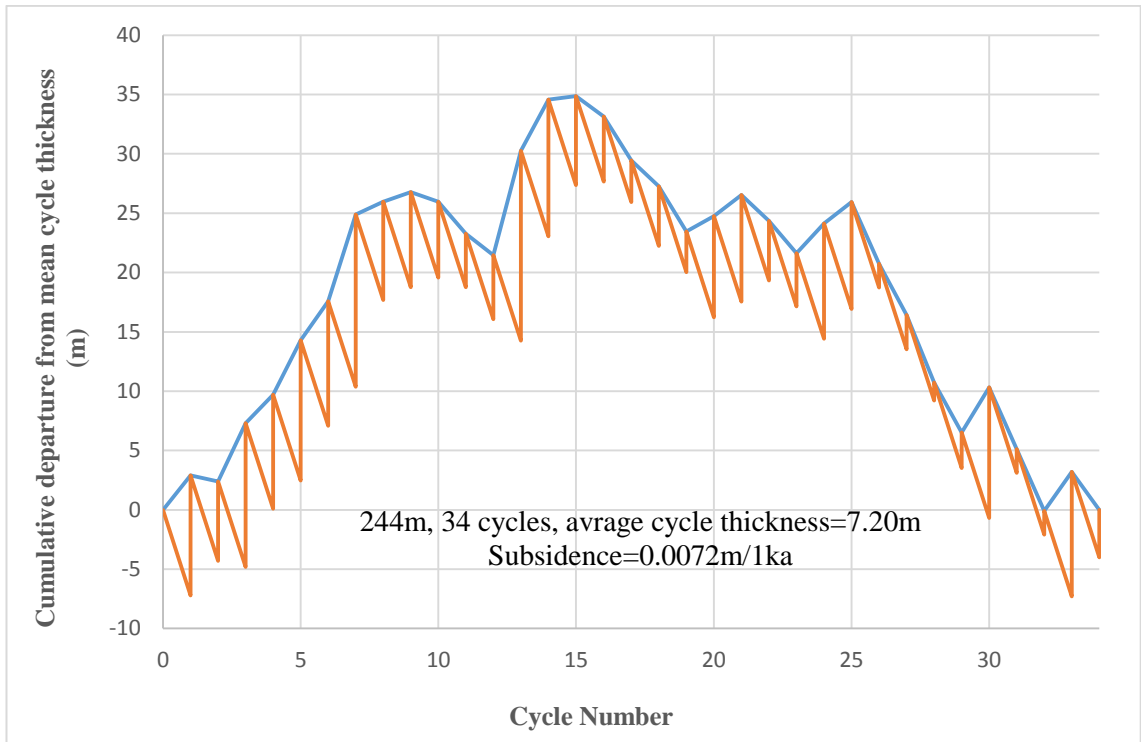


Figure 4-18 Fischer plot of the carbonate-evaporite cycles of the Fatha Formation from Takiya section. The plots represent the standard Fischer plot as constructed between cumulative departure of mean cycle thickness and cycle number (upper plot), as well as revised Fischer plot as presented between cumulative departure of mean cycle thickness and cycle thickness (lower plot).

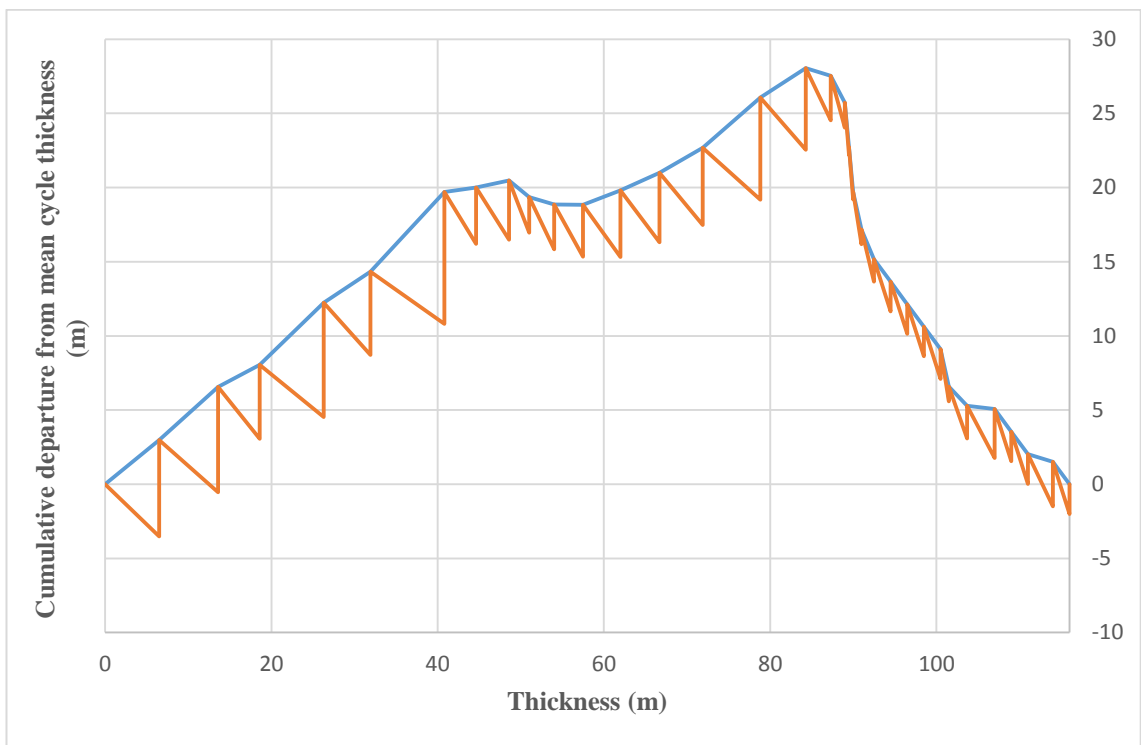
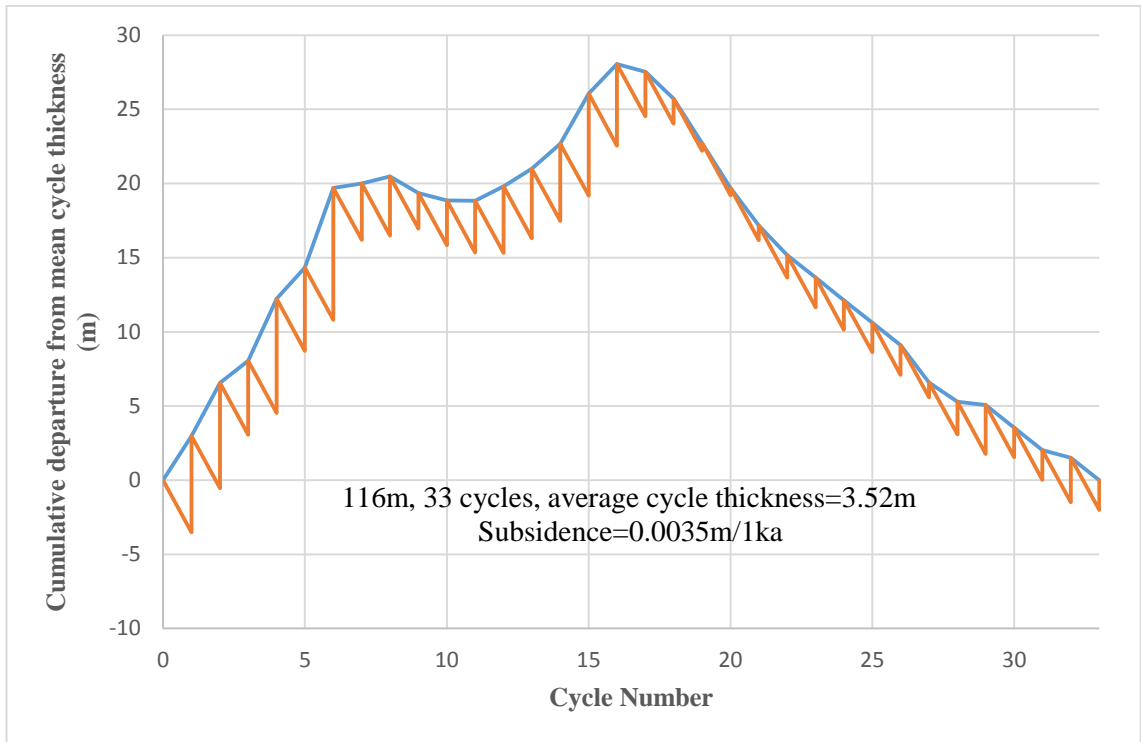


Figure 4-19 Fischer plot of the carbonate-evaporite cycles of the Fatha Formation from Krbchna section. The plots represent the standard Fischer plot as constructed between cumulative departure of mean cycle thickness and cycle number (upper plot), as well as revised Fischer plot as presented between cumulative departure of mean cycle thickness and cycle thickness (lower plot).

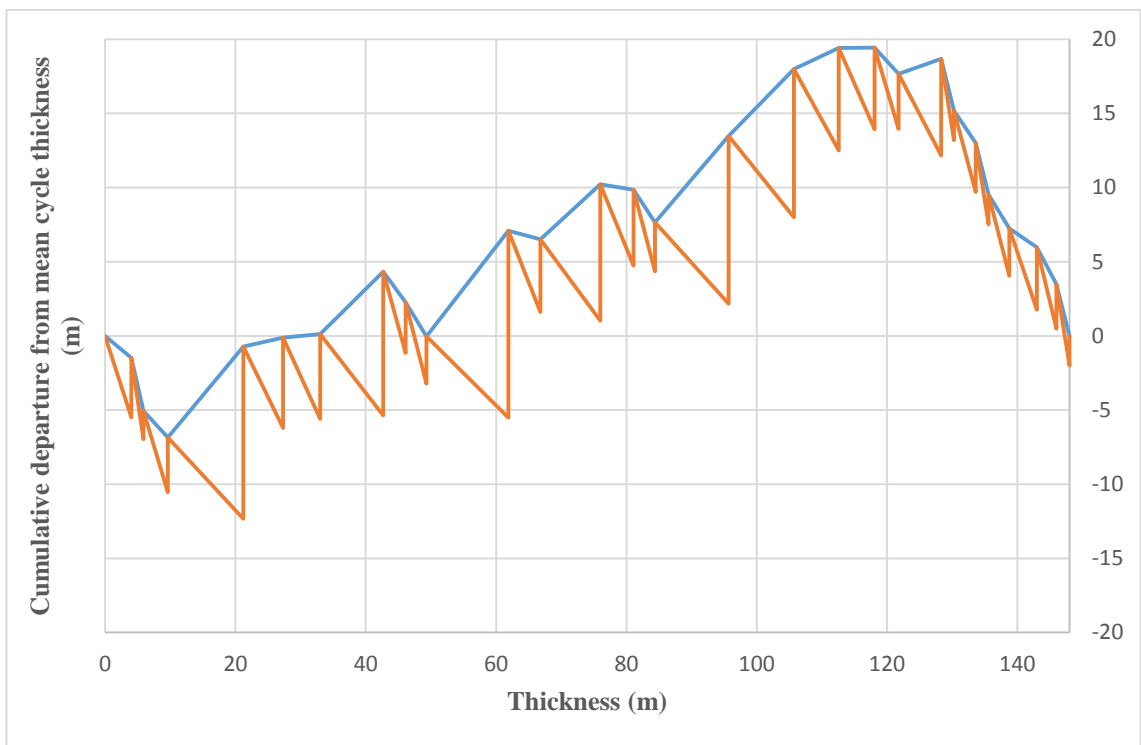
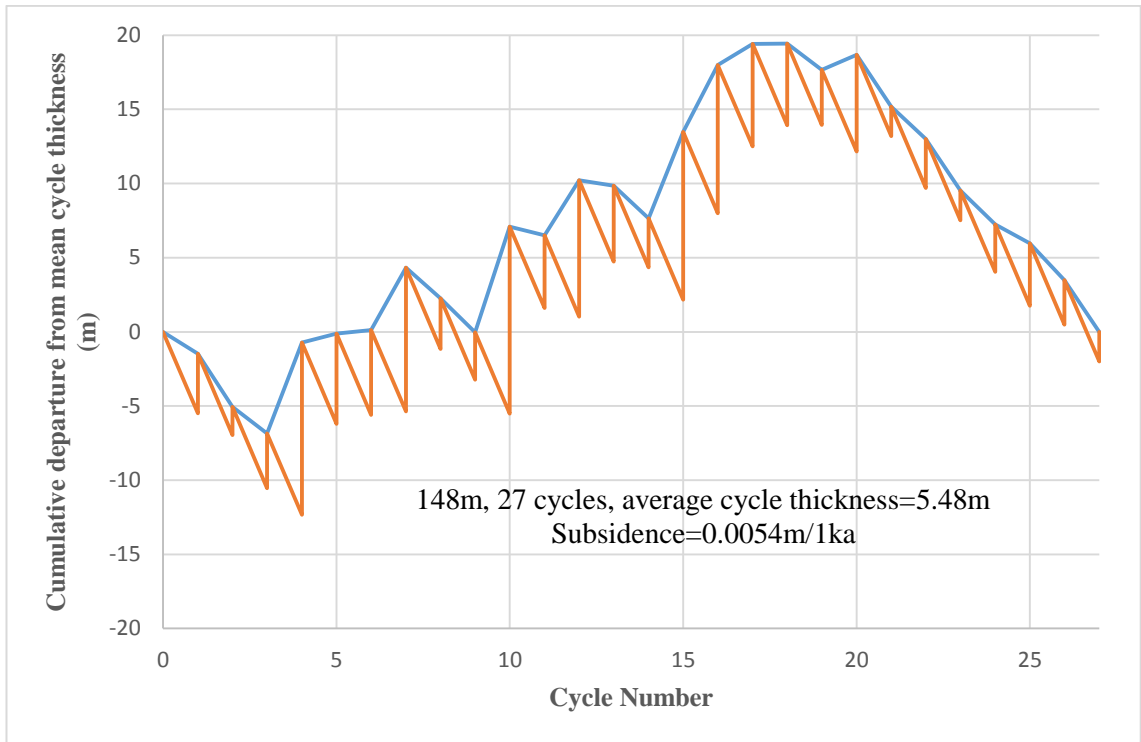


Figure 4-20 Fischer plot of the carbonate-evaporite cycles of the Fatha Formation from Darbandikhan section. The plots represent the standard Fischer plot as constructed between cumulative departure of mean cycle thickness and cycle number (upper plot), as well as revised Fischer plot as presented between cumulative departure of mean cycle thickness and cycle thickness (lower plot).

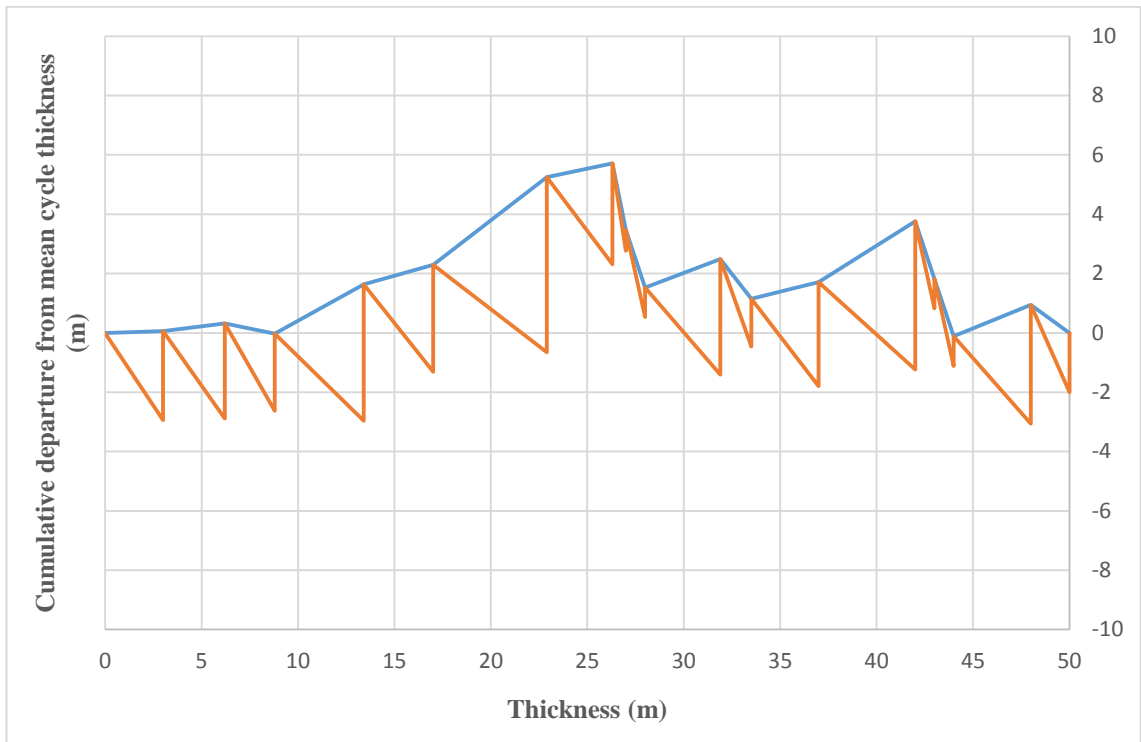
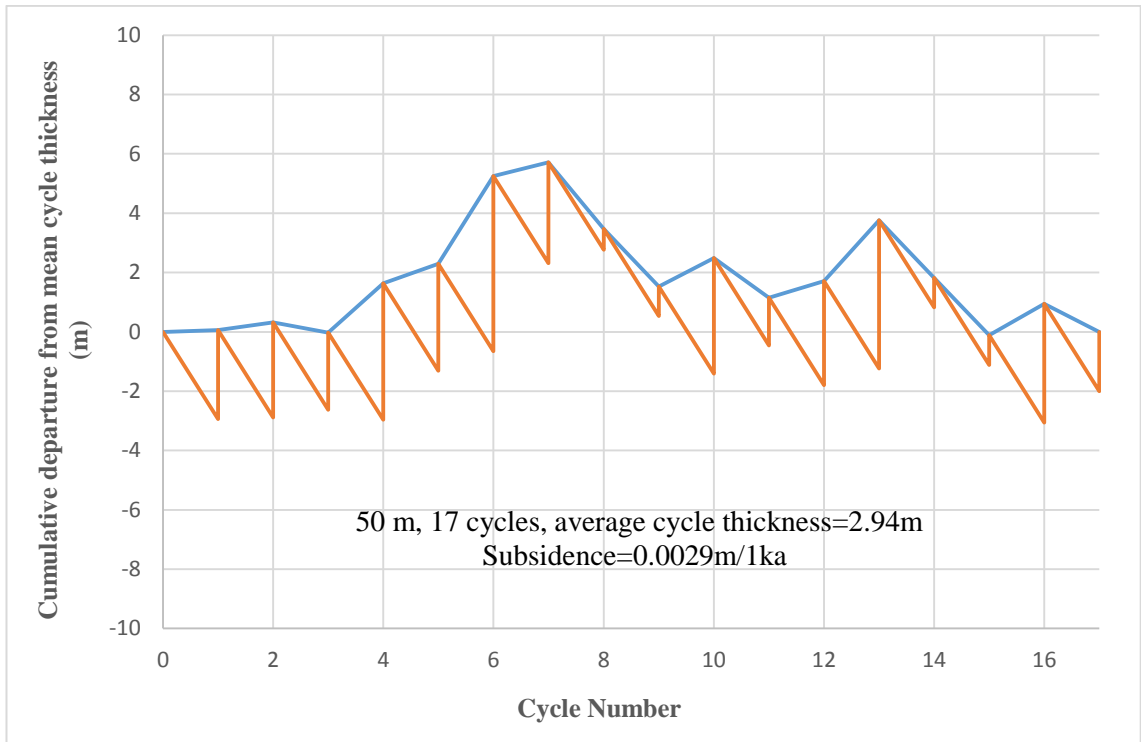


Figure 4-21 Fischer plot of the carbonate-evaporite cycles of the Fatha Formation from Chnarah section. The plots represent the standard Fischer plot as constructed between cumulative departure of mean cycle thickness and cycle number (upper plot), as well as revised Fischer plot as presented between cumulative departure of mean cycle thickness and cycle thickness (lower plot).

Standard Fischer plots are presented of the cyclic succession of the Fatha Formation (Figures 4-13 to 4-21). These are constructed with cumulative departure from mean cycle thickness on the vertical scale and cycle numbers on the horizontal scale. Revised Fischer plots are also presented with cumulative departure from mean cycle thickness on the vertical scale and cycle thicknesses on the horizontal scale. The rising slopes in the left-hand part of each of the graphs represent the thicker cycles of the lower part of the succession, whereas the falling slopes at the right-hand side of each of the graphs include the thinner cycles of the upper part of the succession. The Fischer plots presented show nearly similar trends in all the studied sections; an increase and then a decrease in slope (i.e., positive rising and negative falling). This means that the thicker cycles on the rising slopes of the graphs were deposited during increasing, higher accommodation space generation, whereas the thinner cycles on the falling slopes of the graphs were accumulated during a phase of relatively reduced accommodation space generation. It can be concluded that the Fatha Formation was deposited during transgressive (rising slopes) to highstand (falling slopes) system tracts and the Fischer plot reveals elements of a 3rd order depositional sequence, which started with a rise in sea-level and evolved to a highstand (stillstand).

4.9.2 Parasequence sets

A parasequence set comprises a number of parasequences that accumulated during a specific phase of sea-level change. Therefore, by detecting parasequence stacking patterns, system tracts can be interpreted. In general, the Fatha Formation was deposited during a sea-level rise in the lower part and evolved toward a 3rd order highstand sea-level in the upper part. This is consistent with the formation being divided into two parasequence sets on the plots; transgressive and highstand parasequence sets.

1. Retrogradational parasequence set

A retrogradational parasequence set is defined by farther landward deposition of successively younger parasequences or cycles, in which the rate of accommodation generation is more than the rate of deposition. Transgressive system tracts are characterized by retrogradational parasequence sets, which onlap and downlap onto pre-existing surfaces in landward and basinward directions, respectively (Van Wagoner *et al.*, 1987). However, if sedimentation rates are higher than the accommodation creation,

then progradational stacking patterns may be preserved within a transgressive system tract.

This type of stacking pattern is recognized at the base of the Fatha Formation by landward onlap of the underlying sequence boundary by successive parasequences. Thus a retrogradational stacking pattern has been observed. On Fischer plots, the positive slope represents the transgressive system tract, which was generated by upward thickening of stacked cycles during a prolonged period of high accommodation space generation. The thicknesses of the cycles are greater than the average thickness. In this parasequence set, a thick carbonate-evaporite succession was deposited that are consistent with the high rates of accommodation space generation. Therefore, these cycles are interpreted to have been deposited during the relative sea-level rise of a third order transgressive system tract.

2. Progradational parasequence set

A progradational stacking pattern is defined by farther basinward deposition of successively younger parasequences (cycles), in which the rate of accommodation generation is less than that of the rate of deposition. This is a characteristic of the highstand system tract that may start with one or more aggradational cycle and passes up to progradational cycles with prograding geometries (Van Wagoner *et al.*, 1987). There is a maximum flooding surface between the retrogradational transgressive system tract and the aggradational early highstand system tract. However, the recognition of the maximum flooding surface is complicated in high frequency sea-level events. Therefore, stacking patterns have been used to identify this transition. In these cases, a maximum flooding zone (MFZ) and sequence boundary zone (SBZ) have been invoked by some authors (Montanez and Osleger, 1993; Tucker, 2003).

On Fischer plots, this zone is located at the falling part of the curve. Correlated Fischer plots from the Fatha parasequences show a transition from thick cycles of carbonate-evaporite facies to thinner cycles. This transition is gradational and rounded in most of the studied sections. This parasequence set is characterized by the falling slope on the Fischer plot and thinning upward, in which the thicknesses of the cycles are smaller than the average. This indicates decelerating accommodation creation and a high rate of deposition. Therefore, these cycles were deposited during a relatively slow relative sea-level rise of the early highstand system tract. In this part of the plot, the evaporite unit is

typically missing and the marine deposits become very thin with occasional evidence of meteoric diagenesis.

Table 4-4 Descriptions and definitions of the high-frequency cycles, cycle-set, and 3rd-order sequence of the Late Burdigalian Fatha Formation.

Hierarchy	Lateral extent (km)	Thickness (m)	Time (k.y.)	Definition
High-frequency parasequences	>10	5-10, up to 13	60	Shallowing-upward cycles, passing up from hypersaline lagoonal deposits into shallow carbonate deposits, then to supratidal and fluvial deposits.
Cycle-set	Basin-wide	100-150	1-1.5	Distinguished by changes in stacking patterns and cycle thicknesses.
3rd-order sequence	Basin-wide	50-300	2.5-3	3 rd -order accommodation creation.

4.9.3 Distributions of the parasequences on the Fischer plots

Fischer plots have been applied for correlation across a large area to explore the effects of tectonics and long-term accommodation space creation during deposition of a cyclic succession (Grottsch, 1996). In the current study, each parasequence had different ranges of thickness and was documented from different parts of the succession or different parts of the basin (Figures 4.22 and 4.23). However, in general, they all have some significant criteria in common, which represent shallowing-upward changes.

Type D parasequences are the most common parasequence in the studied areas. This type constitutes the majority of the parasequences in the lower part of the succession, while types A, B and C cycles occur sporadically. This means that these three types are not common at the basin margin. However, they are more common in the basin centre. On the Fischer plots, these four types are located on the rising limb of the plot (Figures 4.22 and 4.23). However, the types of parasequence show greater variations on the falling limb (HST) of the Fischer plot. These variations exhibit decreasing thickness, missing evaporites and increasing siliciclastic deposits. On this part of the Fischer plot, type E and type F parasequences are more abundant, while type G and type H parasequences become abundant in the uppermost part of the succession and at the end of the falling slope of the Fischer plot. Toward the uppermost part of the succession, the

marine deposits become a lesser component until the succession becomes a fully fluvial deposit in the Injana Formation.

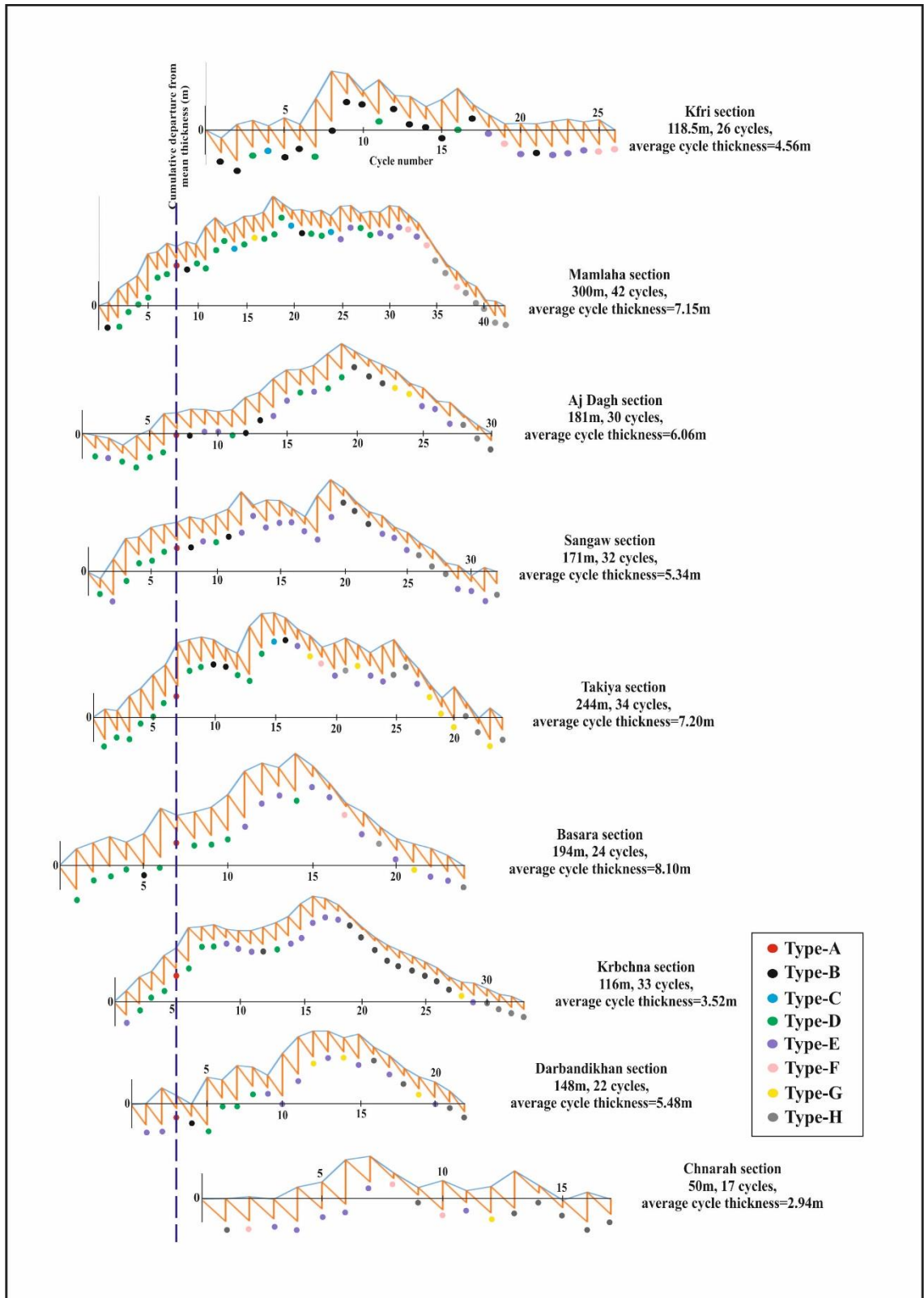


Figure 4-22 Correlation of the Fischer plots from the studied sections and distributions of parasequences types along the plots. The shape of the plots are nearly similar in all the studied sections. Most of the parasequences at the lower succession are of type-D, whereas type-H is predominate at the upper succession. The dotted blue line is the position of the laminated evaporite.

A high number of type D cycles were observed in the lower part of the succession. For example, more than 15 cycles were documented in the lower part of the succession in the Mamlaha area, while the number of type D parasequences reduces to approximately 10 cycles in the Basara and Takiya areas and less than 8 parasequences at Krbchna and Darbandikhan. It is absent in the Chnarah section where the majority of the parasequences are composed of type E parasequences. However, the majority of the parasequences in the Lower Member of the basin centre are composed of type A, B and C parasequences, followed by type D parasequences (lack or presence of red clastic deposits) in the Upper Member (after (Tucker, 1999; Aqrawi *et al.*, 2010)). A number of type B parasequences are preserved in the Kfri area in the SW of the study area.

The high abundance of type D parasequences in the lower part of the succession and on the rising slope of the Fischer plot indicates higher accommodation space and subsidence. During that time a number of thick cycles were accumulated. However, the abundance of types E, F, G and H in the upper part of the succession and on the falling limb of the Fischer plots suggest relatively low accommodation creation and subsidence. In this context, relatively thin parasequences are preserved. The reduced number of type D parasequences in the Krbchna and Darbandikhan areas and their absence in the Chnarah section allow an inference of very low subsidence during deposition close to the hinterlands. Reduced numbers of parasequences in an individual set from Basara and Takiya to Krbchna and Darbandikhan areas suggest missed cycles in between. This could be the result of very low subsidence or uplift around the margin.

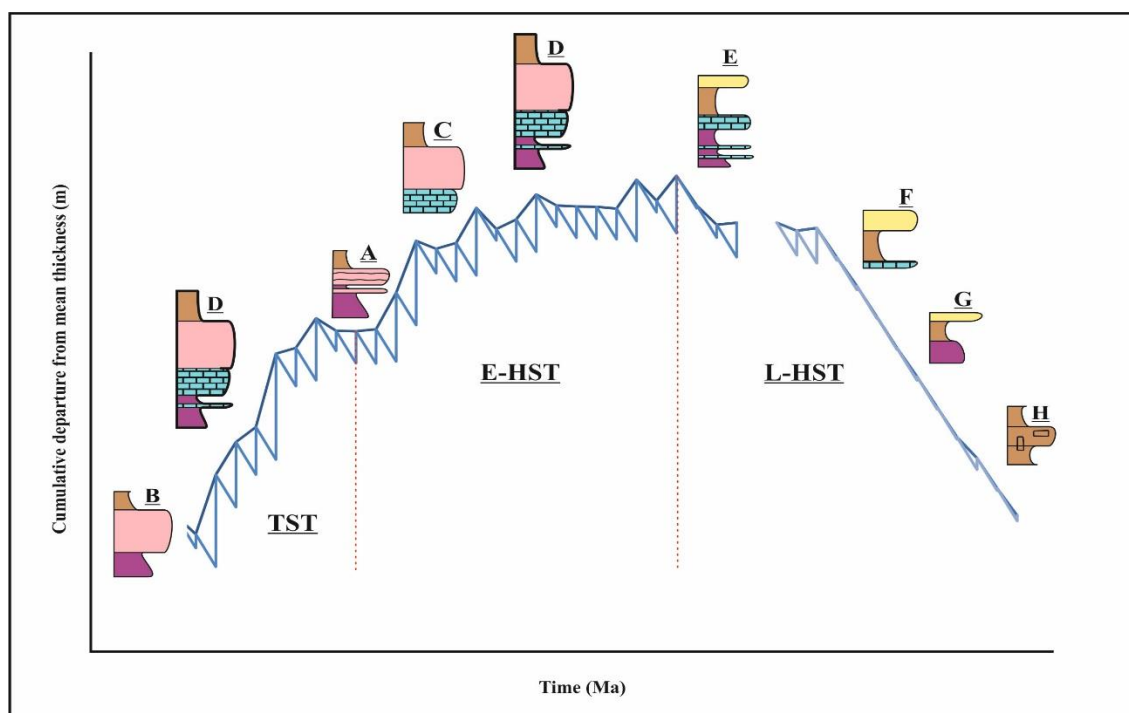


Figure 4-23 Schematic illustration of the distribution of parasequence types on a Fischer plot. Thick carbonate-evaporite parasequences are located in the lower part of the succession with high accommodation space creation; however, the parasequences in the upper part of the succession become thinner due to decelerating accommodation space. Furthermore, siliciclastics become abundant and evaporites are missing.

4.10 Sequence boundaries

Sequence stratigraphy may be used to divide genetically related units into system tracts and parasequences based on hierarchical cycles of relative sea-level change. Moreover, it is an important tool that links stratigraphy, basin analysis and aspects of petroleum geology. In order to create a sequence stratigraphic description of the Fatha Formation, the lower and upper boundaries need to be defined, as well as sedimentary facies, and the nature of parasequences which have been described in detail.

4.10.1 The lower boundary

In all previous studies it has been suggested that the lower boundary of the Fatha Formation at the basin margin with the underlying Late Eocene Pila Spi Formation is unconformable. A *Basal Fars Conglomerate* (BFC) was described at the boundary without any recognition of early Miocene and Oligocene formations (van Bellen *et al.*, 1959; Buday, 1980; Al-Juboury and McCann, 2008; Aqrabi *et al.*, 2010). However, the Early Miocene formations (e.g. Euphrates, Dhiban and Jeribe) and Oligocene

formations have recently been identified by a number of authors in Kurdistan region (Kharajiany, 2008; Khanaqa *et al.*, 2009; Ghafur, 2012) Hussein, 2016).

In the current study, the *Basal Fars Conglomerate* (BFC) is recognized in the Darbandikhan area below the Fatha Formation, where a thick fluvial unit (9m) of conglomerate, breccia, claystone and sandstone is recorded between the Late Eocene Pila Spi and Miocene Fatha Formations (Figures 4.24 and 4.25). However, this fluvial unit is also documented below the Early Miocene formations (Euphrates, Dhiban and Jeribe) in the Garmian areas. It thins (to 1.5-2m) toward the Garmian area, where the Mamlaha, Sangaw and Aj Dagh sections have been logged. It is absent toward the basin centre.

The Early Miocene formations (e.g. Euphrates, Dhiban and Jeribe) have not previously been recorded along the Sargrma-Qishlagh Mountains. However, in the current study, three packages of carbonates and green marls were recorded along the Sargrma-Qishlagh Mountains just below the Fatha Formation whilst they are absent toward the Darbandikhan area. So, the Basal Fars Conglomerate is located below these carbonate packages along the Sargrma-Qishlagh Mountains. The first carbonate unit, which is about 4m thick, may be the Euphrates Formation by indicating the Early Miocene index fossil *Borelis melo*. However, the two carbonates and green marl packages above the first carbonate unit may represent the Jeribe Formation. These results were determined by studying all the sedimentary facies and microfacies of the packages and correlating them to the Euphrates and Jeribe Formations along the Aj-Dagh and Qara-Wais anticlines, SW of Kurdistan region (Aj Dagh, Sangaw and Mamlaha sections), which were recently recorded by Hussein (2016). In addition, these carbonate packages have also been studied in Basara gorge and their age is determined to be between Late Oligocene and Early Miocene by using index fossils (Khanaqa *et al.*, 2009). As a result, the Early Miocene and Fatha Formations must have diachronously overlapped the unconformity surface (BFC) toward the basin margin.

In the basin centre, the lower boundary of the Fatha Formation is conformable with the Early Miocene Jeribe Formation, the boundary being marked by a change from carbonate of the Jeribe Formation to the basal anhydrite of the Fatha Formation. However, elsewhere the boundary is unconformable on the Euphrates Formation (Buday, 1980).

4.10.2 The upper boundary

The upper boundary of the Fatha Formation is gradational and conformable with respect to the overlying Injana Formation (van Bellen *et al.*, 1959; Buday, 1980). In the current study, the boundary is taken to be the transition from marine deposits of the upper part of the Fatha Formation to fluvial deposits of Injana Formation. Therefore, the boundary is a diachronous lithostratigraphic boundary and becomes younger towards the basin. There is no subaerial unconformity present.

4.10.3 The upper boundary of Injana Formation

The upper boundary of the Injana Formation is unconformably overlain by the Mukdadiya Formation (previously termed the Lower Bakhtiari Formation), as indicated by the first pebbly sandstone of the Mukdadiya Formation (Al-Rawi *et al.*, 1993) and local angular unconformity (Pirouz *et al.*, 2011).

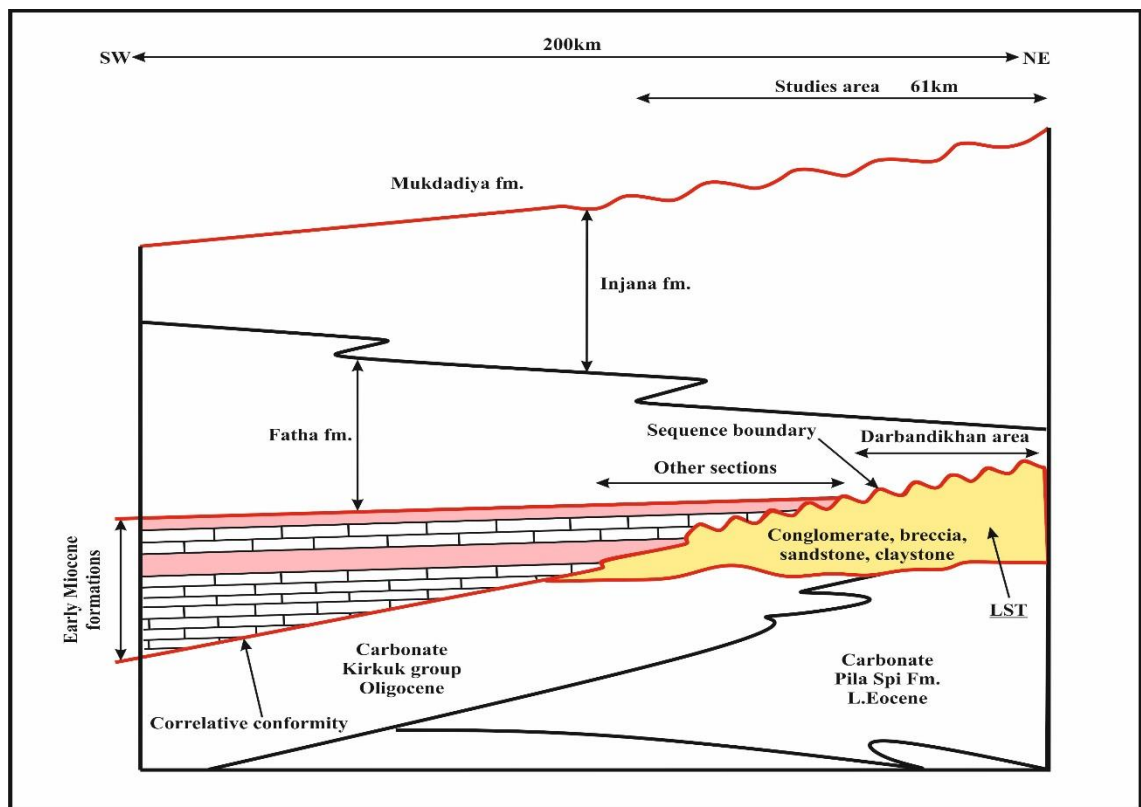


Figure 4-24 Lower boundary of the Fatha Formation with the Early Miocene formations (Euphrates, Dhiban and Jeribe). There is an unconformity surface toward the margin that represents a sequence boundary at the Oligocene-Miocene boundary. Both the Early Miocene formations and the Fatha Formation onlap the sequence boundary.

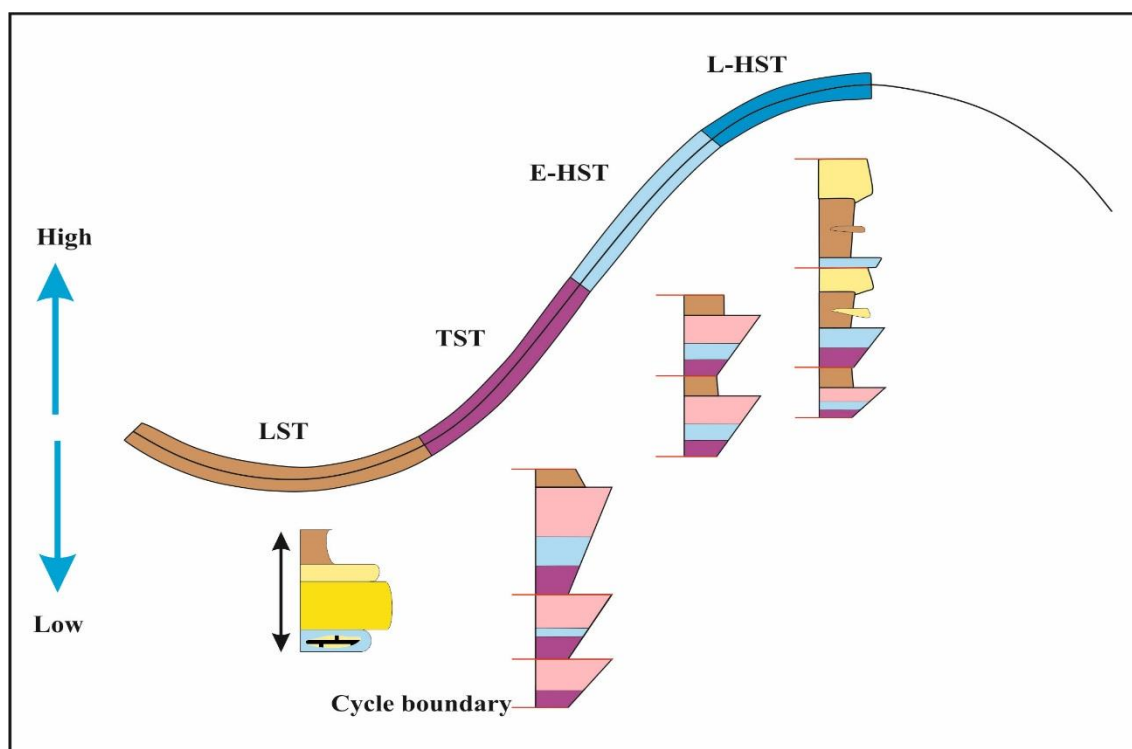


Figure 4-25 3rd order sea-level changes including system tracts during deposition of the Fatha Formation marginal deposits, and variations in cycle types throughout the regressive succession.

The Fatha and Injana Formations were deposited during a 3rd order depositional sequence, which is bounded by sequence boundaries at the base and the top. The sequence boundaries are characterized by subaerial exposure at the basin margin and correlative conformities within the basin depocentre. In addition, the Fatha depositional sequence includes a number of high-frequency parasequences.

4.11 Mechanisms controlling the Miocene high-frequency parasequences

The most important variables that affected high-frequency relative sea-level changes are eustatic sea-level change, climate, tectonics and depositional rate. These factors may separately or all together control the depositional architecture of a sedimentary basin. Eustatic sea-level changes have an effect on accommodation space for sediment accumulation, while tectonics is a major control on accommodation but also on sedimentation, through hinterland uplift processes which influence erosion and sediment supply rates, and which may control changes of the basin configuration during subsidence and uplift. In addition, deposition rate can change the geometry and form of stacking patterns within the basin.

In the current study, three main controls were recognized on Fatha deposition, these being sedimentary process, glacio-eustasy and tectonics, as discussed below.

4.11.1 Glacio-eustasy and orbital forcing

Eustatic sea-level variations have been estimated on different time scales: **(i)** long-term scale (10^7 to 10^8 years) that is influenced by variations in sea-floor spreading; **(ii)** million-year time scale that is recognized by seismic stratigraphic methods and regionally correlatable sequence boundaries; and **(iii)** 10^4 - 10^5 year time scale that is influenced by climate changes and Milankovitch cycles (Vail *et al.*, 1977; Haq *et al.*, 1988; Kominz, 2001; Miller *et al.*, 2005; John *et al.*, 2011). In general, variations in eustatic sea-level are controlled by changes in the volume of the ocean basins (tectono-eustasy) and volume of water in the oceans (glacio-eustasy) (Kominz, 2001; Coe and Church, 2003; Miller *et al.*, 2005). The main driving force causing variation in the volume of the ocean and long-term sea-level change is tectonic, which changes the volume and shape of the ocean basins. For example, during collision of the Indian and Asian continental plates and generation of the Tibetan Plateau and the Himalayan Mountains, sea-level has probably fallen about 70m over the last 50 million years (Kominz, 2001). Moreover, collision, subduction, sea-floor ridge development, rifting, large igneous province evolution, and transient mantle upwelling all contribute to controlling the long-term sea-level changes. However, variations in the water volume in the oceans can be largely attributed to climate changes. Palaeo-climate can be estimated by observing oxygen-18 to oxygen-16 ratios in the tests of dead organisms. The variation in $\delta O^{18}/O^{16}$ from microfossil remains allow the inference of a general cooling over the last 50 million years (e.g. Zachos *et al.*, 2001).

The Miocene ranges between 23 and 5.3 Ma. It represents a period of long-term cooling that continues today, as estimated from deep-sea oxygen-isotope records (Zachos *et al.*, 2001; Haupt and Seidov, 2012). The earliest Oligocene glaciation event was suggested as a major change in climate from long-term warming to the long-term cooling that continues today. The long-term cooling since the earliest Oligocene alternated with warming episodes, such as the latest Oligocene and the mid-Miocene Climatic Optimum that lasted 10^4 - 10^6 years (Haupt and Seidov, 2012).

There was a cooling event at the Oligocene-Miocene boundary (Figure 4.26), which caused a period of ice growth in the Antarctic (Miller *et al.*, 1991). This event at the

Oligocene-Miocene boundary resulted in a global sea-level fall, known as the ice growth maximum (Mi-1) (Miller *et al.*, 1991). This event can be correlated with the Oligocene-Miocene sequence boundary on the Arabian Plate at a regional scale and in this studied area on a local scale.

The second ice growth (Mi-1a) and associated sea-level fall occurred during the late Aquitanian to early Burdigalian and are separated from the previous cooling phase (Mi-1) by a minor sea-level rise, which is indicated by a shift in oxygen-isotope ratios. These events were succeeded by a warmer period, known as “the Mid-Miocene Climatic Optimum”, which lasted from the middle Burdigalian to the Langhian and was separated by two glacial maxima (Mi-1b and Mi-2). This was followed by a lowering of temperatures, including the Mi-3 to Mi-7 glacial maxima, a cooling trend which has continued until today (Miller *et al.*, 1991; Rasmussen, 2004). In general, the marine oxygen isotope record during the Miocene records several climatic fluctuations or warm spikes and sea-level rises (Zachos *et al.*, 2001; Rasmussen, 2004). But overall, large ice sheets in East Antarctica have developed at least since the Oligocene, driving a sea-level change equivalent to at least 35m (Zachos *et al.*, 1994). These fluctuations of climate created metre-scale to decametre-scale high-frequency cyclical sea-level changes, expressed in stratigraphic records, at the three different periodicities of orbital forcing that are known as the Milankovitch cycles. These three episodes have rhythms of precession (ca. 20kyr), obliquity (ca. 40kyr) and eccentricity (ca. 100 and 400 kyr). These changes in orbital forcing cause variation in temperature and solar radiance reaching the Earth, which in turn affect ice volumes and hence sea-level. Therefore, there is a significant relationship between climate and sea-level. The magnitude of sea-level fluctuations has been greater during icehouse climatic phases than during greenhouse phases, due to the increased availability of polar ice during icehouse conditions. For example, sea-level has fluctuated by about 100m during eccentricity phases of the icehouse maximum during the Pleistocene (Miall, 2010). A good example of probable Milankovitch cyclicity is seen in the Turonian succession within the Western Interior Basin, between Utah and Kansas. Elder *et al.* (1994) have correlated two major shallowing-upward successions; one from Utah that comprises shallowing-upward cycles of marine mudstone to siltstone and shoreline sandstone, while the second from Kansas comprises couplets of marl and carbonate. They attributed these two successions as being controlled by Milankovitch timescale climatic fluctuations. They interpreted that during cold/wet periods, the rate of sediment supply would have

increased and led to coastal progradation, whereas during hot/dry periods, the rate of sediment supply would have decreased, leading to carbonate-rich sediments being deposited in the basin centre (Elder *et al.*, 1994). Thus the climatic variability may be expressed either as shifts in the position of coastlines due to sea-level fluctuations or to differences in sediment supply rates and progradation rates.

The presence of high-frequency cyclicity with periodicities of less than one million years and which can be traced over large areas regionally, even globally, and correlated across different tectonic and/or climatic situations, provide the main evidence for the Milankovitch climatic-forcing control of stratigraphic architectures (Tucker and Wright, 1990; Tucker and Garland, 2010) (Figure 4.27). High-frequency cyclicity is very common in the Miocene worldwide. It occurs in a carbonate-siliciclastic succession in the Lorca Basin, SE Spain (Thrana and Talbot, 2006); a mixed siliciclastic-carbonate shelf in the Guadix Basin, Spain (García-García *et al.*, 2009); Messinian evaporites in the Mediterranean Basin (Manzi *et al.*, 2012); siliciclastic cycles in Western Louisiana and Central Texas (Ye *et al.*, 1995; Hentz and Zeng, 2003), and in shallow marine, fluvio-deltaic and lacustrine sediments of the Vienna Basin (Paulissen and Luthi, 2011).

The Miocene high-frequency carbonate-evaporite-clastic cycles in the current study are extend to Syria and Iran and are continuous over about 2000km, and are well preserved throughout the entire basin. The cycles are traceable for tens of kilometres, this distance usually only being limited by outcrop continuity. This is strong evidence for orbital forcing having been a control on the basin stratigraphy. Other strong evidence of orbital forcing and a eustatic control is the regularity of the cycles and the correlation of parasequence sets across the region. This has been indicated by the correlation of the parasequence sets expressed in the Fischer plots.

The total duration of the deposition of the Fatha Formation was estimated to be 5.0 Myr by its stratigraphical position (van Bellen *et al.*, 1959; Buday, 1980; Jassim and Goff, 2006). The number of cycle that were recorded from the basin-centre is about 50 cycles (Tucker, 1999). By dividing the total duration of the deposition by the number of cycles, in the basin-centre, 100Kyr is the inferred average cycle duration. However, a radiometric strontium isotope study calculated the total duration of deposition of the formation to be 3.0 Myr (Grabowski and Liu, 2009; Grabowski and Liu, 2012). Now, a similar strontium isotope study has been conducted in this study for calculating the total duration of the formation, and the duration is determined to be 2.55Myr. Moreover, the

cycles were completely preserved in the basin-centre, whereas toward the basin-margin, due to onlapping of the cycles, not all the cycles are preserved. As a result, 17 to 42 cycles were recorded in the basin-margin, whereas 50 cycles were documented in the basin-centre. By dividing the total duration of the formation (3.0Myr) by the number of cycles in the basin-centre (50), a mean cycle duration of 60Kyr is obtained. These values fall in the vicinity of the Earth's short eccentricity cycle that is modulated in the range from 95 to 123 k.y. (Berger, 1977). This means that a mix of obliquity and eccentricity-forced cycles are probably being expressed. This assumes that the amplitude of eccentricity insolation variation is bigger than the amplitude of insolation variations forced by obliquity variations (of ca. 40 Kyr periodicity) are that these are in turn bigger than precession-forced variations (of ca. 20 Kyr periodicity).

The 3rd-order accommodation cycle represents the whole Fatha succession and is a longer-term, low frequency cycle, including a number of 4th-order cycles. This long-term trend is described by the vertical stacking patterns of the 4th-order cycles, which progressively thin from the lower part of the succession (5 to 15m thick) to the upper part (1 to 5m thick). This accommodation cycle is probably developed in response to long-term subsidence patterns. The thicker 4th-order cycles at the lower part of the succession were accumulated during a higher subsidence rate phase when higher rates of accommodation space generation occurred. Whereas, the thinner 4th-order cycles in the upper part of the Fatha Formation were deposited when the rate of accommodation space generation and therefore probably subsidence rates decelerated.

It can be concluded that the Oligocene-Miocene was a time of high-frequency climatic changes and basin margin sequence architectures were largely controlled by glacio-eustatic sea-level changes (Kominz, 2001; Miller *et al.*, 2005; John *et al.*, 2011), including in the studied area. The Miocene succession in the Zagros foreland basin is characterized by a high-frequency cyclicity, with an average periodicity of about 60 kyr, which probably means that a mix of obliquity and eccentricity-forced cycles are expressed. Over the Fatha Formation as a whole, alternations of warm and cold periods, and associated sea level fluctuations, occurred during the mid-Miocene Climatic Optimum. This was followed by high frequency climatic alternations during a period when globally there was a gradual decrease in temperature and net sea-level fall. This event resulted in the deposition of the thick fluvial succession (Injana Formation and younger deposits) that prograded toward the basin throughout the rest of the Miocene

and Pliocene. During the mid-Miocene Climatic Optimum, in the hot/dry periods, carbonate and evaporite were deposited, whereas during the cold/wet periods, siliciclastic supply from the hinterlands was enhanced causing progradation and regression of the coastal facies belt.

To conclude, the nine logged sections of the Miocene cycles show consistent patterns of coincident changes in stacking patterns, accommodation space and a distribution of cycle types that support control by high frequency eustatic sea-level changes and associated climatic variation that governed sediment supply rates.

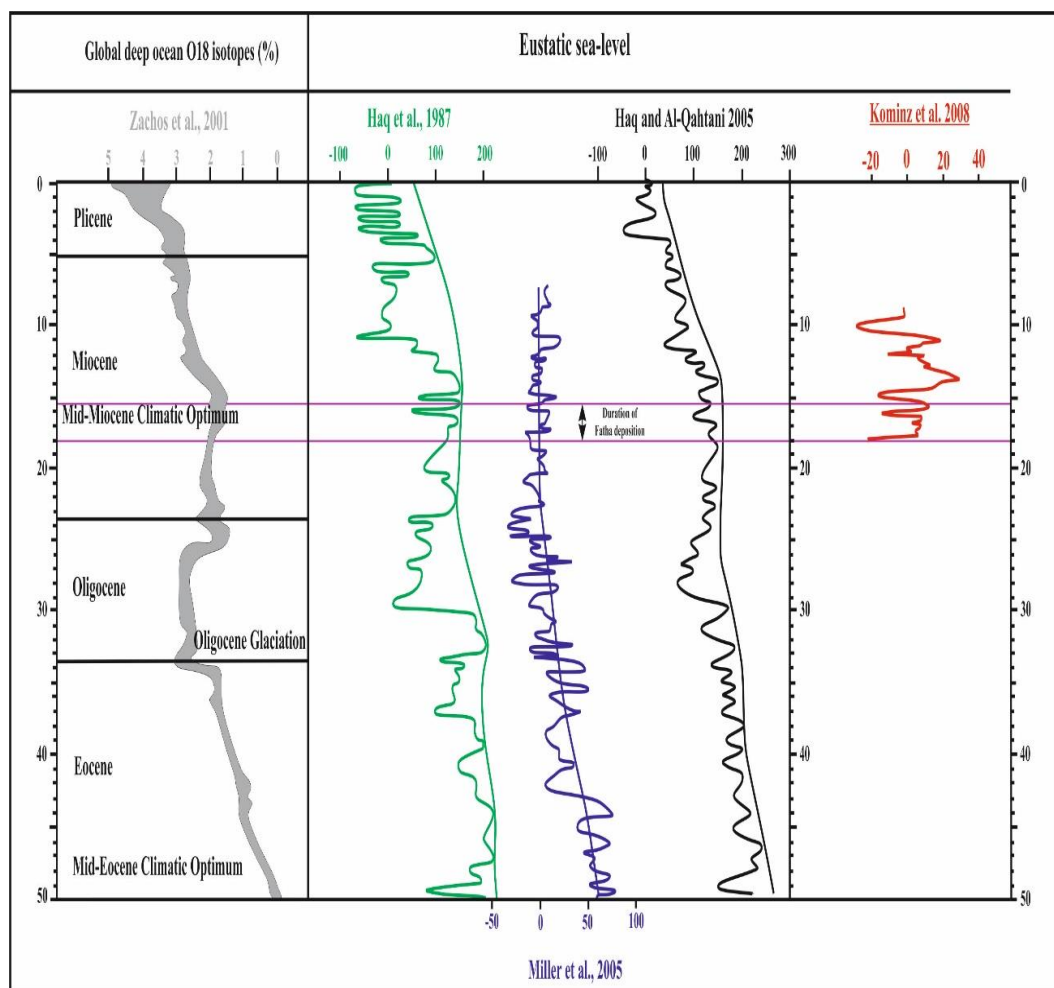


Figure 4-26 Eustatic sea-level estimations and global oxygen isotope ratios between 50 Ma and the present. The eustatic sea-level estimations are after Haq *et al.*, (1987, the green curve), Miller *et al.*, (2005, the blue curve), Haq and Al-Qahtani (2005, the black curve) and Kominz *et al.*, (2008, the red curve). The Haq *et al.* curve estimates higher amplitudes of sea-level variations. In contrast, the other curves of Kominz *et al.*, and Miller *et al.*, estimate lower amplitudes. The global oxygen isotope curve is after Zachos *et al.* (2001), against which Fatha Formation deposition occurred during the mid-Miocene Climatic Optimum (from ca. 18.0 to 15.5 Ma, the purple line).

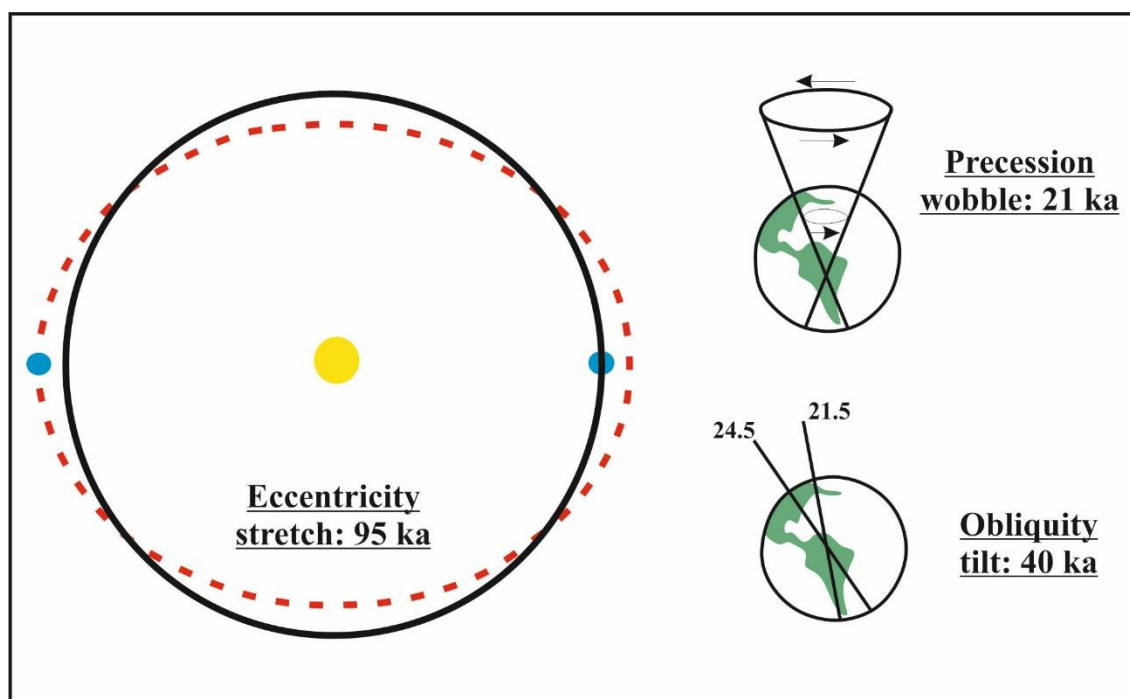


Figure 4-27 Components of orbital forcing of the earth, showing their periodicities and causes.

4.11.2 Tectonics

A number of geological processes can affect the subsidence evolution of a sedimentary basin, e.g. rifting, thermal relaxation, sediment loading and intraplate stresses. These processes work on subsidence evolution in low frequency (thermal relaxation) and relatively high frequency (intraplate stress and rifting) time scales (Cloetingh, 1988; Nottvedt *et al.*, 1995; Nielsen *et al.*, 2002).

The Arabian plate has undergone a complex tectonic history as well as eustatic sea-level changes since the Proterozoic era, which have caused changes in subsidence rate that in turn caused significant new accommodation space, or led to the development of erosional unconformities (Haq and Al-Qahtani, 2005). The subsidence evolution of the Zagros foreland basin during the Cenozoic era has been assumed to be influenced by tectonics of the Arabian Plate margin, obduction and final continent-continent collision between the Arabian and Iranian Plates (Koop *et al.*, 1982). In addition, possible reactivation of the basement Khanaqin fault (KHF) and Hail Ga'ara lineament (HRA) during the Miocene, and development of the Kirkuk and Sinjar salt sub-basins in Iraq could have influenced the subsidence of the Fatha sub-basins (Bahroudi and Koyi, 2004) (Figure 4.28). These basement faults are syn-sedimentary tectonic structures that

separated the Fatha basin in to six sub-basins along the north eastern part of the Zagros foreland Basin. The presence of palaeo-highs that have separated the sub-basins have affected the distribution of sedimentary facies, thickness variation, subsidence and the development of accommodation space in the Fatha cycles across the Zagros Basin. These effects on the Fatha cycles are evidenced by increasing thickness further away from the palaeo-highs (Al-Juboury and McCann, 2008), whereas thicknesses decrease toward the basin margin due to lower subsidence. It is clear from Figure (4.29) that the rate of subsidence decreased from the lower to the upper part of the succession and that this in turn created higher accommodation space in the lower part of the formation.

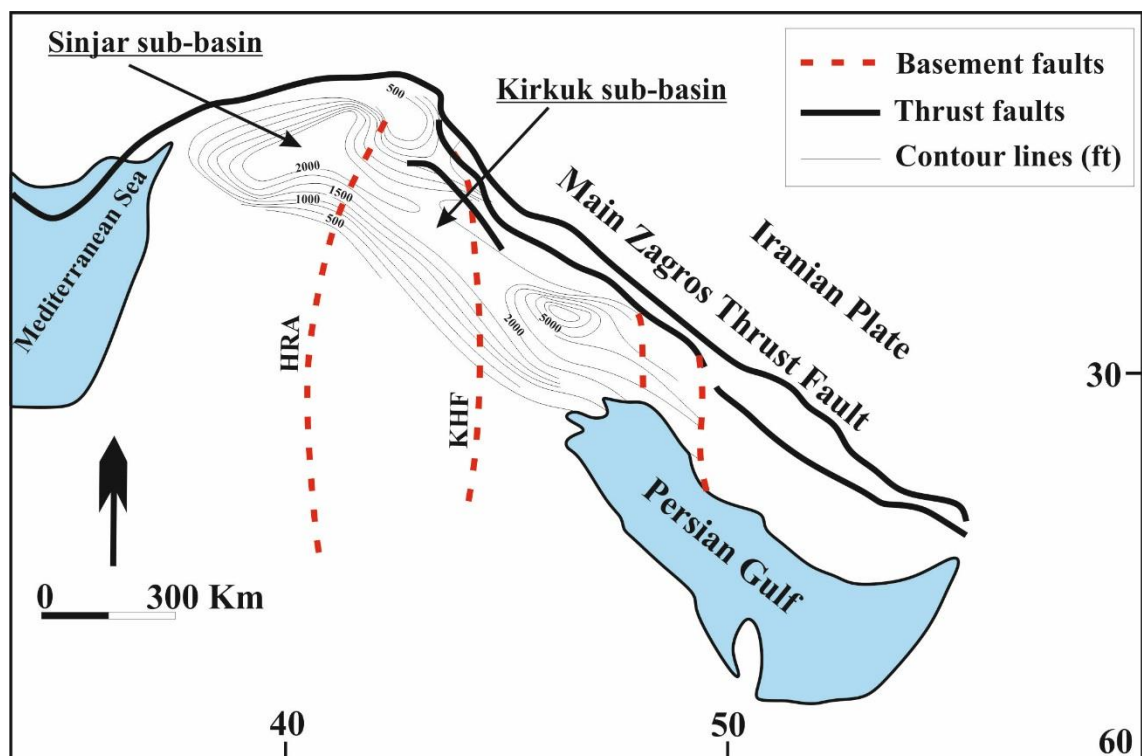


Figure 4-28 Isopach map of the Fatha (Gachsaran) Formation on the Arabian Plate. The (possibly syn-sedimentary) basement Khanaqin fault (KHF) and Hail Ga'ara lineament (HRA) are shown in the context of the separate Sinjar and Kirkuk salt sub-basins in Iraq (Bahroudi and Koyi, 2004).

Whilst basement faults and lineaments may have determined the geographical location of depocentres, and regional thickness variations, they had no apparent influence on stratigraphic cyclicity. The distances over which correlations of the high-frequency cycles of the Fatha Formation are possible make it unlikely that the cyclicity originated as a result of these tectonic activities. However, the deposition of the first red fluvial claystone in the Miocene happened during the deposition of the Fatha Formation. This means that the Zagros Mountains had probably started to grow in the late Burdigalian

and continued throughout the Miocene and Pliocene. This is evidenced by an apparent increase in sediment supply upward through the Fatha succession, as well as in the Injana and Mukdadiya Formations in the upper Miocene. Additionally, climatic cooling, accompanied by increasing rainfall, followed the Mid-Miocene Climatic Optimum, and this probably resulted in increased clastic deposition represented by the upper Miocene and Pliocene siliciclastic deposits.

4.11.3 Sedimentary process

Autogenic sedimentary processes that include tidal-flat progradation, have previously been used to explain the origin of sedimentary cyclicity (Ginsburg, 1975). This is not excluded in the Miocene cyclicity of the studied area because of the presence of tidal-flat and supratidal deposits at the top of many cycles. Typical cycles from the studied area pass up from low energy hypersaline conditions to shallow water carbonate of variable depositional environments and then pass up to supratidal evaporite and an alluvial/fluvial unit above. In general, the Fatha Formation cycles have laterally persistent pattern in cycle thickness, accommodation space and stacking patterns that all indicate a regular eustatic control. However, in tracing one cycle or a set of cycles laterally, some cycles are missing between the sections. For example, the Takiya and Basara sections have a higher number of cycles in the lower part than the Krbchna section. A possible explanation is that such duplications or omissions of cycles may be indicative of an autogenic sedimentary mechanism contributing to the control of cyclicity (Tucker and Garland, 2010).

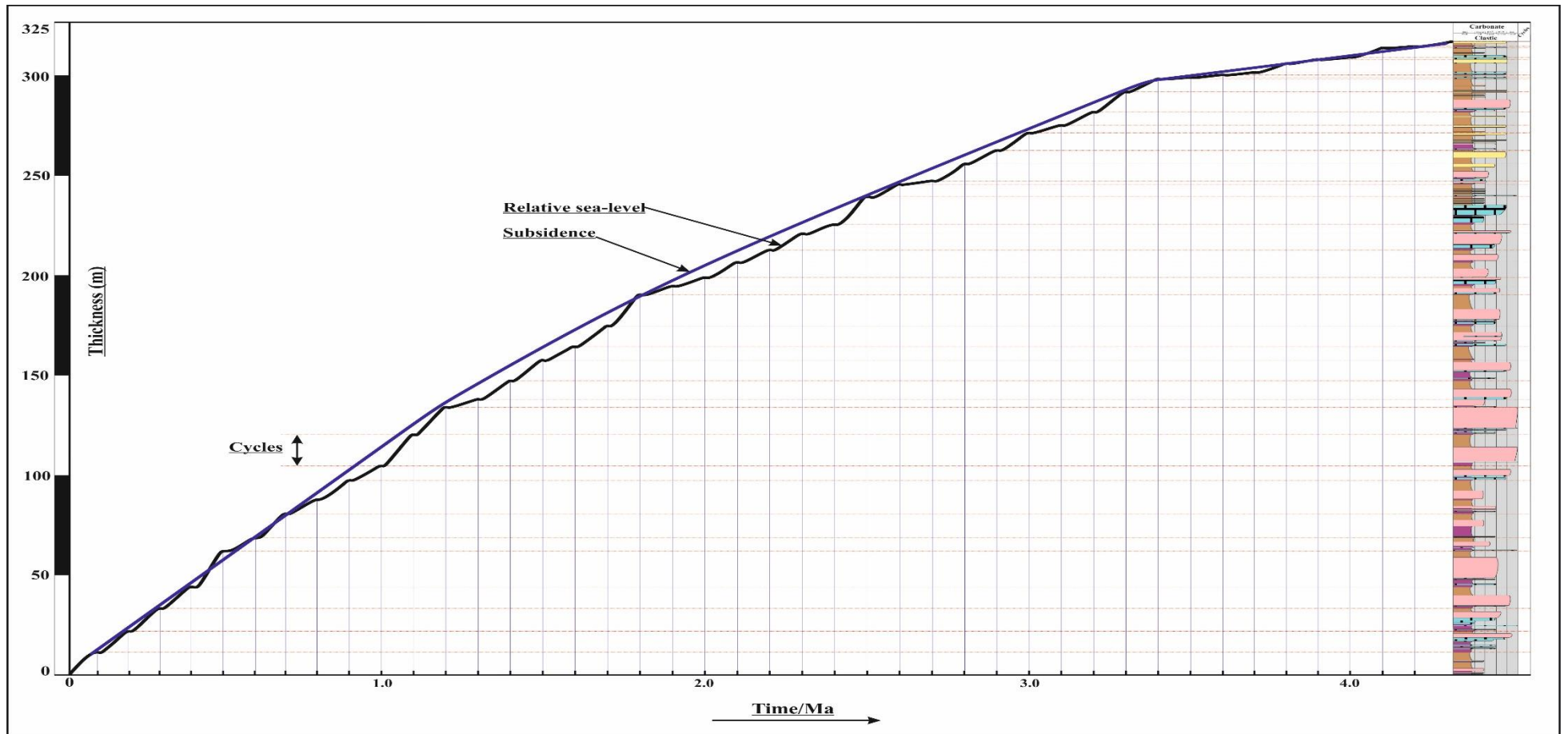


Figure 4-29 The effects of relative sea-level changes and subsidence on the Fatha cyclicity, based on the Mamlaha section. The subsidence is high at the lower succession, where the thicker cycles were deposited. Whereas, it shows a dramatic decrease in subsidence upward through the upper succession.

4.12 Conclusion

The late Burdigalian carbonate-evaporite deposits of the Fatha Formation were studied in the periphery of the Zagros foreland Basin in Kurdistan Region/NE Iraq. For this purpose, nine outcrop sections were studied around Slemani city to investigate sequence stratigraphic studies and analysis the carbonate-evaporite cycles. The formation is composed of a stacked succession of carbonate-evaporite shallowing-upward cycles that represent a long term accommodation history. Approximately 17 to 42 shallowing-upward cycles are recorded and defined as parasequences that are bounded by flooding surfaces. Shallowing-upward trend in an individual cycle is evidenced in all the particular facies by changing microfacies, fossil size and abundance, and lithology. These changes record environmental variations that include upward shoaling and salinity changes.

Standard and revised Fischer plots are constructed for the Fatha parasequences. The Fischer plots record a systematic variation in parasequence stacking pattern that can be used to define system tracts, parasequence set, and sequence boundary. The plots presented for all the studied sections have the same shape, an increase, and then a decrease in slope. The parasequences of the Fatha Formation form retrogradational and progradational parasequence sets, the individual parasequences ranging in thickness from 5-13 and 1-5 metres, in the lower and upper parts, respectively. They can be traced laterally for tens of kilometres at outcrop. Each parasequence in the lower part of the Fatha Formation has onlapped landward, overstepping pre-existing parasequences, whereas the parasequences in the upper part have prograded farther basinward relative to the previous parasequences. In this way, the upper part of the succession prograded basinward and created a diachronous relationship between the basinal and marginal facies belts and the fluvial wedge represented by the Injana Formation above. This means that the thicker cycles at the lower succession (rising slopes of the Fischer plots) were deposited during a higher accommodation space that was probably created by tectonic subsidence. Whereas, the thinner cycles at the upper succession (falling slopes of the Fischer plots) were accumulated during a relatively reduced accommodation creation that was probably enhanced by tectonic uplift. The high accommodation space at the lower succession was created during transgressive system tract (TST), whereas accommodation space at the upper succession was reduced during highstand system tract (HST). The transgressive system tract at the lower succession was recognized by

onlapping parasequences landward on a sequence boundary. By this way not all the parasequences were preserved at the margin.

Each individual cycle and the whole succession have some criteria in common. For example, firstly, both individual cycles and the succession represent a shallowing upward trend that indicates a decrease in water depth. Secondly, each cycle starts with a rapid increase in accommodation space generation and terminates with a decreasing rate of accommodation space generation. This criterion is also seen in the whole succession with high accommodation space generation in the lower part compared with progressively less accommodation space generation toward the upper part. Two types of parasequence sets resulted, in part seen as an increase and a decrease in the cycle thicknesses from the lower to upper parts of the succession, respectively.

The components and thicknesses of the parasequences change from basin margin to basin centre. Eight different types of parasequences (A to H) are recognized in the studied areas. These types of parasequences are plotted on the Fischer plots that are correlated across the studied areas. Type-D parasequence that is composed of calcareous mudstone, carbonate, evaporite, and red claystone, from base to top, is the thickest parasequence and most common type in the lower succession. Whereas, type-G and type-H parasequences are the thinnest and most common type in the upper succession where evaporite is missing and siliciclastic becomes predominant.

Strontium isotope method was used to determine the total duration of the whole succession and the origin of the evaporite deposits. The total duration of the deposition of the whole succession is calculated to be 2.55 m.y., as well as the duration of an individual parasequence is estimated to be 60 k.y. by dividing the total duration of the whole succession into the maximum cycle number. Additionally, all the evaporite samples show the Miocene marine signal. This means that the evaporites are originally marine deposits.

After an evaluation of eustatic, tectonic, and sedimentary mechanisms for the generation of the Fatha cyclicity, it can be called on high-frequency glacio-eustacy as their origins. This conclusion follows from (1) the extensive correlation of the parasequences for tens of kilometres, (2) systematic variation of stacking patterns (retrogradational and progradational), and (3) the high probability of glacio-eustacy in the Miocene worldwide. Secondly, tectonic had an impact on sedimentation that is evidenced by (1)

thickness variations of the succession that probably reflect the influence of tectonic uplift on the sedimentary record, (2) the first appearance of siliciclastic deposits with the deposition of the Fatha Formation, (3) increase of siliciclastic input upward through the succession, and (4) reactivation of basement faults during deposition and formation of several restricted sub-basins. This means that the Zagros Mountains had probably started to grow in the Miocene. Additionally, the climate varied from hot and arid during the deposition of the Fatha Formation into cold and wet during the Injana Formation in the upper Miocene. This is evidenced by ceasing evaporite deposition and increasing siliciclastic deposits from the Zagros Mountains. Lastly, sedimentary mechanism, including tidal flat progradation, is also included that follows by (1) the presence of supratidal and tidal flat deposits, and (2) missing of some cycles laterally between the studied sections.

It can be concluded that the Miocene period was a time of high-frequency climatic changes and basin margin sequence architectures were largely controlled by glacio-eustatic sea-level changes. Over the Fatha Formation as a whole, alternations of warm and cold periods, and associated sea level fluctuations, occurred during the mid-Miocene Climatic Optimum. This was followed by high frequency climatic alternations during a period when globally there was a gradual decrease in temperature and net sea-level fall. This event resulted in the deposition of the thick fluvial succession (Injana Formation and younger deposits) that prograded toward the basin throughout the rest of the Miocene and Pliocene. During the mid-Miocene Climatic Optimum, in the hot/dry periods, carbonate and evaporite were deposited, whereas during the cold/wet periods, siliciclastic supply from the hinterlands was enhanced causing progradation and regression of the coastal facies belt.

Chapter Five

Comparison of carbonate-evaporite cyclical successions of the Zechstein, Paradox and Zagros Basins

5.1 Introduction

Cyclic deposition may be defined as a systematic arrangement of a group of sedimentary facies that is regularly repeated several or many times through an accumulated succession (Tucker, 2003). Cyclic successions of sedimentary strata are locally recorded during most geological times but during a few specific time intervals they are widespread, and at these times cyclic successions accumulated with worldwide distribution (Goldhammer *et al.*, 1994). For example during the Pennsylvanian and Permian, widespread cyclic deposition of mixed carbonate, evaporite, and siliciclastic rock types occurred over large parts of Europe (e.g. the Zechstein Basin, late Permian) and the United States (e.g. the Paradox Basin, SW USA, Pennsylvanian-Permian) (Baars, 1976; Baars and Stevenson, 1982; Tucker, 1991; Brown, 2002; Becker and Bechstädt, 2006). In these basins, up to 1.5 and 2 km of predominately evaporites were accumulated, respectively (Baars and Stevenson, 1982; Geluk, 2000b). Facies analysis and distribution of the sedimentary facies in these basins reveal shelf depositional configurations (Tucker, 1991; Weber *et al.*, 1995) where the evaporite deposition, comprising both anhydrite and salt deposits, was restricted to the basin centre, whereas the carbonate deposition accumulated on the shelf at the basin margins. In contrast, the Miocene carbonate-evaporite cycles of the Fatha Formation of Kurdistan were accumulated on a gently sloping ramp. The carbonate ramp and shelf configurations, as well as tectonic settings and eustatic sea-level fluctuations, each exerted an important role in controlling the accumulation and distribution of the sedimentary facies.

One of the important features to consider in comparing the Miocene succession of Kurdistan to the Pennsylvanian-Permian successions of NW Europe and SW USA is the well-developed carbonate-evaporite cyclicity in these basins. Climate, tectonics, and glacio-eustatic sea-level fluctuations, as well as sedimentary mechanisms, were likely controls on these cyclic arrangements. The main aim of this chapter is to review the developments of the Zechstein and Paradox Basins and then to compare the fill of the Miocene carbonate-evaporite cycles of the Fatha Formation with the carbonate-

evaporite cycles of the Pennsylvanian to Permian Basins. Specific research objectives are as follows: (i) to review the development histories, tectonics and palaeoclimates, as well as depositional configurations of the Zechstein and Paradox basins; (ii) to summarize their depositional facies and their distributions in the carbonate shelf settings; (iii) to review the components of the cycles, and their correlations across the basins; (iv) to present the hierarchies of the cycles in term of sequence stratigraphic frameworks; (v) to compare the Miocene cycles to the Zechstein and Paradox cycles in term of depositional facies, basin configuration, tectonics, and climates, as well as local and global mechanisms that controlled the cyclicities.

This chapter comprises three main sections: the first section reviews the characteristics and context of the Zechstein Basin and the second section similarly examines the Paradox Basin, whereas the third section includes a comparison and analysis of the Miocene cycles of the Fatha Formation in the Zagros Basin with the other two case-study examples.

5.2 Zechstein Basin

One of the most interesting areas where high-resolution basin analysis has been undertaken is the carbonate-evaporite cycles of the late Permian (Lopingian) Zechstein Basin in NW Europe. The basin extends from northern England, across the North Sea through the Netherlands, Denmark, Germany and Poland, with a length of 2500 km and a width of 600 km (Roscher and Schneider, 2006) (Figure 5.1). The name Zechstein Group is defined in Nederlandse Aardolie Maatschappij and Rijks Geologische Dienst (1980). The Zechstein Group developed in the late Permian (Lopingian) and was deposited after the Late Carboniferous Variscan Orogeny (Geluk, 2000a; Geluk, 2007). The Zechstein deposits formed in a major epicontinental shallow marine basin that covered much of Central Europe, and which had a connection of restricted size with the upper Permian open marine sea through a narrow strait between Greenland and the Scandinavian Peninsula. The strait was narrow and over 1000 km long; its development was originated by tectonic evolution of the Greenland-Norwegian Sea rift (Wagner and Peryt, 1997). The formation of the rift led to a sudden transgression over the low-lying southern and northern Permian basins (Ziegler, 1990; Taylor, 1998) (Figure 5.1). The main depocentre in the southern Permian basin was located in the northeastern and northern part of the offshore Netherlands territorial waters of the present-day North Sea.

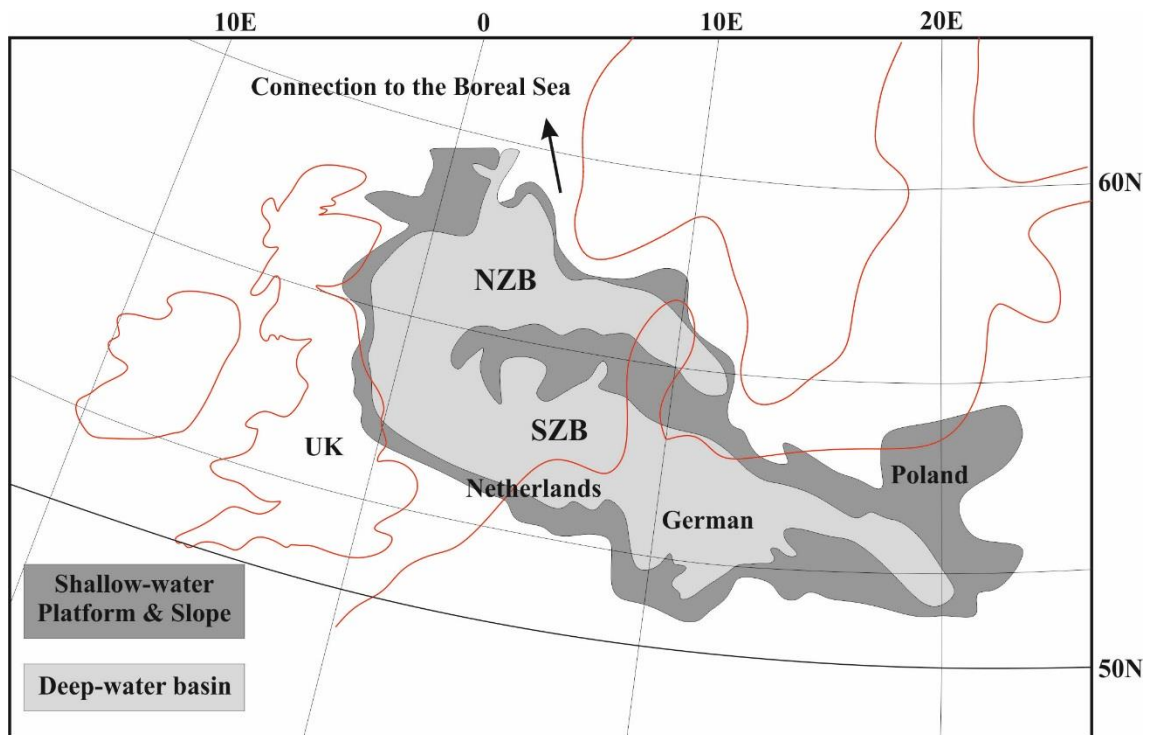


Figure 5-1 Late Permian palaeogeography of the Zechstein Sea, including both Northern Zechstein Basin (NZB) and Southern Zechstein basin (SZB). The shallow and deep water areas of sedimentation are also included (Taylor, 1998).

In general, the Zechstein Group consists of carbonate and evaporite cycles with thin claystone intercalations (Taylor, 1998). The carbonates were deposited in platform, slope and basin settings, whereas the evaporites, which consist of anhydrite and rock salt, accumulated principally down in the basin in shallow-water lagoons. However, toward the edge of the basin, claystone and sandstone gradually replace the evaporites and, to a lesser degree, the carbonates. The upper boundary is gradational with the Lower Triassic Sherwood Sandstone Group onshore and the Bacton and Heron groups offshore, whereas the lower boundary is unconformable with the Carboniferous strata of the Upper Rotliegend Group. The Zechstein Group is divided into five evaporite-bearing cycles (Z1-Z5) (Taylor, 1998). The Z1 and Z2 cycles were deposited in various settings from lagoon to sabkha/mudflat at the margin, to deep marine in the basin centre. A very thick salt layer was deposited during the Z2 cycle. The Z3 cycle was deposited in a shallow marine setting. However, toward the higher cycles (Z4 and Z5), marine deposits are less common; carbonates are not present and alternations of claystone and halite are more common; these were deposited in a playa lake depositional setting. The Zechstein Upper Claystone Formation, at the top of the group, rests on the underlying cycles with an unconformable relationship (Geluk, 2007).

5.2.1 Tectonic development of the Zechstein Basin

The development of the Permian Basin followed the Variscan Orogeny, and it originated largely by thermal subsidence (Smith, 1979), although tectonic processes were locally significant, as outlined below. During the latest Carboniferous to early Permian, Central Europe was occupied by the collapsing Variscan mountain chain and adjacent basin development was accompanied by thermal destabilization of the lithosphere and intense magmatism (McCann, 2008). Strike-slip fault movements, crustal stretching, and igneous activity were the main characteristics of this stage. At this stage, the late Variscan Orogeny led to the development of trans-tensional rifting and formation of a number of pull-apart basins where clastic and volcanic detritus of the Lower Rotliegend Group were accumulated (Ziegler, 1990). Then, the Saalian Orogeny, which was a deformation phase (post-Carboniferous-Early Permian) (Schulmann *et al.*, 2014), terminated the deposition of the Lower Rotliegend Formation in most of the NW European Basin and resulted in a lengthy period of uplift, and erosion of hundreds to thousand metres of deposits (Ziegler, 1990). This unconformity surface is known as the Saalian unconformity (Ziegler, 1990) or Basal Permian Unconformity (Geluk, 2007). A broad continental depression was developed during the Permian and was repeatedly flooded during the Zechstein (Ziegler, 1990). Continental rifting, thermal subsidence and magmatic activity after the Saalian Orogeny resulted in the development of the Northern and Southern Permian Basins that stretched from England to Poland (Ziegler, 1990). The Mid-North Sea, Ringkobing-Fyn, and Texel structural highs separated these basins with axes that trended WNW-ESE (Geluk, 2000a). Continental to marginal marine deposits of the Upper Rotliegend Formation were accumulated in these intermountain basins with basinal halite-dominated evaporitic sequences (McCann, 2008). On gently inclined platform margins along the southern edge of the basin, a cross-laminated sandstone-dominated desert unit (the Yellow Sand in England) accumulated, overstepping the Saalian unconformity surface (Benton *et al.*, 2002).

During the late Permian to Mid-Triassic times, subduction of the Palaeotethys Ocean and rifting of the Norwegian-Greenland Sea continued and the Neotethys Ocean started opening (Roscher and Schneider, 2006). The development of a rift zone between Greenland and Scandinavia and global glacio-eustatic sea-level rise in the late Permian resulted in a rapid transgression into the low-lying Northern and Southern Permian Basins where the Zechstein cyclic succession of carbonate-evaporite and minor clastic

detritus accumulated (McCann, 2008). The Southern Permian Basin is divided into sub-basins due to tectonic activity that resulted in variations in composition and thickness of the Zechstein deposits (Geluk, 2007). The depocentre of this basin was located in the northern offshore and northeastern Netherlands where thick salt sequences of the Z2 and Z3 cycles were accumulated (Geluk, 2005). The basin was bordered by the Mid-North Sea and Ringkobing-Fyn Highs to the north, and the Texel High to the south. Siliciclastic deposits derived from these highs are locally included within the cycles (Geluk, 2007). Toward the margins of the basin, claystone and sandstone deposits replaced the evaporite members (Ziegler, 1990). During the deposition of the Z1 to Z3, a thick succession of halite-dominated evaporitic deposits accumulated, whereas towards the end of the late Permian, the basin became filled, and evaporite precipitation was less widespread (Geluk, 2005; Geluk, 2007).

The deposition of the thick evaporite cycles of the Zechstein Basin played a crucial role during post-Zechstein structural development when the ductile salt beds migrated in response to changing stress fields (Roscher and Schneider, 2006), leading to the development of a series of salt-walled mini-basins that influenced later Triassic sediment distribution patterns (Geluk, 2000b).

5.2.2 Permian climate in Central Europe

The Carboniferous-Permian strata, including siliciclastic and carbonate deposits, were succeeded by deltaic, swampy and often non-marine red-bed deposits, indicate a falling trend in sea-level (McCann, 2008). This eustatic sea-level lowstand was the result of the Carboniferous-Permian glaciations on Gondwana, and was emphasized by Variscan tectonic uplift. The absence of marine influence on earliest Permian deposition in many parts of the Europe was the result of this combined tectono-eustatic condition (McCann, 2008). Later in the Permian, eustatic sea-level rise, combined with initial rifting in the North Atlantic or North Sea areas and denudation of the Variscan highs, resulted in marine transgression comprising, lastly, the development of the Zechstein Sea (Roscher and Schneider, 2006). A combination of climate changes, basin dynamics and eustatic sea-level fluctuations controlled the sedimentary history and distribution of facies of the Zechstein Sea (McCann, 2008). Eustatic sea-level changes during the sedimentation of the Zechstein Limestone resulted in episodic subaerial exposure of the carbonate platforms and extreme meteoric diagenesis. The following regression in the latest

Permian occurred simultaneously with the eustatic sea-level lowstand (Haq and Schutter, 2008), the Pangaea coalescence and the incipience of more humid climates.

The desert-dominated facies of the Upper Rotliegend Group indicates an arid to semi-arid climate (Roscher and Schneider, 2006). At the southern basin margin, alluvial and aeolian dune facies are preserved, whereas evaporitic lake deposits occur in the basin centre. In addition, Roscher and Schneider (2006) state that the Permo-Carboniferous climate was characterized by a trend towards increasing aridity that was interrupted by multiple wet stages. These wet stages were the result of the waxing and waning of the Gondwana icecap and can be recognized in all major European and North African basins. Later, the Zechstein Transgression occurred as a rapid flooding event governed by a eustatic sea-level highstand and ongoing rifting (Benton *et al.*, 2002; McCann, 2008). These events exerted a marine influence on the otherwise highly continental climate of northern Pangaea. Additionally, no large glacial deposits are found in the late Permian and the climatic belts were spread out latitudinally at that time, which is inferred from the presence of forest in the Antarctic Continent, comprising cold temperate and humid vegetation (Cúneo, 1996).

In general, the Zechstein carbonate-evaporite cyclothems resulted from transgressive-regressive cycles of different duration and intensity. The supply of new sea-water was coincident with transgression and carbonate deposition, whereas the lack of new sea-water or restricted inflow during regression resulted in anhydrite and salt deposition (Wagner and Peryt, 1997). Generally, the climate was very dry and the intensity of aridity was variable. The more arid phases of the second Zechstein cycle (Z2) alternated with less dry periods of the third Zechstein cycle (Z3). At the end of accumulation of the Z3 cycle, the climate changed to become more humid. Consequently, in the latest Zechstein cycles (Z4-Z5), the arid phases were interrupted by humid ones due to the increasingly reduced connection of the Zechstein Sea with the Late Permian Ocean (Wagner and Peryt, 1997). This reduction in connection resulted from the Late Permian global regression that in turn resulted in the cessation of carbonate deposition and the onset of accumulation of a new type of siliciclastic-evaporitic cycle. In arid periods, evaporites – mainly halite and with minimal amounts of anhydrite – were precipitated. By contrast, during humid phases siliciclastic and siliciclastic-saline deposits were accumulated. In the lowermost part of the Z4 cycle connection with the open sea was completely cut off, resulting in the deposition of clayey-saline deposits in the

continental salt pan during relatively humid periods and the deposition of clayey rock salt in the dry phase. Finally, fluvial siliciclastic deposits prograded out to the palaeo-shorelines of the salt lakes (Wagner and Peryt, 1997).

5.2.3 Zechstein stratigraphy

The Permian stratigraphy includes three groups, the Lower Rotliegend (early to mid-Permian), Upper Rotliegend (middle into the late Permian), and Zechstein (late Permian). The boundary between the Lower Rotliegend and the overlying strata (whether the Upper Rotliegend or Zechstein), as well as the boundary of the Upper Rotliegend Group and the overlying Zechstein Group are unconformable (Geluk, 2007). The high-frequency carbonate-evaporite cycles are related to the Zechstein Group. The Zechstein Group was originally divided into five carbonate-evaporite cycles (Z1-Z5) (Figure 5.2), each of formation rank, and these can be correlated as equivalent carbonate-evaporite cycles from the UK to the Netherlands, Germany, Denmark and to Poland (Van Adrichem Boogaert and Kouwe, 1994; Taylor, 1998). The Zechstein Upper Claystone Formation overlies the carbonate-evaporite cycles unconformably.

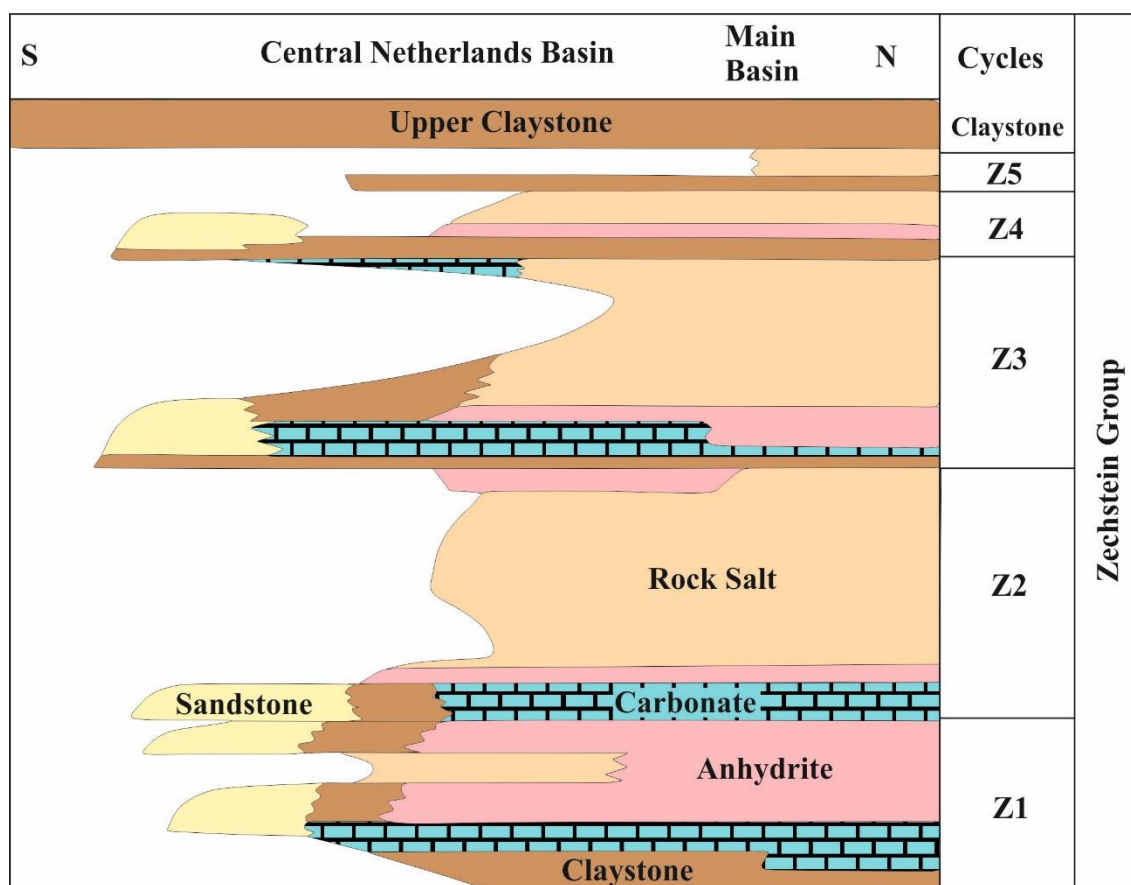


Figure 5-2 Lithostratigraphic diagram of the Zechstein cycles, including five carbonate-evaporite cycles (Z1-Z5). The Upper Claystone Formation overlies the Zechstein cycles unconformably (Van Adrichem Boogaert and Kouwe, 1994). Two thick halite deposits were accumulated during the Z2 and Z3 cycles, and carbonate deposition ceases toward the upper cycles.

5.2.4 Zechstein cycles

The late Permian Zechstein deposits are traditionally divided into five main carbonate-evaporite cycles, Z1 to Z5 (Tucker, 1991; Geluk, 2000a). Each cycle includes clastic deposits (claystone) at the base, followed by carbonates, sulphates and rock salt. Depending on the palaeogeographic position and subsidence state of the basin at the time of accumulation, the thickness of each cycle ranges from a few tens to several hundreds of metres (Geluk, 2000a).

5.2.4.1 First Zechstein cycle: Z1

Deposition of the Z1 cycle began with the finely laminated claystone of the Coppershale or Kupferschiefer (Marl Slate in England) (Figure 5.3A), which was deposited in a stratified anoxic sea, inferred to have been about 200m deep (Tucker, 1991). This deposit marks the first Zechstein transgression over the underlying desert sands and playa lakes (Yellow Sand in England). Above this, the cycle comprises of the Z1 carbonate, Z1 anhydrite and Z1 salt (Tucker, 1991; Becker and Bechstädt, 2006). Up to 300 m of rock salt was deposited in a series of locally fault-bounded depressions in the anhydrite platform (Ziegler, 1990). However, toward the southern part of the basin the formation consists of claystone. The platform and slope deposits of the Z1 carbonate comprise a thick (200m) marl and carbonate succession, in contrast to a thin carbonate unit in the sediment-starved basin centre. The Z1 carbonate (Ca1) unit in England is represented by the Raisby, Ford, and Cadeby Formations (Tucker, 1991), whereas their lateral equivalents in the Netherlands and Germany are represented by the equivalent Werra Formation (Geluk, 2007). The Raisby Formation is generally dolomitized and consists of lime mudstone and bioclastic and bioturbated wackestone (Figure 5.3B). In Tyne and Wear County the top of the formation is marked by a major slide-slump horizon (Tucker, 1991) (Figure 5.3F). The Ford Formation is characterized by shelf-margin reef and back-reef facies (Figure 5.3B-E). In addition, the Z1 anhydrite (A1) in England consists of the Hartlepool and Hayton anhydrites, whereas the lateral equivalent in the Netherlands and Germany is the Werra Anhydrite (Geluk, 2000a; Becker and Bechstädt, 2006).

5.2.4.2 Second Zechstein cycle: Z2

The Z2 cycle consists of a basal carbonate unit (Ca₂), followed by the basal anhydrite (A2) and a thick salt layer (Tucker, 1991; Becker and Bechstädt, 2006). The carbonates of the second Zechstein Z2 cycle are represented by the Roker Dolomite (shelf facies, 50m thick) and the Concretionary Limestone (foreslope facies, 110m thick) (Figure 5.3F), as well as the Edington Formation (shelf lagoon facies) in the Durham Province in England, whereas it comprises the Kirkham Abbey Formation (shelf-margin and foreslope facies) in the Yorkshire province (Tucker, 1991). The lateral equivalent of the second carbonate cycle in the other countries comprises the Stassfurt Formation (50 to 700 m thick). The shallow-shelf facies of the Roker Dolomite in England commonly consists of cross-bedded bioclastic oolite (Figure 5.4A-B) (Tucker, 1991). In the area of Blackhall Rocks in England, stromatolites and microbialite domes (Figure 5.4C-D) are developed and pass up to oolites (Figure 5.4A-B), whereas, the slope carbonate facies of the Roker Formation consists of laminated dolomite and dedolomite (Figure 5.4F) and turbidites (Figure 5.4E) (Tucker, 1991). Similar to England, three facies realms (platform, slope, and basin) are identified in the Z2 carbonates in the Netherlands (Geluk, 2007). The deposition of the second carbonate was followed by evaporites (the Fordon Evaporite in England and the Stassfurt Evaporite in other countries) that completely filled the basin (>300m thick) and then was succeeded by the deposition of several hundred metres of halite (>600m) (Tucker, 1991).

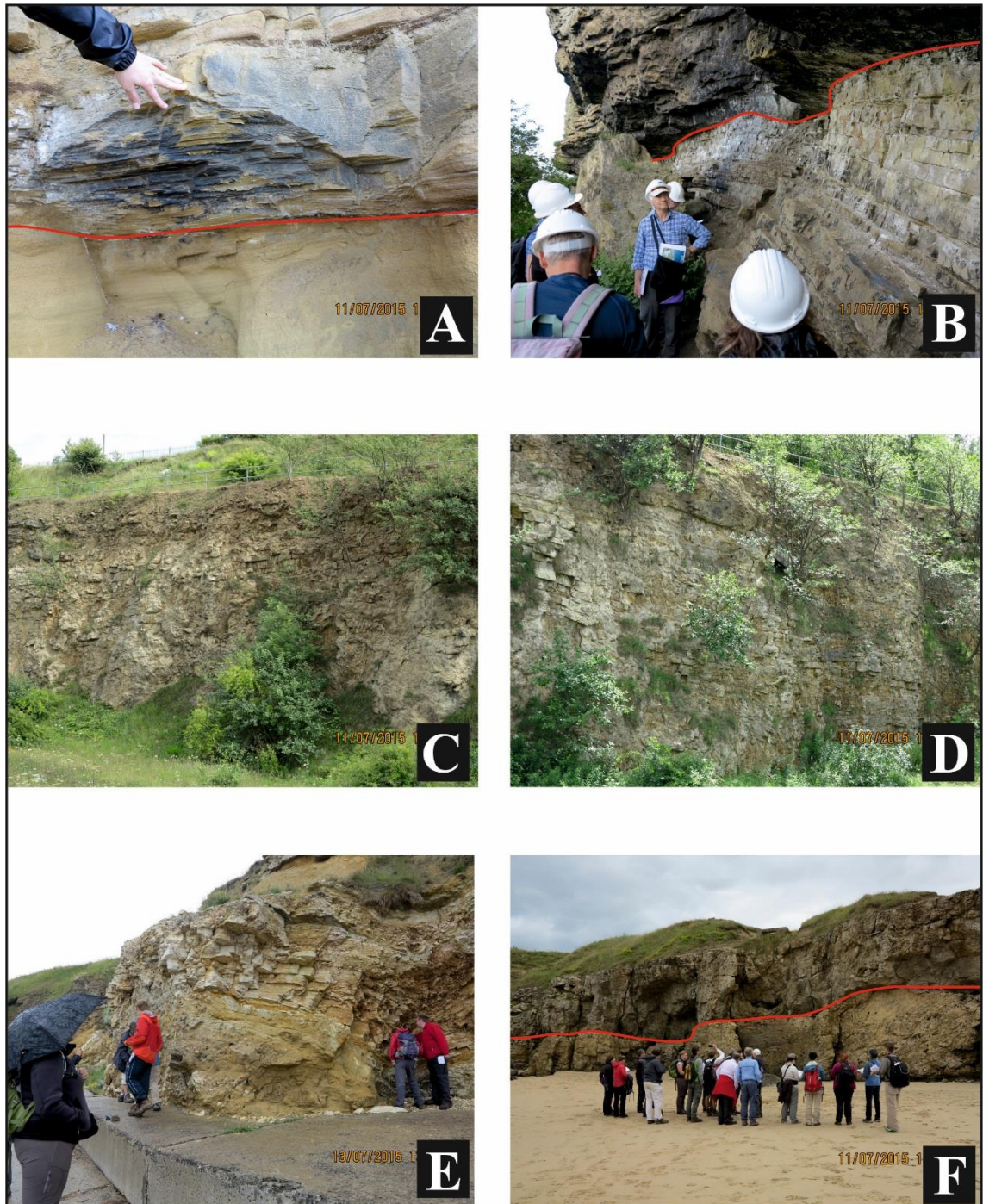


Figure 5-3 Field photographs of the Zechstein carbonate units in England.

A: The first Zechstein unit the Z1 Marl Slate (Copper Shale), the first transgression of the Zechstein Sea over the desert facies of the Yellow Sand (Upper Rotliegend Group) from Claxheugh Rock, Sunderland. **B:** Well-bedded carbonate unit of the lagoonal facies of the Z1 Raisby Formation, overlain by the massive carbonate of the reef facies of the Z1 Ford Formation from Claxheugh Rock, Sunderland. **C and D:** The massive carbonate unit of the reef facies overlain by or laterally changed to the well-bedded carbonate unit of the back-reef facies Z1 of the Ford Formation from Sunderland. **E:** Old abandoned quarry in the lagoonal facies of the Z1 Ford Formation, Wingate Quarry. **F:** Well-exposed megabreccia slide deposits of the uppermost Z1 Raisby Formation overlain by the Trow Point Bed (10cm thick, equivalent to the Ford Formation) and then followed by the collapse-brecciated carbonate of the Z2 Concretionary Limestone of the Roker Formation. These two units are separated by a sequence boundary with the residue of the Hartlepool Anhydrite.

5.2.4.3 Third Zechstein cycle: Z3

The Z3 cycle began with the deposition of a thin clay unit (Illitic Shale in England, Grey Salt Clay in the Netherlands and Grauer Salzton in Germany) that represents an important regional marker bed (Tucker, 1991; Strohmenger *et al.*, 1996a; Geluk, 2007). This basal bed is followed by the third cycle Z3 carbonate, the Seaham and Brotherton Formations in England, comprising peloidal mudstone-packstone and bioclastic/ooidal grainstone with cross-lamination and storm-generated bedding features. These facies represent quiet, relatively shallow aggraded shelf deposits (Tucker, 1991) with occasional storm activity. Stromatolitic mudstone and several sabkha parasequences are identified in the upper part of the Seaham Formation. The Z3 carbonate in the Netherlands (Leine Formation) consists of a thin, dark-coloured limestone (basinal facies), laminated and bioturbated mudstone (slope facies), and grey microcrystalline dolomite and algal boundstone (platform facies). These carbonate facies were followed by the deposition of evaporite and salt. The evaporite deposits (Billingham Anhydrite (0-20m) and Boulby Halite (50m) in England) indicate subaerial (sabkha) to shallow subaqueous (lagoonal) deposition (Tucker, 1991).

5.2.4.4 Fourth Zechstein cycle: Z4

The Z4 cycle was initiated with a thin carbonate member (the Uppang Formation, <1m thick) in England, whereas it began with a thin claystone (Red Salt Clay) in the Netherlands. The carbonate unit (Uppang Formation) comprises sandy oolitic dolomite and argillaceous dolomite that represent hypersaline conditions, as indicated by the lack of marine fossils (Tucker, 1991). The cycle is then characterised by the deposition of anhydrite and salt. The Z4 Pegmatite Anhydrite in the Netherlands has a wide distribution while the Z4 Salt is only accumulated in the depocentres (Geluk, 2000a). The Z4 Sherburn Anhydrite (in England) is just 0 to 9 m thick and probably accumulated in a shallow hypersaline sea (Tucker, 1991). The anhydrites were followed by the deposition of the Z4 Salt (Sneaton Halite in England) that ranges from 0 to 60 m in thickness in England (Tucker, 1991), whereas in the Netherlands, it reaches 150m thick (Geluk, 2000a; Geluk, 2005). Along the basin margins, sabkha facies and coarse-grained fluvial sandstone were deposited (Geluk, 2005).

5.2.4.5 Fifth Zechstein cycle: Z5

The Z5 cycle became restricted in the depocentres and started with the Littlebeck Anhydrite in England (Tucker, 1991), and a thin claystone in the Netherlands (Geluk, 2000a). The claystone was followed by the deposition of the Z5 Salt (up to 15m thick), whereas the Littlebeck Anhydrite was followed by the deposition of claystone, siltstone and sandstone (Roxby Formation) of distal alluvial fan, coastal plain and shallow lagoonal environments (Tucker, 1991).

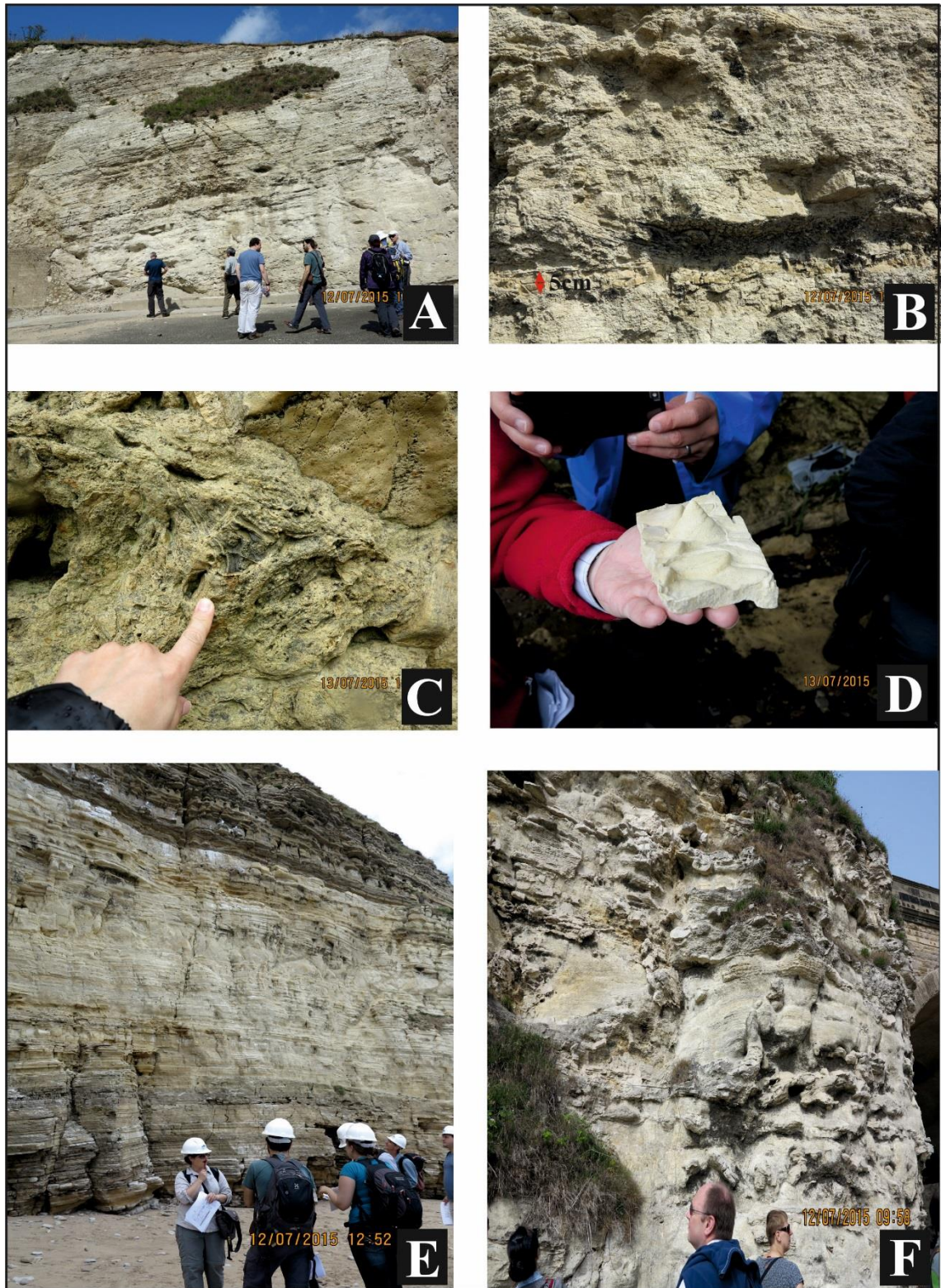


Figure 5-4 Field photographs of the Zechstein carbonate units in England.

A: Cross-bedded oolitic shelf-margin facies of the Z2 Roker Formation from Seaburn, Sunderland. **B:** Close-up view of the cross-bedded oolitic facies of the previous photo. **C and D:** Microbial dolomite and stromatolites of the Z2 Roker Formation from Blackhall Rocks. **E:** Lower slope turbidite facies of the Roker Formation from Marsden Bay. **F:** Dedolomitized foreslope facies of the Roker Formation underlying the oolitic shelf-margin facies, a lateral equivalent of the Concretionary Limestone, at Seaburn, Sunderland.

5.2.5 Sequence stratigraphy of the Zechstein cycles

Lithostratigraphically, the Zechstein Group comprises five main carbonate-evaporite cycles (Figure 5.2). Each begins with a basal claystone followed by carbonate, anhydrite and rock salt at the top. Various sequence stratigraphic models are proposed for the Zechstein cycles from different parts of the basin that show some differences (Tucker, 1991; Strohmenger *et al.*, 1996a; Wagner and Peryt, 1997; Becker and Bechstädt, 2006). The entire Zechstein depositional event represents a 2nd-order cycle, whereas each depositional sequence may be considered a 3rd-order sequence with well-developed system tracts. In addition, 4th- and 5th-order shallowing-upward parasequences are also identified (Tucker, 1991; Wagner and Peryt, 1997).

A new approach to Zechstein stratigraphy was proposed by Tucker (1991) for the English succession, identifying seven depositional sequences separated by regional sequence boundaries on the western edge of the Northern Zechstein Basin (Figure 5.5). The first depositional sequence was interpreted to start with a type 1 sequence boundary at the base of the lowstand facies of the Yellow Sand. The Marl Slate facies (Copper Shale) represents deposit of the first transgression of the Zechstein Basin and can be correlated across the Netherlands (Geluk, 2007), Germany (Becker and Bechstädt, 2006), and Poland (Wagner and Peryt, 1997). Then the succeeding carbonate deposits (Raisby Formation) represent the deposits of the HST. Similarly, the other depositional sequences each commence with a sequence boundary at their base with a well-developed lowstand facies accumulated in the basin depocentre regions (anhydrite and halite), and then succeeded by the TST and HST, mainly of carbonates. The sequence boundaries are well developed at the top of the carbonate members with evidence of subaerial exposure. According to this model, the sequence boundaries are placed at the base of evaporites, and carbonates were not originally linked chronostratigraphically to the following evaporites. In addition, in the Tucker (1991) model, each depositional sequence commences with evaporites which originated as a marginal lowstand gypsum wedge and basin halite-fill during the period of relative sea-level fall and sea-level low. These evaporites are followed by carbonates deposited as the TST and HST. More carbonates were accumulated in the lower sequences, whereas the upper sequences are dominated by evaporate accumulation.

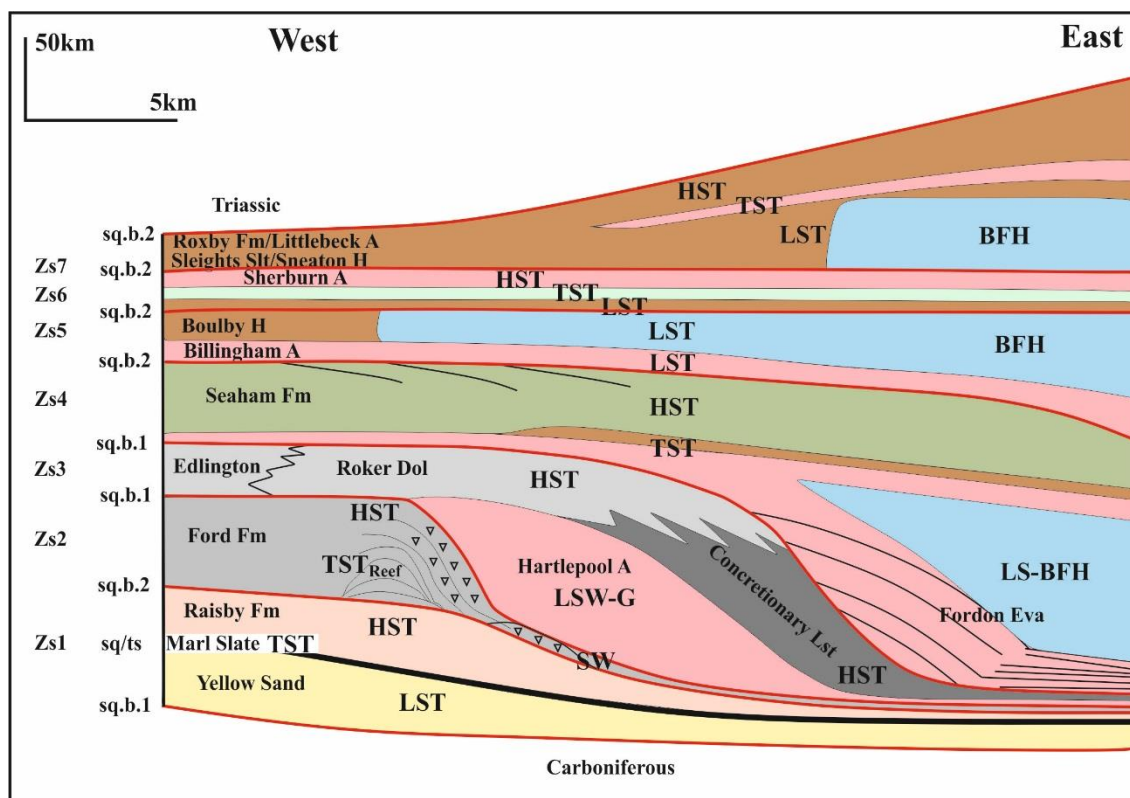


Figure 5-5 Sequence stratigraphy and lithostratigraphy of the English Zechstein group (Tucker, 1991).

Seven depositional sequences (ZS1-ZS7) are identified that are separated by sequence boundaries (red lines). BFH: basin-fill halite, LSW-G: lowstand wedge, SW: slope wedge, LST: lowstand system tract, TST: transgressive system tract, HST: highstand system tract, A: anhydrite, H: halite, sq.b.1: sequence boundary type1, sq.b.2: sequence boundary type2, and ZS1-ZS7: depositional sequences.

Wagner and Peryt (1997) considered that the lower four of Tucker's sequences (ZS1-ZS4) should be treated as 3rd-order sequences, whereas the upper three sequences (ZS5-ZS7) could be parasequences of one 3rd-order sequence. Goodall *et al.* (1992) argued that the duration of the entire Zechstein succession (5 to 7 Myr) could lie within the range of a single 3rd-order sequence (duration of 1 to 10 Myr), thereby indicating that the 3rd-order sequences defined by Tucker are more logically assigned as 4th-order sequences. Tucker (1992b) recognized that the entire Zechstein succession is more carbonate-dominated at its base and more evaporite-dominated at its top. This is consistent with these packages having accumulated during a 2nd-order relative sea-level rise and fall, respectively.

The first sequence stratigraphic division of the German Zechstein cycles was proposed by Strohmenger *et al.* (1996a) and they divided the succession into sequences and

parasequences (Figure 5.6). According to this model, and in contrast to Tucker's (1991) model, the evaporites are not correlated with the lowstand deposits and the carbonates with the transgressive and highstand deposits. In addition, they conclude that there is no indication of subaerial exposure at the top of Ca1 carbonate platform in this region, and the Z1 evaporites (A1) are mainly HST deposits and not LST as placed by Tucker. Strohmenger *et al.* (1996a) put a maximum flooding surface at the top of the Ca1 and the A1 is interpreted as a HST deposit. The main significant differences in the Strohmenger *et al.* (1996a) model is the presence of LST deposits in the upper part of the Main Dolomite unit.

German Zechstein Cycles	Chronostratigraphy of German Zechstein Cycles		3rd order Zechstein sequences (Strohmenger <i>et al.</i> , 1996)	3rd order Zechstein sequences (Tucker, 1991)	3rd order Zechstein sequences (Wagner and Peryt, 1997)
	North	South			
Z7	HST		GZS8	EZS7	PZS4-C3
Z6	TST				PZS4-C2
Z5	LST				PZS4-C1
Z4	HST		GZS7	EZS6	PZS4
	TST				
Z3	LST		GZS6	EZS5	PZS3
	HST				
	TST				
Z2	LST		GZS5	EZS4	PZS3
	HST				
	TST		GZS4		
Z1	LST		GZS3	EZS3	PZS2
	HST				
	TST		GZS2		
	LST		GZS1	EZS2	PZS1
	HST			EZS1	
	TST				
	CS				
	Upper Carboniferous/Lower Permian				

Figure 5-6 Lithostratigraphic cycles and chronostratigraphic division of the Zechstein cycles in German and sequence stratigraphic comparison of the Zechstein succession in German, England, and Poland.

Another sequence stratigraphic model of the Zechstein cycles, from Poland, was proposed by Wagner and Peryt (1997) (Figure 5.7). The main significant difference

between the Poland Zechstein and the surrounding countries is the development of evaporitic-terrigenous cycles in the upper part of the Zechstein Group and the complete absence of carbonate deposits in this eastern region of the Southern Zechstein Basin. This contrasts with the thin carbonate deposits that were deposited in England, in the western Northern Zechstein Basin (Uppgang Formation) (Tucker, 1991; Taylor, 1998). In their model, Wagner and Peryt (1997) divided the Poland Zechstein cycles into four 3rd-order sequences (PZS1-PZS4), and they identified three climatic sequences (PZS4-C1 to PZS4-C3) within the uppermost (youngest) of these sequences. These climatic sequences reflect the climatic changes and interruption from humid conditions – when terrigenous sediments were accumulated – to arid conditions – when halite was precipitated. The origin of the halite that precipitated in the lower two climatic sequences in the youngest 3rd order sequence (PZS4-C1-PZS4-C2) is from the sea-water whereas this condition changed significantly in the last climatic sequence (PZS4-C3) to a continental source supplied to the salt lakes and playas (Wagner and Peryt, 1997).

Galloway (1989). Two main mechanisms may have controlled the cyclicity of the Zechstein Basin: glacio-eustatic sea-level changes and tectonics.

5.2.6.1 Glacio-eustatic sea-level changes

Broad continuity of the Zechstein cycles across the basin can be interpreted as being controlled by global sea-level fluctuations (Baars and See, 1968; Ziegler, 1990; Cúneo, 1996; Roscher and Schneider, 2006; Geluk, 2007; Mawson and Tucker, 2009). The duration of the whole Zechstein deposition is considered to be 5 Myr (Menning et al., 1988) or 7 Myr (Menning and Commission, 2002) that would represent a second-order cycle (Tucker, 1991). In addition, the determined duration of approximately 2 Myr for the Zechstein 1 (Z1) cycle (Menning and Commission, 2002) is on the scale of third-order cycles. The cycles may be further subdivided into higher frequency orders, if so developed, with five orders of eustatic sea-level changes being described by Plint *et al.* (1992).

The aeolian and evaporitic deposits of the pre-Zechstein Group and the thick evaporitic cycles of the Zechstein Group were influenced by arid to semi-arid climatic conditions that were characteristic of large parts of Europe during the late Permian (Legler and Schneider, 2013). However, high-frequency climatic fluctuations were recorded during the deposition of the lower Zechstein cycles and were interpreted to be related to the waxing/waning cycles of ice shields (Glennie, 1986) and to occur within the Milankovitch frequency bands.

Richter-Bernburg (1985) identified laminated and mosaic-like anhydrite cycles, recording the various varve laminae in the Zechstein carbonate-anhydrite laminites and these were interpreted as Milankovitch band cycles, of duration approximately 50-100 k.y. In addition, Mawson and Tucker (2009) interpreted the interbedded turbidites and laminated lime-mudstones of the Z2 carbonate (Roker Formation) unit in England and they distinguished well-developed cyclicity of thinning-upward and thickening-upward packages of turbidite facies. Four orders of cyclicity are revealed and were interpreted as being induced by Milankovitch-style orbital forcing and associated glacio-eustasy, including short-eccentricity (100 kyr), precession (20 kyr), semi-precession (10 kyr), and sub-Milankovitch, millennial-scale cycles. The origin of these turbidite cycles is concluded to be controlled by relative sea-level changes in response to climate and

environmental changes, which in turn influenced carbonate productivity. Tectonic controls on cycles of these short durations are considered unlikely.

Cyclicality is a very common of sedimentation during the Permian and numerous cyclic successions are documented worldwide, for example: in Texas (Fracasso and Hovorka, 1986; Borer and Harris, 1991; Eide, 1993), in Australia (Michaelsen and Henderson, 2000), in Tunisia (Soua, 2012), in Pakistan (Ghazi *et al.*, 2015), and in Antarctica (Fielding and Webb, 1996). In addition, the development of the Paradox Basin cycles in Utah and Colorado continued into the Permian (Condon, 1997; Jordan and Mountney, 2012; Venus *et al.*, 2015). These cyclical successions are all consistent with a significant control of marginal marine successions by glacio-eustasy and by climatic fluctuations that would have been occurring over similar timescales.

5.2.6.2 Tectonic controls

Tectonic or syn-sedimentary, fault-related uplift may control sedimentary basin fill and play a major role in basin configuration (Miall, 2010). These tectonic controls could also provide a local influence on sedimentation. In the case of the late Permian Zechstein Basin, active tectonic control, on a large or broad scale, is inferred to be unlikely; however, it is likely evidenced on a small scale. For example, Mawson and Tucker (2009) found evidence implicating syn-sedimentary, fault-related uplift on the cyclic turbidite packages of the Z2 Roker Formation at Marsden Bay in England. However, these turbidite packages are traceable throughout the Roker Formation, or even throughout the whole basin, indicating that basin-wide relative sea-level changes, not local tectonic changes, may be the more likely dominant control upon cyclicities.

5.3 Paradox Basin

The Paradox Basin is located mostly in SE Utah and SW Colorado, and extends into NE Arizona and NW New Mexico (Baars and Stevenson, 1981) (Figure 5.8). It is bordered to the west by the Circle Cliffs Uplift, in the northwest by the San Rafael Swell and in the east by the tectonically uplifted Uncompahgre Plateau (Baars and Stevenson, 1982). It is a large elongate and asymmetric foreland basin that is oriented NW to SE and extended for approximately 300 km in length, and 150 km in width (Nuccio and Condon, 1996). The basin started development in the Early Pennsylvanian (Condon, 1997), covered an area of about 28,500 km² in which more than 4,600 m of sedimentary

strata was accumulated in the depocentre (Brown, 2002). It contains complex, mixed open marine carbonate, evaporite and siliciclastic deposits in cyclic sedimentary deposits. Because it contains thick salt sequences, salt tectonics has played a major role in the post-Pennsylvanian tectonic deformation of the basin and its later infill. The basin occupied an equatorial setting between five degrees north and south of the palaeo-equator at time of deposition. As the basin developed, a 2 km-thick succession of evaporite sediments accumulated during an episode of extremely arid climate in the Desmoinesian (Baars and Stevenson, 1982).

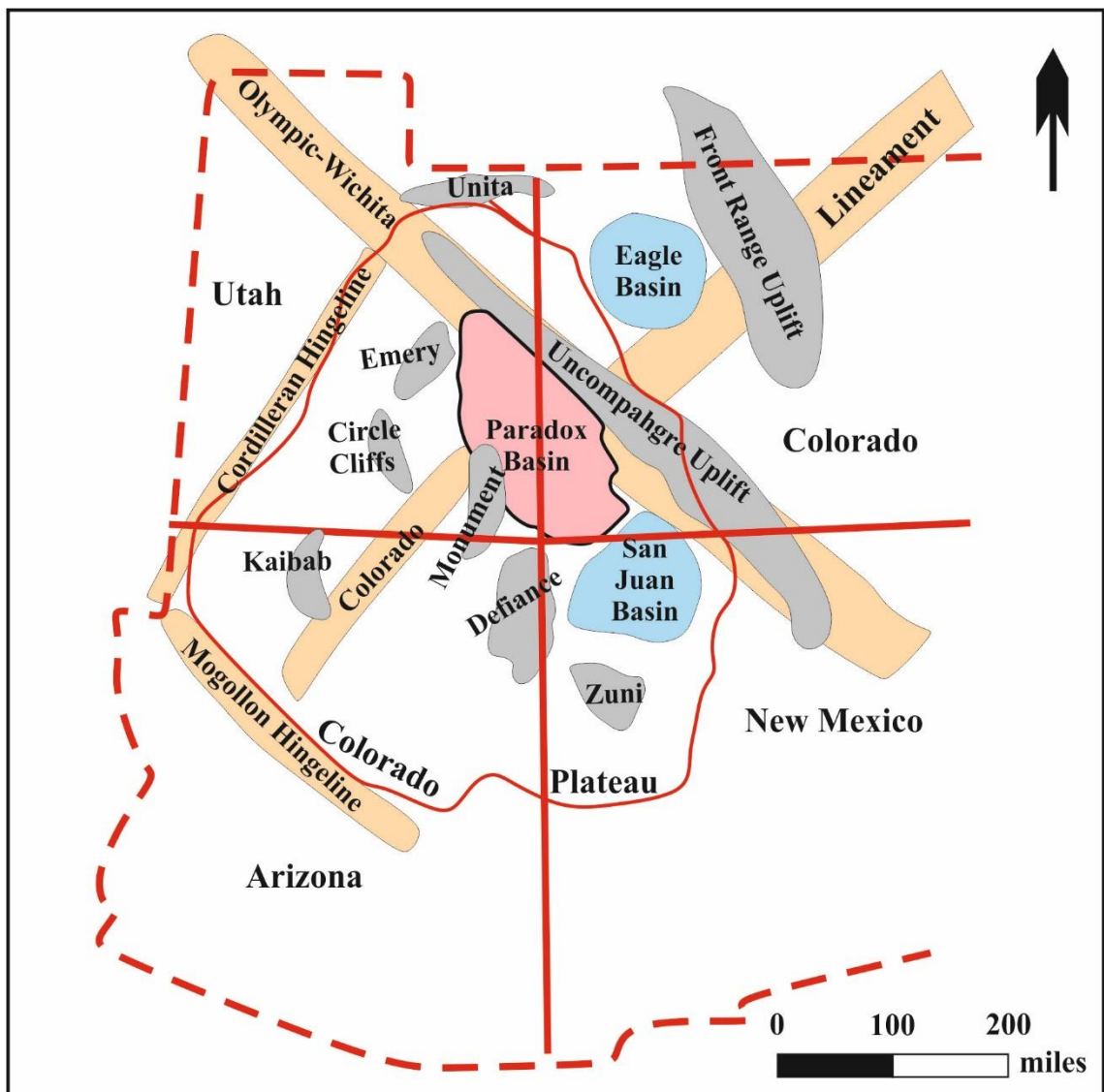


Figure 5-8 Structural and location map of the Paradox Basin and basement lineaments showing north-western Olympic-Wichita Lineament and north-eastern Colorado Lineament with bounding uplifts (Baars and Stevenson, 1982).

5.3.1 Development of the Paradox Basin

The Paradox Basin is a palaeo-tectonic depression of the Palaeozoic Era. The pre-Pennsylvanian depositional facies accumulated in a relatively stable and extensive shelf depositional setting of shallow water carbonate and clastics (Baars and Stevenson, 1982). By the Early Pennsylvanian epoch (Atokan), the basin covered most of east-central Utah and SW Colorado and into NW New Mexico and NE Arizona (Figure 5.8). It was created as a structurally subsiding, elongate NW-SE oriented basin. The basin was bordered by low-lying emergent barriers of the Zuni, Defiance, Monument, Circle Cliffs and Emery highs to the south, west, and north respectively (Baars and See, 1968). In Early Pennsylvanian time, the Uncompahgre high underwent a major tectonic uplift and this resulted in the onset of rapid subsidence of the basin, leading to the development of the eastern and north-eastern depositional border of the basin (Brown, 2002). The Uncompahgre uplift was the most significant structural element and it this mountain belt supplied the great majority of the siliciclastic deposits to the proximal part of the basin, resulting in the south-westward progradation of a large clastic wedge (Weber *et al.*, 1995; Williams, 2009). This palaeo-uplift occupied the same location as the current Uncompahgre Mountains (Raup and Hite, 1992). Thus, the Paradox Basin developed proximal to the south-western bounding faults of the Uncompahgre highland where it was affected by oblique, right-lateral divergent activity along the Olympic-Wichita Lineament (Baars, 1976).

The basin development during Desmoinesian to Permian times underwent three stages of deposition, which are a) terminal basin fill during the Desmoinesian-lower Missourian, b) reconfiguration of the basin during the upper Missourian, and c) south-westward progradation during late Pennsylvanian-Permian times (Williams, 2009).

5.3.2 Palaeo-tectonic setting

Two older, major rift systems traverse the Paradox Basin and they form a conjugate set (Baars and Stevenson, 1981) (Figure 5.8). They were tectonically active at about 1700 Ma during the Late Precambrian. One of them is the NW-trending group of faults that extends from the San Juan Mountains (SW Colorado) to NW Vancouver Island and extends toward the SE (Oklahoma's Wichita aulacogen). It is called the Olympic-Wichita Lineament (Baars, 1966). The second is the NE-trending swarm of faults that extends from the Grand Canyon and Arizona through the Colorado Mineral Belt to Lake

Superior, and this is termed the Colorado Lineament (Warner, 1978). The Olympic-Wichita and Colorado Lineaments displaced the basement rocks with right and left lateral strike-slip offsets, respectively (Hite, 1975). The timings of their displacements are dated at 1780 to 1460 Ma and about 1700 Ma, respectively.

The southern Rockies and Colorado Plateau were relatively quiescent during the early Palaeozoic Era (Baars, 1966; Baars and See, 1968), however, during Cambrian, Devonian and Mississippian times, a minor rejuvenation along the Olympic-Wichita Lineament occurred in the basin (Baars and Stevenson, 1981; Baars and Stevenson, 1982). Despite the fact that the early Palaeozoic tectonic activity on the faults was minor, some vertical movement took place and led to development of local shoaling conditions and an alteration in composition of the sedimentary facies (Goldhammer *et al.*, 1991). This structural activity resulted in the isolation of offshore sand bars in the Elbert Formation during the Upper Devonian and provided sites for the development of the crinoidal bioherms of the Mississippian Leadville Formation on the fault block highs (Baars and Stevenson, 1982). The relatively calm tectonic activity of the early Palaeozoic changed dramatically by the Middle Pennsylvanian (Atokian). The basement faults of the Paradox Basin and southern Rockies were displaced vertically throughout the Middle Pennsylvanian (Desmoinesian). During this time, the major uplifts of the Ancestral Rockies developed and became major sources of siliciclastic sediments. The Uncompahgre highlands were uplifted nearly a thousand metres, yielding clastic debris into the subsiding Paradox Basin to its south-west (Goldhammer *et al.*, 1994). About 4,500 to 6,000 metres of coarse siliciclastics were shed from the uplift into the developing eastern trough of the basin.

It was in Early Desmoinesian times that cyclic successions of carbonates began accumulating along the extensive western and south-western shelf of the Paradox Basin, and they covered much of what is now southern Utah and north-western New Mexico (Baars and Stevenson, 1982). The cyclic deposition of shallow marine carbonate shelf sediments throughout the Desmoinesian combined with the exposure of the low-lying barriers that dramatically restricted the basin downdip caused an evaporite basin to develop across a broad and gently sloping shelf (Baars and Stevenson, 1981).

Development of the major structures in the proximity of the Paradox Basin had been completed by the end of the Pennsylvanian, except for the development of major salt diapirs, generation of which commenced in the late Pennsylvanian to early Permian

(Trudgill, 2011; Banham and Mountney, 2013) and were still effectively developing into the Mesozoic. Tectonic activity in the vicinity of the Uncompahgre Uplift commenced during the Atokan and it had possibly reached its zenith by the Permian (Baars and Stevenson, 1981). However, the middle (north-western) segment of the uplift continued its uplift and underwent denudation well into the Permian (Baars and Stevenson, 1982). In addition, the north-western segment did not begin yielding clastic deposits to the basin until the Desmoinesian. Finally, the Nacimiento, Zuni, and Defiance basement uplifts, the Emery uplift and most of the salt diapirs were progressively buried by Permian red-bed sediments derived from the Uncompahgre uplift (Baars and Stevenson, 1981; Baars and Stevenson, 1982).

5.3.3 Stratigraphy

5.3.3.1 Mississippian

The stratigraphy of the Paradox Basin comprises Carboniferous strata of Mississippian and Pennsylvanian age. The Mississippian stratigraphy is represented by the Leadville Formation, a single carbonate unit that is mostly composed of dolomite (Baars and Stevenson, 1982; Brown, 2002). It also contains carbonates, especially in the upper part. Based on presence of an intraformational disconformity, the Leadville Formation is divided into Lower and Upper Members. The Leadville Formation is composed of crinoid mound buildups and represents restricted shallow water deposits (Brown, 2002). The Leadville Formation is underlain by the Ouray Formation which grades up into it, and overlain by the red palaeosol of the Molas Formation (Baars and Stevenson, 1982). This palaeosol records the result of post-Leadville weathering that altered the carbonate unit due to reactivation of Precambrian basement faults. A significant unconformity surface separates the Mississippian from the Pennsylvanian unit (Baars and Stevenson, 1982). This surface left a gap in the stratigraphic record for approximately 20 Myr (Brown, 2002).

5.3.3.2 Pennsylvanian

As previously mentioned, the Paradox Basin developed adjacent to the Uncompahgre uplift, and the deepest part of the basin was located adjacent to the uplift (Figures 5.9; 5.10). During the Middle Pennsylvanian, evaporites were deposited throughout the Desmoinesian due to a restricted exchange of water with the open ocean along the

margins of the basin (Weber *et al.*, 1995). Chemical deposition occurred of saline facies, with 1500 to 2400 metres of salt, in the deeper faulted troughs, characterised by cyclical accumulations in the evaporite basin (Raup and Hite, 1992) (Figure 5.9). The basin was continuously sinking along the active extensional basement faults due to the continuous or episodic rising of the Uncompahgre uplift through the Pennsylvanian (Baars and Stevenson, 1982). The open Middle Pennsylvanian sea entered the evaporitic basin through several entryways to recharge the salt supply to the Paradox Formation (Brown, 2002). The entryways were through the Palaeo-San Juan Basin from the south, through the Fremont embayment between the Embry highlands and Circle Cliffs from the west, through the Oquirrh Basin from the northwest, and another possible connection was through the palaeo-Black Mesa Basin, from the southwest (Stevenson and Baars, 1988).

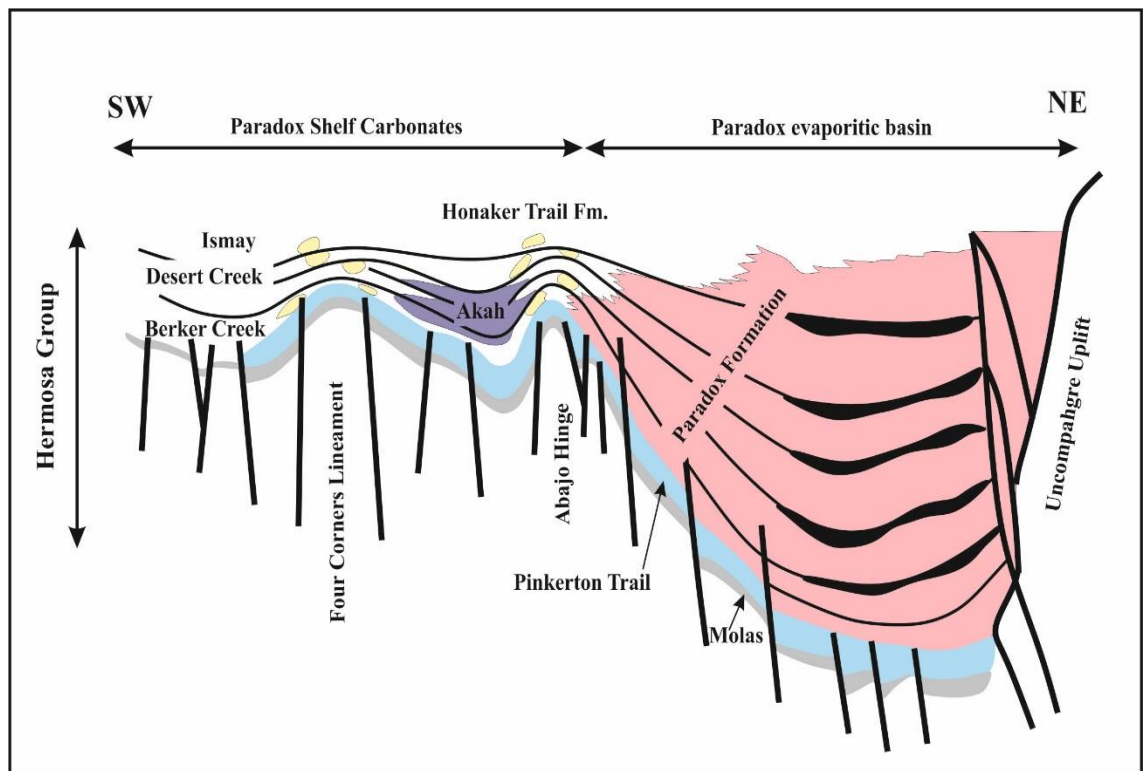


Figure 5-9 Structure and stratigraphic cross-section of the Paradox Basin showing the north-eastern evaporitic basin, and the south-western shelf carbonates (Baars and Stevenson, 1982).

The carbonate and evaporite, including the thick salt, are related to the Paradox Formation. The shelf carbonate of the Paradox Formation has very diverse lithofacies that reflect combinations of clastic, physiochemical and biochemical sedimentation (Weber *et al.*, 1995). This diversity in the carbonate lithofacies resulted from the

shallow-water environment of the shelf together with minor sea-level changes (Goldhammer *et al.*, 1994). The abrupt lateral facies changes within the carbonate lithofacies could result from the palaeo-topographic configuration of the seafloor (Baars and Stevenson, 1981). In general, the Pennsylvanian stratigraphy is represented by the large evaporite succession of the Hermosa Group, which includes the evaporitic Paradox Formation and its carbonate equivalents, the Barker Creek, Akah, Desert Creek, and Ismay Members (Weber *et al.*, 1995) (Figure 5.9). These formations are overlain by the Honaker Trail Formation, which is a siliciclastic-dominated succession. The Hermosa Group was first subdivided into three members by Baker *et al.* (1933), namely the Lower, Paradox and Upper Members. These units were later elevated to formation status and renamed the Pinkerton Trail, Paradox, and Honaker Trail formations, respectively, by Wengerd and Matheny (1958). This group is conformably overlain by the Cutler Group that is in turn unconformably overlain by the Kaibab Limestone (Condon, 1997).

The Pinkerton Trail Formation (Early to Middle Pennsylvanian) overlies the red palaeosol of the Molas Formation, and is composed of a succession of marine carbonate with shale and minor detrital deposits. The deposition of this marine succession reflects a new transgression after the Mississippian regression. Coarse siliciclastic deposits are lacking in the formation, which suggests that the early development of the Uncompahgre Uplift had little effect on Pinkerton Trail Formation deposition (Baars and Stevenson, 1981).

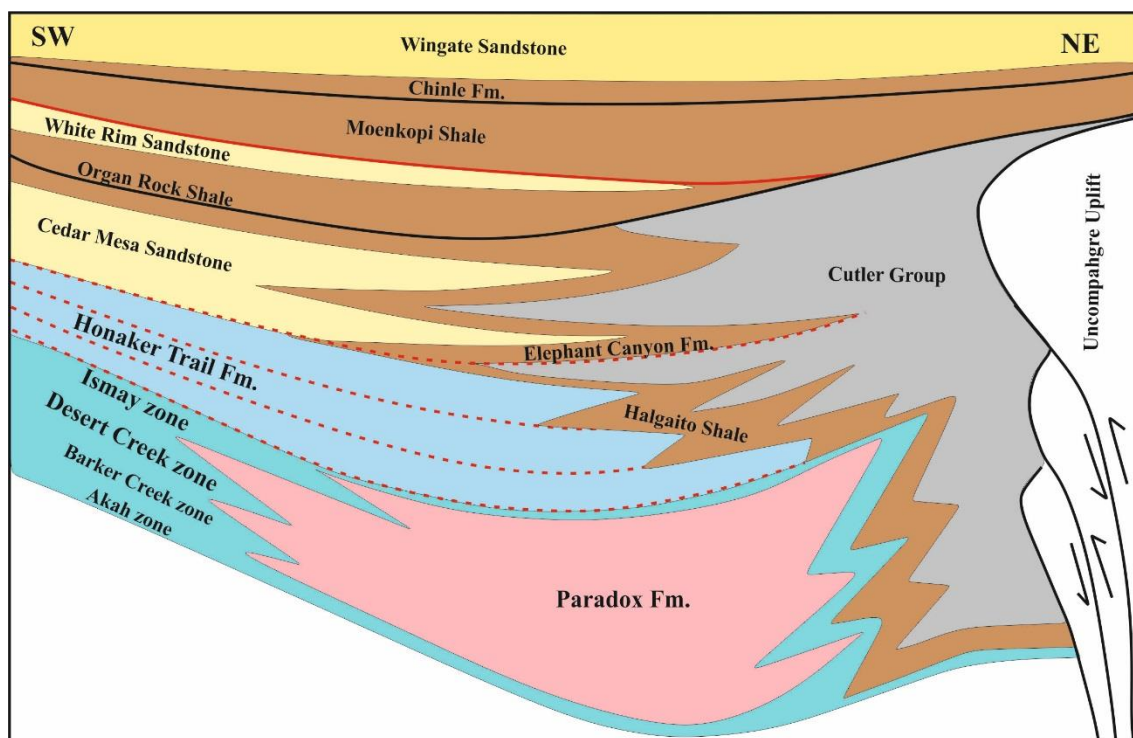


Figure 5-10 Stratigraphic relationships of the Paradox Basin during Pennsylvanian to Permian times (Wengerd and Matheny, 1958; Baars and Stevenson, 1981). The basin overfilled with the Pennsylvanian carbonate-evaporite cycles, and then the siliciclastics, derived from the Uncompahgre Uplift, prograded south-westward into the basin through time.

The Paradox Formation (Desmoinesian) is the evaporitic unit of the group. It is composed of interbedded evaporites with open marine carbonate deposits and shoaling-up carbonate buildups to the west, and siliciclastic deposits to the north-northeast. The evaporites form a cyclic succession and interbed with black marine shale. The evaporitic-dominated cycles in the north-northeastern part of the basin are laterally correlated to the open marine carbonate-dominated cycles on the platform top at the west and south of the basin. The carbonate-dominated succession on the platform top is stratigraphically divided into the Baker Creek, Akah, Desert Creek and Ismay Members. The thickness of the formation reached its maximum in the deepest, north-northeastern part of the basin, at approximately 1500-1800 metres (Baars and Stevenson, 1981).

The Honaker Trail Formation (Missourian) is a siliciclastic-dominated succession and it is composed of interbedded marine carbonates and siliciclastic alluvial fan-delta successions. It is underlain by the salt cycles of the Paradox Formation (Figure 5.10). The boundary is defined by a colour change from grey-dark grey and black in the Paradox Formation to reddish brown, red and buff in the Honaker Trail strata (Williams,

2009). The Paradox-Honaker trail contact is placed at the top of the uppermost halite cycle. The loading of the Honaker Trail Formation on the evaporitic part of the basin is believed to have led to early salt diapirism that was still active until the Jurassic (Peterson and Hite, 1969; Baars and Stevenson, 1982; Rasmussen and Rasmussen, 2009; Jordan and Mountney, 2012; Venus *et al.*, 2015).

The Cutler Group (Permian) overlies the Hermosa Group and encompasses the lower Cutler beds (formally the Elephant Canyon Formation), Cedar Mesa Sandstone, Organ Rock Formation, White Rim Sandstone, De Chelly Sandstone, and the undifferentiated Cutler Group (Condon, 1997; Jordan and Mountney, 2012) (Figure 5.10). The Cutler Group is a mixed siliciclastic-carbonate cyclic succession. The lower Cutler beds are dark reddish-brown and are dominated by aeolian dune, fluvial (braided stream and flood plain) and shallow marine carbonate sediments (Jordan and Mountney, 2012; Wakefield and Mountney, 2013). The fluvial systems of the Cutler Group episodically prograded south-westward into the basin and loaded the underlying salt, which in turn moved to develop salt deformation structures and finally resulted in the successive development of a series of salt-walled mini-basins (Rasmussen and Rasmussen, 2009; Trudgill and Arbuckle, 2009; Trudgill and Paz, 2009). Even though the first salt movement probably commenced in Late Pennsylvanian times, the first notable phase of salt migration and consequent influence on the development of fluvial systems likely occurred in the early Permian (Trudgill and Paz, 2009). Salt migration and mini-basin development continued, periodically, into the Jurassic (Lorenz and Cooper, 2009).

5.3.4 Palaeoclimate

The Carboniferous climate was characterized by the main Gondwana Glaciation (Haq and Schutter, 2008) (Figure 5.11). This glaciation came to an end in the early Permian and is marked as an eustatic sea-level fall at the Mississippian-Pennsylvanian boundary (Haq and Schutter, 2008). During the Pennsylvanian to the Jurassic, the Paradox Basin was located near the west coast of Pangaea (Ziegler *et al.*, 1983). It migrated northward from a position approximately 20° south of the palaeo-equator in the Pennsylvanian to a location nearly 30° north of the palaeo-equator in the Jurassic (Ziegler *et al.*, 1983). The Paradox cycles tend to support the assumption of expanding and contracting equatorial areas proposed by Sarnthein (1978). When continental ice cover expanded in the southern hemisphere, very arid conditions expanded in equatorial areas. The climate of the Paradox Basin at this stage was dry and cool, and sea-level was low, resulting in the

development of restricted basins with evaporite precipitation (Rueger, 1996). In contrast, during each inter-glacial period when glacial melting predominated, the result was a global sea-level rise. The Paradox Basin at this stage was warmer and wetter. The relationship between the Paradox cycles and climate is inferred to have been as follows (Rueger, 1996): The deposition of black shale was coincident with the wet and warm climatic conditions (transgressive phase), whereas the evaporite deposition occurred in the cooler and drier conditions (regressive phase). During the cool and dry phases the temperature did not decrease sufficiently to stop the evaporite deposition.

During the early Permian, the basin was located five degrees north of the palaeo-equator (Baars and Stevenson, 1981). Permian stratigraphic records in the Paradox Basin reveal evidence of aridity comprising well-developed aeolian dunes, aeolian sand sheets, and sabkha facies (Roscher and Schneider, 2006). Although the evidence of aridity is abundant, periodical input of moisture is revealed by the presence of fluvial and floodplain deposits that contain palaeosols and rhyzolith facies (Loope, 1984; Loope, 1988; Stanesco *et al.*, 2000). These features, including a repeated upward change from aeolian deposits into fluvial facies, indicate alternating dry and wet phases (Stanesco *et al.*, 2000). This is clearly recognized in the Pennsylvanian to Permian succession of the Cutler Group in Utah (Jordan and Mountney, 2012).

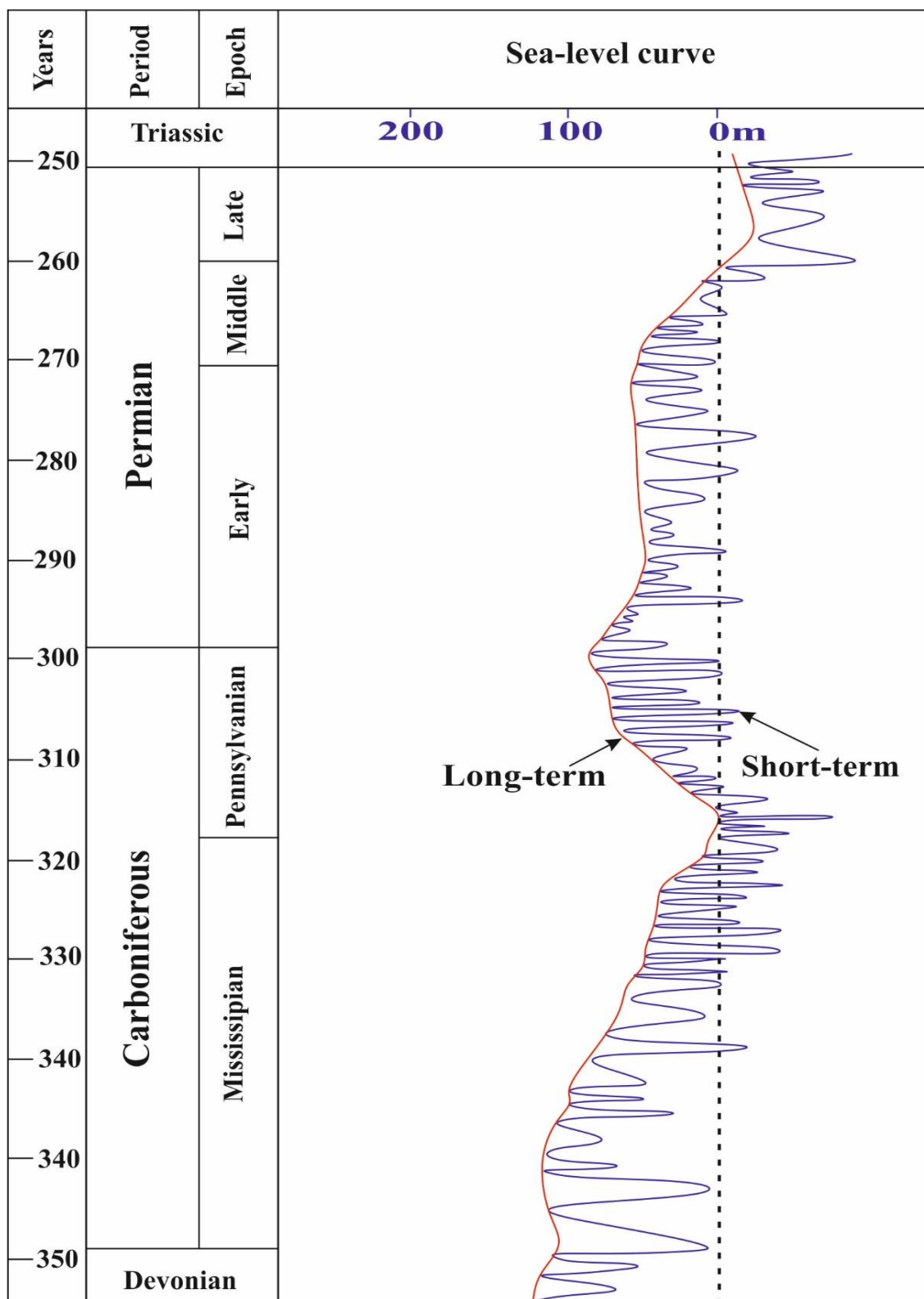


Figure 5-11 Carboniferous to Permian eustatic sea-level curve, including long- and short-term sea-level fluctuations, showing eustatic rise in the latest Pennsylvanian, and eustatic falls at the Mississippian-Pennsylvanian boundary and in the latest Permian (Haq and Schutter, 2008). The eustatic fall at the Mississippian-Pennsylvanian boundary was related to the main Gondwana Glaciation. The magnitude of sea-level changes during the Palaeozoic is estimated to have varied from a few tens metres to nearly 125 metres.

5.3.5 Paradox cyclicity

The cyclic sedimentation first developed during deposition of the Pinkerton Trail Formation occurred as cyclic deposition of clastic and carbonate layers. Progressively, the cycles show a vertical increase in carbonate content, and eventually grade through dolomite and black shale into the overlying Paradox evaporite cycles (Weber *et al.*, 1995). The overlying carbonate and evaporitic parts of the basin succession belong to the Paradox Formation, which includes the basinal evaporite cycles (north-northeast) and their laterally equivalent carbonate shelf cycles (west-southwest). The evaporite cycles of the Paradox Formation, and their equivalents – the shelf carbonate cycles – are overlain by carbonate and siliciclastic cycles of the Honaker Trail Formation that are somewhat similar to the pre-Pennsylvanian carbonate and siliciclastic cycles (Pinkerton Trail Formation) (Weber *et al.*, 1995; Williams, 2009). The carbonate and siliciclastic cycles continued to the Lower Permian, and the succession eventually grades upward to entirely siliciclastic cycles (Peterson and Hite, 1969).

Goldhammer *et al.* (1991), Goldhammer *et al.* (1994) and Weber *et al.* (1995) divided the Paradox cycles into a number of hierarchally arranged third- and fourth-order sequences that are each bounded by regional unconformities or subaerial exposure surfaces. In addition, they identified fifth-order cycles that are bounded by either flooding surfaces or diastem. Twenty-nine regionally correlative shale-evaporite cycles of Desmoinesian age are identified in the Paradox depocentre of the Paradox Formation (Peterson and Hite, 1969). These evaporite cycles are laterally correlated to the carbonate shelf cycles that decrease in number toward the shelf due to onlapping of the lower cycles. To calculate the correct duration of these cycles, the total number of the basinal evaporite cycles (29) is divided by the total duration of the Desmoinesian, for which estimates range from 4 My (Odin and Gale, 1982) to 10 My (Van Eysinga, 1975). The average periodicity of the cycles is thus between 138 and 345 kyr per sequence, falling in the 4th-order range (Goldhammer *et al.*, 1991). These 4th-order sequences contain a number of 5th-order shallowing-upward cycles (average 9 cycles). By dividing the periodicities of the 4th-order sequences (138 to 345 kyr) by the average number of 5th-order cycles (9 cycles), a duration of approximately 15 to 38 kyr would be obtained for the 5th-order cycles. Thus the 4th and 5th order cyclicities are consistent with being a response to 1) eccentricity- and 2) obliquity and/or precessional Milankovitch orbital forcing of climate changes.

The rapid rise of the Uncompahgre Uplift, cyclic restriction of circulation, and increasing evaporation within the semi-enclosed basin resulted in deposition of three types of cyclic successions: 1) evaporitic cyclic deposition (in the basin centre) that includes salt, anhydrite, dolomite, and black shale; 2) shelf carbonate cycles (in the south-western basin) that include mound-like buildups of biogenic carbonates; and 3) siliciclastic (arkosic) cycles, which accumulated in narrow belts close to the Uncompahgre Uplift (in the north-eastern part of the basin) (Raup and Hite, 1992).

5.3.5.1 Evaporitic cycles

Hite (1960) first numbered the evaporite cycles of the Paradox Formation into sequences from the lowest (oldest) to the uppermost (youngest) and identified twenty-nine halite-bearing cycles in the deep part of the basin. Each idealized evaporitic cycle (basinal cycle) of the Paradox Formation is about 45 to 60 metres in thickness and is composed of lower transgressive and upper regressive parts (Figures 5.12 and 5.13). The lower part has been characterised as beginning with a rapid transgression that is marked by a disconformity surface at the top of the salt bed of the previous cycle. This grades upward from transgressive laminated anhydrite at the base into nodular anhydrite that is overlain by dolomite and then by marine black shale (Raup and Hite, 1992). By contrast, the upper regressive part of each cycle begins with dolomite deposition at the base that grades up to anhydrite and then into salt at the top (Peterson and Hite, 1969; Raup and Hite, 1992). The black shale units are traceable shelf-ward to equivalent carbonate cycles. The lower parts of the cycles were initiated in response to a rapid rise in relative sea-level and an inflow of sea water into the basin. The rise in sea level reached its maximum during the black shale deposition, at which time the deeper parts of the basin were largely sediment starved (Raup and Hite, 1992). Consequently, in the latter stage of each cycle, evaporite deposition rapidly overrode the basin subsidence and overfilled the basin with thick anhydrite and salt deposits (Raup and Hite, 1992; Goldhammer *et al.*, 1994).

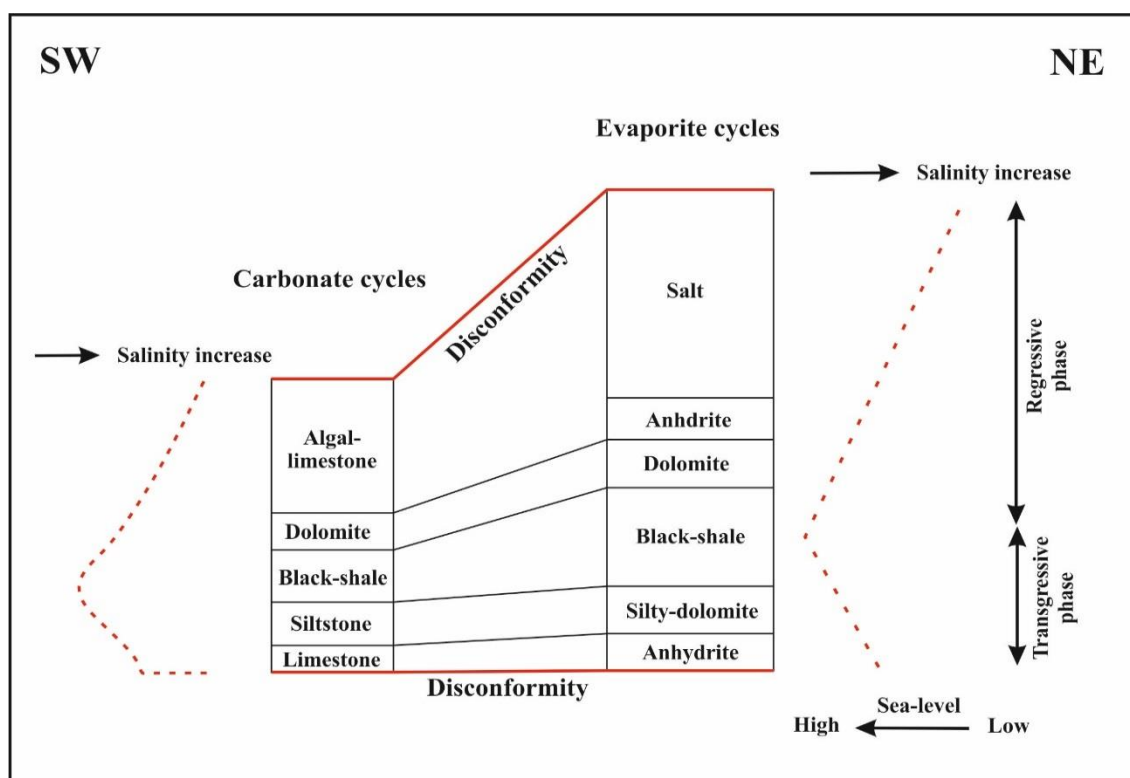


Figure 5-12 Stratigraphic logs of an idealized carbonate and evaporitic cycle bounded by disconformities. Each cycle represents a full cycle of sea-level change and salinity variations (Hite and Buckner, 1981; Trudgill and Arbuckle, 2009).

5.3.5.2 Shelf carbonate cycles

An idealized carbonate platform cycle ranges from 10 to 40 metres in thickness (average 35m) and consists of a thin, transgressive black shale or dark carbonate mudstone at the base, overlain by a regressive (shallowing-upward) succession of shelf carbonates (Raup and Hite, 1992; Weber *et al.*, 1995), as represented in Figures 5.12 and 5.13. The regressive carbonate succession includes thick phylloid algal bioherm facies capped by ooid grainstone facies. The cycles are each separated by unconformities, with evidence of subaerial exposure at the bounding surfaces (Figure 5.12). The carbonate cycles show three cyclo-stratigraphic orders with a systematic vertical succession of facies, cycle, and sequence stacking patterns (Goldhammer *et al.*, 1991; Weber *et al.*, 1995; Grammer *et al.*, 1996). Fifth-order cycles (inferred to be of ca. 29 kyr duration) are packaged into fourth-order sequences (ca. 257 kyr duration), which in turn are grouped to define third-order sequences (ca. 2-3 Myr) (Goldhammer *et al.*, 1991).

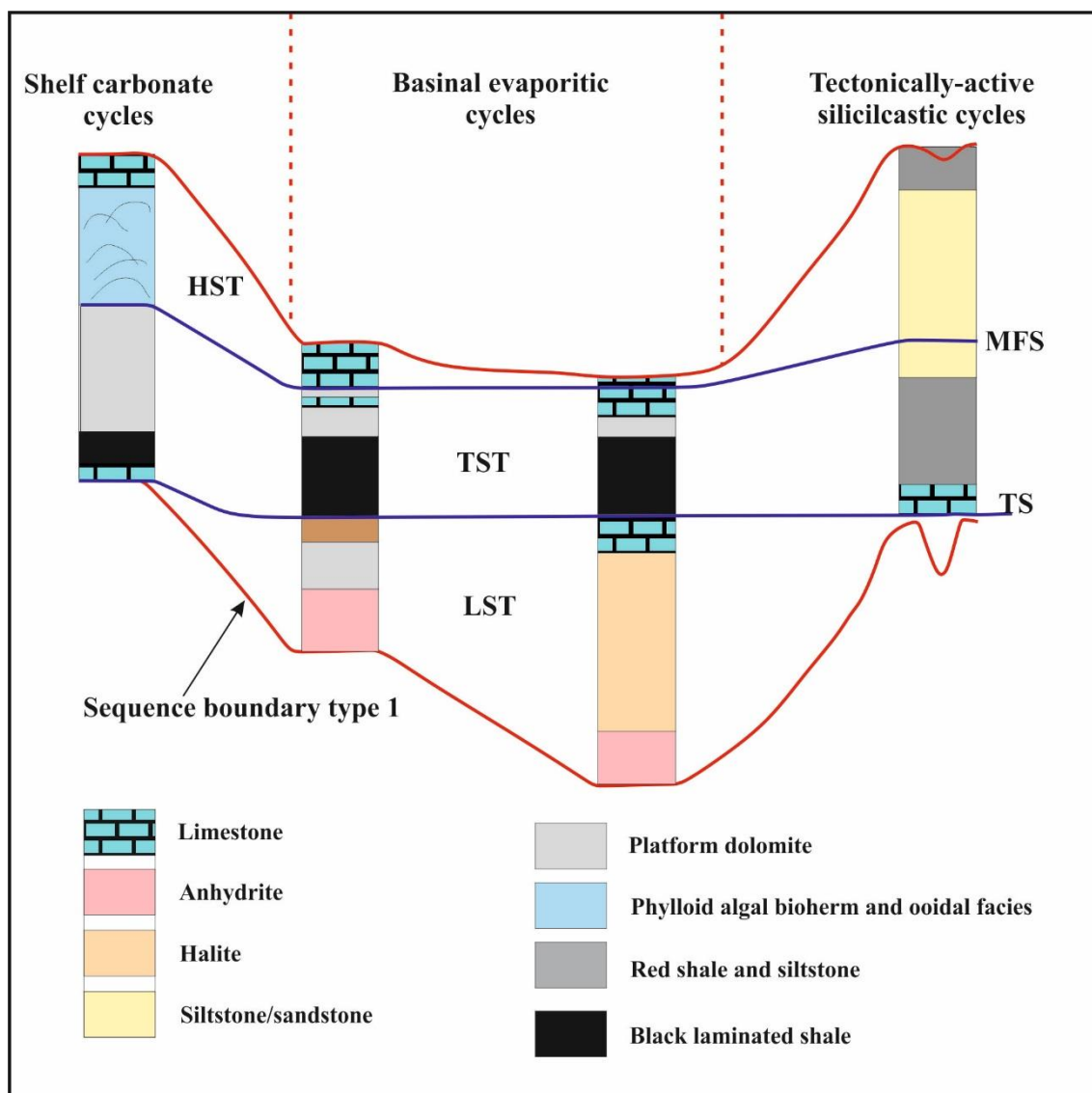


Figure 5-13 Correlation of depositional cycles showing three types of cycles from tectonically-active siliciclastic-dominated through basinal evaporite-dominated cycles to shelf carbonate cycles (Weber *et al.*, 1995).

5.3.5.3 Arkosic (siliciclastic) cycles

The arkosic cyclic facies reached maximum thickness toward the southeastern edge of the basin during the Atokian and Desmoinesian, and along the northeastern part of the basin during the Late Pennsylvanian (post-Desmoinesian) and Permian (Figure 5.13). The post-Desmoinesian siliciclastic deposits are represented by the Cutler Group that comprises a mixed siliciclastic-carbonate succession (Rankey, 1997; Jordan and Mountney, 2012). The considerable influx of siliciclastic debris into the basin occurred simultaneously with maximum growth of the Uncompahgre Uplift (Peterson and Hite,

1969). Eventually, during the late Pennsylvanian and Permian, the siliciclastic deposits from the Uncompahgre Uplift prograded south-westward across the basin (Loope, 1984; Mountney, 2006). Field investigations indicate that most of these deposits were transported and deposited by streams, probably of braided type (Cain and Mountney, 2009).

The Cutler cyclic succession is characterized by mixed siliciclastic-carbonate deposits during the Permian. Each cycle passes up from a basal sandstone of exclusively aeolian dune origin into a fluvial deposit of both channel and floodplain origin. Shallow marine carbonate forms the capping unit of each cycle (Rankey, 1997; Jordan and Mountney, 2012). Each cycle varies from non-marine-dominated deposits (aeolian and fluvial) towards the northeastern (landward) part of the basin to marine-dominated deposits southwest-wards towards the basin centre.

5.3.6 Sequence stratigraphy of the Paradox succession

Weber *et al.* (1995) divided the Desmoinesian succession into five 3rd-order composite sequences, comprising lowstand, transgressive, and highstand systems tracts, each composed of higher-order sequences (4th-order sequences). The total duration of the 3rd-order composite sequences was estimated to range between 800 kyr to 2 Myr and these are included within a 2nd-order transgressive-regressive “super-sequence” in the terminology of these authors. A type 1 sequence boundary is recognized at the base of the lowstand system tract, and is characterized by exposure of the shelf and erosion on the slope (Raup and Hite, 1992; Weber *et al.*, 1995) (Figure 5.14). The basinal correlative conformity of this surface is characterized by the presence of an evaporitic wedge that onlaps the sequence boundary. The transgressive surface (TS) between the lowstand and transgressive systems tracts is defined by an upward change from basinal restricted siltstone facies to skeletal lime mudstone/wackestone facies (Weber *et al.*, 1995). The transgressive facies are in the form of the black laminated mudstone that is traceable across the whole basin. The maximum flooding surface (MFS), separating the transgressive system tract from the overlying highstand system tract, is composed of a marine condensed section in basinward areas that is associated with a hardground (Peterson and Hite, 1969; Weber *et al.*, 1995). In platform settings, it is defined by the top of a silty dolomudstone/wackestone facies that sits above the early transgressive black shale (Weber *et al.*, 1995). The highstand facies is represented by a thin lime mudstone/wackestone facies in the basin, whereas on the platform it consists of thick

phyloid algal mounds and peloid/ooid packstone/grainstone facies (Goldhammer *et al.*, 1994). Each systems tract comprises a set of high-frequency 4th-order sequences (Goldhammer *et al.*, 1991; Goldhammer *et al.*, 1994; Weber *et al.*, 1995) which in turn include packages of 5th-order parasequences.

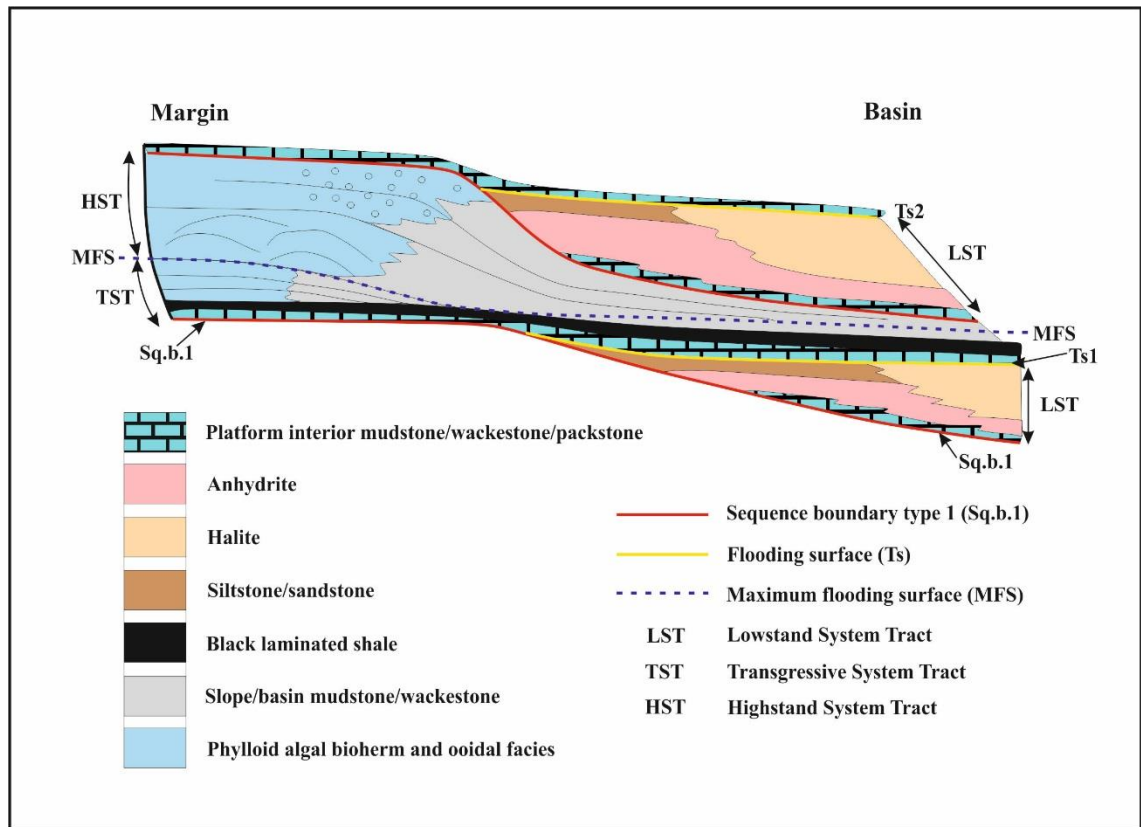


Figure 5-14 Sequence stratigraphic model for the carbonate-evaporite cycles of the Paradox Basin (Weber *et al.*, 1995).

The lower two composite sequences are represented by the Pinkerton Trail and Baker Creek formations, and exhibit stratal geometries which backstep in a landward direction, whereas the upper three sequences are represented by aggradational (Akah and Desert Creek Formations) to progradational geometries (of the Ismay and Honaker Trail Formations) (Weber *et al.*, 1995). Each sequence begins with a lowstand evaporite unit (lowstand wedge) in the basin centre, which is equivalent to the subaerial exposure of the shelf carbonates. Three 4th-order sequences and nineteen 5th-order parasequences are recognized (Goldhammer *et al.*, 1991; Goldhammer *et al.*, 1994; Weber *et al.*, 1995).

5.3.7 Origin of cyclicity

Analysis of cycles in term of facies architecture, broad lateral correlation of the cycles, and variations in cycle types are commonly used for analysing the origin of the cycles. Two main mechanisms are inferred to have controlled the cyclicity of the Paradox Basin, these being glacio-eustatic sea-level changes and tectonics.

5.3.7.1 Glacio-eustasy sea-level changes

Numerous examples of Pennsylvanian to Permian cyclicity have been recorded, and their origins have been evaluated as due to climatic and glacio-eustatic controls on their deposition (Busch and Rollins, 1984; Driese and Dott Jr, 1984; Algeo and Wilkinson, 1988; Corrochano *et al.*, 2012; Alasad *et al.*, 2014; Khodjanyazova *et al.*, 2014).

Interpretations of the origin of the Paradox cycles generally relate these to glacio-eustatic sea-level fluctuations that were triggered by the southern hemisphere glaciation of Gondwana. This interpretation has been supported by the broad lateral correlation of the cycles, subaerial exposure events, and the asymmetric nature of the internal facies architecture (Goldhammer *et al.*, 1994).

More specifically, the major control on the carbonate and evaporite cyclicity in the Paradox Formation has similarly been attributed to periodic sea-level changes in response to retreat and advance of Gondwanaland glaciers during the Pennsylvanian (Raup and Hite, 1992). During interglacial stages, sea-level rose due to glacial melting leading to increases in accommodation space across the shelf and resulting in a lowering of salinity and an increase in circulation of the basin waters. In contrast, during glacial stages, sea-level fell resulting in a restricted circulation and a rise in the brine salinity.

The composite stratigraphic cyclicity of the Paradox Formation, including fifth-order cycles, fourth-order sequences, and third-order accommodation cycles are interpreted as a composite of fourth- and fifth-order glacio-eustatic cycles (Goldhammer *et al.*, 1991). These authors evaluated two viable scenarios for the formation: a) a model dominated by long eccentricity and obliquity cycles, versus b) a model dominated by short eccentricity and precession cycles. In the first model, the duration of the fourth-order sequences ranges from ca. 216 to 345 kyr, a periodicity which approaches that of the Earth's long eccentricity cycle (413 kyr). Additionally, each fourth-order sequence includes approximately nine fifth-order cycles, with each cycle approximately 38 kyr in

duration, close to the Earth's obliquity cycle. In the second model, the minimum duration of the fourth-order sequences is 138 kyr, which is close to the Earth's short eccentricity cycle (dominant periodicities of ca. 95 and 123 kyr). By dividing the time duration of the fourth-order sequences (138 kyr) by the 9 fifth-order cycles, approximately 15.33 kyr is obtained and this is close to the Earth's precession cycle.

Additionally, the major interpretation of the development of the mixed siliciclastic-carbonate cycles from the Cutler Group during Permian times that these are considered to be both climatic and eustatic in origin (Jordan and Mountney, 2012). The non-marine aeolian and fluvial units at the base of the cycles may represent an external climatic influence on the depositional system, whereas the presence of marine deposits at the top of the cycles demonstrates rhythmic episodes of relative sea-level change of likely eustatic origin (Jordan and Mountney, 2012). Deposition of the aeolian dune deposits occurred during sea-level lowstand episodes and climatic aridity, whereas deposition of the fluvial deposits were coincident with sea-level rise and climatic humidity. Additionally, carbonate deposition occurred during sea-level highstand and maximum humidity.

5.3.7.2 Tectonic mechanism

Baars and Stevenson (1982) state that small-scale oscillating vertical displacements occurred along the basement faults throughout early Palaeozoic time, and they suggest that the same structural activity was responsible for the distribution of the Middle Pennsylvanian carbonate lithofacies. This structural activity resulted in the formation of positive fault blocks favourable to shallow-water carbonate production. However, Goldhammer *et al.* (1991) and Goldhammer *et al.* (1994) state that there are no indicators of any syn-Desmoinesian faulting across the southwestern Paradox shelf and they insist that localized tectonics (gentle uplifts) were responsible for the distribution of the algal mound development. Additionally, extensive correlation of the high-frequency cycles is a feature unlikely to have formed from tectonic oscillations.

5.4 Comparison between basin types and their evolution

5.4.1 Basin-fill stratigraphy

The late Permian basin in Central Europe was developed after the Variscan orogeny which was succeeded, or probably occurred with, an east-west relative movement

between the Gondwanan and Laurasian continents (McCann, 2008). This resulted in right-lateral wrench movements of its northern foreland between Poland and Britain and the Variscan fold belt. These wrench movements caused a rapid collapse of the Variscan fold belt. At the time of the collapse of the Variscan fold belt, its northern foreland also underwent east-west tension. Tension and regional stresses affected many parts of Europe, resulting in volcanic extrusions in the North German-Polish plain, and dyke and sill intrusions in NE Britain. These volcanic activities belong to the Lower Rotliegend Group. Eventually, the east-west trending Northern and Southern Permian Basins developed as a result of the regional extension followed by thermal subsidence of the earlier areas of subsidence. These two basins were separated by the Mid North Sea-Ringkobing-Fyn palaeohigh and are together called the Rotliegend Basin. The Rotliegend Basin is characterized by fluvial, aeolian, lake-sabkha, and desert lake deposits (Benton *et al.*, 2002). These deposits indicate a hot and dry climate (Glennie, 1986). The late Permian transgression of the Zechstein marks a main and rapid transgression over the aeolian deposits. The hot and arid climate continued through the late Permian and resulted in the deposition of a cyclic succession of carbonate-evaporite cycles (Geluk, 2007). The Zechstein stratigraphy represents a transgressive-regressive cycle during overall eustatic sea-level rise and fall, respectively (Glennie, 1986). The thick carbonate cycles of the Z1-Z3 were deposited during the transgressive phase while the regressive phase is characterized by the disappearance of carbonate deposits, and deposition of thin terrigenous-halite cycles (Wagner and Peryt, 1997). Toward the upper cycles (Z4-Z5), the marine deposits were reduced in significance and ephemeral fluvial environments, salt lakes and playas were predominant. This condition continued until the Triassic which is dominated by terrestrial conditions and is completely lacking in marine fossils (Słowakiewicz and Gąsiewicz, 2013). Through time, the marginal coarse sediments prograded basinwards.

The Paradox Basin comprises a thick succession that passes up from the evaporite cycles, in the Paradox trough itself, and their shelf carbonates, at the shelf margin, of the Paradox Formation into carbonate-siliciclastic cycles of the Honaker Trail Formation. Consequently, the formation is followed by or changes laterally to siliciclastic-dominated units of the Halgaito Shale, Elephant Canyon, and Cedar Mesa Sandstone Formations (Williams, 2009) (Figures 5.15; 5.16). A number of sedimentary facies, including cherty mudstone to wackestone, skeletal wackestone to packstone, planar to wavy bedded sandstone, amalgamated carbonate-quartz, laminated carbonate-

siliciclastic, large scale, cross-bedded sandstone, and mottled heterolithic sandstone/shale facies are documented in the Honaker Trail and lower Cutler beds (formerly the Elephant Canyon Formation) (Williams, 2009). These sedimentary facies were interpreted to have accumulated in peritidal settings that include deep-subtidal, shallow-subtidal, upper shoreface, intertidal, supratidal, and flood-plain settings, respectively.

The cycles of the Paradox (A cycle-set of Williams, 2009) and the lower part of the Honaker Trail (B cycle-set of Williams, 2009) formations expand north-eastward to the original Paradox trough. This is evidenced by facies trends of the cycle-sets, cycle thicknesses, and observed upward changes in facies diversity, bed thickness, and evidence of subaerial exposure. However, the cycles of the middle part (C cycle-set of Williams, 2009) of the Honaker Trail Formation preserve a reversal in the overall direction of sediment transport being from the northeast to being from the southwest. Finally, the cycles of the upper Honaker Trail and Elephant Canyon formations, including D and E cycle-sets, record overall south-westward expansion (Williams, 2009) (Figure 5.15).

In general, the stacking patterns and northeastern stratal expansion of the A-B cycle-sets indicate Paradox Basin infilling, whereas the southwestern stratal expansion of the C cycle-set indicates a stage of reconfiguration of the basin towards the southwest. Finally, the stacking patterns and south-westward palaeo-current directions of the D-E cycle-sets suggest filling of the basin and shifting of the available accommodation space to the southwestern part of the basin, as represented by the southwest-wards progradation (Williams, 2009) (Figure 5.15).

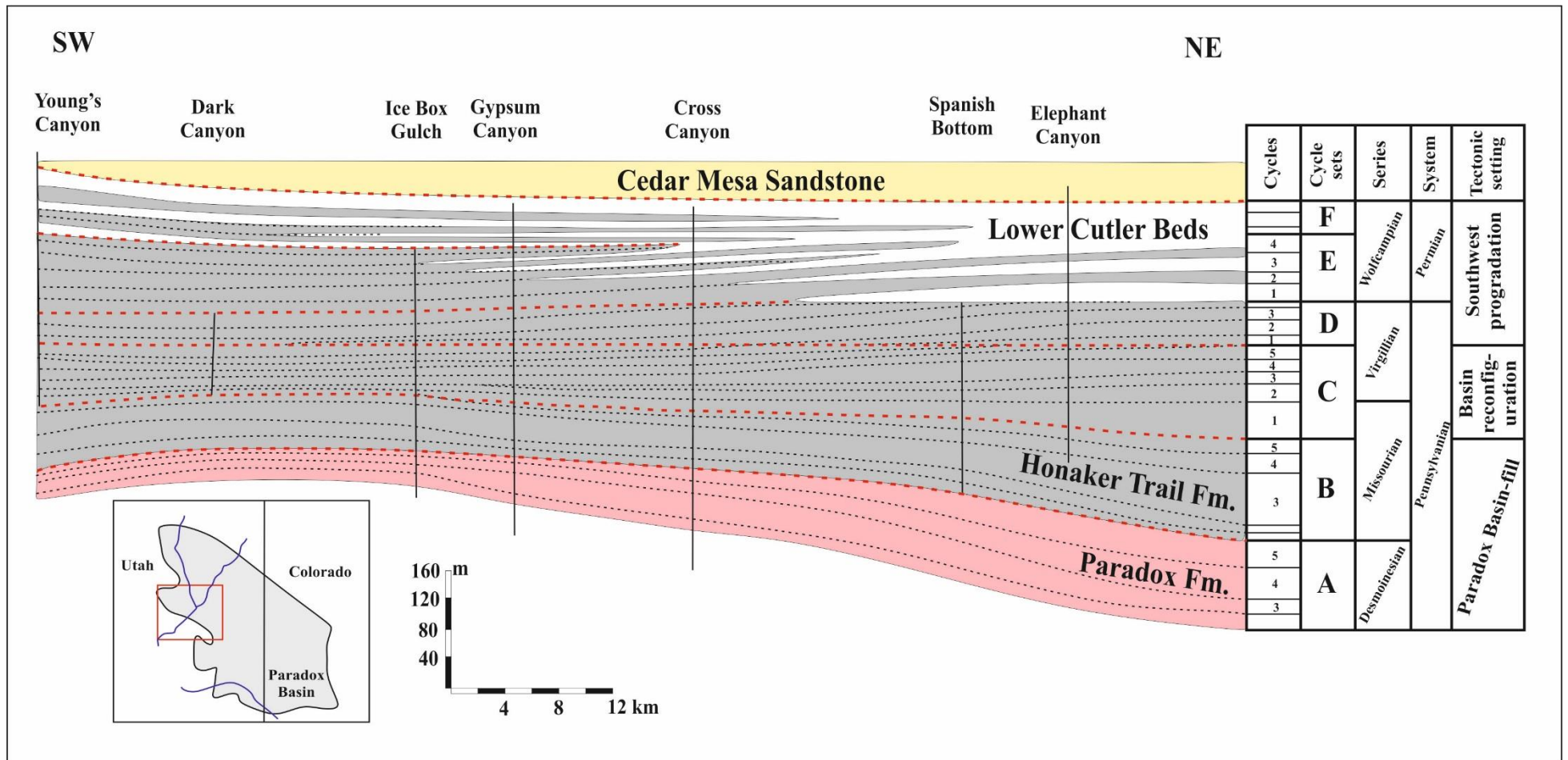


Figure 5-15 Cross-section through Cataract Canyon showing cycle sets, high-frequency cycles, and tectonic settings of the Pennsylvanian-Permian of the Paradox Basin, as well as the approximate location of the measured logs (Williams, 2009). The red dash-lines represent the cycle-set boundaries, and black dash-lines are cycle boundaries. The basin underwent three tectonic stages of basin-fill, basin-reconfiguration, and basin progradation.

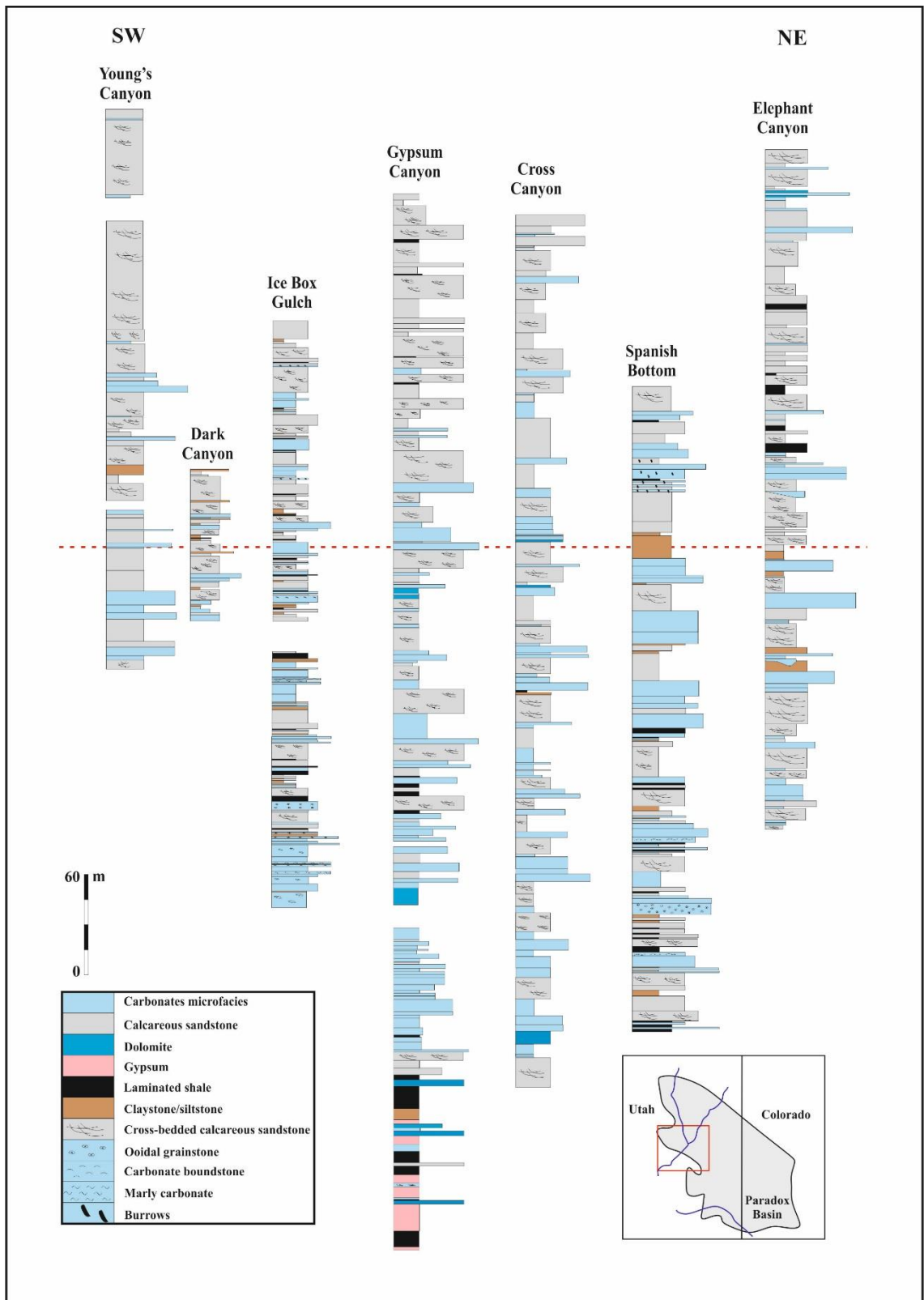


Figure 5-16 Stratigraphic logs of the Pennsylvanian-Permian cycles of the Paradox Basin in Utah (Williams, 2009), showing the carbonate-siliciclastic cycles. the dotted red line is the boundary between cycle-sets C and D.

5.4.2 Basin configuration

The Miocene Fatha Formation was accumulated on a gently sloping ramp; this is evidenced by the gradual changes of the carbonate microfacies from basin margin towards the basin centre. The accumulation of carbonates with packstone and grainstone microfacies at the basin margin, changing to mudstone and wackestone microfacies down-dip in the formation are the indicators of the presence of this carbonate ramp. In addition, the lack of abrupt lithological changes or collapse-brecciated carbonates indicate that no steep depositional slope was developed. As has been described previously, the identified sedimentary facies in the formation as seen at outcrop, including the twenty-one carbonate microfacies, are interpreted to have accumulated in the inner ramp setting (Chapter Three).

By contrast, both the Paradox and Zechstein successions were accumulated in shelf carbonate to basinal depositional settings. The presence of a deep evaporitic trough just beside the Uncompahgre Uplift in the Paradox Basin and its shelf carbonate equivalents are consistent with a shelf or distal-steepened ramp carbonate depositional setting. In addition, the presence of collapse-brecciated carbonate, the Concretionary Limestone, and a lowstand gypsum wedge in the Zechstein Basin strongly indicate a significant slope in the depositional environment. Moreover, the restriction of the evaporite deposition toward the basin centre in both the Paradox and Zechstein Basins, and the presence of subaerial exposure on the shelf carbonate suggest shelf settings. However, a ramp-like depositional setting was locally developed along the margins of the Zechstein Basin, for example the carbonates of the Z2 Roker Formation in England and Poland (Tucker, 1991; Słowakiewicz and Tucker, 2012). These carbonates are dominated by stromatolites and peritidal facies that are interbedded with oolitic grainstone microfacies. Different microbial and oolitic lithofacies of subtidal, oolitic shoals, tidal flat, tidal-channel, intertidal, and supratidal settings are recognized within the formation (Słowakiewicz and Tucker, 2012). Moreover, several evaporitic facies, comprising nodular, chicken-wire structure, irregular anhydrite, and pseudomorphs after lenticular gypsum, are recognized in the German Zechstein and are interpreted to have precipitated in supratidal sabkha (Betzler and Pawellek, 2014).

5.4.3 Stratigraphy

In the Miocene Zagros foreland basin, the Early Miocene units rest on the Oligocene-Miocene sequence boundary that changes from an unconformity surface (presumably with incised valleys updip) at the basin margin, where the Oligocene and Early Miocene units are missing, to the correlative conformity in the basin centre, where the Early Miocene is underlain by a thick Oligocene unit. The Early Miocene Serikagni Formation records the first Miocene transgression over the regional unconformity surface or its correlative conformity, and it is characterized by a deep calcareous mudstone facies that riches with planktonic foraminifera (Aqrawi *et al.*, 2010). The formation grades up or laterally to the carbonate-dominated facies of the Euphrates Formation which then grades up to carbonate-evaporitic-dominated facies of the Dhiban, Jeribe and Fatha formations. The deposition of the Fatha Formation records the first progradational geometry by the red siliciclastic unit, derived from the emerging Zagros mountain hinterlands, southwest-wards towards the basin, and this progradation continued up into the Upper Miocene-Pliocene when the previous carbonate-evaporite depositional settings changed to completely siliciclastic deposits of fluvial facies (of the Injana, Mukdadiya and Bai Hassan Formations) (Figure 5.17).

This stratigraphic trend, from dominantly carbonate facies to carbonate/evaporite and then to siliciclastic facies, is also clearly documented in the Paradox Basin (Williams, 2009) (Figure 5.15). The Pennsylvanian units rest on the regional unconformity surface that is underlain by the red shale and siltstone facies of the Molas Formation. This unit grades up to the carbonate unit of the Pinkerton Trail Formation, which then grades up to evaporitic-dominated facies of the Paradox Formation and its carbonate equivalent at the shelf. The Paradox Formation is overlain by the carbonate-siliciclastic cycles of the Honaker Trail Formation which in turn is overlain by the coarse grained clastic unit of the Cutler Group.

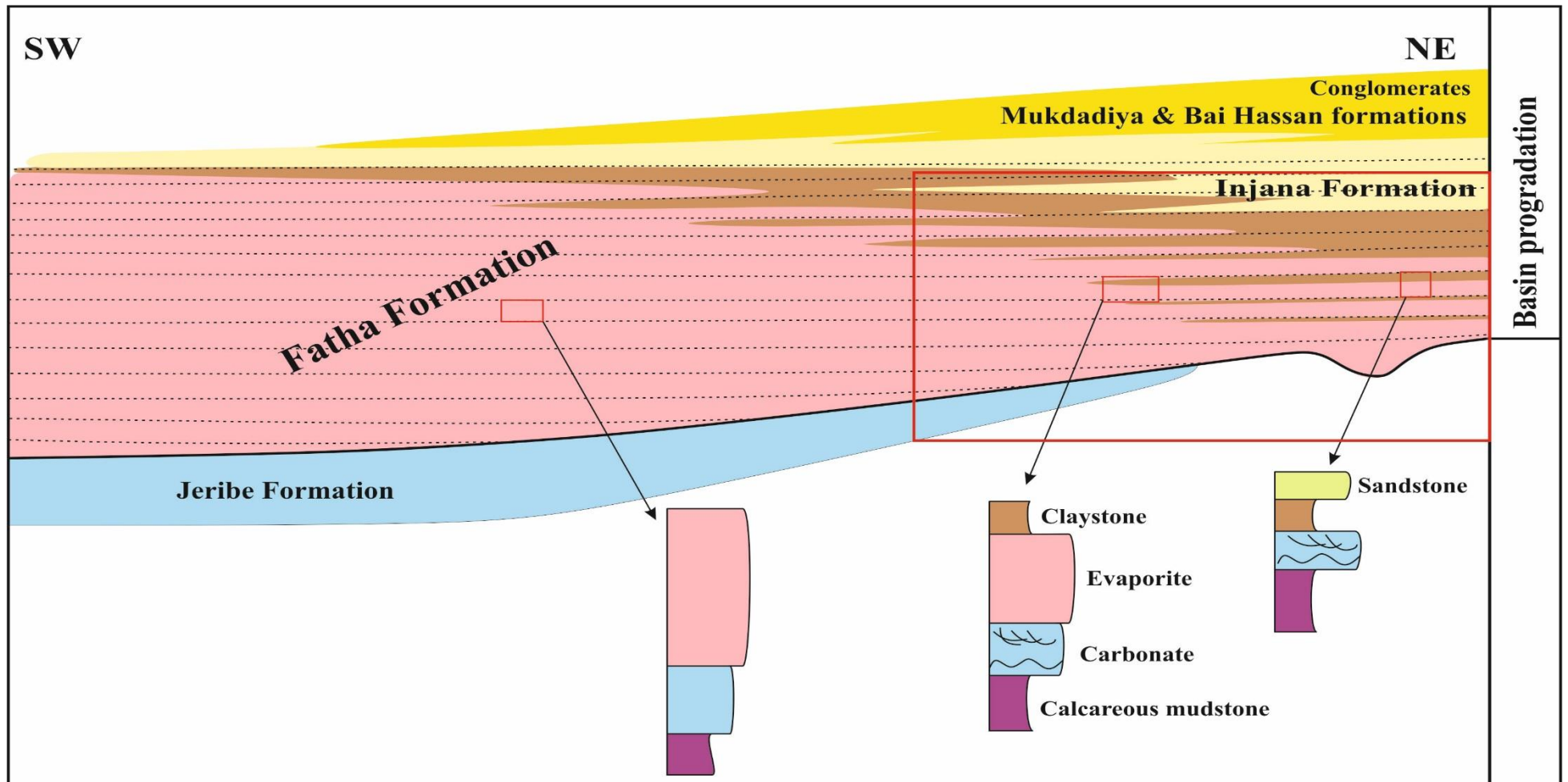


Figure 5-17 Stratigraphic relationships between the Miocene formations showing the final stage of progradation of the Zagros foreland basin and conceptual location of the measured logs from basin margin. Approximate horizontal scale (from basin margin to basin centre): 200km.

The siliciclastic unit was derived from the Uncompahgre Uplift and prograded towards the basin centre in the Permian (Peterson and Hite, 1969; Gianniny and Miskell-Gerhardt, 2009; Williams, 2009).

The late Permian stratigraphic trend of Central Europe in some ways resembles the Miocene and Pennsylvanian basins. It is underlain by the Lower and Upper Rotliegend groups, which are volcanic and siliciclastic dominated facies. The basal Marl Slate (Copper Shale) of the late Permian time is defined as the first Zechstein transgression. The Zechstein cycles start with a thick carbonate and evaporite (predominately salt) package in the lower three cycles (Z1-Z3), whereas the proportion of carbonate and evaporite facies is reduced up into the upper two cycles (Z4-Z5). The deposits in the upper cycles become shallower and consist of terrigenous-salt couplets that indicate the deposits of fluvial, lakes, rivers, and playas (Wagner and Peryt, 1997). The deposition of these terrestrial deposits continued into the Triassic when further progradation continued toward the basin.

Overall, the pattern of deposition of these basins records progressive filling of the basins and progradation. These conditions are evidenced by overall shallowing in the basins, decreasing, or in some parts of the basin disappearance, of carbonate deposits, and increasing fluvial siliciclastic deposits at the last stage of their deposition and accumulation.

5.4.4 Sedimentary facies

Three main sedimentary facies assemblages were predominant during the development of the Pennsylvanian-Permian and Miocene basins, these essentially being made up of evaporite, carbonate, and siliciclastic facies.

5.4.4.1 Evaporite facies

1- The Miocene evaporites of the Fatha Formation comprise mainly chicken-wire structure gypsum units that overlie shallow-marine carbonate facies. These evaporites are interpreted to have accumulated in supratidal sabkha which in turn are overlain by the red fluvial units. In some cycles, especially in less proximal areas, the chicken-wire evaporite is overlain by either a bedded (laminated) evaporite or a thick salt layer (Tucker, 1999). This upward transition represents the shallowing-upward trend of the cycles. The laminated evaporites were subaqueously precipitated in

shallow lagoons. The upward transition from laminated anhydrite to nodular anhydrite at the base of the evaporite cycles in the Paradox Formation possibly resulted from a new influx of sulphate and calcium into the basin during sea-level rise (Raup and Hite, 1992). During the early phases of the influx, when the salinity of the brine in the basin was still very high, the laminated anhydrite would have been precipitated. The inflowing brine was mixed with the higher salinity brine that was already in the basin (Raup and Hite, 1992). This could have resulted in changes of the brine from a higher to a lower salinity. However, the nodular anhydrite was possibly formed as the result of early diagenesis. The nodules may have formed when the original gypsum changed to anhydrite, as evidenced by the presence of traces of laminations through the nodules. This indicates a secondary origin of the nodules that resulted from the diagenesis of the primary laminated gypsum (Raup and Hite, 1992). By contrast, the laminated evaporite and carbonate in the Zechstein Basin are interpreted to have accumulated as a condensed section in the basin centre.

- 2- The evaporite deposition in the Paradox Formation was trapped in a deep, relatively narrow depression (the Uncompahgre Trough), and a shallow shelf along the western margins of the basin inhibited access to the open ocean. The lack of indicators of complete desiccation, mud cracks and ripple marks, in the Paradox Basin's evaporites indicates an absence of subaerial exposure, and shallow-water deposition along the basin margin. However, the Miocene evaporite in the Zagros Basin accumulated subaerially in a flat and wide marine-derived sabkha.
- 3- The evaporitic cycles of Paradox Basin, similar to those of the Zechstein evaporites, are terminated by thick halite deposits that were restricted to the basin centre. These deposits are interpreted to have been precipitated subaqueously from the brine waters. However, in the Zagros Basin, not all the Miocene cycles are terminated by halite deposition, but the Miocene cycles are generally capped by halite in the basin centre. These halite deposits are related to have precipitated from the final remnants of the shrinking sea and were probably deposited in salinas or salt pans (Al-Juboury and McCann, 2008).
- 4- The Paradox and Zechstein evaporites, including anhydrite and salt, are interpreted to have been precipitated subaqueously from shallow-restricted waters. However, several evaporitic facies, comprising nodular, chicken-wire structure, irregular anhydrite, and pseudomorphs after lenticular gypsum, are recognized in the German Zechstein cycles by (Betzler and Pawellek, 2014) and are interpreted to have been formed subaerially in a sabkha setting. These sabkha evaporitic facies are widespread

around the basin. Nodular, chicken-wire structure, and pseudomorphs after lenticular gypsum are also abundant in the Miocene Fatha Formation. The pseudomorphs after lenticular gypsum are very common in the Fatha carbonate members and can be interpreted to have accumulated in intertidal settings.

- 5- The main evidence supporting the depositional setting of the Fatha evaporite as sabkha facies are the abundant nodular and chicken-wire structures and their associations with intertidal facies. Specific recognizable features of the intertidal facies in the Fatha carbonates are the presence of fenestrate pores, pseudomorphs after lenticular gypsum, and algal mats and stromatolites. Such evidence from within the carbonates, as well as their associations with nodular and chicken-wire evaporites, and with fluvial deposits strongly support the inference of a sabkha depositional setting for the evaporites.

5.4.4.2 Carbonate facies

The Pennsylvanian carbonates of the Paradox Basin were deposited along a shelf and are characterized by the presence of phylloid algal bioherms. These facies were accumulated on relatively high structural blocks as a result of basement fault movements. Abrupt changes in carbonate facies are documented which are inferred to have been due to the tectonic activity. These carbonates are equivalents of the evaporitic cycles of the Paradox Formation downdip in the basin. The proportion of carbonate components declines upwards into the Honaker Trail Formation in which siliciclastic deposits entered the basin. The carbonates of the Zechstein Basin accumulated along the shelf and on a distally-slope, as well as in a condensed section in the basin centre. Different carbonate facies of shelf margin, reef, back-reef, slope, and shelf lagoon are recognized in the carbonates of the English Zechstein (Tucker, 1991). The amount of the carbonate components decreases to zero toward the upper cycles. By contrast, the carbonates of the Miocene succession of the Zagros Basin are characterized by deposition in a variety of shallow marine depositional environments.

Unlike the Paradox and Zechstein carbonates, no evidence of subaerial exposure is recognized at the top of the Miocene carbonates. Subaerial exposures, including karstification, leaching, and erosion, are recognized at the top of the Paradox and Zechstein carbonates, indicating the presence of a Type 1 sequence boundary. In contrast, there is a gradational change between the carbonates and the overlying evaporites in the Miocene succession. In addition, the carbonate microfacies record

gradational changes from mudstone and wackestone, at the base, into packstone and grainstone or algal mats and stromatolites, at the top, describing a shallowing-up regressive trend.

5.4.4.3 Siliciclastic facies

In all the basins the siliciclastic facies increase in proportion and thickness toward the upper part of the succession as a result of progradation. Different fluvial facies, comprising alluvial fans, rivers, lakes, playa, deserts, and palaeosols are recognized within the siliciclastic deposits. These deposits are composed of claystone, siltstone, sandstone, and conglomerate.

The main sources of the siliciclastic deposits into the Paradox Basin were the Uncompahgre Uplift to the east and the San Luis Uplift near the southern periphery of the basin (Trudgill and Arbuckle, 2009), whereas the clastic supply into the Miocene Basin in Kurdistan was from the Zagros and Torus Mountains to the northeast and north, respectively.

5.4.5 Carbonate-evaporite cycles

Although carbonate-evaporite cyclicity is a common feature in the Paradox, Zechstein, and Miocene Basins, some differences occur. First of all, in contrast to the Paradox cycles, according to the sequence stratigraphic investigations that have been done on the Zechstein carbonate-evaporite cycles, the carbonates (largely highstand deposits) were not laterally equivalent to the evaporites that defined as the lowstand deposits. Therefore, the carbonates and evaporites are not time-related. However, the carbonates of the Paradox Basin are interpreted to be laterally time-equivalent to the evaporites in the basin centre. On the other hand, the carbonates of the Miocene Fatha Formation cycles gradationally pass up into the evaporites at the top of each cycle's regressive phase, with no subaerial exposure at the top of the carbonates.

Secondly, the carbonate-evaporite cycles of these basins are different in terms of hierarchy and thickness. For example, the Zechstein succession reaches a thickness of 2km (Taylor, 1998) and individual halite and anhydrite bodies are up to 600 and 280 m thick, respectively (Van den Belt and de Boer, 2007). Similarly, the carbonate-evaporite succession of the Paradox Basin reaches a thickness of 2km, and an individual cycle is up to 300m thick (Catacosinos *et al.*, 1990). On the other hand, the Miocene Fatha

Formation succession reaches a maximum total thickness of 600 to 900 m in the basin centre, whereas it is 100 to 300 m thick toward the basin margin, in this study's field area. In contrast to the Miocene cycles, the carbonate-evaporite successions of the Paradox and Zechstein Basins are defined as 2nd-order "super-sequences", and the individual carbonate-evaporite cycles as 3rd-order sequences. Additionally, a number of high-frequency cycles are also recognized and defined as 4th-order sequences and 5th-order parasequences. This contrasts with the Miocene Fatha Formation succession which is interpreted in this study to represent a 3rd-order sequence, and the individual cycles are defined as 4th-order parasequences.

Thirdly, the evaporitic cycles of the Paradox Formation in the basinal trough can be correlated into the carbonate cycles at the shelf margin. This can be applied by the correlation of the transgressive black shale over the basin. In addition, Hite and Buckner (1981) correlated the carbonate and evaporitic cycles across about 40 km and they were able to correlate the 29 evaporitic cycles of the Paradox Formation with the carbonate cycles of the Ismay, Desert Creek, Akah, Barker Creek, and Alkali Gulch formations. Lateral correlations of the cycles over a large distance can be applied with little difficulty. This extensive correlation over a large distances is similarly a common feature in the Zechstein cycles that can be correlated over England, Germany, Poland, and the Netherlands. Moreover, the lateral correlations of the Fatha cycles in the Zagros Basin have been conducted between the studied sections over tens of kilometres in distance.

5.4.6 Palaeoclimate

The major Gondwana glaciation was initiated in the Carboniferous period and the major icehouse phase terminated during early Permian times. After that the climate throughout the Permian and Triassic times became mainly hot and arid at the palaeo-latitudes of the Paradox and Zechstein Basins. Most of the classic Permo-Triassic strata in England and Europe comprise of red beds that indicate hot conditions either in rivers and lakes or deserts (Benton *et al.*, 2002). A lowstand 1st-order cycle has been suggested in the Late Palaeozoic (Fischer, 1984). In addition, Vail *et al.* (1977) inferred a 2nd-order lowstand at the end of the Mississippian, whereas the Pennsylvanian was marked by 2nd-order transgression (Haq and Schutter, 2008).

The proximity of the Paradox Basin to the palaeo-equator during the Pennsylvanian resulted in the high rates of evaporation and the development of high salinity brines. High rates of evaporation in the late Permian Zechstein Basin were also a response to hot and arid climatic conditions. On the other hand, the Zagros Basin in the Miocene period is characterised by high-frequency climatic fluctuations and a number of climatic cycles, arid-humid couplets, are recognized. The high rates of evaporation represented in the Miocene successions across the Middle East relate to hot and arid climates, especially during the deposition of the Fatha evaporites that were accumulated during the Miocene Climatic Optimum.

It is believed that the arid climate, together with sea-level changes, had direct influence on the rate of the evaporation in Zechstein seawater, and resulted in a gradual salinity increase in the seawater. This salinity trend, due to climatic influence, is clearly documented in the carbonate members also. The first carbonate cycle of the Zechstein Basin was deposited under normal marine water, evidenced by abundant normal marine fauna, while the second and third carbonate cycles were accumulated under higher salinities, evidenced by restricted fauna (Słowakiewicz and Gąsiewicz, 2013). However, the aridity became less intensive through time and interrupted by humid phases. This is clearly observed in the upper Zechstein cycles in the form of reduced evaporite deposits and increased terrigenous sediments. A comparable climatic trend is inferred as being recorded in the Miocene strata of the Zagros Basin, where the thickest evaporite deposits accumulated during the Early-Middle Miocene due to the high evaporation rate and arid climate, whereas the evaporation rates and aridity decreased through the Upper Miocene and Pliocene.

5.4.7 Mechanisms controlling cyclicity

Three main mechanisms, including glacio-eustatic sea-level fluctuations, tectonics, and sedimentary autocyclicity have invoked to explain high-frequency cyclicity in different basins (Grotzinger, 1986a; Grotzinger, 1986b; Goldhammer *et al.*, 1987a; Tucker and Garland, 2010). Facies analysis and depositional environments, cycle and cycle-set extensions, and stacking patterns are the tools that can be used to determine the controlling mechanisms on cyclicity.

5.4.7.1 Glacio-eustatic sea-level fluctuations

Global sea-level fluctuations and climate changes are reflected in the sedimentary rock records by sediment composition and cyclicity. Correlation of thin stratigraphic units or an individual cycle over large distances is one of the main features of glacio-eustatic control. This has been documented in all the Paradox, Zechstein, and Zagros Basin cycles. The Pennsylvanian and Permian cycles of the Paradox Basin have been analysed and can be traced over significant distances from the basinal areas to the shelf areas (Raup and Hite, 1992; Goldhammer *et al.*, 1994; Williams, 2009; Jordan and Mountney, 2012). Additionally, the transgressive black shale deposit has been traced from the evaporitic cycles of the Paradox Formation, in the basin trough, into the shelf carbonates, at the shelf margin (Baars and Stevenson, 1982; Goldhammer *et al.*, 1994). Moreover, regional and local tectonics, sediment availability and supply, climate, subsidence, and glacio-eustatic sea-level fluctuations resulted in the development of the observed cyclicity within the Paradox Formation (Trudgill and Arbuckle, 2009). These authors believed that the eustatic sea-level fluctuations, as a main factor influencing the Paradox cyclicity, were the result of the Gondwana Glaciations. Of greater lateral extent, reflecting the greater dimensions of the basin, the carbonate-evaporite cycles of the Zechstein Basin have been studied and correlated widely over Germany (Strohmeier *et al.*, 1996a), Poland (Wagner and Peryt, 1997), the Netherlands (Geluk, 2000a), and England (Tucker, 1991).

Different orders of eustatic sea-level fluctuations, including 2nd, 3rd, 4th, and 5th orders, have been documented in both the Paradox and Zechstein Basins (Goldhammer *et al.*, 1991; Tucker, 1991). Additionally, orbital forcing are interpreted on the timescales of Milankovitch cycles, including precession (ca. 20kyr), obliquity (ca. 40kyr), and eccentricity (ca. 100kyr and 400kyr), are recognized within the higher frequency orders (4th and 5th orders) from both basins (Goldhammer *et al.*, 1991; Mawson and Tucker, 2009).

These features are similarly documented from the Zagros Basin Miocene Fatha Formation cycles, in which cycles (or parasequences) can be traced over large distances. The cyclicity in the Fatha Formation is widely documented in its equivalents in surrounding countries, including Iran and Syria, and it is a predominant Miocene feature in the Middle East, as well as worldwide. In addition, the correlation of the cycle-sets (parasequence sets) from the Fatha Formation, including retrogradational and

progradational cycle-sets, is widely traceable over all the studied areas. What does vary is the number of cycles in an individual cycle-set, which is variable from place to place. This is not documented in the analysis of cycle-sets from the Paradox Basin (Williams, 2009). Instead, here five cycle-sets are consistently correlated over a large distance from the evaporite and carbonate-siliciclastic cycles of the Paradox, Honaker Trail, and Elephant Canyon Formations (Williams, 2009).

Overall, glacio-eustatic sea-level fluctuations appear to have generated a dominant stratigraphic signal in all the Paradox, Zechstein, and Zagros cycles.

5.4.7.2 Tectonic mechanism

Tectonic mechanisms exert a major influence on the configuration of a sedimentary basin and a first order control upon the distribution of the sedimentary facies. In addition, syn-sedimentary faults or tectonic activity could make local changes in a basin. These tectonic conditions have been clearly observed in the shelf carbonates of the Paradox Basin. The presence of a thick phyloid algal bioherm and abrupt lithological changes within the shelf carbonates in the Paradox Basin indicate local tectonic and syn-depositional reactivation of the basement faults (Baars and Stevenson, 1981; Goldhammer *et al.*, 1994). However, the extensive correlation of the high-frequency cycles of both the Paradox and Zechstein Basins is unlikely to be controlled by such local tectonic activity.

A similar condition is seen in the Miocene Fatha Formation of the Zagros Basin. There is evidence for syn-sedimentary tectonic activity on basement faults in the region. Movement on tectonic basement faults created a number of palaeo-highs which in turn cut the Miocene basin into several sub-basins (Bahroudi and Koyi, 2004). Two main sub-basins, comprising the Sinjar and Kirkuk depocentres, are located in Iraq while the other depocentres extend into Iran. However, this tectonic activity apparently exerted only a minor influence on local Fatha Formation cyclicity. This can be concluded by the extensive correlation of the high-frequency cycles of the Fatha Formation. This feature of extensive continuity of high-frequency cycles in the Paradox, Zechstein, and Zagros Basins indicates that, with the expectation indicated above, local tectonic activity had only minor effect, if any, on depositional geometries.

5.5 Conclusions

In this chapter, the carbonate-evaporite cycles of the Paradox and Zechstein Basins have been compared to the Miocene carbonate-evaporite cycles of the Fatha Formation in the Zagros Basin. The comparisons have been made in terms of basin configurations and development, tectonics, stratigraphy, lateral and vertical facies variations, the nature of the carbonate-evaporite cyclicities, and the mechanisms that have led to these cyclicities. The Carboniferous-Permian Paradox Basin is a long and asymmetric foreland basin that extends in a NW-SE direction. The basin covered most of east-central Utah and SW Colorado and into NW New Mexico and NE Arizona, and was bordered by several palaeo-highs. The most significant palaeo-high was the Uncompahgre Uplift to the northeast of the basin that was a main source for terrigenous deposits. A thick evaporite cyclical succession accumulated in the basin centre to the east, whereas a carbonate cyclical succession was deposited on the shelf margin to the west.

By contrast, the late Permian Zechstein Basin developed in a broad epicontinental shallow marine basin that covered much of north-central Europe and had a small connection with the upper Permian open sea through a narrow strait between Greenland and the Scandinavian Peninsula. In this basin five main carbonate-evaporite cycles were accumulated and extended from northern England, across the North Sea through the Netherlands, Denmark, Germany and Poland.

Unlike the Miocene succession of the Fatha Formation in the NE Zagros Basin, which was accumulated on a gentle ramp, the Paradox and Zechstein successions were deposited on shelf platforms or distally-steepened ramps. However, some local, more continuously sloping ramp-like depositional settings were formed around the margins of the basins, where they are characterized by shallow-water carbonate and evaporite facies of peritidal and sabkha settings.

Similar in stratigraphic character to the Miocene succession of the Zagros Basin, the Paradox succession passes up from the carbonate facies of the Pinkerton Trail Formation, at the base, into the evaporite cycles of the Paradox Formation and its lateral carbonate equivalents of the Barker Creek, Akah, Desert Creek, and Ismay Formations. These pass up to the carbonate-siliciclastic cycles of the Honaker Trail Formation and finally to the siliciclastic-carbonate cycles of the Cutler Group. This stratigraphic trend

suggests basin-filling and progradation into the basin in a south-westward direction. This is similarly seen in the Miocene Fatha Formation, with the Zagros Basin undergoing progradational basin-filling from north-east to south-west.

The deposits of the Paradox and Zechstein Basins form thick cyclical successions; each reaches about 2km in thickness, whereas the Miocene Fatha Formation reaches 900m in thickness at the basin centre. Unlike the Miocene succession, which is composed of a number of shallowing-upward cycles that are bounded by flooding surfaces, the Paradox and Zechstein successions are characterised as sequences that define cycles of sea-level change, but in which each cycle is bounded by regional sequence boundaries that define each depositional sequence.

Extensive correlation of the Paradox and Zechstein cycles and also the Fatha Formation cycles are possible over large distances. This suggests that the carbonate-evaporite cycles of the Paradox, Zechstein and Zagros Basins have originated primarily as a result of glacio-eustatic sea-level fluctuations and climate changes. Pennsylvanian-Early Permian times were characterized by the main Gondwana Glaciation that resulted in a fall in sea-level but the proximity of the Paradox Basin to the palaeo-equator created an arid and hot climate and resulted in the deposition of the thick evaporitic succession. However, the intensity of the glaciation reduced in the early Permian and the climate changed to hot and arid condition throughout the Permian at low latitudes. The evaporitic succession of the Zechstein Basin was developed in this arid and hot context during the late Permian.

Overall, it can be concluded that climate has a dominant role in the deposition of the studied carbonate-evaporite cyclical successions. Evaporite deposition needs an arid to semi-arid climate and a restricted basin that has some connection to an open ocean. This climatic condition is observed in all the carbonate-evaporitic successions. In the case of cyclical successions of carbonate-siliciclastic character, both tectonic uplift, as a source of siliciclastic sediments, and climate are believed to have major roles in their development.

Chapter Six

General Discussion

Cyclical carbonate-evaporite successions are important deposits in the sedimentary record, whether in terms of being an archive for the study of sedimentary processes and palaeoenvironmental change or for hydrocarbon exploitation, or for economic geology such as the widespread extraction of salt, as for example in the case of the Zechstein Basin. This has motivated geologists to study these deposits worldwide. In this PhD project, an investigation has been carried out of the carbonate-evaporite cycles of the late Burdigalian-Langhian Fatha Formation from the periphery of the Zagros foreland basin in the Kurdistan region of Iraq. Cycles have been analysed and their origins evaluated, largely based upon the detailed characterization of outcrop sections which have been logged close to the palaeo-basin margin, and through the comparison of these logs with published records of cycles from the basin centre. This Zagros Basin cyclical succession has then been compared to the carbonate-evaporite cycles of the Paradox and Zechstein Basins. In this chapter, the controls that interacted to determine depositional architectures in each of these basins are discussed, to try to assess which controls or combination of controls were the dominant factors determining architectures in each of these cases. From this, lessons can be drawn for the interpretation of carbonate-evaporite successions elsewhere. Methodological issues and preliminary implications for understanding and predicting the hydrocarbon reservoir geometries in these and similar successions will also be discussed.

Controls on architectures of cyclical carbonate-evaporite successions: The first and main control on carbonate-evaporite basins is the *tectonic setting*, which determines basin physiography (Table 6-1). The Zagros Basin is a foreland basin that developed as a result of the tectonic compression between the Eurasian and Arabian plates. This tectonic setting developed a broad depression in the Early Miocene with gently sloping ramps around its margins. In the north-east of the basin, in the studied area, the ramp dipped southwestwards toward the basin centre. Similarly, the Paradox Basin (Pennsylvanian to Early Permian) also formed as a foreland basin. The basin was tectonically controlled by the shortening and growth of the Uncompahgre Uplift to the northeast of the basin and the concurrent formation of a deep trough which allowed the accumulation of the evaporites and marginal carbonates. In this example, favourable

conditions for the development of algal bioherms on the margin resulted in distally-steepened carbonate ramp or platform geometries around the margin of the basin. In contrast, the Zechstein Basin developed as a much broader depression, largely as a result of thermal subsidence. The accumulation of carbonate and evaporites in these three basins was largely controlled by their tectonic settings. The carbonates of the Paradox Basin at the shelf margin, for example, were mainly controlled by the basement block movements that created favourable places for algal bioherm colonisation and aggradation. The carbonates of the Zechstein Basin are largely composed of reefal bioherms and grainstones around the margin, with laterally equivalent laminated mudstones in the basin centre. However, bioherms and corals are not developed on the Zagros carbonate ramp. This could be due to slightly elevated salinities or to highly energetic hydrodynamic conditions toward the edge of the basin inhibiting colonisation by reef-builders. Instead, gastropods, bivalves, and benthic foraminifera (rotaliids and miliolids) were common in the Zagros Basin. The latter, high energy marginal environment interpretation is not really supported by the sparse sedimentary structures that are preserved, therefore the elevated salinities model is preferred.

The second major control on carbonate-evaporite successions is *climate*. Climate is an important factor for the deposition of evaporites that need evaporation to match or exceed marine water recharge, typically hot and dry conditions. The palaeoclimatic context of the Paradox Basin during the Pennsylvanian was that deposition was occurring across the peak of the main Gondwanan ice-house event, a palaeoclimatic phase that diminished through the early Permian. The deposition of the Paradox evaporites occurred during this main Pennsylvanian glaciation, but the position of the basin very close to the palaeo-equator meant that during high frequency episodes of high insolation the climate was hot and arid and led to evaporite deposition. By the late Permian palaeoclimate was in the late stages of the broad Pennsylvanian-Permian glaciation, but the climate at the palaeolatitudes of central Europe, where the Zechstein Basin developed, was arid and hot. But there appears to have been little expression of the high frequency (4th order) insolation fluctuations seen in the earlier Paradox Basin. The palaeoclimate during the Miocene in what is now NE Iraq was in the early stages of global ice-house development, but at this location the climate of the Zagros foreland basin was hot and arid. However, the arid/hot climate was cyclically interrupted by a shift towards increased marine water recharge compared to evaporation rates that resulted in relative sea-level rise, a return from hypersalinity towards more normal (but

perhaps still slightly elevated) marine salinities, and the deposition of the carbonates and shales. In the case of these late Burdigalian-Langhian Fatha Formation cycles, the high frequency cycles included increasingly wet/humid phases around the basin margin bordered by the Zagros Mountains. This led to cessation of the deposition of sabkha evaporites around the margin and increased siliciclastic input and progradation. This inference of a climatic evolution toward increasingly significant wet and humid conditions may also be recorded in the late stages of the Paradox Basin, when the carbonate and more siliciclastic-rich cycles developed and prograded toward the southwest within the basin. So regional increases in humidity are implied in the later stages of both the Zagros and Paradox Basins' evolution. It is possible that this records an orographic effect of increased rainfall in response to growing mountain belt elevations and/or widths. The problem is that increased mountain elevations and hence relief also promote enhanced erosion rates, even for a stable climatic state, such that it is not possible to invoke an absolute increase in humidity with high levels of certainty.

Table 6-1 Comparison of three carbonate-evaporite basins, including Zagros, Zechstein, and Paradox, in terms of their depositional developments, climates, and tectonics.

Factors\Basins	Zagros Basin	Zechstein Basin	Paradox Basin
Age	Late Burdigalian-Langhian	Lopingian (late Permian)	Pennsylvanian to Cisuralian (early Permian)
Tectonic setting	Early foreland basin	Mainly thermal subsidence (local early rifting-related basins)	Foreland basin
Palaeoclimate context	Early ice-house	Late ice-house	Peak ice-house
Local climate context	Arid, probably with developing humidity over growing mountain belt	Arid, probably with developing humidity in later stages	Arid (close to palaeo-equator), probably with developing humidity into the Cisuralian (early Permian), after uplift phase of the Uncompahgre Mountains
Basin-margin physiography	Ramp	Distally-steeped ramp (after Read, 1985), evolving to ramp	Distally-steeped ramp
Stratigraphic context of evaporites	Regressive sabkhas in margin (highstand and falling stage) and basinal lowstand gypsum and halite (falling stage and/or early transgressive)	Few marginal sabkhas in late highstand (e.g. Z3 Seaham Formation) and basinal falling stage/lowstand evaporites (gypsum and halite)	Lowstand evaporites (gypsum and halite) and highstand carbonate
Basin width	500 km (northeast to southwest)	>1000km (northeast to southwest length)	150km (northeast to southwest)
Lateral extent (proximal to basinal) of proximal facies (whether upper to lower ramp or shelf to slope)	Tens of kilometres	Tens to hundreds of kilometres	Tens of kilometres
Carbonate dominant types	Packstones/grainstones	Reefal bindstones and grainstones	Algal bioherms and grainstones
Siliciclastic progradation	Late	Very late (minor)	Late
Cycle frequencies	Third-order sequences and 4 th -order (and probably also 5 th order)	Third-order sequences and some 4 th -order parasequences	Third- and fourth-order sequences and 5 th -order parasequences

	parasequences		
--	---------------	--	--

Lateral extent of carbonate-evaporite cycles: Another important point to discuss is the distances over which lateral correlation of high-frequency cycles is possible, which has implications for the origins of the cycles. Three main factors have invoked to explain their origins, these being glacio-eustasy, tectonics, and sedimentary autocyclicity. The first factor can be recognized by evaluating the lateral extent and continuity of the cycles, where high continuity would support a glacio-eustatic origin. Local tectonic activity, on the other hand, is not likely to develop such laterally extensive, traceable cycles. The distances over which cycles might be developed would likely be controlled by the spacing of tectonic features, separating areas undergoing accommodation growth from areas undergoing concurrent accommodation reduction and so having different depositional geometries. Lastly, sedimentary factors that might develop high-frequency cycles, but of limited lateral extent, might include for example the progradation and autocyclic lateral switching in the position of tidal flat deposits along a basin margin. These three factors have been evaluated for the late Burdigalian-Langhian cycles of the Zagros Basin for the first time in this study. There are two critical observations which have been used to conclude that the Fatha Formation cycles originated as glacio-eustatic effects. These are: 1) the extensive correlation of the depositional cycles for many tens of kilometres, and 2) this being consistent with the glacio-eustatic fluctuations recorded worldwide during the Miocene. These three factors have been evaluated for Paradox and Zechstein Basins as well. In both cases, the presence and lateral continuity of high-frequency cycles (Table 6.1) of these basins, and their occurrence during known periods of global palaeoclimate variability, allow the inference that the principal control on their cyclical sedimentary architectures were similarly a result of glacio-eustatic sea-level fluctuations and associated regional, high frequency palaeoclimate fluctuations.

Implications for sequence stratigraphic models of carbonate-evaporite successions: In term of sequence stratigraphy, different models have been proposed for carbonate-evaporite deposits (Tucker, 1991; Handford and Loucks, 1993; Weber *et al.*, 1995; Strohmenger *et al.*, 1996a; Sarg, 2001). Most of these models have been applied to the Paradox and Zechstein deposits. The position of carbonate and evaporite deposits in the basins have been critically analysed in term of system tracts and sequence boundaries (see Chapter Five). Each of individual cycle (Z1-Z3) in the Zechstein Basin represents a third-order sequence that is bounded by type-1 sequence boundaries (Tucker, 1991). This type-1 sequence is recognized based on the evidence of sea-level falling to below the level of a shelf break. However, in the upper cycles (Z4-Z5), the sequence

boundaries change to type-2 sequence boundaries (Tucker, 1991). This is due to evolution of the basin margin (on the western margin of the Northern Zechstein Basin) from a shelf slope (or over-steepened ramp to use original terminology of Read, 1985) to a carbonate ramp. On the other hand, 3rd order type-1 sequence boundaries are recognized throughout the Paradox cycles (Weber *et al.*, 1995). These differences in the type of sequence boundary are probably due to the basin margin physiography that is largely controlled by tectonic setting but also by the presence or absence of slope-steepening coral or algal bioherms.

The Fatha Formation cycles have been interpreted as parasequences that developed within a 3rd order transgressive-regressive sequence (TST-RST). This interpretation has been made based on vertical facies changes within the individual cycles that are dominated by of shallowing-upward/shoaling-up RST trends. These shallowing-upward parasequences are bounded by flooding surfaces that can be placed at the base of the calcareous mudstones. Each cycle starts with a flooding event and then shoals up, and then progrades toward the basin. Over the formation as a whole, progradation is clearly evidenced by the first appearance and then progradation of the red siliciclastic deposits, derived from the Zagros Mountains, during the deposition of the Fatha Formation. This may also imply the progressive filling to overflowing (completed in the succeeding Injana Formation) of the basin and the tectonic growth of the Zagros Mountains during the late Burdigalian. The marginal evaporites of the Fatha cycles were accumulated during highstand system tract and falling stage in a broad supratidal sabkha setting. Lowstand evaporites do also occur in the basin centre. In contrast, the bulk of the Paradox and Zechstein evaporites were subaqueously deposited within lowstand system tracts. The deposition of lowstand evaporite simultaneously occurred with subaerial exposure of the shelf margin. This is clearly observed in all the Paradox cycles and some of the Zechstein cycles (Tucker, 1991; Weber *et al.*, 1995).

A new depositional model has been presented for the carbonate-evaporite cycles of the Fatha Formation in Chapter 3 and is summarised in Figure (3-6). This model is a significant departure from previously published carbonate-evaporite sequence architectures (Handford and Loucks, 1993; Weber *et al.*, 1995; Strohmenger *et al.*, 1996a; Sarg, 2001) and is necessitated by the recognition of the exclusively carbonate ramp geometry, without any over-steepened slope, that characterised the north-eastern margin of the Zagros Basin at time of deposition.

Uncertainties in the analysis of carbonate-evaporite successions: The first point that is worth mentioning is that the sedimentological and sequence stratigraphical investigations on the Fatha facies have been undertaken at the basin margin where not all the cycles are preserved. This creates difficulty in the interpretation and correlation of cycles from the margin to the basin centre because of the proximal-distal variabilities that have been seen in the cycles. These variabilities include both lateral variations from north-east to south-west and upward variations through the succession. The majority of the cycles in the lower part of the basin margin succession comprise four main depositional facies, these being from base to top; calcareous mudstone, shallow-marine carbonate, nodular evaporite, and red siliciclastic units. Whereas, the cycles vary the basin centre are composed of calcareous mudstone\carbonate and evaporites (anhydrite and halite). These variabilities are due to the siliciclastic input to the basin around the margin as a result of the tectonic growth of the Zagros Mountains, and to the restriction of the basin toward the basin centre, most notably during the relative lows in sea-level. In addition, the variabilities of the cycles upward through the succession, including decreasing cycle thicknesses, missing evaporite deposits, decreasing marine deposits, and increasing siliciclastic facies, are due to the progradation and migration of the shoreline south-westwards into the basin. These trends have been interpreted as representing progressive shallowing throughout Fatha Formation deposition. This shallowing-upward trend has been enhanced by progradation of the siliciclastic deposits from the basin margin to the SW of the basin. This resulted in the migration of the shoreline through time that in turn resulted in the formation of the variations in the cycles around the margin where not all the cycles are preserved.

The second point that is worth mentioning is the interpretation of extensive chicken-wire and nodular evaporites in the Fatha Formation. The best evidence that leads to high levels of certainty in the primary origin of the Fatha evaporites can be listed as the follows: 1) Lack of diagenetic origin of the evaporite: Secondary nodular evaporites originate from diagenesis of pre-existing laminated evaporites, and so traces of the original laminations are likely still to be preserved locally. This is used as a good indicator for the detection of secondary nodular evaporites. However, such traces of original laminations have not been observed in the Fatha Formation evaporites. Only one depositional parasequence includes laminated evaporite facies and these are consistently well preserved. 2) The association of the nodular evaporites above shoaling-upwards shallow-marine carbonates and intertidal facies is another factor

increasing certainty in the primary origin of the nodular evaporites. The intertidal facies are composed of algal mats and stromatolites that include fenestrate pores and evaporite pseudomorphs. 3) The last factor confirming the primary sabkha origin of the proximal evaporites is the continuation of the vertical facies trend into overlying red siliciclastics (the red claystones), which are consistent with a continuing regressive trend with clastics over-riding the marginal sabkha environments.

It is worth mentioning that palaeo-salinities appear to have varied upward through the individual Fatha Formation cycles, as well as through the whole succession. The calcareous mudstone units, at the base of each cycle, were deposited during transgression in initially hypersaline conditions. This is indicated by the presence of hypersalinity indicator fossils, including rotaliids and miliolids. This elevated salinity may have only applied around the laterally extensive shallow basin margin due to locally high evaporative conditions in shallow waters, whereas toward the basin centre, the calcareous mudstone represents a deeper water facies that contains planktonic foraminifera and therefore probably more normal marine salinities (Shawkat, 1979). Salinities increase upward through an individual cycle where restricted lagoonal environments are recorded, as evidenced by the presence of evaporite pseudomorphs in restricted carbonate microfacies. More normal marine carbonate microfacies are developed around the shoals. However, overall the salinity decreases upward through the succession as indicated by the increasing presence of normal marine fossils, including bryozoas and oyster. This would be consistent with a decrease in the ratio of evaporation to recharge, whether marine or freshwater input. The consistent marine signal in the strontium isotope record does not, however, resolve a freshwater source or increasing freshwater input through the Fatha Formation succession.

Methodological issues: The Fischer plot methodology has been used to show the variation in high-frequency parasequence architecture in the Fatha Formation. It is a useful method to aid interpretation of the stacking patterns, systems tracts, and correlation of the cycles (Sadler *et al.*, 1993). It can be used to evaluate the lateral extension of the cycles that in turn can be used to evaluate the origins of the cycles. Importantly, Fischer plots are best used for the characterisation of successions of shallowing-upward cycles and it is recommended that it be applied where at least 50 cycles are developed. However, it is worth mentioning that compaction of the sediments will introduce an error in the plots that in turn affects the amount of the accommodation

space inferred through time. It is because the cycles are similar in lithological character that such errors are considered likely to be a second order effect in the context of the overall plot trends. Fischer plots have not been generated for the Paradox Basin and Zechstein Basin cycles due to the lack of availability of published continuous detailed logs in the Chapter 5 secondary study, and because of the poor chronostratigraphic constraint of top and base of each succession.

Implications for hydrocarbon reservoir geometries: The association of carbonates and evaporites in cyclical successions can have significance in petroleum systems. The carbonates can act as good reservoirs, if either good or well-connected primary porosities or good and well-connected secondary or fracture porosities are developed, whereas the evaporites may provide good cap rocks. Recently, Cenozoic carbonate reservoirs have been investigated in Kurdistan and north-central Iraq. The lateral extent of these potential carbonate reservoirs on the margins of Burdigalian-Langhian Zagros Basin, traceable for tens of kilometres basinward and potentially hundreds of kilometres parallel to the basin margin is significant. . The sabkha evaporites could act as extensive intraformational seals, capping the carbonate facies of each cycle. This would mean that the formation as a whole will behave as a series of separated reservoir units, with potentially high lateral permeabilities and connectivity, but much lower vertical permeabilities and connectivity due to the presence of the mudstones and the evaporites in each cycle. Moreover, the regularity in the stacking patterns that are correlated across the whole area would be another important point in any evaluation of the carbonate reservoirs and evaporite seals.

Suggestions for future work: Throughout this PhD project, sedimentological and sequence stratigraphical tools have been used to study the carbonate-evaporite cycles of the Late Burdigalian-Langhian Fatha Formation. However, the studied outcrops have been logged in detail only around the basin margin where the succession has reduced thickness and numbers of cycles compared to in the basin centre. In addition, there was no available detailed characterization of basinal facies that could be used to aid correlation of basinal facies to the facies of the basin margin. In order to study the succession in the whole basin, these recommendations should be considered for future work: 1) Using well logs, cores and seismic profiles to extend the study to cover both marginal and basinal facies, over the whole basin. This would allow the development of a depositional model for the whole basin. It is worth mentioning that analysis of the

cycles in terms of lateral correlation and sequence stratigraphic interpretation would require a complete section in the basin centre. This would allow correlation the cycles basin-wide and further evaluation of the origin of the cycles. 2) Hydrocarbon potential and reservoir characterization would be another topic worthy of further investigation, with respect to the carbonates as reservoirs and evaporites as regional hydrocarbon seal. This would require petrophysical studies of the carbonate facies, including the links between porosity and permeability and primary facies, together with analysis of any secondary diagenetic or fracture modification of porosity and permeability distributions, that would then allow rock typing (in the sense of Hollis *et al.* (2010)) and mapping of rock types. 3) Geochemistry of the evaporite units could further help understanding of the precipitation history and origin of the evaporites. This may also need detailed core sampling of evaporites to observing the structure of the evaporites. Lastly, 4) an approximate water depth has been determined from the benthic foraminifera around the margin of the basin. However, the water depth in the basin centre has yet to be characterized by studying benthic and planktonic foraminifera. This is another tool which would allow estimation of the variation in the water depth from the basin margin to the basin centre.

Chapter Seven

Conclusions

This study has aimed to investigate the variations in cyclical carbonate-evaporite depositional systems of three main cyclic successions, comprising the late Burdigalian-Langhian Fatha Formation in the Zagros Foreland Basin, the Pennsylvanian to Permian of the Paradox Basin in the USA and the late Permian of the Zechstein Basin in north-central Europe. The focus of the study was to determine the depositional settings and to analyze the high-frequency cyclical geometries of the carbonate-evaporite succession of the Fatha Formation on the margin of the Zagros Foreland Basin in the Kurdistan region. The second aim was to analyze the carbonate-evaporite cycles of the Paradox and Zechstein Basins and then to compare them to the carbonate-evaporite cycles of the Miocene Fatha Formation.

The Miocene Fatha Formation at the periphery of the Zagros Foreland Basin comprises of a number of carbonate-evaporite cycles and crops out extensively in the Kurdistan region. Nine outcrops of the Fatha Formation were selected in the vicinity of the city of Sulaimani and nine sedimentary sections were logged. Thin section preparation and analysis, microfacies analysis, fossil extractions, and the characterization of lateral and vertical facies variations, as well as cycle analysis, have been conducted for this purpose. These investigations have produced the following conclusions.

At the margin of the Zagros Foreland Basin, the Fatha Formation overlies either the Jeribe Formation conformably or Oligocene/Late Eocene sediments unconformably, further to the north-east. The Lower Miocene formations, including the Euphrates, Dhiban, and Jeribe Formations, are recognized for the first time in this study area along the Qishlagh-Sargrma Mountain below the Fatha Formation. Oligocene rocks have also been recognized locally.

At the margin of the Zagros Basin in the Kurdistan region the Fatha Formation comprises 17 to 42 carbonate-evaporite cycles. A typical cycle passes up from a calcareous mudstone unit into a shallow-marine carbonate member and this passes up into a nodular evaporite deposit. Each cycle is typically capped by a red siliciclastic unit. The boundaries between the calcareous mudstones and the following carbonates, as well as the carbonates and the succeeding evaporites, are gradational. However, there

are typically abrupt changes between the evaporites and the overlying red siliciclastic units. Additionally, there is an abrupt change between the red siliciclastic unit with the overlying calcareous mudstone unit of the next cycle.

The calcareous mudstones, in the lower part of the succession, were deposited in hypersaline conditions, perhaps 20-30m deep, whereas toward the upper part of the succession they were accumulated in normal marine waters in relatively shallow settings. Twenty-one carbonate microfacies were identified that were deposited in a variety of environments, including hypersaline lagoons, restricted lagoons, shallow-lagoons, sand shoals and beaches, sand shoal edges, intertidal, tidal-flats, and coastal settings. These carbonates shoal up to supratidal sabkha evaporites that are characterized by nodular and chicken-wire structures. Occasionally, laminated evaporites are subaqueously deposited in shallow-lagoons. The overlying red siliciclastic deposits that occur above the evaporite unit within each cycle are composed of detritus derived from the Zagros Mountains to the northeast of the basin, and were deposited in different alluvial depositional environments of a distal alluvial plain, as river channel deposit, palaeosols, but probably also with significant aeolian dust input in an arid coastal setting. These results allow the inference that the depositional settings record accumulation mainly in an inner ramp setting, on a continuously and gradually dipping ramp that generally dipped from north-east to south-west.

The cycles show variations from the basin margin to the basin centre. The margin of the basin has covered approximately 50km of the area where the cycles comprise interbeddings of calcareous mudstone, carbonate, evaporite, and red siliciclastic deposits upward throughout each of the cycles. In contrast, the cycles at the basin centre are predominately composed of interbedded calcareous mudstone/carbonate and evaporite with the only occurrence of red siliciclastics being as minor accumulations in the upper part of cycles in the upper member of the formation. A number of significant observations can be made with respect to the carbonate-evaporite cycles, as well as the succession as a whole: (i) the preserved thickness of the formation decreases from the basin centre towards the basin margin. At the basin margin it is between 50 and 300m thick, whereas in the basin centre it is between 600 to 900m thick; (ii) the number of cycles decreases toward the margin where 12 to 40 cycles are documented, whereas about 50 cycles have been recorded in the basin centre; and (iii) the thickness of each

cycle is 5 to 13 m in the lower part of the formation, but only 1 to 5 m in the upper part of the formation.

The succession reveals a stack of high-frequency shallowing-upward cycles. Each cycle is passes up from hypersaline conditions, through shallow marine packstones and grainstones to shallow-lagoons, sand shoals or beaches, and intertidal deposits, into the supratidal sabkha and distal alluvial plain deposits. This trend varies toward the upper part of the succession where the evaporite component is reduced or missing, marine deposits including calcareous mudstone and shallow marine carbonate deposits decline, and siliciclastic deposits become predominant. These changes in depositional components toward the upper part of the succession indicate an overall shallowing-upward or regressive succession that prograded toward the basin, to the south-west. The cycles prograded through time which in turn resulted in the migration of the shoreline toward the southwest of the basin. The progradation continued throughout the Miocene and into the Pliocene, when fluvial deposits of the overlying Injana and Mukdadiya Formations covered the whole region. Thickness variations in the cycles, as well as of the whole succession, from the basin margin into the basin centre, reflect this progradation and migration of the shoreline. This resulted in the preservation of a minimum number of cycles and thinner succession around the basin margin, whereas a thicker succession was accumulated at the basin centre. The preservation of only a reduced number of cycles at the basin margin was also due to onlapping the cycles onto a sequence boundary at the base of the succession that resulted in the whole succession not being preserved at the basin margin.

The deposition of the thick evaporite succession of the Fatha Formation was a response to hot and arid climatic conditions during the Miocene that is known as the Miocene Climatic Optimum, in the early stages of the longer-term Neogene-Quaternary ice-house. However, the reduction or absence of evaporites in the upper part of the Fatha Formation succession may record an increasingly wet and humid climate around the north-eastern margin of the basin (close to the growing Zagros mountain range), this decrease in the intensity of the aridity toward the upper part of the succession being different from the time-equivalent, highly evaporative conditions in the basin centre where evaporites were still accumulating. The more humid climate is clearly also reflected in the upper Miocene to Pliocene fluvial deposits of the Injana and Mukdadiya

Formations, which are predominately composed of fluvial deposits with very minor marine deposits.

Sequence stratigraphic investigations and isotope dating of the Fatha Formation reveal that it was deposited during a 3rd-order accommodation cycle (50-300m thick, 2.5 Myr duration) that is in turn composed of a number of 4th-order parasequences (12-40 cycles, each approximately 60,000 years in duration). The Fatha Formation was deposited between about 18 and 15.45 million years ago. The 3rd-order sequence is bounded by a sequence boundary at the base that is characterized by an erosional unconformity at the margin, and correlative conformity in the basin centre. The parasequences are characterized by shallowing-upward cycles that are bounded by flooding surfaces. The parasequences in the lower part of the Fatha Formation succession overlapped the sequence boundary and form a retrogradational stacking pattern, whereas the parasequences in the upper part of the succession form a progradational stacking pattern. The correlation of the parasequences reveals that (i) the individual parasequences may be correlated over at least several tens of kilometres across the studied sections, (ii) several carbonate marker beds are extensive and may be used for correlation, (iii) two main retrogradational and progradational cycle-sets are recognized and extensively correlated over the whole studied area, and (iv) the number of cycles in each cycle-set varies from place to place and a few cycles pinch out laterally, possibly as the result of autogenic sedimentary mechanisms. The retrogradational parasequence set accumulated during increasing accommodation creation due to either sea-level rise or increased subsidence rates, whereas the progradational set was deposited during decelerating accommodation space as a result of high sediment supply and/or possibly lower subsidence rates. Systematic variations in thickness define a third-order accommodation cycle that is regionally correlative over the whole studied area. The lateral extent of the 4th-order stacking patterns are characteristic of glacio-eustatic sea-level fluctuations during the Miocene. These glacio-eustatic sea-level fluctuations are generated as a result of waxing and waning of glaciation due to orbital forcing of climate variations. In addition, the extensive correlation of the parasequence sets is unlikely to be the result of tectonic oscillations. However, overall thickness variations away from palaeo-highs are probably the result of syn-sedimentary tectonic activity (regional variations in subsidence rates) or of subtle compaction differentials due to underlying stratigraphic thickness variations.

The Paradox Basin (Pennsylvanian-Permian, USA) and the Zechstein Basin (late Permian, Central Europe) are well-known examples of cyclical carbonate-evaporite successions with high-frequency and composite orders of cyclicity and have been the focus of a number of high-resolution sequence stratigraphic studies. Comparison of these with the carbonate-evaporite cycles of the Fatha Formation helps to explain the interactions of the various factors that influenced and controlled the architecture of these basins. Among these factors, palaeo-climate variations, tectono-stratigraphic trends, and basin configurations have been the main influences and controls on these basins' depositional architectures. Glacio-eustatic sea-level fluctuations are inferred to have been the main mechanism that generated the higher-frequency cyclicities in each case. These basins have some criteria in common: (i) they contain high-frequency composite orders of carbonate-evaporite parasequences, (ii) the parasequences, as well as parasequence sets and lower order sequences, are regionally correlative across the whole of each basin, (iii) they all include sites of accumulation of thick halite deposits, and (iv) they were developed during arid and semi-arid climates. In general, the cycles of the Fatha Formation more closely resemble those of the Paradox Basin cycles in term of stratigraphic trends and stacking geometries, and they were both terminated by the progradation of siliciclastics infilling the basin.

A distinct sequence stratigraphic model for cyclical carbonate-evaporite successions on a ramp margin has been developed, based upon the study of the Fatha Formation. It is suggested that this may also be applicable to the uppermost cycles of the Zechstein Basin, where developed on a gradually dipping basin margin, where sabkha deposits developed. Access to more detailed log records of the Zechstein cycles would be needed to test this. This new sequence stratigraphic model for cyclical carbonate-evaporite successions on a ramp margin may have wider application to similar successions elsewhere in the geological record.

References

- Abdol Rassul, A.H. and Al-Sheikhly, S.S. 2001. Ostracoda of Fatha Formation (M. Miocene), from Central Iraq. *Al-Rafidain Journal of Science*. **12**(4), pp.47-59.
- Abou-Ouf, M., Durgaprasada Rao, N. and Taj, R. 1988. Benthic foraminifera from littoral sediments of Al Lith-Al Qunfidhah coast, southeastern Red Sea. *Indian journal of marine sciences*. **17**(3), pp.217-221.
- Abreu, V., Pederson, K., Neal, J. and Bohacs, K.M. 2014. A Simplified Guide For Sequence Stratigraphy: Nomenclature, Definitions and Method. In: *2014 GSA Annual Meeting in Vancouver, British Columbia*.
- Aghwan, T.A. 2004. Mineralogical maturity, weathering index, climate and tectonic setting of Injana Formation based on petrographic constituents of sandstones in Komal syncline-north Iraq. *Iraqi journal of earth science*. **4**(1), pp.47-57.
- Ahr, W.M. 1973. The carbonate ramp: an alternative to the shelf model. *Gulf Coast Association of Geological Societies Transactions*. **23**, pp.221-225.
- Ajel, M. 2004. *Sedimentology of the transitional zone of non-marine deposits in the Fatha Formation (Middle Miocene) in selected sections in N and NW of Iraq*. MSc thesis, University of Baghdad.
- Al-Juboury, A. 2009. Palygorskite in Miocene rocks of northern Iraq: environmental and geochemical indicators. *Acta Geologica Polonica*. **59**(2), pp.269-282.
- Al-Juboury, A., Al-Naqip, S. and Al-Juboury, A. 2001. Sedimentology, Mineralogy and Depositional Environments of the Clastic Units, Fatha Formation, (Middle Miocene), South of Mosul, Iraq. *Dirasat*. **28**(1), pp.80-105.
- Al-Juboury, A., Al-Tarif, A. and Al-Eisa, M. 2007. Basin analysis of the Burdigalian and Early Langhian successions, Kirkuk Basin, Iraq. In: Schreiber, B.C. Lugli, S. and Ba, Bel, M. eds. *Evaporites Through Space and Time*. London: Geological Society, London, Special Publications, pp.53-68.
- Al-Juboury, A., McCann, T. and Ghazal, M. 2009. Provenance of Miocene sandstones in northern Iraq: constraints from framework petrography, bulk-rock geochemistry and mineral chemistry. *Russian Geology and Geophysics*. **50**(6), pp.517-534.
- Al-Juboury, A.I. and McCann, T. 2008. The Middle Miocene Fatha (Lower Fars) formation, Iraq. *GeoArabia*. **13**(3), pp.141-174.
- Al-Juboury, Z.A. and Al-Kawaz, H.A. 2008. Geochemistry of marl sidements within Fatha Formation at selected localities, northern Iraq. *Iraqi journal of earth science*. **8**(2), pp.27-46.
- Al-Kawaz, H.A. and Al-Juboury, Z.A. 2006. Mineralogy and petrography of marl sediments within the Fatha Formation in selected parts of northern Iraq. *Rafidain Journal Society*. **17**(1), pp.19-31.
- Al-Mubarak, M. and Youkhana, R. 1977. *The Regional Geological Mapping of Al-Fatha-Mosul Area*. Baghdad: State Organization for Minerals (SOM) Library Reports.
- Al-Rawi, Y.T., Sayyaeb, A.S., Jassim, J.A., Tamar-Agha, M., Al-Sammarai, A.I., Karim, S.A.B., M.A. , Dhiab, S.H., Faris, F.M. and Anwar, F. 1993. New names for some of the late Early Miocene-Pliocene formations of Iraq (Fatha, Injana, Mukdadiya and Bai-Hassan Formations). *Iraqi Geological Journal*. **25**, pp.1-18.
- Al-Juboury, A., Al-Ghrear, J. and Al-Rubaii, M. 2010. Petrographic and diagenesis characteristics of the Late Oligocene-Lower Miocene Ghar Formation in SE Iraq. *Journal of Petroleum Geology*. **33**(1), pp.67-85.

- Alasad, R., Montanez, I., Holterhoff, P.F. and Calvo, J.P. 2014. Precessional-driven climate cyclicity in Pennsylvanian Benwood Fm, Dunkard Basin, eastern Ohio. In: *2014 GSA Annual Meeting in Vancouver, British Columbia*.
- Algeo, T.J. and Wilkinson, B.H. 1988. Periodicity of mesoscale Phanerozoic sedimentary cycles and the role of Milankovitch orbital modulation. *The Journal of Geology*. pp.313-322.
- Alsharhan, A.S. and Kendall, C.G.S.C. 2003. Holocene coastal carbonates and evaporites of the southern Arabian Gulf and their ancient analogues. *Earth-Science Reviews*. **61**(3), pp.191-243.
- Ameen, B.M. 2006. Geological relations between clastic, evaporite and limestone layers of Fatha Formation in the High Folded Zone, NE-IRAQ. *Journal of Iraqi geological society*.
- Ameen, B.M. and Karim, K.H. 2007. Evidence of tempestite and possible turbidite in the middle Miocene lagoonal deposits of Lower Fars Formation, Kurdistan region, NE Iraq. In: *The second international conference of geo-resource of the middle east and north Africa, Feb., Cairo University*. Geo resource of the Middle East and north Africa-II, pp.745-756.
- Amirshahkarami, M. 2013. Microfacies correlation analysis of the Oligocene-Miocene Asmari Formation, in the central part of the Rag-e-Safid anticlinal oil field, Zagros Basin, south-west Iran. *Turkish Journal of Earth Sciences*. **22**(2), pp.204-219.
- Amirshahkarami, M., Vaziri-Moghaddam, H. and Taheri, A. 2007. Sedimentary facies and sequence stratigraphy of the Asmari Formation at Chaman-Bolbol, Zagros Basin, Iran. *Journal of Asian Earth Sciences*. **29**(5), pp.947-959.
- Aqrawi, A. 1993. Miocene evaporitic sequence of the southern Mesopotamian Basin. *Marine and Petroleum geology*. **10**(2), pp.172-179.
- Aqrawi, A.A., Horbury, A. and Sadooni, F. 2010. *The Petroleum Geology of Iraq*. Beaconsfield, UK: Wiley Online Library.
- Aref, M.A., Attia, O.E. and Wali, A.M. 1997. Facies and depositional environment of the Holocene evaporites in the Ras Shukeir area, Gulf of Suez, Egypt. *Sedimentary Geology*. **110**(1), pp.123-145.
- Arthur, M.A. and Garrison, R.E. 1986. Cyclicity in the Milankovitch band through geologic time: an introduction. *Paleoceanography*. **1**(4), pp.369-372.
- Baars, D. 1966. Pre-Pennsylvanian Paleotectonics--Key to Basin Evolution and Petroleum Occurrences in Paradox Basin, Utah and Colorado. *AAPG Bulletin*. **50**(10), pp.2082-2111.
- Baars, D. 1976. The Colorado Plateau aulacogen—key to continental-scale basement rifting: . In: *Proceedings of the Second International Conference on Basement Tectonics*, pp.157-164.
- Baars, D. and See, D.P. 1968. Pre-Pennsylvanian stratigraphy and paleotectonics of the San Juan Mountains, southwestern Colorado. *Geological Society of America Bulletin*. **79**(3), pp.333-350.
- Baars, D. and Stevenson, G. 1981. Tectonic evolution of the Paradox basin, Utah and Colorado. In: Wiegand, D.L. ed. *Geology of the Paradox Basin*. . Rocky Mountain Association of Geologists, field conference, pp.23-31.
- Baars, D. and Stevenson, G. 1982. Subtle stratigraphic traps in Paleozoic rocks of Paradox basin. In: Halbouty, M.T. ed. *The Deliberate Search for the Subtle Trap*. The American Association of Petroleum Geologists, Memior 32, pp.131-158.
- Bahroudi, A. and Koyi, H.A. 2004. Tectono-sedimentary framework of the Gachsaran Formation in the Zagros foreland basin. *Marine and Petroleum Geology*. **21**(10), pp.1295-1310.

- Baker, A.A., Dane, C.H. and Reeside Jr, J.B. 1933. Paradox formation of eastern Utah and western Colorado. *American Association of Petroleum Geologists Bulletin*. **17**(8), pp.963-980.
- Banham, S.G. and Mountney, N.P. 2013. Controls on fluvial sedimentary architecture and sediment-fill state in salt-walled mini-basins: Triassic Moenkopi Formation, Salt Anticline Region, SE Utah, USA. *Basin Research*. **25**(6), pp.709-737.
- Bate, R. 1971. The distribution of recent ostracoda in the Abu Dhabi Lagoon, Persian Gulf. *Paleoecologie des Ostracodes. Bull Rech Pau-SNPA*. **5**, pp.239-225.
- Becker, F. and Bechstädt, T. 2006. Sequence stratigraphy of a carbonate-evaporite succession (Zechstein 1, Hessian Basin, Germany). *Sedimentology*. **53**(5), pp.1083-1120.
- Benton, M., Cook, E. and Turner, P. 2002. *Permian and Triassic red beds and the Penarth Group of Great Britain*. Peterborough: Geological Conservation Review Series, Joint Nature Conservation Committee. p.337.
- Berger, A. 1977. Support for the astronomical theory of climatic change. *Nature*. **269**(5623), pp.44-45.
- Berger, A. 1988. Milankovitch theory and climate. *Reviews of geophysics*. **26**(4), pp.624-657.
- Betzler, C. and Pawellek, T. 2014. Facies, stratigraphic architecture and high-resolution sequence stratigraphy of the Zechstein anhydrite (Werra Anhydrite) in Menslage area (Lower Saxony, N Germany). *Zeitschrift der Deutschen Gesellschaft für Geowissenschaften*. **165**(3), pp.331-344.
- Beydoun, Z., Clarke, M.H. and Stoneley, R. 1992. Petroleum in the Zagros Basin: A Late Tertiary Foreland Basin Overprinted onto the Outer Edge of a Vast Hydrocarbon-Rich Paleozoic-Mesozoic Passive-Margin Shelf: Chapter 11. In: Macqeen, R. and Leckie, D.A. eds. *Foreland basins and fold belts*. American Association of Petroleum Geologists Memoir 55, pp.309-339.
- Beydoun, Z.R. 1991. Arabian plate hydrocarbon geology and potential. *American Association of Petroleum Geologists, Studies in Geology*. **33**, p77.
- Bodergat, A.-M. 1983. *Les ostracodes, témoins de leur environnement: approche chimique et écologie en milieu lagunaire et océanique*. Département des sciences de la terre, Université Claude-Bernard.
- Bodergat, A.-M. 2008. Ecophenotypic ornamentation of ostracods species and salinity of the ambient water. In: *Workshop "Methods in Ostracodology: Citeseer*, pp.7-12.
- Boersma, A. 1978. Foraminifera. In: Haq, B.U. and Boersma, A. eds. *Introduction to Marine micropaleontology*. New York: Elsevier, pp.19-77.
- Boltovskoy, E. and Wright, R. 1976. *Recent foraminifera*. The Hague, Netherlands.: Junk, W.
- Borer, J. and Harris, P. 1991. Lithofacies and Cyclicity of the Yates Formation, Permian Basin: Implications for Reservoir Heterogeneity (1). *AAPG Bulletin*. **75**(4), pp.726-779.
- Börner, K. 2004. Evaporite basins with emphasis on the Permian Zechstein. *Institute of Geology, Freiberg University of Mining and Technology, Germany*.
- Bosence, D., Procter, E., Aurell, M., Kahla, A.B., Boudagher-Fadel, M., Casaglia, F., Cirilli, S., Mehdie, M., Nieto, L. and Rey, J. 2009. A dominant tectonic signal in high-frequency, peritidal carbonate cycles? A regional analysis of Liassic platforms from Western Tethys. *Journal of Sedimentary Research*. **79**(6), pp.389-415.
- Bosence, D.W. and Wilson, R.C. 2003. Carbonate depositional systems. In: Coe, A.L. ed. *The sedimentary record of sea-level change*. Cambridge, UK: Open University, pp.209-233.

- Bradshaw, J. 1961. Laboratory experiments on the ecology of foraminifera. *Contributions from the Cushman Foundation for Foraminiferal research*. **12**(3), pp.87-106.
- Brown, A.L. 2002. *Outcrop to Subsurface Stratigraphy of the Pennsylvanian Hermosa Group Southern Paradox Basin USA*. PhD thesis, West Virginia University.
- Brown, L. and Fisher, W. 1977. Seismic-stratigraphic 46 interpretation of depositional systems: Examples from the Brazilian rift and pull-apart basins. In: Payton, C. ed. *Seismic stratigraphy: application to hydrocarbon exploration*. American Association of Petroleum Geologists Memoir 26.
- Buday, T. 1980. *Regional Geology of Iraq: Stratigraphy and Paleogeography*. Mosul, Iraq: Dar Al-Kutub.
- Burchette, T. and Wright, V. 1992. Carbonate ramp depositional systems. *Sedimentary Geology*. **79**(1), pp.3-57.
- Busch, R.M. and Rollins, H.B. 1984. Correlation of Carboniferous strata using a hierarchy of transgressive-regressive units. *Geology*. **12**(8), pp.471-474.
- Busk, H.G. 1918. Some notes on the geology of the Persian oilfields. *Institution of petroleum technologists*. **5**, pp.3-26.
- Cain, S.A. and Mountney, N.P. 2009. Spatial and temporal evolution of a terminal fluvial fan system: the Permian Organ Rock Formation, South-east Utah, USA. *Sedimentology*. **56**(6), pp.1774-1800.
- Carozzi, A.V. 1961b. Distorted oolites and pseudoolites. *Journal of Sedimentary Research*. **31**(2), pp.262-274.
- Catacosinos, P., Daniels Jr, P. and Harrison III, W. 1990. Structure, stratigraphy, and petroleum geology of the Michigan Basin. In: Leighton, M.W., Kolata, D.F., Oltz, D.F. and Eidel, J.J. eds. *Interior cratonic basins*. Tulsa: AAPG Memoir 51, pp.561-601.
- Catuneanu, O. 2006. *Principles of sequence stratigraphy*. New York: Elsevier.
- Chassefiere, B., Lundhardt, O. and Levy, A. 1969. Données nouvelles sur les cadoules (édifices coquilliers) de la lagune de Thau (Hérault.). *Compte Rendu Sommaire Des Séances De La Société Géologique De France*. **5**, pp.140-142.
- Cloetingh, S. 1988. Intraplate stresses: a new element in basin analysis. In: Kleinspehn, K., Paolo, C. ed. *New perspectives in basin analysis*. Berlin: Springer, pp.205-230.
- Coe, A.L. and Church, K.D. 2003. Sea-level change. In: Coe, A.L. ed. *The Sedimentary Record of Sea-Level Change*. The Open University: Cambridge University Press, pp.34-55.
- Condon, S.M. 1997. *Geology of the Pennsylvanian and Permian Cutler group and Permian Kaibab limestone in the Paradox Basin, southeastern Utah and southwestern Colorado*. US. Department of the Interior, U.S. Geol. Surv. Bull. 46
- Corrochano, D., Barba, P. and Colmenero, J.R. 2012. Glacioeustatic cyclicality of a Pennsylvanian carbonate platform in a foreland basin setting: an example from the Bachende Formation of the Cantabrian Zone (NW Spain). *Sedimentary Geology*. **245**, pp.76-93.
- Crevello, P.D. 1991. High-frequency carbonate cycles and stacking patterns: interplay of orbital forcing and subsidence on Lower Jurassic rift platforms, High Atlas, Morocco. *Sedimentary Modeling: Computer Simulations and Methods for Improved Parameter Definition: Kansas Geological Survey, Bulletin*. **233**, pp.207-230.
- Cúneo, N.R. 1996. Permian phytogeography in Gondwana. *Palaeogeography, Palaeoclimatology, Palaeoecology*. **125**(1), pp.75-104.

- Curran, H.A. 1985. *Biogenic structures: Their use in interpreting depositional environments*. Tulsa: Society of Economic Paleontologists and Mineralogists Special Publication.
- De Deckker, P. 2002. Ostracod palaeoecology. *The ostracoda: applications in Quaternary research*. pp.121-134.
- Debenay, J.-P., Geslin, E., Eichler, B.B., Duleba, W., Sylvestre, F. and Eichler, P. 2001. Foraminiferal assemblages in a hypersaline lagoon, Araruama (RJ) Brazil. *The Journal of Foraminiferal Research*. **31**(2), pp.133-151.
- Driese, S.G. and Dott Jr, R. 1984. Model for Sandstone-Carbonate. *AAPG Bulletin*. **68**(5), pp.574-597.
- Dunham, R.J. 1962. Classification of carbonate rocks according to depositional textures. In: Ham, W.E. ed. *Classification of Carbonate Rocks*. Tulsa: Memoir of the American Association of Petroleum Geologists, pp.108-121.
- Dunnington, H.V. 1958. Generation, migration, accumulation, and dissipation of oil in northern Iraq: Middle East. In: Weeks, L.G. ed. *Habitat of oil*. Tulsa, Oklahoma, USA: American Association of Petroleum Geologists, pp.1194-1251.
- Eide, M.G. 1993. *The facies, depositional environment, and cyclicity of the Queen Formation (Guadalupian, Permian), North Ward-Estes Field, Ward County, Texas*. PhD thesis, Texas A&M University.
- Elder, W.P., Gustason, E.R. and Sageman, B.B. 1994. Correlation of basinal carbonate cycles to nearshore parasequences in the Late Cretaceous Greenhorn seaway, Western Interior USA. *Geological Society of America Bulletin*. **106**(7), pp.892-902.
- Embry, A. 2009. Practical sequence stratigraphy. *Canadian Society of Petroleum Geologists*. **79**.
- Embry, A., Johannessen, E.P., Owen, D. and Beauchamp, B. 2007. Recommendations for sequence stratigraphic surfaces and units (abstract). In: *Arctic Conference Days, Tromso, Norway*.
- Embry, A.F. 2001. The six surfaces of sequence stratigraphy. In: *Hedberg Conference on sequence stratigraphic and allostratigraphic principles and concepts, Dallas*. American Association of Petroleum Geologists, pp.26-27.
- Embry, A.F. and Klovan, J.E. 1971. A Late Devonian reef tract on northeastern Banks Island, NWT. *Bulletin of Canadian Petroleum Geology*. **19**(4), pp.730-781.
- Fielding, C.R. and Webb, J.A. 1996. Facies and cyclicity of the Late Permian Bainmedart Coal Measures in the Northern Prince Charles Mountains, MacRobertson Land, Antarctica. *Sedimentology*. **43**(2), pp.295-322.
- Fischer, A.G. 1964. The Lofer cyclothems of the alpine Triassic. In: Merriam, D.F. ed. *Symposium of cyclic sedimentation*. State Geological Survey of Kansas Bulletin, pp.107-150.
- Fischer, A.G. 1984. The two Phanerozoic supercycles. In: Berggren, W.A. and Van Couvering, J.A. eds. *Catastrophes and Earth History: The New Uniformitarianism*. Princeton University Press Princeton, NJ, pp.129-150.
- Fischer, A.G. 1986. Climatic rhythms recorded in strata. *Annual Review of Earth and Planetary Sciences*. **14**, p351.
- Flügel, E. 2004. *Microfacies of Carbonate Rocks: Analysis, Interpretation and Application*. New York: Springer-Verlag.
- Fracasso, M. and Hovorka, S. 1986. Cyclicity in the Middle Permian San Andres Formation, Palo Duro Basin, Texas Panhandle, Texas Bureau of Economic Geology, UT Austin, Texas. *Report of Investigations*. (156).
- Galloway, W.E. 1989. Genetic stratigraphic sequences in basin analysis I: architecture and genesis of flooding-surface bounded depositional units. *AAPG bulletin*. **73**(2), pp.125-142.

- Garbett, E.C. and Maddocks, R.F. 1979. Zoogeography of Holocene cytheracean ostracodes in the bays of Texas. *Journal of Paleontology*. pp.841-919.
- García-García, F., Soria, J.M., Viseras, C. and Fernández, J. 2009. High-Frequency Rhythmicity in a Mixed Siliciclastic–Carbonate Shelf (Late Miocene, Guadix Basin, Spain): A Model of Interplay Between Climatic Oscillations, Subsidence, and Sediment Dispersal. *Journal of Sedimentary Research*. **79**(5), pp.302-315.
- Garrison, R., Schreiber, B., Bernoulli, D., Fabricius, F., Kidd, R. and Melieres, F. 1978. Sedimentary petrology and structures of Messinian evaporitic sediments in the Mediterranean Sea, leg 42A, Deep Sea Drilling Project. In: Hsu, K. and Montadert, L. eds. *Initial Reports of the Deep Sea Drilling Project*. Washington: U.S. Government Printing Office, pp.571-612.
- Geel, T. 2000. Recognition of stratigraphic sequences in carbonate platform and slope deposits: empirical models based on microfacies analysis of Palaeogene deposits in southeastern Spain. *Palaeogeography, Palaeoclimatology, Palaeoecology*. **155**(3), pp.211-238.
- Geluk, M. 2000a. Late Permian (Zechstein) carbonate-facies maps the Netherlands. *Geologie en Mijnbouw*. **79**(1), pp.17-28.
- Geluk, M. 2000b. Steps towards successful prediction of the internal tectonics of salt structures. In: *Proceedings of the 8th World Salt Symposium*. Elsevier (Amsterdam), pp.125-130.
- Geluk, M. 2007. Permian. In: Wong, T.E., Batjes, D.a.J. and De Jager, J. eds. *Geology of the Netherlands*. Royal Netherlands Academy of Arts and Sciences, pp.63-83.
- Geluk, M.C. 2005. *Stratigraphy and tectonics of Permo-Triassic basins in the Netherlands and surrounding areas*. PhD thesis, Utrecht University.
- Gertsch, B., Keller, G., Adatte, T., Berner, Z., Kassab, A., Tantawy, A., El-Sabbagh, A. and Stueben, D. 2010. Cenomanian–Turonian transition in a shallow water sequence of the Sinai, Egypt. *International Journal of Earth Sciences*. **99**(1), pp.165-182.
- Ghafur, A. 2012. *Sedimentology and reservoir characteristics of the Oligocene-Early Miocene carbonates (Kirkuk Group) of southern Kurdistan*. PhD thesis, Cardiff University.
- Ghazi, S., Mountney, N.P. and Sharif, S. 2015. Lower Permian fluvial cyclicity and stratigraphic evolution of the northern margin of Gondwanaland: Warchha Sandstone, Salt Range, Pakistan. *Journal of Asian Earth Sciences*. **105**, pp.1-17.
- Gheith, A.G. and Auf, M.A.A. 1996. Textural characteristics, mineralogy and fauna in the shore zone sediments at Rabigh and Sharm Al-Kharrar, eastern Red Sea, Saudi Arabia. *Marine Sciences-Ceased Issuerg*. **17**(1), pp.1-2.
- Ghosh, A.K. and Sarkar, S. 2013. Facies analysis and paleoenvironmental interpretation of Piacenzian carbonate deposits from the Guitar Formation of Car Nicobar Island, India. *Geoscience Frontiers*. **4**(6), pp.755-764.
- Gianniny, G.L. and Miskell-Gerhardt, K.J. 2009. Progradational mixed siliciclastic/carbonate sequence sets on the tectonically active eastern margin of the Pennsylvanian Paradox Basin, southwestern Colorado. In: Houston, W.S., Wray, L.L. and Moreland, P.G. eds. *The Paradox Basin Revisited-New Developments in Petroleum Systems and Basin Analysis*. Colorado: The Rocky Mountain Association of Geologists Special Publication, pp.310-380.
- Gill, W.D. and Ala, M.A. 1972. Sedimentology of Gachsaran Formation (lower Fars series), Southwest Iran. *American Association of Petroleum Geologists Bulletin*. **56**(10), pp.1965-1974.
- Ginsburg, R.N. ed. 1975. *Tidal deposits, a casebook of recent examples and fossil counterparts*. New York: Springer-Verlag.

- Glennie, K. 1986. Development of NW Europe's Southern Permian gas basin. *Geological Society, London, Special Publications*. **23**(1), pp.3-22.
- Goff, J.C., Jones, R.W. and Horbury, A.D. 1995. Cenozoic basin evolution of the northern part of the Arabian Plate and its control on hydrocarbon habitat. In: *Middle East Petroleum Geosciences, GEO94, Bahrain*. pp.402-412.
- Goldhammer, R., Oswald, E. and Dunn, P. 1991. Hierarchy of stratigraphic forcing: Example from Middle Pennsylvanian shelf carbonates of the Paradox Basin. In: Franseen, E.K., Watney, L.K. and Kendall, C.G.S.C. eds. *Sedimentary Modeling: Computer Simulations and Methods for Improved Parameter Definition*. Kansas Geological Survey Bulletin, pp.361-413.
- Goldhammer, R., Oswald, E. and Dunn, P. 1994. High-Frequency, Glacio-Eustatic Cyclicality in the Middle Pennsylvanian of the Paradox Basin: An Evaluation of Milankovitch Forcing. In: Boer, P.L. and Smith, D.G. eds. *Orbital Forcing and Cyclic Sequences*. International Association of Sedimentologists, Special Publication 19, pp.243-283.
- Goldhammer, R.K., Dunn, P.A. and Hardie, L. 1987a. High frequency glacio-eustatic sealevel oscillations with Milankovitch characteristics recorded in Middle Triassic platform carbonates in northern Italy. *American Journal of Science*. **287**(9), pp.853-892.
- Goldhammer, R.K., Dunn, P.A. and Hardie, L.A. 1987b. High frequency glacio-eustatic sealevel oscillations with Milankovitch characteristics recorded in Middle Triassic platform carbonates in northern Italy. *American Journal of Science*. **287**(9), pp.853-892.
- Goodall, I., Harwood, G., Kendall, A. and McKie, T. 1992. Discussion on sequence stratigraphy of carbonate– evaporite basins: models and application to the Upper Permian (Zechstein) of northeast England and adjoining North Sea. *Journal*, vol. 148, 1991, pp. 1019-1036. Reply. *Journal of the Geological Society*. **149**, pp.1050-1054.
- Grabowski, G.J. and Liu, C. 2009. Ages and Correlation of Cenozoic Strata of Iraq. In: *International Petroleum Technology Conference, 7-9 December, Doha, Qatar*. International Petroleum Technology Conference.
- Grabowski, G.J. and Liu, C. 2012. Age, Correlation, Depositional Environments, and Sedimentary History of the Fat'ha Formation (Burdigalian, Lower Miocene) of Iraq. In: *GEO 2012*.
- Grammer, G.M., Eberli, G.P., Van Buchem, F.S., Stevenson, G.M. and Homewood, P. 1996. Application of high-resolution sequence stratigraphy to evaluate lateral variability in outcrop and subsurface—Desert Creek and Ismay intervals, Paradox Basin. In: *Rocky Mountain Section (SEPM)*.
- Grotzinger, J. 1996. Cycle stacking and long-term sea-level history in the Lower Cretaceous (Gavrovo Platform, NW Greece). *Journal of Sedimentary Research*. **66**(4), pp.723-736.
- Grotzinger, J.P. 1986a. Cyclicality and paleoenvironmental dynamics, Rocknest platform, northwest Canada. *Geological Society of America Bulletin*. **97**(10), pp.1208-1231.
- Grotzinger, J.P. 1986b. Upward shallowing platform cycles: A response to 2.2 billion years of low-amplitude, high-frequency (Milankovitch band) sea level oscillations. *Paleoceanography*. **1**(4), pp.403-416.
- Hamid, S.F. 1994. *Sedimentological studies of Fatha Formation in sheikh Ibrahim and Butmah anticlines, SW Iraq*. thesis, University of Mosul.
- Handford, C.R. and Loucks, R.G. 1993. Carbonate depositional sequences and systems tracts-responses of carbonate platforms to relative sea-level changes. In: Loucks,

- R.G.a.S.J.F. ed. *Carbonate sequence stratigraphy, recent developments and applications*. Tulsa, Oklahoma, USA: AAPG memoir 57, pp.3-3.
- Haq, B.U. and Al-Qahtani, A.M. 2005. Phanerozoic cycles of sea-level change on the Arabian Platform. *GeoArabia, Manama*. **10**(2), pp.127-160.
- Haq, B.U. and Boersma, A. eds. 1998. *Introduction to marine micropaleontology*. Singapore: Elsevier.
- Haq, B.U., Hardenbol, J. and Vail, P.R. 1988. Mesozoic and Cenozoic chronostratigraphy and cycles of sea-level change. In: Wilgus, C.K., Hastings, B. S., Kendall, C. G. St. C., Posamentier, H. W., Ross, C. A., and Van Wagoner, J. C. ed. *Sea-level Changes: an integrated approach*. Society of Economic Paleontologists and Mineralogists Special Publication 42, pp.71–108.
- Haq, B.U. and Schutter, S.R. 2008. A chronology of Paleozoic sea-level changes. *Science*. **322**(5898), pp.64-68.
- Hardie, L.A. 1986. Carbonate tidal-flat deposition: ten basic elements. *Colorado School of Mines Quarterly*. **81**(1), pp.3-6.
- Hardie, L.A. and Eugster, H.P. 1971. The depositional environment of marine evaporites: a case for shallow, clastic accumulation. *Sedimentology*. **16**(3-4), pp.187-220.
- Hariri, M.S. 2008. Effect of hydrographic conditions on the ecology of benthic foraminifera in two different hypersaline lagoons, eastern Red Sea coast, Kingdom of Saudi Arabia. *Journal of King Abdulaziz University: Marine Science*. **19**, pp.3-13.
- Haupt, B.J. and Seidov, D. 2012. Modeling geologically abrupt climate changes in the Miocene: Potential effects of high-latitude salinity changes. *Natural science*. **4**(3), pp.149-158.
- Hawramy, O.A. and Khalaf, S.K. 2013. Ostracoda of Fat'ha Formation (Middle Miocene) from (Darbandikhan and Aghjalar) sections, Sulaimani-Kurdistan Region/Northeastern Iraq. *Journal of Zankoy Sulaimani-Part A (JZS-A)*. **15**(3), p3.
- Hentz, T.F. and Zeng, H. 2003. High-frequency Miocene sequence stratigraphy, offshore Louisiana: Cycle framework and influence on production distribution in a mature shelf province. *AAPG bulletin*. **87**(2), pp.197-230.
- Hite, R. and Buckner, D. 1981. Stratigraphic correlations, facies concepts, and cyclicity in Pennsylvanian rocks of the Paradox Basin. In: Wiegand, D.L., ed. *Geology of the Paradox Basin: Rocky Mountain Association of Geologists, Field Conference*. pp.147-159.
- Hite, R.J. 1960. Stratigraphy of the saline facies of the Paradox Member of the Hermosa Formation of southeastern Utah and southwestern Colorado. In: *Geology of the Paradox basin fold and fault belt: 3rd Annual Field Conference: Four Corners Geological Society*, pp.86-89.
- Hite, R.J. 1975. An unusual northeast-trending fracture zone and its relations to basement wrench faulting in northern Paradox Basin, Utah and Colorado. In: Fasset, J., ed. *Four Corners Geological Society 8th Field Conference, Guidebook, Canyonlands country*. pp.217-223.
- Hoffman, P. 1976b. Stromatolite Morphogenesis in Shark Bay, Western Australia. In: Walter, M.R. ed. *Stromatolites*. Amsterdam: Elsevier, Developments in Sedimentology, pp.261-271.
- Hollis, C., Vahrenkamp, V., Tull, S., Mookerjee, A., Taberner, C. and Huang, Y. 2010. Pore system characterisation in heterogeneous carbonates: An alternative approach to widely-used rock-typing methodologies. *Marine and Petroleum geology*. **27**(4), pp.772-793.

- Hudson, J. 1963. The recognition of salinity-controlled mollusc assemblages in the Great Estuarine Series (Middle Jurassic) of the Inner Hebrides. *Palaeontology*. **6**(2), pp.318-326.
- Hussein, D.O. 2016. *Reservoir characterization of ramp carbonates: Lessons from the Lower Miocene Euphrates and Jeribe Formations, Kurdistan, northern Iraq*. Unpublished PhD thesis, University of Leeds, UK.
- Ibrahim, G. 1979. Sabkha sediments of Lower Fars Formation, northern Iraq. *Unpublished MSc Thesis University of Bristol*.
- Inden, R.F. and Moore, C.H. 1983. Beach Environment. In: Scholle, P.A., Bebout, D. G. And Moore, C. H. ed. *Carbonate depositional environments*. Tulsa, Oklahoma: The American association of petroleum geologists, pp.212-240.
- Ingo, S. and Lehmann, C. 2002. Detailed Sequence Stratigraphic Interpretation of Mixed Carbonate-Evaporite Reservoir Systems: The Permian (Zechstein) of Germany and the Lower Cretaceous of NE Mexico. In: *AAPG Annual Meeting 2002, Texas*.
- James, G.A. and Wynd, J.G. 1965. Stratigraphic nomenclature of Iranian oil consortium agreement area. *American Association of Petroleum Geologists bulletin*. **49**(12), pp.2182-2245.
- Jassim, S.Z. and Goff, J.C. 2006. *Geology of Iraq*. First ed. Zelny trh 6, Brno, Czech Republic: Dolin, Prague and Moravian Museum, Brno.
- John, C.M., Karner, G.D., Browning, E., Leckie, R.M., Mateo, Z., Carson, B. and Lowery, C. 2011. Timing and magnitude of Miocene eustasy derived from the mixed siliciclastic-carbonate stratigraphic record of the northeastern Australian margin. *Earth and Planetary Science Letters*. **304**(3), pp.455-467.
- Jordan, O.D. and Mountney, N.P. 2012. Sequence Stratigraphic Evolution and Cyclicity of An Ancient Coastal Desert System: The Pennsylvanian–Permian Lower Cutler Beds, Paradox Basin, Utah, USA. *Journal of Sedimentary Research*. **82**(10), pp.755-780.
- Karim, K.H. 2010. Modification of the time-expanded stratigraphic column of north east Iraq. *Petroleum geology of Iraq, Baghdad. Abstract Book*, p4.
- Kassim, S.A. 2006. Paleoenvironmental Indicators of Clay Minerals in Miocene Sediments, Northern Iraq. *Damascus University Journal for Basic Sciences*. **22**(1), pp.59-70.
- Keen, A.M. and Coan, E.V. 1974. *Marine molluscan genera of western North America: An illustrated key*. Stanford, California: Stanford University Press.
- Keen, M. 1977. Ostracod assemblages and the depositional environments of the Headon, Osborne and Bembridge Beds (Upper Eocene) of the Hampshire Basin. *Palaeontology*. **20**(2), pp.405-445.
- Kendall, A.C. 1978b. Facies models 12. Subaqueous evaporites. *Geoscience Canada*. **5**(3), pp.124-139.
- Kendall, A.C. 1992. Evaporites. In: Walker, R.G., James, Noel P. ed. *Facies Models: Responses to sealevel change*. Geological Association of Canada, pp.375-409.
- Kendall, A.S., AlSharhan, C.G.S.C. and Cohen, A. 2002. The Holocene tidal flat complex of the Arabian Gulf coast of Abu Dhabi. In: Boer, B. and Barth, H.J. eds. *The sabkhas of the Arabian Peninsula region: Distribution and ecology*. Dordrecht, the Netherlands: Kluwer Academic Publishers, pp.21-35.
- Kendall, C.G.S.C. and Patrick, A. 1969. Holocene shallow-water carbonate and evaporite sediments of Khor al Bazam, Abu Dhabi, southwest Persian Gulf. *AAPG Bulletin*. **53**(4), pp.841-869.
- Kendall, C.G.S.C., Weber, L.J. and Alsharhan, A.S. 2009. The Giant Oil Field Evaporite Association: A Function of the Wilson Cycle, Climate, Basin Position and Sea Level. In: *AAPG Annual Convention, June 7-10, Denver, Colorado*.

- Khalaf, S.K. 1988. Middle Miocene ostracoda from northern Iraq. *Developments in Palaeontology and Stratigraphy*. **11**, pp.1113-1124.
- Khalifa, M.A., El Ghar, M.S., Helal, S.A. and Hussein, A.W. 2004. Depositional history of the Eocene drowned carbonate platform (Drunka Formation), west of Assiut-Minia Stretch, western Desert, Egypt. In: *7th international conference on the geology of the Arab world, Feb. , Cairo University*. pp.233-254.
- Khanaqa, P.A., Karim, S.A., Sissakian, V.K. and Karim, K.H. 2009. Lithostratigraphic study of a Late Oligocene–Early Miocene succession, south of Sulaimaniyah, NE Iraq. *Iraqi Bulletin of Geology and Mining*. **5**(2), pp.41-57.
- Kharajiany, S. 2008. *Sedimentary facies of Oligocene rock units in Ashdagh mountain—Sangaw district—Kurdistan region, NE Iraq*. MSc thesis, University of Sulaimani.
- Khodjanyazova, R.R., Davydov, V.I., Montañez, I.P. and Schmitz, M.D. 2014. Climate- and eustasy-driven cyclicality in Pennsylvanian fusulinid assemblages, Donets Basin (Ukraine). *Palaeogeography, Palaeoclimatology, Palaeoecology*. **396**, pp.41-61.
- Kilenyi, T.I. 1972. Transient and balanced genetic polymorphism as an explanation of variable nodding in the ostracode *Cyprideis torosa*. *Micropaleontology*. pp.47-63.
- Kinsman, D.J. 1969. Modes of formation, sedimentary associations, and diagnostic features of shallow-water and supratidal evaporites. *AAPG Bulletin*. **53**(4), pp.830-840.
- Kinsman, D.J. and Park, R.K. 1976. Algal belt and coastal sabkha evolution, Trucial Coast, Persian Gulf. *Developments in Sedimentology*. **20**, pp.421-433.
- Kominz, M. 2001. Sea level variations over geologic time. *Encyclopedia of Ocean Sciences*. pp.2605-2613.
- Koop, W., Stoneley, R., Ridd, M., Murphy, R., Osmaston, M. and Kholief, M. 1982. Subsidence history of the Middle East Zagros basin, Permian to Recent [and discussion]. *Philosophical Transactions of the Royal Society of London A: Mathematical, Physical and Engineering Sciences*. **305**(1489), pp.149-168.
- Kushnir, J. 1981. Formation and early diagenesis of varved evaporite sediments in a coastal hypersaline pool. *Journal of Sedimentary Research*. **51**(4), pp.1193-1203.
- Lasemi, Y., Jahani, D., Amin-Rasouli, H. and Lasemi, Z. 2012. Ancient carbonate tidalites. In: Davis, R.a.a.D., R. W. ed. *Principles of Tidal Sedimentology*. Dordrecht Heidelberg London New York: Springer, pp.567-607.
- Legler, B. and Schneider, J. 2013. High-frequency cyclicality preserved in nonmarine and marine deposits (Permian, Germany and North Sea). In: Lucas, S.G., Dimichele, W.A., Barrick, J.E., Schneider, Joerg W., Spielmann, J.A. ed. *The Carboniferous-Permian Transition*. New Mexico Museum of Natural History and Science Bulletin, pp.200-211.
- Logan, B.W. 1987. *The MacLeod evaporite basin, Western Australia: Holocene environments, sediments and geological evolution*. American Association of Petroleum Geologists.
- Loope, D.B. 1984. Eolian origin of upper Paleozoic sandstones, southeastern Utah. *Journal of Sedimentary Research*. **54**(2).
- Loope, D.B. 1988. Rhizoliths in ancient eolianites. *Sedimentary Geology*. **56**(1), pp.301-314.
- Lorenz, J.C. and Cooper, S.P. 2009. Extension-Fracture Patterns in Sandstones Above Mobile Salt: The Salt Valley Anticline, Arches National Park, Utah. In: Houston, W.S.Wray, L.L. and Moreland, P.G. eds. *The Paradox Basin Revisited - New Developments in Petroleum Systems and Basin Analysis*. RMAG Special Publication pp.198-220.

- Machel, H.G. and Burton, E.A. 1991. Burial-diagenetic sabkha-like gypsum and anhydrite nodules. *Journal of Sedimentary Research*. **61**(3), pp.394-405.
- Mahdi, A.I. 2007. Fossils Mollusca (Bivalve) from the Fatha Formation of northern Iraq. *Iraqi Bulletin of Geology and Mining*. **3**(1), pp.41-53.
- Manzi, V., Gennari, R., Lugli, S., Roveri, M., Scafetta, N. and Schreiber, B.C. 2012. High-frequency cyclicity in the Mediterranean Messinian evaporites: evidence for solar–lunar climate forcing. *Journal of Sedimentary Research*. **82**(12), pp.991-1005.
- Mawson, M. and Tucker, M. 2009. High-frequency cyclicity (Milankovitch and millennial-scale) in slope-apron carbonates: Zechstein (Upper Permian), North-east England. *Sedimentology*. **56**(6), pp.1905-1936.
- McArthur, J., Donovan, D., Thirlwall, M., Fouke, B. and Matthey, D. 2000. Strontium isotope profile of the early Toarcian (Jurassic) oceanic anoxic event, the duration of ammonite biozones, and belemnite palaeotemperatures. *Earth and Planetary Science Letters*. **179**(2), pp.269-285.
- McCann, T. 2008. Mesozoic and Cenozoic. In: McCann, T. ed. *The Geology of Central Europe, volume 2*: . Bonn University, Germany: Geological Society of London, p.748.
- Menning, M. and Commission, G.S. 2002. A geologic time scale 2002. *Stratigraphic Table of Germany*. pp.3-00.
- Miall, A. 2010. *The geology of stratigraphic sequences*. Berlin Heidelberg: Springer Science & Business Media.
- Michaelsen, P. and Henderson, R.A. 2000. Facies relationships and cyclicity of high-latitude, Late Permian coal measures, Bowen Basin, Australia. *International Journal of Coal Geology*. **44**(1), pp.19-48.
- Miller, K.G., Feigenson, M.D., Wright, J.D. and Clement, B.M. 1991. Miocene isotope reference section, Deep Sea Drilling Project Site 608: an evaluation of isotope and biostratigraphic resolution. *Paleoceanography*. **6**(1), pp.33-52.
- Miller, K.G., Kominz, M.A., Browning, J.V., Wright, J.D., Mountain, G.S., Katz, M.E., Sugarman, P.J., Cramer, B.S., Christie-Blick, N. and Pekar, S.F. 2005. The Phanerozoic record of global sea-level change. *science*. **310**(5752), pp.1293-1298.
- Mitchum, R.M., Vail, P. and Thompson III, S. 1977. Seismic stratigraphy and global changes of sea level: Part 2. The depositional sequence as a basic unit for stratigraphic analysis Section 2. Application of seismic reflection configuration to stratigraphic interpretation. In: Payton, C. ed. *Seismic stratigraphy: application to hydrocarbon exploration*. AAPG Memoir 26, pp.53-62.
- Mitchum, R.M. and Van Wagoner, J.C. 1991. High-frequency sequences and their stacking patterns: sequence-stratigraphic evidence of high-frequency eustatic cycles. *Sedimentary Geology*. **70**(2), pp.131-160.
- Mohamed, M., Madkour, H. and El-Taher, A. 2013. Recent benthic foraminifera in the saline pool and its surrounding areas at ras shuukier and Gulf of Suez, Egypt. *Indian Journal of Geo-Marine Sciences*. **42**(3), pp.293-299.
- Montanez, I.P. and Osleger, D.A. 1993. Parasequence Stacking Patterns, Third-Order Accommodation Events, and Sequence Stratigraphy of Middle to Upper Cambrian Platform Carbonates, Bonanza King Formation, Southern Great Basin: Chapter 12. In: Loucks, R.G.a.S., J. F. ed. *Carbonate sequence stratigraphy, recent developments and applications*. Tulsa, Oklahoma, USA: AAPG Memoir
- Mountney, N.P. 2006. Periodic accumulation and destruction of aeolian erg sequences in the Permian Cedar Mesa Sandstone, White Canyon, southern Utah, USA. *Sedimentology*. **53**(4), pp.789-823.

- Murray, J.W. 1973. *Distribution and ecology of living benthic foraminiferids*. New York, Crane, Russak.
- Murray, J.W. 1991. *Ecology and palaeoecology of benthic foraminifera*. Essex: Longman, Harlow.
- Nagy, Z.R., Somerville, I.D., Gregg, J.M., Becker, S.P. and Shelton, K.L. 2005. Lower Carboniferous peritidal carbonates and associated evaporites adjacent to the Leinster Massif, southeast Irish Midlands. *Geological Journal*. **40**(2), pp.173-192.
- Neal, J. and Abreu, V. 2009. Sequence stratigraphy hierarchy and the accommodation succession method. *Geology*. **37**(9), pp.779-782.
- Nederlandse Aardolie Maatschappij, B.V. and Rijks Geologische Dienst. 1980. *Stratigraphic nomenclature of the Netherlands*. Koninklijk Nederlands Geologisch Mijnbouwkundig Genootschap.
- Nielsen, S., Paulsen, G., Hansen, D., Gemmer, L., Clausen, O., Jacobsen, B., Balling, N., Huuse, M. and Gallagher, K. 2002. Paleocene initiation of Cenozoic uplift in Norway. *Geological Society, London, Special Publications*. **196**(1), pp.45-65.
- Nissenbaum, A. 1980. Hypersaline brines and evaporitic environments. In: *Bat-Sheva Seminar on Saline Lakes and Natural Brines (1977: Weizmann Institute of Science)*: Elsevier Scientific Pub. Co.; distribution for the US and Canada, Elsevier/North-Holland.
- Nottvedt, A., Gabrielsen, R. and Steel, R. 1995. Tectonostratigraphy and sedimentary architecture of rift basins, with reference to the northern North Sea. *Marine and Petroleum Geology*. **12**(8), pp.881-901.
- Nuccio, V.F. and Condon, S.M. 1996. *Burial and thermal history of the Paradox Basin, Utah and Colorado, and petroleum potential of the Middle Pennsylvanian Paradox Basin*. US. Department of the Interior, U.S. Geol. Surv. Bull. 41
- Numan, N.M. 1997. A plate tectonic scenario for the Phanerozoic succession in Iraq. *Iraqi Geological Journal*. **30**(2), pp.85-110.
- O'Brien, C. 1957. Salt diapirism in south Persia. *Geologie en Mijnbouw*. **19**, pp.357-376.
- Odin, G.S. and Gale, N.H. 1982. Mise à jour d'échelles des temps calédoïens et hercyniens. *Académie des Sciences, Comptes Rendus*. **249**(2), pp.453-456.
- Ogniben, L. 1955. Inverse graded bedding in primary gypsum of chemical deposition. *Journal of Sedimentary Research*. **25**(4), pp.273-281.
- Osleger, D. 1991. Subtidal carbonate cycles: implications for allocyclic vs. autocyclic controls. *Geology*. **19**(9), pp.917-920.
- Paszkowski, M. and Szydłowski, T. 1986. Evidence of hypersaline sedimentation in Dinantian carbonate deposits in area of Krzeszowice near Kraków. In: *Annales Societatis Geologorum Poloniae*, pp.385-397.
- Paulissen, W.E. and Luthi, S.M. 2011. High-frequency cyclicity in a Miocene sequence of the Vienna Basin established from high-resolution logs and robust chronostratigraphic tuning. *Palaeogeography, Palaeoclimatology, Palaeoecology*. **307**(1), pp.313-323.
- Payton, C.E. 1977. *Seismic stratigraphy: applications to hydrocarbon exploration*. American Association of Petroleum Geologists Tulsa, OK.
- Peterson, J.A. and Hite, R.J. 1969. Pennsylvanian evaporite-carbonate cycles and their relation to petroleum occurrence, southern Rocky Mountains. *American Association of Petroleum Geologists Bulletin*. **53**(4), pp.884-908.
- Pirouz, M., Simpson, G., Bahroudi, A. and Azhdari, A. 2011. Neogene sediments and modern depositional environments of the Zagros foreland basin system. *Geological Magazine*. **148**(5-6), pp.838-853.

- Plint, A.G., Eyles, N., Eyles, C.H. and Walker, R.G. 1992. Control of sea level change. In: Walker, R.G. and James, N.P. eds. *Facies Models–Response to Sea Level Change*. Geological Association of Canada, St. Johns, pp.15-25.
- Posamentier, H. and Vail, P. 1988. Eustatic controls on clastic deposition II: sequence and systems tract models. In: Wilgus, C.K., Hastings, B. S., Kendall, C. G. St.C., Posamentier, H. W., Ross, C. A. And Van Wagoner, J. C. ed. *Sea level changes: an integrated approach*. SEPM Special Publication 42, pp.125-154.
- Posamentier, H.W., Jervey, M. and Vail, P. 1988. Eustatic controls on clastic deposition I: conceptual framework. In: Wilgus, C.K., Hastings, B. S., Kendall, C. G. St.C., Posamentier, H. W., Ross, C. A. And Van Wagoner, J. C. ed. *Sea level changes: an integrated approach*. SEPM Special Publication 42, pp.109-124.
- Rameil, N. 2005. *Carbonate sedimentology, sequence stratigraphy, and cyclostratigraphy of the Tithonian in the Swiss and French Jura Mountains*. thesis, Université de Fribourg.
- Rankey, E.C. 1997. Relations between relative changes in sea level and climate shifts: Pennsylvanian–Permian mixed carbonate-siliciclastic strata, western United States. *Geological Society of America Bulletin*. **109**(9), pp.1089-1100.
- Rasmussen, E. 2004. The interplay between true eustatic sea-level changes, tectonics, and climatic changes: what is the dominating factor in sequence formation of the Upper Oligocene–Miocene succession in the eastern North Sea Basin, Denmark? *Global and Planetary Change*. **41**(1), pp.15-30.
- Rasmussen, L. and Rasmussen, D.L. 2009. Burial history analysis of the Pennsylvanian petroleum system in the deep Paradox Basin Fold and Fault Belt, Colorado and Utah. In: Houston, W.S.Wray, L.L. and Moreland, P.G. eds. *The Paradox Basin revisited-new Developments in Petroleum systems and Basin Analysis*. RMAG Special Publication, pp.24-95.
- Raup, O.B. and Hite, R.J. 1992. *Lithology of evaporite cycles and cycle boundaries in the upper part of the Paradox Formation of the Hermosa Group of Pennsylvanian age in the Paradox Basin, Utah and Colorado*. Washington: US Geological Survey Bulletin 2000-B. 1-37
- Read, J. and Goldhammer, R. 1988. Use of Fischer plots to define third-order sea-level curves in Ordovician peritidal cyclic carbonates, Appalachians. *Geology*. **16**(10), pp.895-899.
- Read, J.F., Osleger, D. and Elrick, M. 1991. Two-dimensional modeling of carbonate ramp sequences and component cycles. *Sedimentary modeling: Computer simulations and methods for improved parameter definition: Kansas Geological Survey Bulletin*. **233**, pp.473-488.
- Richter-Bernburg, G. 1955. Stratigraphische Gliederung des deutschen Zechsteins. *Zeitschrift der deutschen geologischen Gesellschaft*. pp.843-854.
- Richter-Bernburg, G. 1985. Zechstein-Anhydrite-Fazies und Genese. *Geologisches Jahrbuch Reihe* **85**, pp.3-82.
- Roscher, M. and Schneider, J.W. 2006. Permo-Carboniferous climate: Early Pennsylvanian to Late Permian climate development of central Europe in a regional and global context. *Geological Society, London, Special Publications*. **265**(1), pp.95-136.
- Rueger, B.F. 1996. *Palynology and its relationship to climatically induced depositional cycles in the Middle Pennsylvanian (Desmoinesian) Paradox Formation of southeastern Utah*. USA: Geological Survey Bulletin 2000-K. 1-22
- Sadler, P.M., Osleger, D.A. and Montanez, I.P. 1993. On the labeling, length, and objective basis of Fischer plots. *Journal of Sedimentary Research*. **63**(3).

- Sami, T.T. and James, N.P. 1994. Peritidal carbonate platform growth and cyclicity in an early Proterozoic foreland basin, upper Pethei Group, northwest Canada. *Journal of Sedimentary Research*. **64**(2), pp.111-131.
- Sandberg, P.A. 1964. The ostracod genus cyprides in the Americas. *Stockholm Contributions in Geology*. **12**, pp.1-78.
- Sarg, J. 2001. The sequence stratigraphy, sedimentology, and economic importance of evaporite-carbonate transitions: a review. *Sedimentary Geology*. **140**(1), pp.9-34.
- Sarnthein, M. 1978. Sand deserts during glacial maximum and climatic optimum. *Nature* **272**, pp.43-46.
- Schlanger, S.O. 1963. Subsurface geology of Enewetak Atoll. U.S. *Geological Survey Professional Paper*. **260bb**, pp.991-1066.
- Schmitt, W.L. 1957. Barnacles. In: Laad, H.S. ed. *Treatise on marine ecology and paleoecology*. Geological society of America Memoir, pp.1158-1159.
- Scholle, P.A. and Ulmer-Scholle, D.S. 2003. *A Color Guide to the Petrography of Carbonate Rocks: Grains, Textures, Porosity, Diagenesis*. Tulsa, Oklahoma, U.S.A: American Association of Petroleum Geologists Memoir 77.
- Schreiber, B., Tucker, M. and Till, R. 1986. Arid shorelines and evaporites. *Sedimentary environments and facies*. pp.189-228.
- Schreiber, B.C. 1987. Environments of subaqueous gypsum deposition.
- Schreiber, B.C. and Hsü, K.J. 1980. Evaporites. In: Hobson, G.D. ed. *Developments in Petroleum Geology*. Barking: Elsevier, pp.87-138.
- Schreiber, B.C. and Tabakh, M.E. 2000. Deposition and early alteration of evaporites. *Sedimentology*. **47**(s1), pp.215-238.
- Schulmann, K., Catalán, J.R.M., Lardeaux, J.M., Janoušek, V. and Oggiano, G. 2014. The Variscan orogeny: extent, timescale and the formation of the European crust. *Geological Society, London, Special Publications*. **405**(1), pp.1-6.
- Seilacher, A. 1967. Bathymetry of trace fossils. *Marine geology*. **5**(5), pp.413-428.
- Sharland, P.R., Archer, R., Casey, D.M., Davies, R.B., Hall, S.H., Heward, A.P., Horbury, A.D. and Simmons, M.D. 2001. *Arabian Plate Sequence Stratigraphy*. Gulf PetroLink, Bahrain: GeoArabia Special Publication 2.
- Sharland, P.R., Archer, R., Casey, D.M., Davies, R.B., Simmoins, M.D. and Sutcliffe, O.E. 2004. *Arabian Plate Sequence Stratigraphy-revisions to Special Publication 2*. Bahrain: GeoArabia.
- Shawkat, M.G. 1979. *The sedimentology of the Lower Fars Formation (Miocene) of Northern Iraq*. PhD thesis, University of Newcastle Upon Tyne.
- Shawkat, M.G. and Tucker, M.E. 1978. Stromatolites and sabkha cycles from the Lower Fars Formation (Miocene) of Iraq. *Geologische Rundschau*. **67**(1), pp.1-14.
- Sloss, L. 1949. Integrated facies analysis. In: *Sedimentary facies in geologic history: conference at meeting of the Geological Society of America November 11, 1948, New York*. Geological Society of America, p.91.
- Sloss, L. 1963. Sequences in the cratonic interior of North America. *Geological Society of America Bulletin*. **74**(2), pp.93-114.
- Słowakiewicz, M. and Gąsiewicz, A. 2013. Palaeoclimatic imprint, distribution and genesis of Zechstein Main Dolomite (Upper Permian) petroleum source rocks in Poland: Sedimentological and geochemical rationales. *Geological Society, London, Special Publications*. **376**(1), pp.523-538.
- Słowakiewicz, M. and Tucker, M.E. 2012. Microbialites in Zechstein Cycle 2 Carbonates (NE England and Poland): Types and Source Rock Perspectives. In: *AAPG Hedberg Conference "Microbial Carbonate Reservoir Characterization" June 4-8, Houston, Texas*

- Smith, D.B. 1979. Rapid marine transgressions and regressions of the Upper Permian Zechstein Sea. *Journal of the Geological Society*. **136**(2), pp.155-156.
- Soua, M. 2012. Orbital forcing and Milankovitch cyclicity constraint during Permian deposition on the Northern margin of Africa, Southern Tunisia. In: *North Africa Technical Conference and Exhibition*: Society of Petroleum Engineers.
- Spence, G.H. and Tucker, M.E. 2007. A proposed integrated multi-signature model for peritidal cycles in carbonates. *Journal of Sedimentary Research*. **77**(10), pp.797-808.
- Stanescio, J.D., Dubiel, R.F. and Huntoon, J.E. 2000. Depositional environments and paleotectonics of the Organ Rock Formation of the Permian Cutler Group, southeastern Utah. In: Spinkel, D.A., Chidsey, T.C., Jr., and Anderson, P.B. ed. *Geology of Utah's National Parks and Monuments* Utah Geological Association, Publication 28, pp.591-605.
- Stevenson, G. and Baars, D. 1988. Overview: carbonate reservoirs of the Paradox Basin. In: *Occurrence and petrophysical properties of carbonate reservoirs in the Rocky Mountain region: Rocky Mountain Association of Geologists Field Conference*, pp.148-162.
- Strasser, A. 1986. Ooids in Purbeck limestones (lowermost Cretaceous) of the Swiss and French Jura. *Sedimentology*. **33**(5), pp.711-727.
- Strasser, A., Arnaud, H., Baudin, F. and Röhl, U. 1995. Small-scale shallow-water carbonate sequences of Resolution Guyot (Sites 866, 867, and 868): Northwest Pacific atolls and guyots. In: *Proceeding of the ocean drilling program, scientific results, College Station, Texas*. pp.119-131.
- Strohmenger, C., Voigt, E. and Zimdars, J. 1996a. Sequence stratigraphy and cyclic development of Basal Zechstein carbonate-evaporite deposits with emphasis on Zechstein 2 off-platform carbonates (Upper Permian, Northeast Germany). *Sedimentary Geology*. **102**(1), pp.33-54.
- Taufiq, J. and Domas, J. 1977. *Report on the Regional Geological Mapping of Duhok-Ain Zala Area*. Baghdad: GEOSURV.
- Taylor, J. 1998. Upper Permian—Zechstein. In: Glennie, K.W. ed. *Petroleum Geology of the North Sea: Basic Concepts and Recent Advances, Fourth Edition*. Oxford, United Kingdom,: Blackwell Science, pp.174-211.
- Thrana, C. and Talbot, M.R. 2006. High-frequency carbonate-siliciclastic cycles in the Miocene of the Lorca Basin (Western Mediterranean, SE Spain). *Geologica acta*. **4**(3), p343.
- Trudgill, B. 2011. Evolution of salt structures in the northern Paradox Basin: controls on evaporite deposition, salt wall growth and supra-salt stratigraphic architecture. *Basin Research*. **23**(2), pp.208-238.
- Trudgill, B. and Arbuckle, W. 2009. *Reservoir characterization of clastic cycle sequences in the Paradox Formation of the Hermosa Group, Paradox Basin, Utah*. Utah Geological Survey Open-File Report 543. 106
- Trudgill, B.D. and Paz, M. 2009. Restoration of mountain front and salt structures in the northern Paradox Basin, SE Utah. In: Houston, W.S.Wray, L.L. and Moreland, P.G. eds. *The Paradox Basin Revisited - New Developments in Petroleum Systems and Basin Analysis*. RMAG Special Publication, pp.132-177.
- Tucker, M.E. 1991. Sequence stratigraphy of carbonate-evaporite basins: models and application to the Upper Permian (Zechstein) of northeast England and adjoining North Sea. *Journal of the Geological Society*. **148**(6), pp.1019-1036.
- Tucker, M.E. 1992a. Carbonate diagenesis and sequence stratigraphy. In: Wright, V.P. ed. *Sedimentology Review 1*. London: Blackwell Scientific Publications Oxford, pp.51-72.

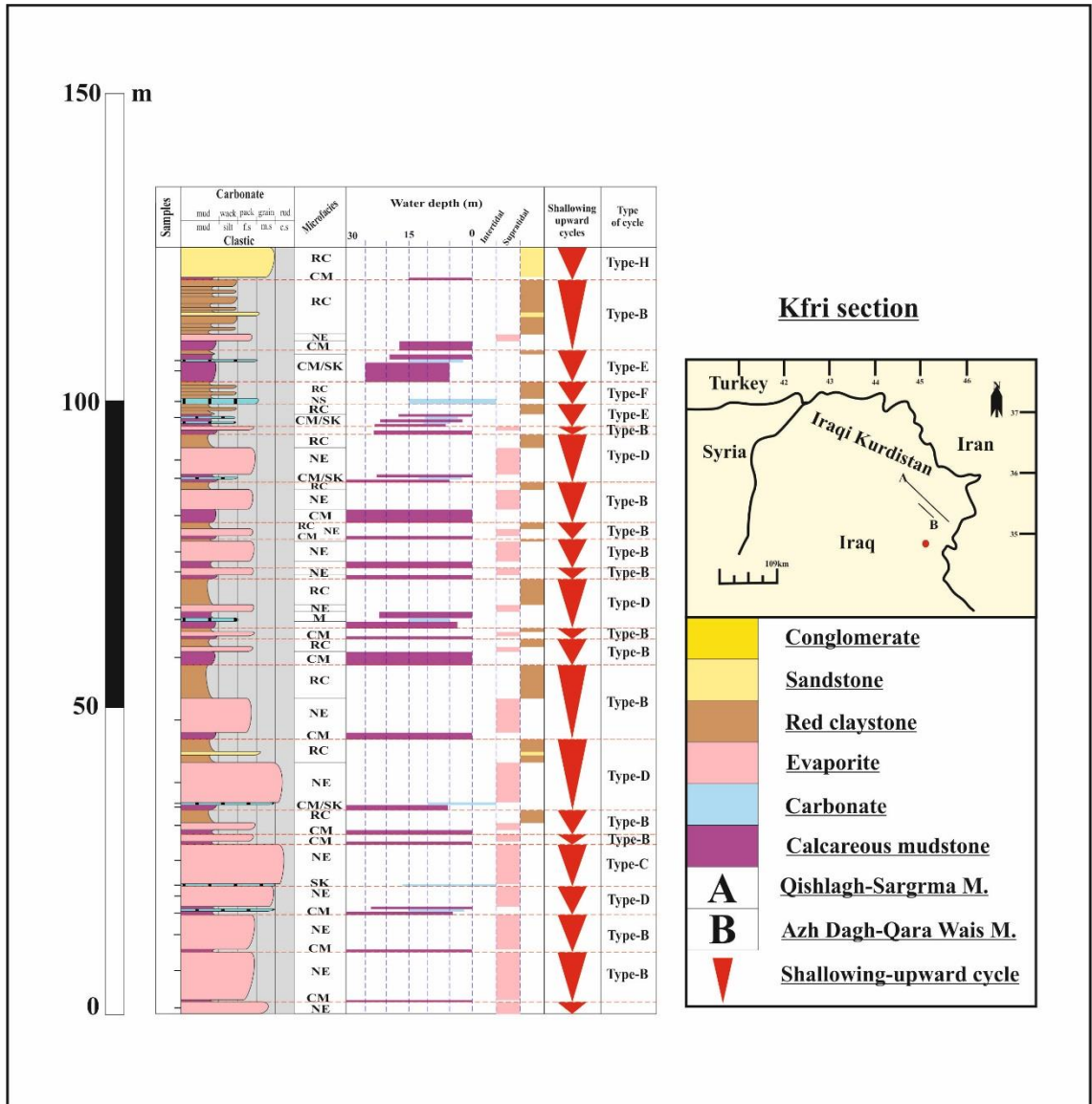
- Tucker, M.E. 1992b. Discussion on sequence stratigraphy of carbonate– evaporite basins: models and application to the Upper Permian (Zechstein) of northeast England and adjoining North Sea. *Journal*, vol. 148, 1991, pp. 1019-1036. Reply. *Journal of the Geological Society*. **149**, pp.1050-1054.
- Tucker, M.E. 1999. Sabkha cycles, stacking patterns and controls: Gachsaran (Lower Fars/Fatha) Formation, Miocene, Mesopotamian Basin, Iraq. *Neues Jahrbuch fur Geologie und Palaontologie-Abhandlungen*. **214**(1-2), pp.45-69.
- Tucker, M.E. 2003. *Sedimentary rocks in the field*. England: John Wiley & Sons.
- Tucker, M.E. and Garland, J. 2010. High-frequency cycles and their sequence stratigraphic context: orbital forcing and tectonic controls on Devonian cyclicity, Belgium *Geologica Belgica*. **13**(3), pp.213-240.
- Tucker, M.E. and Wright, V.P. 1990. *Carbonate Sedimentology*. Oxford, UK: Blackwell Scientific Publications.
- Vail, P.R., Mitchum Jr, R. and Thompson III, S. 1977. Seismic Stratigraphy and Global Changes in Sea Level: Part 3. Relative Changes of Sea Level from Coastal Onlap. In: Payton, C.E. ed. *Seismic Stratigraphy: Applications to Hydrocarbon Exploration*. American Association of Petroleum Geologists, Memoir 26, pp.49-212.
- Vail, P.R. and Todd, R.G. 1981. Northern North Sea Jurassic unconformities, chronostratigraphy and sea-level changes from seismic stratigraphy. In: Illing, L.a.H., G. ed. *Petroleum geology of the continental shelf of northwest Europe*. Heyden London Son, Ltd, pp.216-235.
- Van Adrichem Boogaert, H.A. and Kouwe, W.F.P. 1994. Stratigraphic nomenclature of the Netherlands, revision and update by RGD and NOGEP. *Mededelingen Rijks Geologische Dienst*. **50**.
- van Bellen, R.C., Dunnington, H.V., Wetzel, R. and Morton, D.M. 1959. *Lexique Stratigraphique International, III, Asie, Iraq*. Paris: Centre National de la Recherche Scientifique.
- Van den Belt, F.J. and de Boer, P.L. 2007. A shallow-basin model for ‘saline giants’ based on isostasy-driven subsidence. In: Nichols, G.Williams, E. and Paola, C. eds. *Sedimentary Processes, Environments and Basins: A Tribute to Peter Friend (Special Publication 38 of the IAS)*. Blackwell publishing Ltd., pp.241-251.
- Van Eysinga, F.W. 1975. Geologic Time Table. *Elsevier Scientific Publication Company, Amsterdam*. p1.
- Van Harten, D. 1975. *Cyprideis baetica* n. sp.(Ostracoda, Cytheridae) from the Miocene of southeastern Spain. *Scripta Geologica*. **32**, pp.1-17.
- Van Harten, D. 2000. Variable nodding in *Cyprideis torosa* (Ostracoda, Crustacea): an overview, experimental results and a model from Catastrophe Theory. *Hydrobiologia*. **419**(1), pp.131-139.
- Van Wagoner, J., Mitchum Jr, R., Posamentier, H. and Vail, P. 1987. Seismic Stratigraphy Interpretation Using Sequence Stratigraphy: Part 2: Key Definitions of Sequence Stratigraphy. In: Bally, A.W. ed. *Atlas of seismic stratigraphy*. AAPG Studies in Geology 27, pp.11-14.
- Van Wagoner, J., Mitchum, R., Champion, K. and Rahmanian, V. 1990. Siliciclastic sequence stratigraphy in well logs, cores, and outcrops. *AAPG Methods in Exploration*. (7), p55.
- Van Wagoner, J., Posamentier, H.W., Mitchum, R.M., Vail, P.R., Sarg, J.F., Loutit, T.S. and Hardenbol, J. 1988. An overview of the fundamentals of sequence stratigraphy and key definitions. In: Wilgus, C.K., Hastings, B. S., Kendall, C. G. St.C., Posamentier, H. W., Ross, C. A. And Van Wagoner, J. C. ed. *Sea level changes: an integrated approach*. SEPM Special Publication 42, pp.39-46.

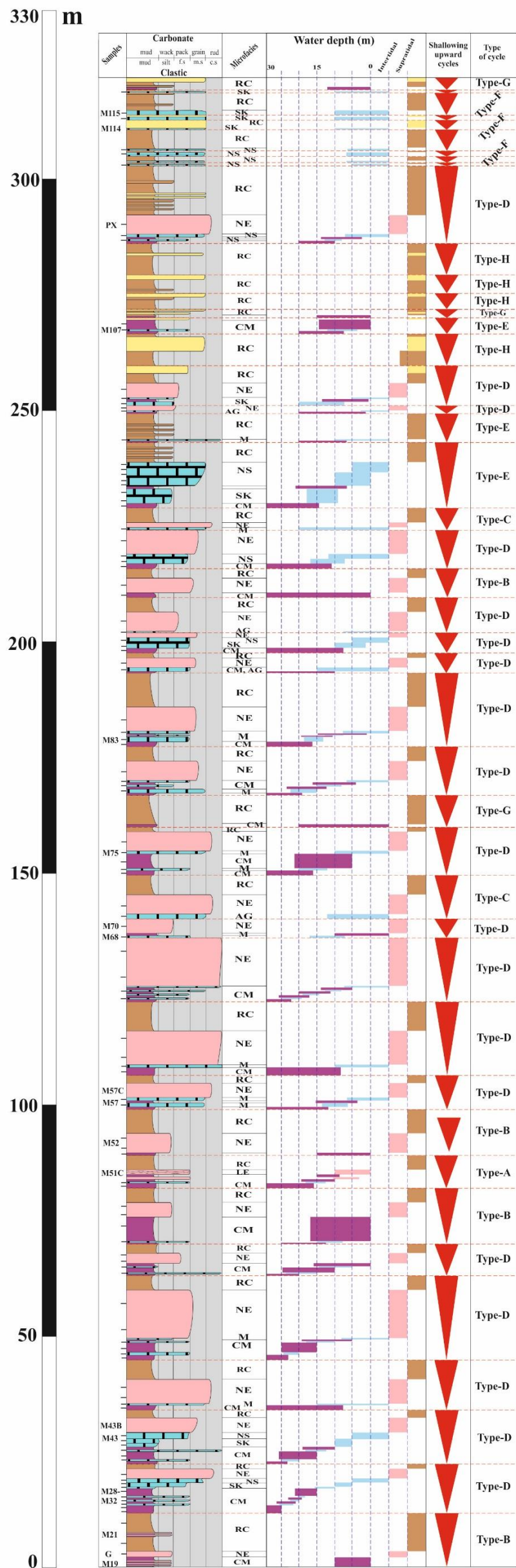
- Van Wagoner, J.C. 1995. Overview of sequence stratigraphy of foreland basin deposits: terminology, summary of papers, and glossary of sequence stratigraphy. In: Van Wagoner, J.C., Bertram, G.T. ed. *Sequence Stratigraphy of Foreland Basin Deposits: Outcrop and Subsurface Examples from the Cretaceous of North America*. American Association of Petroleum Geologists.
- Vaziri-Moghaddam, H., Seyrafian, A., Taheri, A. and Motiei, H. 2010. Oligocene-Miocene ramp system (Asmari Formation) in the NW of the Zagros basin, Iran: microfacies, paleoenvironment and depositional sequence. *Revista Mexicana de Ciencias Geológicas*. **27**(1), pp.56-71.
- Venus, J.H., Mountney, N.P. and McCaffrey, W.D. 2015. Syn-sedimentary salt diapirism as a control on fluvial-system evolution: an example from the proximal Permian Cutler Group, SE Utah, USA. *Basin Research*. **27**(2), pp.152-182.
- Vesper, B. 1975. To the problem of nodding on *Cyprideis torosa* (Jones, 1850). *Bulletin of American Paleontology*. **65**, pp.205-216.
- Wagner, R. and Peryt, T.M. 1997. Possibility of sequence stratigraphic subdivision of the Zechstein in the Polish Basin. *Geological Quarterly*. **41**(4), pp.457-474.
- Wakefield, O.J. and Mountney, N.P. 2013. Stratigraphic architecture of back-filled incised-valley systems: Pennsylvanian–Permian lower Cutler beds, Utah, USA. *Sedimentary Geology*. **298**, pp.1-16.
- Warner, L.A. 1978. The Colorado lineament: a middle Precambrian wrench fault system. *Geological Society of America Bulletin*. **89**(2), pp.161-171.
- Warren, J. 1989. *Evaporite Sedimentology: Its importance in hydrocarbon accumulations*. New Jersey: Prentice-Hall Englewood Cliffs p.285.
- Warren, J.K. 2006. *Evaporites: sediments, resources and hydrocarbons*. Brunei: Springer Science & Business Media.
- Warren, J.K. 2010. Evaporites through time: Tectonic, climatic and eustatic controls in marine and nonmarine deposits. *Earth-Science Reviews*. **98**(3), pp.217-268.
- Warren, J.K. and Kendall, C.G.S.C. 1985. Comparison of sequences formed in marine sabkha (subaerial) and salina (subaqueous) settings--modern and ancient. *American Association of Petroleum Geologists Bulletin*. **69**(6), pp.1013-1023.
- Weber, L.J., Sarg, J.F. and Wright, F.M. 1995. Sequence stratigraphy and reservoir delineation of the Middle Pennsylvanian (Desmoinesian), Paradox basin and Aneth field, southwestern USA: Part 3. In: Read, I.E., Kerans, C.L.I., W.Sarg, J.E. and Wright, F.M. eds. *Milankovitch Sea-level changes, Cycles, and Reservoirs on Carbonate Platforms in Greenhouse and Ice-free Worlds*. Society of Economic Paleontologists and Mineralogists Short Course, pp.1-81.
- Wengerd, S.A. and Matheny, M.L. 1958. Pennsylvanian system of Four Corners region. *American Association of Petroleum Geologists Bulletin*. **42**(9), pp.2048-2106.
- Wilgus, C.K., Hastings, B.S., Kendall, C.G.S.C., Posamentier, H.W., Ross, C.A. and Van Wagoner, J.C. 1988. Sea-level changes: an integrated approach. *SEPM (Society of Economic Paleontologists and Mineralogists), Tulsa, Oklahoma. Special Publication 42*, p407.
- Williams, M.R. 2009. Stratigraphy of Upper Pennsylvanian cyclic carbonate and siliciclastic rocks, western Paradox Basin, Utah. In: Houston, W.S., Wray, L.L. and Moreland, P.G. eds. *The Paradox Basin Revisited — New Developments in Petroleum Systems and Basin Analysis*. Rocky Mountain Association of Geologists Special Publication 2009, pp.381–435.
- Wilson, J.L. 1975. *Carbonate facies in geologic history*. Springer Science & Business Media.
- Wright, V. 1986. Facies sequences on a carbonate ramp: the Carboniferous Limestone of South Wales. *Sedimentology*. **33**(2), pp.221-241.

- Ye, Q., Galloway, W. and Robley, R. 1995. High-frequency glacio-eustatic cyclicality of the Miocene in Central Texas and Western Louisiana and its application in hydrocarbon exploration. *Gulf Coast Association of Geological Societies Transactions*. **XLV**.
- Yusuf, N. 1984. Distribution of benthic foraminifera in the sediments in eastern Red Sea between Jeddah and Yanbu. In: *Proceeding Symposium on Coral Reef Environment of the Red Sea, Jeddah*. King Abdulaziz University, Faculty of Marine Science, pp.216-232.
- Zachos, J., Pagani, M., Sloan, L., Thomas, E. and Billups, K. 2001. Trends, rhythms, and aberrations in global climate 65 Ma to present. *Science*. **292**(5517), pp.686-693.
- Zachos, J.C., Stott, L.D. and Lohmann, K.C. 1994. Evolution of Early Cenozoic marine temperature. *Paleoceanography*. **9**(2), pp.353-387.
- Zhao, Q., Jian, Z., Wang, J., Cheng, X., Huang, B., Xu, J., Zhou, Z., Fang, D. and Wang, P. 2001. Neogene oxygen isotopic stratigraphy, ODP Site 1148, northern South China Sea. *Science in China Series D: Earth Sciences*. **44**(10), pp.934-942.
- Ziegler, A., Scotese, C. and Barrett, S. 1983. Mesozoic and Cenozoic paleogeographic maps. In: Brosche, P., and Sundermann, J. ed. *Tidal friction and the earth's rotation, II*. Berlin: Springer-Verlag, pp.240-252.
- Ziegler, M.A. 2001. Late Permian to Holocene paleofacies evolution of the Arabian Plate and its hydrocarbon occurrences. *GeoArabia*. **6**, pp.445-504.
- Ziegler, P. 1990. *Geological Atlas of Western and Central Europe*. Amsterdam: Shell Internationale Petroleum Maatschappij BV/Geological Society of London.

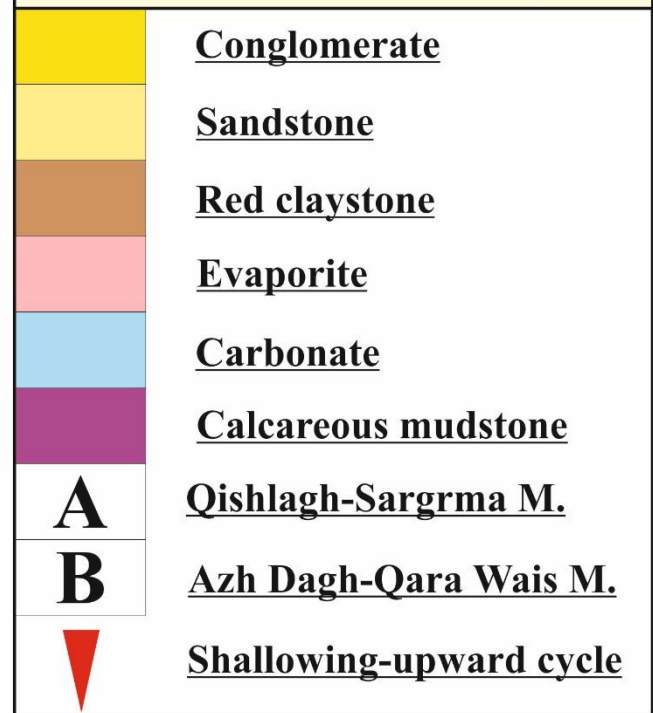
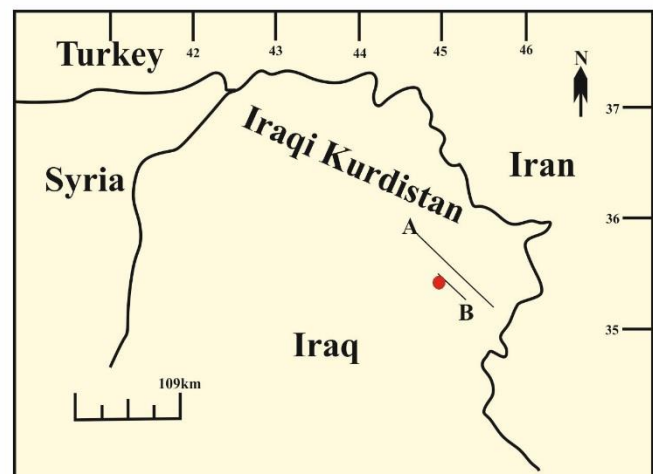
Appendices

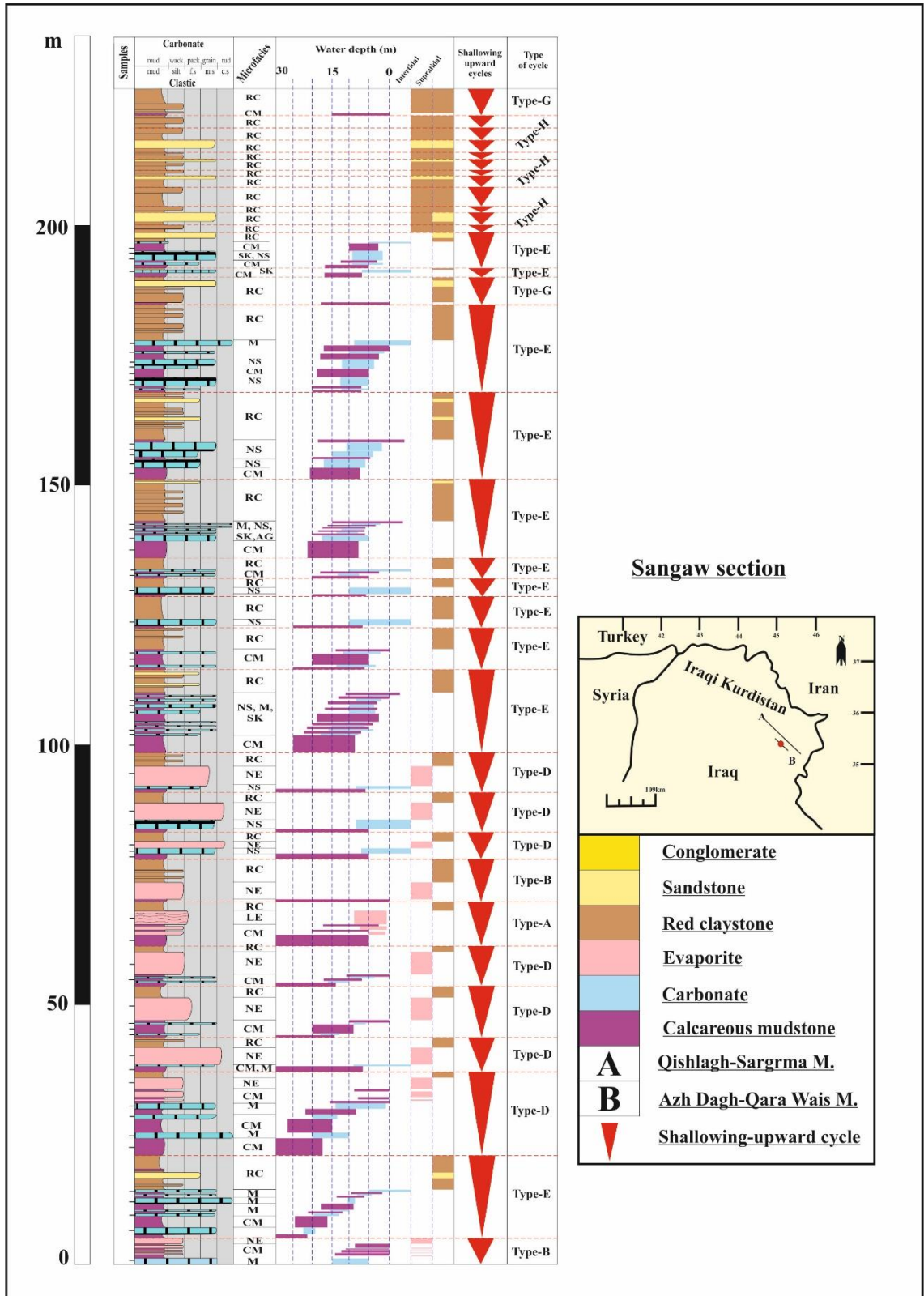
Appendix 1 - Stratigraphic logs of the study areas



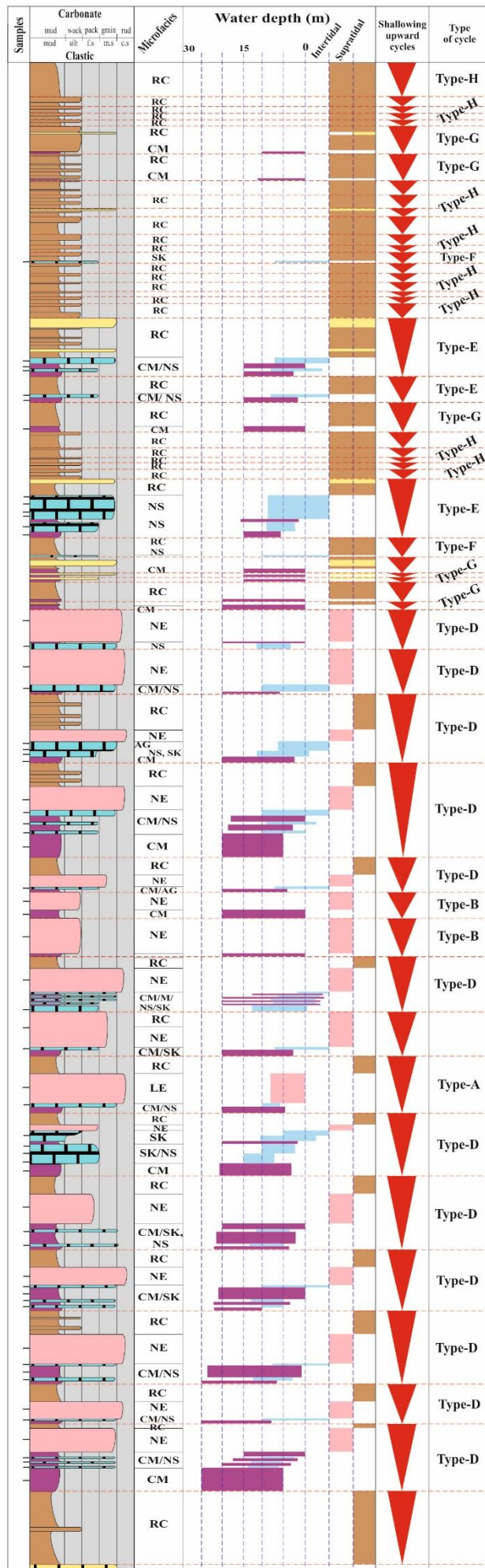


Mamlaha section

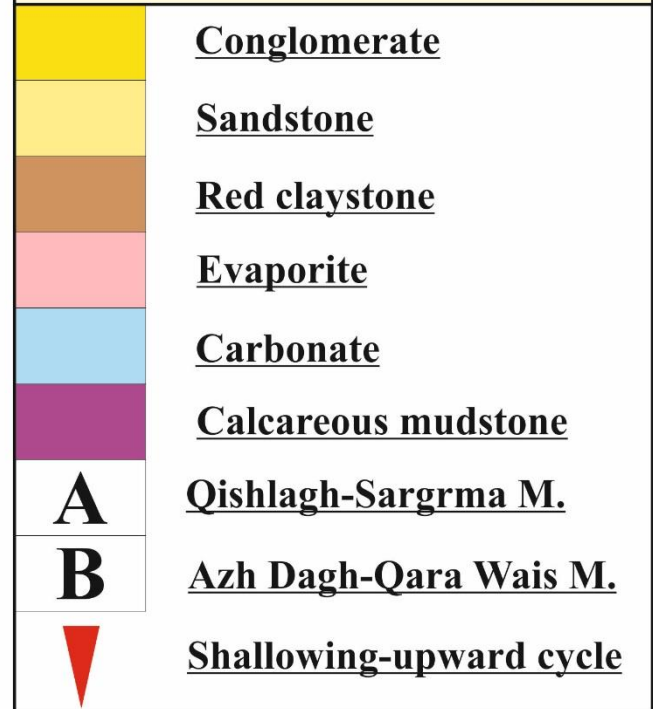


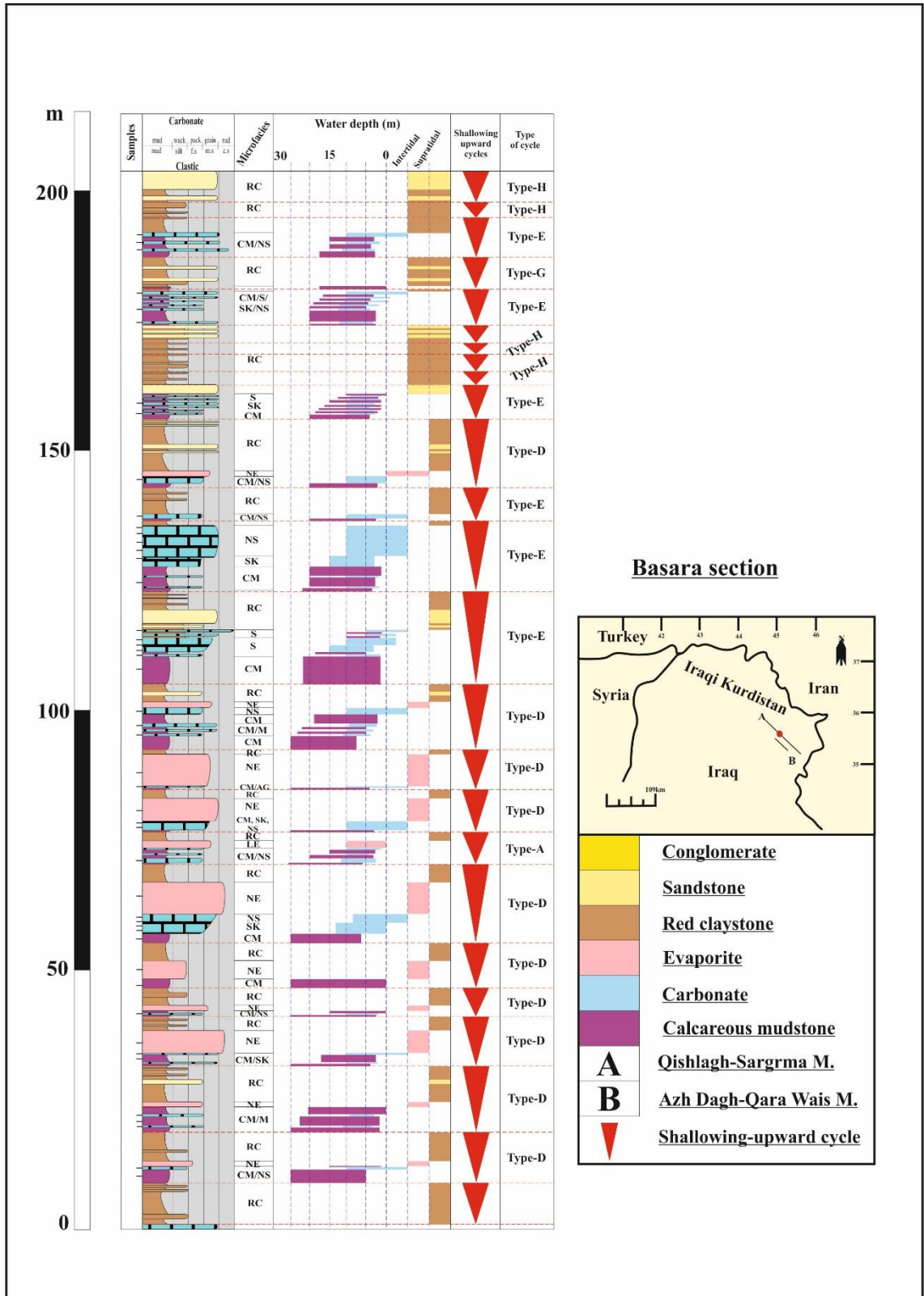


330
300
250
200
150
100
50
0

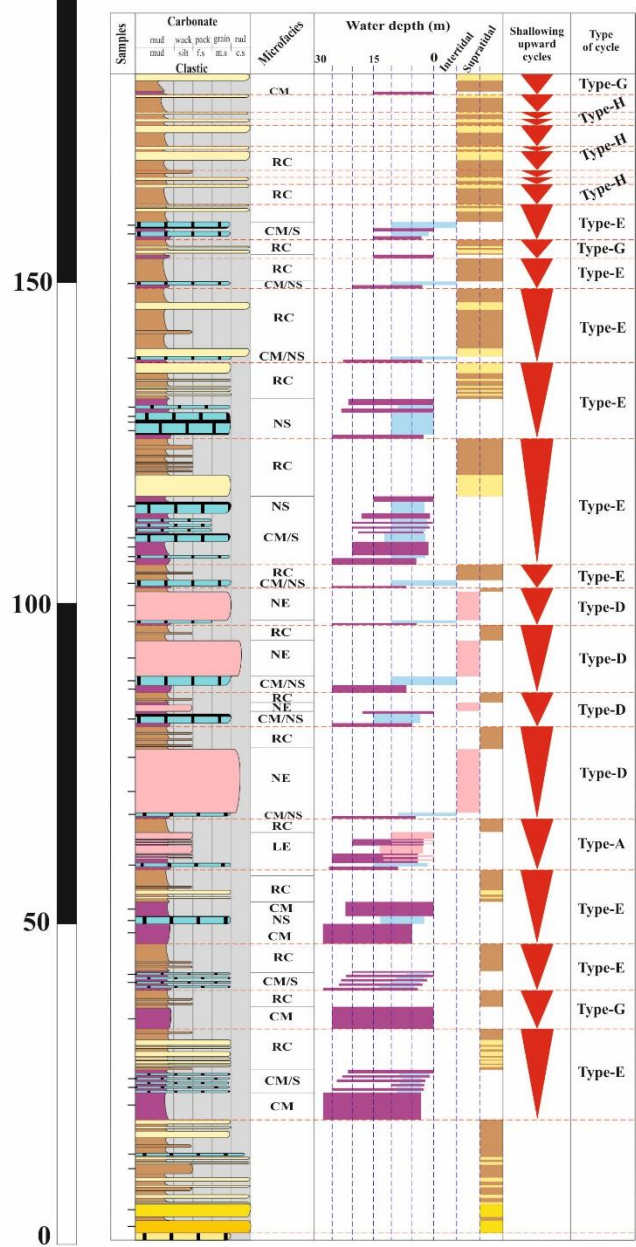


Takiya section

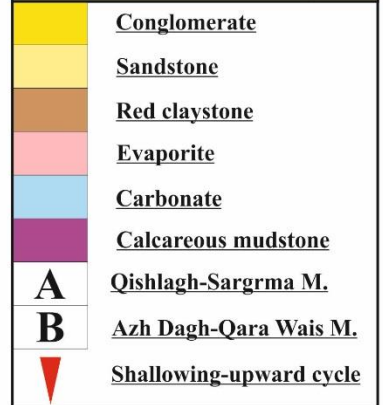




200 m



Darbandikhan section



Appendix 2 - Tables of number, thickness, cumulative thickness, and cumulative departure of the cycles

1- Kfri Section

Cycle No.	Calcareous mudstone (m)	Carbonate (m)	Evaporite (m)	Red siliciclastic (m)	Cycle thickness (m)	Cumulative thickness (m)	Cumulative departure (m)
0	0	0	0	0	0	0.00	0.00
1	0	0	3	0	3	3.00	-1.56
2	0.3	0	7	0	7.3	10.30	1.18
3	0.3	0	5	0	5.3	15.60	1.93
4	0.3	0.2	3	0	3.5	19.10	0.87
5	0	0.2	6	0	6.2	25.30	2.51
6	0.2	0	1	2	3.2	28.50	1.15
7	0.3	0.4	6	3	9.7	38.20	6.30
8	1	0	5	4	10	48.20	11.74
9	2	0	0.6	1.5	4.1	52.30	11.28
10	0.2	0	0.4	0.5	1.1	53.40	7.82
11	1	0.5	1.3	4	6.8	60.20	10.07
12	0.4	0	1	0	1.4	61.60	6.91
13	1	0	3	0.4	4.4	66.00	6.75
14	0.5	0	1	1	2.5	68.50	4.69
15	2	0	3	1	6	74.50	6.13
16	0.5	0.3	4	2	6.8	81.30	8.38
17	0.3	0	1	0	1.3	82.60	5.12
18	0.5	0.5	0	1.5	2.5	85.10	3.06
19	0.2	0.5	0	2	2.7	87.80	1.20
20	4	0.2	0	0.5	4.7	92.50	1.35
21	1.5	0	1	2	4.5	97.00	1.29
22	0	0	0	5	5	102.00	1.73
23	0	0	0	5	5	107.00	2.17
24	0	0	0	4	4	111.00	1.62
25	0	0	0	5	5	116.00	2.06
26	0	0	0	2.5	2.5	118.50	0.00

2- Mamlaha Section

Cycle No.	Calcareous mudstone (m)	Carbonate (m)	Evaporite (m)	Red siliciclastic (m)	Cycle thickness (m)	Cumulative thickness (m)	Cumulative departure (m)
0	0	0	0	0	0	0.00	0.00
1	0.8	0	1	7	8.8	8.80	1.70
2	4	3	5	1	13	21.80	7.60
3	2	3.5	3	1.5	10	31.80	10.51
4	1	0.2	5	4	10.2	42.00	13.61
5	3	0.8	10	3	16.8	58.80	23.31
6	2.7	0.3	2	3	8	66.80	24.21
7	5	0.1	3	3	11.1	77.90	28.22
8	1.5	0.1	1	3	5.6	83.50	26.72
9	0.2	0	4	5	9.2	92.70	28.82
10	0.5	1	3	1.5	6	98.70	27.72
11	1.5	0.5	7	6	15	113.70	35.63
12	0.5	0.5	10	0	11	124.70	39.53
13	0.1	0.1	3	0	3.2	127.90	35.63
14	0	1	4	4	9	136.90	37.53
15	4	0.8	4	1	9.8	146.70	40.24
16	0.5	0	1	6	7.5	154.20	40.64
17	0.5	1	4	3	8.5	162.70	42.04
18	1	1.5	5	7	14.5	177.20	49.44
19	0.3	0.5	2	1	3.8	181.00	46.15
20	1	2.1	1	0	4.1	185.10	43.15
21	0	0.2	4	3	7.2	192.30	43.25
22	1	0	3	2	6	198.30	42.15
23	1	2	5	0	8	206.30	43.05
24	0	0.5	1	3	4.5	210.80	40.46
25	1.5	6	0	4	11.5	222.30	44.86
26	0.1	0.3	0	7	7.4	229.70	45.16
27	0.5	0.2	1	2	3.7	233.40	41.76
28	0.5	1	3	3.5	8	241.40	42.67
29	0	0	0	6.5	6.5	247.90	42.07
30	3	0.2	0	7	10.2	258.10	45.17
31	1.5	0.1	3	2	6.6	264.70	44.67
32	0	0.4	0	3	3.4	268.10	40.98
33	0	0.5	0	3	3.5	271.60	37.38
34	0	0.2	0	0.5	0.7	272.30	30.98
35	0	0.2	0	0.5	0.7	273.00	24.58
36	0	0.5	0	0.5	1	274.00	18.49
37	0	0.3	0	4	4.3	278.30	15.69
38	0	0.3	0	2	2.3	280.60	10.89
39	0	1.5	0	3.5	5	285.60	8.79

40	0	0.3	0	0.5	0.8	286.40	2.50
41	0.5	0.2	0	6	6.7	293.10	2.10
42	0	0	0	5	5	298.10	0.00

3- Sangaw Section

Cycle No.	Calcareous mudstone (m)	Carbonate (m)	Evaporite (m)	Red siliciclastic (m)	Cycle thickness (m)	Cumulative thickness (m)	Cumulative departure (m)
0	0	0	0	0	0	0.00	0.00
1	0.2	0.7	1.5	0.5	2.9	2.90	-2.44
2	4	2.5	0	5.5	12	14.90	4.21
3	6.5	2.5	2	1	12	26.90	10.87
4	1	0.4	3	1.5	5.9	32.80	11.43
5	1.7	0.8	4	2	8.5	41.30	14.58
6	1	0.4	4	1	6.4	47.70	15.64
7	2	0	2.5	1.5	6	53.70	16.29
8	0.2	0	3	4	7.2	60.90	18.15
9	1.6	1.5	0	1.5	4.6	65.50	17.41
10	0.5	1.5	3	2	7	72.50	19.06
11	0.5	0	4	2.5	7	79.50	20.72
12	6	2	0	3	11	90.50	26.38
13	0	0.5	0	0.5	1	91.50	22.03
14	3	0.5	0	3.5	7	98.50	23.69
15	0.3	1	0	4	5.3	103.80	23.64
16	0.2	1	0	1.5	2.7	106.50	21.00
17	0.3	0.3	0	2	2.6	109.10	18.26
18	3.5	1.4	0	7.5	12.4	121.50	25.31
19	2.5	3	0	5	10.5	132.00	30.47
20	0	0	0	2.5	2.5	134.50	27.63
21	0	0	0	1	1	135.50	23.28
22	0	0	0	2	2	137.50	19.94
23	2.2	1.5	0	0.3	4	141.50	18.59
24	0.5	1	0	0	1.5	143.00	14.75
25	0.5	1	0	2	3.5	146.50	12.91
26	0	0	0	2	2	148.50	9.56
27	0	0	0	3	3	151.50	7.22
28	0	0	0	1	1	152.50	2.87
29	0.2	0.3	0	4	4.5	157.00	2.03
30	1	0.5	0	0.5	2	159.00	-1.31
31	2.5	2.5	0	3	8	167.00	1.34
32	0	0	0	4	4	171.00	0.00

4- Aj Dagh Section

Cycle No.	Calcareous mudstone (m)	Carbonate (m)	Evaporite (m)	Red siliciclastic (m)	Cycle thickness (m)	Cumulative thickness (m)	Cumulative departure (m)
0	0	0	0	0	0	0.00	0.00
1	1	0.2	2	2	5.2	5.20	-0.86
2	2.4	0.3	0	2.3	5	10.20	-1.92
3	0	0.3	0	3	3.3	13.50	-4.68
4	1.5	0.3	5	3	9.8	23.30	-0.94
5	1.6	0.7	2	4	8.3	31.60	1.30
6	3	0.5	6	3	12.5	44.10	7.74
7	1.5	0	2	3	6.5	50.60	8.18
8	0.5	0	4	3	7.5	58.10	9.62
9	0.3	1.5	0	4	5.8	63.90	9.36
10	0.5	0.7	0	4	5.2	69.10	8.50
11	0.5	0.4	4	2	6.9	76.00	9.34
12	1	0	4	6	11	87.00	14.28
13	2	0	6	0	8	95.00	16.22
14	3.5	1	0	7	11.5	106.50	21.66
15	4	1	0	4.5	9.5	116.00	25.10
16	0.3	0.1	3	3	6.4	122.40	25.44
17	0.2	0.5	0	7	7.7	130.10	27.08
18	0.2	1.5	4	5	10.7	140.80	31.72
19	2.5	3	1.5	3	10	150.80	35.66
20	0	0	0	3	3	153.80	32.60
21	0	0	0	3	3	156.80	29.54
22	0	0	0	4	4	160.80	27.48
23	1	0.3	0	2	3.3	164.10	24.72
24	0	0.2	0	1	1.2	165.30	19.86
25	0	0.3	0	4	4.3	169.60	18.10
26	0.1	0.1	0	0.5	0.7	170.30	12.74
27	3	2	0	0.5	5.5	175.80	12.18
28	0	0	0	1	1	176.80	7.12
29	0	0	0	2	2	178.80	3.06
30	0	0	0	3	3	181.80	0.00

5- Takiya Section

Cycle No.	Calcareous mudstone (m)	Carbonate (m)	Evaporite (m)	Red siliciclastic (m)	Cycle thickness (m)	Cumulative thickness (m)	Cumulative departure (m)
0	0	0	0	0	0	0.00	0.00
1	4.5	0.6	4	1	10.1	10.10	2.90
2	0.5	0.2	3	3	6.7	16.80	2.39
3	2.5	0.6	5	4	12.1	28.90	7.29
4	3	0.6	3	3	9.6	38.50	9.69
5	3.5	0.3	5	3	11.8	50.30	14.29
6	2.5	5	1	2	10.5	60.80	17.58
7	1	0.5	10	3	14.5	75.30	24.88
8	1	0.3	6	1	8.3	83.60	25.98
9	1	1	4	2	8	91.60	26.77
10	0.4	0	6	0	6.4	98.00	25.97
11	1.5	0	3	0	4.5	102.50	23.27
12	0.3	0.1	2	3	5.4	107.90	21.46
13	6	2	4	4	16	123.90	30.26
14	1	2.5	2	6	11.5	135.40	34.56
15	0	1.5	6	0	7.5	142.90	34.86
16	0.5	0	5	0	5.5	148.40	33.15
17	0.4	0.1	0	3	3.5	151.90	29.45
18	1	0	0	4	5	156.90	27.25
19	0	0.4	0	3	3.4	160.30	23.44
20	1.5	4.5	0	2.5	8.5	168.80	24.74
21	0	0	0	9	9	177.80	26.54
22	1	0	0	4	5	182.80	24.34
23	1	0.5	0	3	4.5	187.30	21.63
24	2	1.2	0	6.5	9.7	197.00	24.13
25	0	0	0	9	9	206.00	25.93
26	0	0	0	2	2	208.00	20.72
27	0.7	0.2	0	2	2.9	210.90	16.42
28	0.5	0	0	1	1.5	212.40	10.72
29	2	0	0	1	3	215.40	6.51
30	1	0	0	10	11	226.40	10.31
31	0	0	0	2	2	228.40	5.11
32	0	0	0	2	2	230.40	-0.09
33	0.5	0	0	10	10.5	240.90	3.20
34	0	0	0	4	4	244.90	0.00

6- Basara Section

Cycle No.	Calcareous mudstone (m)	Carbonate (m)	Evaporite (m)	Red siliciclastic (m)	Cycle thickness (m)	Cumulative thickness (m)	Cumulative departure (m)
0	0	0	0	0	0	0.00	0.00
1	4.5	0.5	1	8	14	14.00	5.90
2	2.5	0.6	3	4	10.1	24.10	7.91
3	2	0.3	5	3	10.3	34.40	10.11
4	0.6	0.5	1	4	6.1	40.50	8.12
5	3	0	4	4	11	51.50	11.02
6	2	4	7	4	17	68.50	19.93
7	0.7	1.4	1.5	2	5.6	74.10	17.43
8	0.2	2	5	2	9.2	83.30	18.53
9	0.4	0.4	7	2	9.8	93.10	20.24
10	5.5	2	1	4	12.5	105.60	24.64
11	7	6	0	3	16	121.60	32.55
12	4.5	5	0	1.5	11	132.60	35.45
13	0.5	1	0	5	6.5	139.10	33.85
14	1	2	1	9	13	152.10	38.76
15	1.5	0.7	0	1.5	3.7	155.80	34.36
16	1	0.2	0	1	2.2	158.00	28.47
17	0	0.2	0	1	1.2	159.20	21.57
18	0	0	0	5	5	164.20	18.48
19	0	0	0	3	3	167.20	13.38
20	1.5	1.5	0	1	4	171.20	9.28
21	0.5	0	0	6	6.5	177.70	7.69
22	2	1.5	0	3	6.5	184.20	6.09
23	0.5	0.1	0	5	5.6	189.80	3.60
24	0	0	0	4.5	4.5	194.30	0.00

7- Krbchna Section

Cycle No.	Calcareous mudstone (m)	Carbonate (m)	Evaporite (m)	Red siliciclastic (m)	Cycle thickness (m)	Cumulative thickness (m)	Cumulative departure (m)
0	0	0	0	0	0	0.00	0.00
1	4	0.5	0	2	6.5	6.50	2.98
2	1.5	0.6	3	2	7.1	13.60	6.57
3	0.6	0.4	1	3	5	18.60	8.05
4	2	0.2	4	1.5	7.7	26.30	12.24
5	2	0.6	1	2	5.6	31.90	14.32
6	1.5	0.4	4	3	8.9	40.80	19.71
7	0.5	1.3	1	1	3.8	44.60	19.99
8	0.5	1	2	0.5	4	48.60	20.48
9	0.2	0.2	0	2	2.4	51.00	19.36
10	0.8	1.2	0	1	3	54.00	18.85
11	2	0	0	1.5	3.5	57.50	18.83
12	0	0	0	4.5	4.5	62.00	19.82
13	0.7	0.5	2	1.5	4.7	66.70	21.00
14	0.5	0.7	0	4	5.2	71.90	22.69
15	0.7	2.2	0	4	6.9	78.80	26.07
16	0.3	0.2	0	5	5.5	84.30	28.06
17	0.5	1.5	0	1	3	87.30	27.54
18	0.5	0.2	0	1	1.7	89.00	25.73
19	0	0	0	0.5	0.5	89.50	22.71
20	0	0	0	0.5	0.5	90.00	19.70
21	0	0	0	1	1	91.00	17.18
22	0	0	0	1.5	1.5	92.50	15.17
23	0	0	0	2	2	94.50	13.65
24	0	0	0	2	2	96.50	12.14
25	0	0	0	2	2	98.50	10.62
26	0	0	0	2	2	100.50	9.11
27	0	0	0	1	1	101.50	6.59
28	0.2	0	0	2	2.2	103.70	5.28
29	0.1	0.2	0	3	3.3	107.00	5.06
30	0	0	0	2	2	109.00	3.55
31	0	0	0	2	2	111.00	2.03
32	0	0	0	3	3	114.00	1.52
33	0	0	0	2	2	116.00	0.00

8- Darbandikhan Section

Cycle No.	Calcareous mudstone (m)	Carbonate (m)	Evaporite (m)	Red siliciclastic (m)	Cycle thickness (m)	Cumulative thickness (m)	Cumulative departure (m)
0	0	0	0	0	0	0.00	0.00
1	0	0	0	4	4	4.00	-1.48
2	0.1	0.3	0	1.5	1.9	5.90	-5.06
3	0	0.2	0	3.5	3.7	9.60	-6.84
4	5	1.6	0	5	11.6	21.20	-0.73
5	3	0.1	0	3	6.1	27.30	-0.11
6	0.7	1	0	4	5.7	33.00	0.11
7	5	1	0	3.7	9.7	42.70	4.33
8	2	0.4	1	0	3.4	46.10	2.25
9	0.2	0	1	2	3.2	49.30	-0.03
10	0.4	0.2	9	3	12.6	61.90	7.09
11	0.7	1.2	1	2	4.9	66.80	6.50
12	1	1.2	5	2	9.2	76.00	10.22
13	0.5	0.1	4	0.5	5.1	81.10	9.84
14	0.5	0.8	0	2	3.3	84.40	7.66
15	5.7	2.6	0	3	11.3	95.70	13.48
16	2	3.5	0	4.5	10	105.70	18.00
17	0.5	0	0	6.4	6.9	112.60	19.41
18	2	0.5	0	3	5.5	118.10	19.43
19	0.2	0	0	3.5	3.7	121.80	17.65
20	0.5	1	0	5	6.5	128.30	18.67
21	0	0	0	2	2	130.30	15.19
22	0.1	0.2	0	3	3.3	133.60	13.01
23	0	0	0	2	2	135.60	9.53
24	0.2	0	0	3	3.2	138.80	7.24
25	0.1	0.1	0	4	4.2	143.00	5.96
26	0	0	0	3	3	146.00	3.48
27	0	0	0	2	2	148.00	0.00

9- Chnarah Section

Cycle No.	Calcareous mudstone (m)	Carbonate (m)	Evaporite (m)	Red siliciclastic (m)	Cycle thickness (m)	Cumulative thickness (m)	Cumulative departure (m)
0	0	0	0	0	0	0.00	0.00
1	0	0	0	3	3	3.00	0.06
2	0	0.2	0	3	3.2	6.20	0.32
3	2	0.1	0	0.5	2.6	8.80	-0.02
4	1.5	0.1	0	3	4.6	13.40	1.64
5	0.5	0.1	0	3	3.6	17.00	2.29
6	1.5	0.4	0	4	5.9	22.90	5.25
7	2.2	0.7	0	0.5	3.4	26.30	5.71
8	0	0.2	0	0.5	0.7	27.00	3.47
9	0	0	0	1	1	28.00	1.53
10	0	0.4	0	3.5	3.9	31.90	2.49
11	0.2	0.4	0	1	1.6	33.50	1.15
12	0.5	0	0	3	3.5	37.00	1.71
13	0	0	0	5	5	42.00	3.76
14	0	0	0	1	1	43.00	1.82
15	0	0	0	1	1	44.00	-0.12
16	0	0	0	4	4	48.00	0.94
17	0	0	0	2	2	50.00	0.00